Contribution of actin cytoskeleton to C. elegans embryonic elongation

Alicia Lardennois

SORBONNE UNIVERSITÉ

Ecole doctorale 515 - Complexité du Vivant

Laboratoire de Biologie du Développement - UMR7622 - IBPS

Contribution of actin cytoskeleton to *C. elegans* embryonic elongation

Contribution du cytosquelette d'actine lors de l'élongation embryonnaire de C. elegans

---

Thèse présentée par :

Alicia LARDENNOIS

Soutenue publiquement le 27 Septembre 2019

Pour obtenir le grade de : **Docteur de Sorbonne Université**

Discipline/Spécialité : Biologie du développement

Thèse dirigée par :
Dr. LABOUESSE Michel — Directeur de Recherche, Sorbonne Université, IBPS

Rapporteur INTERNE/
Présidente de Jury :
Dr. PLASTINO Julie — Directrice de Recherche, Sorbonne Université, Institut Curie

Rapporteurs EXTERNES :
Dr. MANGO Susan — Professeur, Université de Bâle, Biozentrum
Dr. HEISENBERG Carl-Philipp — Professeur, Institute of Science and Technology Austria

Membre invité :
Dr. LLENSE Flora — Maître de conférences, Sorbonne Université, IBPS

ACKNOWLEDGMENTS

It had been quite some journey for me. Science was not my first career choice, but life decided it otherwise. I learned to make the most of it and today I am very happy of the result.

I wish to thank, first and foremost, my thesis director, **Michel**, for handing me over such a wonderful and challenging project, and for trusting me to carry it out. Thank you for your patience, motivation, enthusiasm, and immense knowledge. Your guidance helped me in all the time of research and writing of this thesis. It has not been easy every day, but it was totally worth it. Thank you also for encouraging me when I needed it, for finding the right words.

I consider it an honor to work with **Flora**, my supervisor in the lab, and I am extremely thankful for her support and guidance during these four intense years. Thank for encouraging me all the way, especially during the difficult moments. Thank you for your help with the experiments, your scientific advices, and very stimulating discussions (scientific or else).

I also would like to express my profound gratitude to **Teresa**. Without your scientific contribution, my thesis would not have been the same. Thank you for your support, various scientific discussions and also everyday talks.

Along with **Michel**, **Flora** and **Teresa**, I would also like to thank all present and past members of Labouesse and Robin teams: **François** for insightful scientific discussions (especially about cytoskeleton) but also for precious life hacks - **Saurabh** for teaching some basics about *C. elegans* and how to design CRISPRs - **Shashi** for being available each time I had questions about protocols or else (especially about CRISPR or VAB-10…) - **Loan** for many shared laughs at the bench and in the office, and his kind help with injections - **Serena** for great scientific discussions (as well as cats related and United Wizard discussions) - **Asma** for her kindness and for being a Potterhead just like me - **Camille**, **Thanh**, **Xinyi**, **Vlad** and **Dilyana** for nice conversations about science and life. I want to thank students who helped me with bench work: **Antoine**, **Leïla** and **Camille**. Thank you also to the **Galy team members** for their kind welcome whenever we go for injections. And most importantly, thank you to all for just being there, it was great sharing such a nice time with all of you during these last four years.

I cannot find words to express my gratitude to **Emma**, **Manon** and **Dylan**, who had been there for me all along particularly in the very difficult times. You bear with me anytime I discussed my PhD project, my paper, the difficulties I was facing and most of all the frustration that came with it. I really owe you a lot (and that bottle of Champagne I promised you!).

Special regards to **Michel**, **Flora** and **Teresa** for correcting the science of my thesis, as well as to **Emma** and **my parents**, for editing my thesis, tracking orthograph and layout mistakes of the documents during the last days.

Finally, I deeply thank my family, and Nounoutte, my beloved cat. Thank you, **Mom** and **Dad**, for your unconditional support and love and always standing next to me whenever I need. It has been fifteen years that you trust me with the life choices I make, even the hardest ones. Your trust made me who I am today, I could not have done it without you. I will never be grateful enough.

REMERCIEMENTS

Cette expérience a été déterminante pour moi. La science n'était pas mon premier choix de carrière, mais la vie en a décidé autrement. J'en ai tiré le meilleur parti et aujourd'hui, je suis très heureuse du résultat.

Je tiens avant tout à remercier mon directeur de thèse, **Michel**, de m'avoir confié un projet aussi intéressant et stimulant et de m'avoir fait confiance pour le mener à bien. Merci pour ta patience, ta motivation, ton enthousiasme et tes immenses connaissances. Tes conseils m'ont aidé tout au long de cette thèse et de son écriture. Cela n'a pas été facile tous les jours, mais cela en valait la peine. Merci également de m'avoir encouragée lorsque j'en ai eu besoin et d'avoir trouvé les mots justes.

Ce fut un honneur de travailler avec **Flora**, ma superviseure dans l'équipe, et je suis extrêmement reconnaissante de ton soutien et de tes conseils au cours de ces quatre années intenses. Merci de m'avoir encouragée jusqu'au bout, surtout pendant les moments difficiles. Merci pour ton aide pour les expériences, tes conseils scientifiques et nos discussions très stimulantes (scientifiques ou autres).

Je voudrais également exprimer ma profonde gratitude à **Teresa**. Sans ta contribution scientifique, ma thèse n'aurait pas été la même. Merci pour ton soutien, nos diverses discussions scientifiques et celles plus légères.

En plus de **Michel**, **Flora** et **Teresa**, je voudrais également remercier tous les anciens membres et membres actuels des équipes Labouesse et Robin: **François** pour nos échanges scientifiques approfondis (en particulier sur le cytosquelette) mais aussi pour tes précieux conseils - **Saurabh** pour m'avoir appris quelques manipulations de base sur *C. elegans* et la conception des CRISPRs - **Shashi** pour ta disponibilité à chaque fois que j'avais des questions sur les protocoles ou autres (en particulier sur les CRISPR ou VAB-10…) - **Loan** pour avoir supporté avec bonne humeur de partager la paillasse avec moi pendant deux ans et pour ton aide avec les injections - **Serena** pour nos grandes conversations scientifiques (ainsi que celles sur les chats et United Wizard) - **Asma** pour ta gentillesse et notre passion partagée pour Harry Potter - **Camille**, **Thanh**, **Xinyi**, **Vlad** et **Dilyana** pour nos conversations sur la science et le reste en général. Je tiens à remercier les étudiants qui m'ont aidée sur les expériences : **Antoine**, **Leïla** et **Camille**. Merci également aux membres de l'**équipe Galy** pour leur accueil chaleureux chaque fois que nous injectons. Et surtout merci à tous d'avoir été présents, j'ai beaucoup apprécié votre compagnie au cours de ces quatre dernières années.

Je n'ai pas de mots pour exprimer ma gratitude envers **Emma**, **Manon** et **Dylan**, qui ont toujours été là pour moi, particulièrement dans les moments très difficiles. Vous m'avez supportée à chaque fois que je parlais de ma thèse, de mon papier, de mes difficultés et surtout de la frustration qui en découlait. Je vous dois beaucoup (nous sabrerons le champagne bientôt !).

Merci particulièrement à **Michel**, **Flora** et **Teresa** pour la correction de ma thèse, ainsi qu'**Emma** et **mes parents** pour en avoir perfectionné la mise en page au cours des derniers jours.

Enfin, je remercie profondément ma famille, et Nounoutte, mon chat adoré. Merci, **papa** et **maman**, pour votre soutien inconditionnel et votre amour et pour être à mes côtés à chaque fois que j'en ai eu besoin. Cela fait quinze ans que vous me faites confiance, quel que soient mes choix de vie, même les plus difficiles. Votre confiance a fait de moi ce que je suis aujourd'hui, je n'aurais pas pu le faire sans vous. Je ne serai jamais assez reconnaissante.

TABLE OF CONTENTS

ABBREVIATIONS

ABBREVIATIONS

A/P	Anterior/Posterior
ABD	Actin Binding Domain
ABP	Actin Binding Protein
ABS	Actin Binding Site
AFM	Atomic Force Microscopy
AJ	Adherens Junctions
BMD	Body Morphology Defect
C. elegans	*Caenorhabditis elegans*
CeAJ	*C. elegans* Adherens Junctions
CeHD	*C. elegans* Hemidesmosomes
CH	Calponin Homology (domain)
CRIB	Cdc42/Rac Interactive Binding (domain)
CRISPR	Clustered Regularly Interspaced Short Palindromic Repeats
DIC	Differential Interference Contrast
DLG-1	(*Drosophila*) Discs-Large (homologue)-1
DNA	Deoxyribonucleic Acid
D/V	Dorsal/Ventral
ECM	Extracellular Matrix
FA	Focal Adhesions
FH	Formin Homology (domain)
FRAP	Fluorescence Recovery After Photobleaching
FRET	Förster Resonance Energy Transfer
GAS2	GrowthArrest-Specific protein 2
GBD	GTPase Binding Domain
GFP	Green Fluorescence Protein
GIT	G protein-coupled receptor kinase InTeractor
IF	Intermediate Filament
L1-L4	Larval stages of *C. elegans* development
MHC	Myosin essential Heavy Chain
MLC	Myosin essential Light Chain
MSC	Mesenchymal Stem Cells
MT	Microtubule
MTOC	Microtubule Organizing Center
NGM	Nematode Growth Medium
NMYII	Non-muscle Myosin-II
PAK	p21-Activated Kinase
PAM	Protospacer Adjacent Motif
PCR	Polymerase Chain Reaction
PH	Plecktrin Homology (domain)
PIP2	Phosphatidylinositol-4,5-bisphosphate
PIX	PAK interacting exchange factor
PR	Plectin Repeat
RLC	Regulatory Light Chain (of non-muscle myosin-II)
RNA	Ribonucleic Acid
RNAi	RNA interference
ROCK	Rho-associated Kinase
ROI	Region Of Interest
sgRNA	single guide RNA
SH3	Src Homology (domain)
SR	Spectrin Repeat (domain)

TIRF-SIM	Total Internal Reflection Fluorescence Microscopy - Structured Illumination Microscopy
VBS	Vinculin Binding Site
Y2H	Yeast Two Hybrid
ZP	Zona Pellucida

Common abbreviations for mutant phenotypes in *C. elegans*

Dpy	Dumpy
Let	Lethal
Pat	Paralysed at two-fold
Sma	Small size
Unc	Uncoordinated movement
Vab	Variable abnormal Morphology

Most commonly mentioned genes in this work

fhod-1 encodes for *C. elegans* formin.
mutants are viable and fertile although they show some body wall muscle defects.

gsnl-1 encodes for *C. elegans* gelsolin.
mutants are viable and fertile.

pak-1 encodes for *C. elegans* p21-activated kinase-1.
mutants are viable and fertile, slight BMD (enlarged head) in L1 larvae.

spc-1 encodes for *C. elegans* α-spectrin.
mutants show embryonic lethality and fails to elongate beyond 2-fold.

sma-1 encodes for *C. elegans* β_H-spectrin.
mutants display a Sma phenotype with shortbody length.

unc-70 encodes for *C. elegans* β_G-spectrin.
mutants are short and paralyzed; the defects develop gradually through the larval stages. However embryonic elongation is not affected.

unc-112 encodes for a *C. elegans* dense body component, vertebrate kindlin-homologue
mutants display a Pat phenotype: embryonic arrest due to muscle dysfunction and paralyzation at the 2-fold stage.

vab-10 encodes for *C. elegans* spectraplakin.
mutants have defects in embryonic elongation, body morphology, uterus-vulva connection, and gonad arm migration, the animals have poor mating efficiency.
generates isoforms related either to plectin (VAB-10A) or to microtubule actin cross-linking factor plakins (VAB-10B) that have distinct functions and localizations.

viln-1 encodes for *C. elegans* villin.
mutants are viable and fertile.

ABSTRACTS

(in English and in French)

ABSTRACT

Body axis elongation is a fundamental morphogenetic process, involving cell shape changes powered by mechanical forces through small incremental steps which need to be stabilized. During my PhD, I studied *C. elegans* embryonic elongation to define how the embryo, an elastic material, lengthens progressively upon muscle contractions. Previously, the lab found a kinase, PAK-1, to be mediator of an epidermal mechanotransduction pathway downstream of muscles. Two screens in a *pak-1(Ø)* background identified α-spectrin SPC-1 as an interactor of PAK-1. *spc-1(-)pak-1(-)* embryos elongate up to 1.5-fold and then retract to 1-fold in a muscle dependent manner. I used super-resolution microscopy to show that epidermis circumferential actin bundles are highly disorganized in these embryos; suggesting that actin rearrangement could be the lock counteracting elasticity. With a screen in *spc-1(-)pak-1(-)* background, I identified two severing proteins helping break actin filaments when muscle activity bends them at sharp angles. In addition, the actin bundling formin FHOD-1, was also shown to induce retraction in *fhod-1(-);spc-1(-)* embryos. I overexpressed a C-terminally truncated FHOD-1(ΔFH2/DAD) that partially rescued the *spc-1(-)pak-1(-)* retraction suggesting that FHOD-1 blocks further actin depolymerization at each cycle of contraction. To test it, we modeled the embryo as a Kelvin-Voigt material under acto-myosin force from the epidermis and muscle tension. We predicted embryo lengthening using a viscoplastic component accounting for actin shortening. Altogether I characterized a cellular network conferring mechanical plasticity to stabilize cell shape during a morphogenetic process.

RÉSUMÉ COURT

Les processus morphogénétiques impliquent des changements de forme de cellules, via des forces mécaniques, qui doivent être stabilisés. Ma thèse vise à élucider comment l'embryon de *C. elegans*, matériau élastique, s'allonge progressivement sous l'effet des contractions musculaires. Un crible ARNi en fond *pak-1(Ø),* kinase de l'épiderme impliquée dans une cascade de mécanotransduction en aval des muscles, a identifié SPC-1/α-spectrine, comme partenaire probable. Les embryons *spc-1(-)pak-1(-)* s'allongent jusqu'à 1.5-fold, puis reviennent à leur taille initiale sous l'effet des muscles. Avec la microscopie à super-résolution, j'ai montré que leurs faisceaux d'actine épidermiques sont très désorganisés ; suggérant que le remodelage de l'actine pourrait contrer l'élasticité des cellules. Avec un crible en fond *spc-1(-)pak-1(-),* j'ai identifié deux protéines de fragmentation aidant à rompre les filaments d'actine quand les muscles les courbent fortement. Par ailleurs, la formine de "pontage" FHOD-1 induit aussi une rétraction dans des embryons *fhod-1(-);spc-1(-)*. J'ai surexprimé une construction FHOD-1(ΔFH2/DAD) tronquée en C-terminal qui a partiellement sauvé la rétraction *spc-1(-)pak-1(-)* suggérant que FHOD-1 bloque la dépolymérisation de l'actine à chaque cycle de contraction. Pour tester cela, j'ai modélisé l'embryon en tant que matériau Kelvin-Voigt soumis à une force épidermique et à la tension musculaire et prédit son allongement en utilisant un composant viscoplastique symbolisant le raccourcissement de l'actine. J'ai donc caractérisé un réseau cellulaire conférant une plasticité mécanique et stabilisant la forme des cellules dans un processus morphogénétique.

RÉSUMÉ LONG

En tant qu'organismes vivants, nous interagissons avec notre monde grâce à nos sens. Nous sommes continuellement exposés à des signaux mécaniques, et il en va de même pour nos cellules. Ces dernières ont la capacité de détecter leur environnement physique en traduisant des forces mécaniques et des déformations en signaux biochimiques. À leur tour, ces signaux peuvent ajuster les structures cellulaires et extracellulaires. Au cours des deux dernières décennies, de nombreux processus biologiques répondant à des stress mécaniques ont été mis en évidence tels que : le changement de pression de turgescence dans la réponse au toucher chez *Mimosa pudica,* la différenciation variable des cellules souches mésenchymateuses en fonction de la rigidité du milieu de croissance sous-jacent, la cicatrisation des plaies ou encore la prolifération et la dissémination des cellules cancéreuses. Les différents mécanismes par lesquels le tissu cellulaire convertit le stimulus mécanique en une activité électrochimique ou biochimique sont appelés **mécanotransduction**. La mécanotransduction est à l'origine d'un certain nombre de sens et de processus physiologiques dans le corps, notamment la proprioception, le toucher, l'équilibre et l'audition. Au niveau cellulaire, elle est importante pour de nombreuses fonctions telles que l'adhésion, la migration, la prolifération, la différenciation et l'apoptose et elle est essentielle au développement d'organes.

Une étape clé du développement de l'animal est la mise en place de l'axe du corps définissant sa forme finale lors de la morphogenèse. Ce processus détermine la forme et la structure des tissus, des organes et des organismes. Plus spécifiquement, la morphogenèse embryonnaire désigne des modifications de la forme et de la position des cellules dans l'embryon, en particulier de l'épithélium. L'importance de la morphogenèse épithéliale a été rapportée dans des processus de développement cruciaux tels que la gastrulation (étudiée de manière approfondie dans les ascidies, la drosophile, le poisson zèbre ou le xénope) ou dans la formation du tube neural. Cette étape dépend de manière critique des changements de forme de cellules, eux-mêmes dépendants de l'interaction entre les forces intrinsèques et extrinsèques aux cellules. Comprendre comment les forces mécaniques influencent la morphogenèse au niveau cellulaire et moléculaire reste un défi majeur.

Pour étudier la mécanotransduction et son importance dans la morphogenèse à l'échelle d'un organisme, nous travaillons avec un modèle simple, le nématode *C. elegans*. Depuis son introduction, par Sydney Brenner, dans les laboratoires à la fin des années 1960, *C. elegans* est utilisé comme organisme modèle en biologie du développement, génétique et biologie moléculaire grâce à sa progéniture abondante, son développement rapide, son corps transparent et son génome complètement séquencé. Son épiderme est un épithélium à monocouche séparé des muscles par une mince membrane au niveau basal. Les muscles sont disposés en quatre rangées, deux attachées à l'épiderme dorsal et deux à l'épiderme ventral via les hémidesmosomes, rendant l'épiderme

sensible au stress mécanique résultant de leurs cycles de contraction. Au cours de son élongation embryonnaire, le nématode *C. elegans* voit sa longueur multipliée par un facteur 4 et sa circonférence réduite par un facteur 2,5. Il s'agit d'un processus rapide (trois heures environ) qui a lieu sans réarrangement ni division cellulaire, seulement permis par la déformation des cellules latérales et dorso-ventrales de son épiderme. Cette élongation est initialement activée par la contractilité de l'acto-myosine dans les cellules latérales, via la régulation de la Rho kinase. A partir du stade « 2-fold », la tension fournie par les contractions musculaires permet le recrutement de la protéine adaptatrice GIT-1 aux hémidesmosomes, permettant la seconde phase de l'élongation notamment via activation de la kinase PAK-1. Lorsque l'activité musculaire est inhibée, les embryons sont paralysés à un stade « 2-fold » et GIT-1 n'est plus recrutée. Pourtant les mutants *git-1* et *pak-1* sont viables, suggérant qu'une autre voie agit en parallèle. Par ailleurs, chez *C. elegans,* la contribution du cytosquelette d'actine à la morphogenèse embryonnaire a été rapportée depuis la fin de la gastrulation. Au début, l'actine forme un maillage près du cortex épidermique, et au fur et à mesure elle se réorganise pour former des faisceaux circonférentiels et parallèles d'abord dans les cellules dorso-ventrales, puis dans les cellules latérales. Une fois l'élongation embryonnaire terminée, les faisceaux se désassemblent.

Dans ce contexte, l'objectif de mon projet de thèse a été de caractériser de manière plus détaillée l'apport du cytosquelette d'actine pendant l'élongation embryonnaire de *C. elegans* et la façon dont les câbles d'actine sont remodelés au cours de ce processus.

De précédents travaux de l'équipe ont montré que PAK-1 fait partie d'une voie de mécanotransduction induisant le remodelage des hémidesmosomes, structures de couplage entre les muscles et l'épiderme sus-jacent. Deux cribles ont alors été réalisés en fond sensible *pak-1(-)* pour rechercher de potentiels partenaires de PAK-1 et l'α-spectrine SPC-1 s'est révélée être un fort candidat. Les spectrines ont été décrites pour la première fois dans les érythrocytes en 1968 par Marchesi et Steers. Elles sont un des composants majeurs du cytosquelette de la membrane cellulaire et sont responsables des propriétés mécaniques (stabilité, plasticité et déformabilité) de celle-ci.

À l'aide d'outils génétiques et d'approches d'imagerie *in vivo*, une ancienne doctorante de l'équipe, Gabriella Pàsti, a montré que l'α-spectrine et PAK-1 interagissent génétiquement. En effet, elle a constaté que chez les mutants *spc-1 (-) pak-1 (-),* les embryons s'allongent jusqu'à « 1,5-fold », puis se rétractent jusqu'à leur taille initiale (phénotype de rétraction). Fait intéressant, ce phénotype avait déjà été décrit suite à la dépolymérisation massive de l'actine, via l'usage d'une drogue, suggérant que le réarrangement de l'actine pourrait fonctionner comme un verrou lors de la

morphogenèse embryonnaire. Mon travail a donc consisté à caractériser plus en détail cette interaction entre le cytosquelette d'actine et l'α-spectrine en répondant aux questions suivantes :

- Comment fonctionne le mécanisme de verrou au niveau moléculaire ?
- Comment les câbles d'actine sont-ils remodelés au cours du temps ?
- Quels sont les rôles des différents acteurs identifiés ?
- Peut-on modéliser l'allongement progressif de l'embryon pour comprendre comment les forces contribuent au remodelage de l'actine ?

1. Phénotype de rétraction et activité musculaire

Sachant que les embryons *spc-1(-) pak-1(-)* amorcent leur rétraction lorsque les muscles comment à être actifs, j'ai essayé de déterminer la manière dont l'apport musculaire affecte la rétraction des embryons. Précédemment, Gabriella a montré que si l'activité musculaire était bloquée que chez des mutants *spc-1(-) pak-1(-)*, grâce l'utilisation d'un ARNi contre *unc-112* (kindlin homologue et composant essentiel des muscles), cela empêchait la rétraction des embryons. J'ai terminé cette expérience en ajoutant plusieurs contrôles supplémentaires en mesurant l'élongation des vers *unc-112(-); pak-1(-)* et *unc-112(-); spc-1(-).* Ils ont montré une croissance plus lente très semblable aux vers *unc-112(-)* seuls. Pour comprendre comment les contractions musculaires contribuent au phénotype de rétraction, j'ai quantifié la différence de comportement entre embryons de type sauvage et mutants en utilisant des points de repère sur l'actine épidermique. J'ai mesuré le temps de contraction / relaxation et l'ampleur de la contraction / relaxation. Les doubles mutants ont présenté des contractions plus rapides et plus profondes que les embryons de type sauvage et *pak-1(-)*. Ces deux expériences ont montré que l'apport musculaire est crucial pour le phénotype de rétraction bien qu'il soit perturbé dans le double mutant *spc-1(-) pak-1(-).*

2. Remodelage et dynamique du cytosquelette d'actine

2.a. Organisation de l'actine

En plus de contracter plus rapidement, les embryons *spc-1(-) pak-1(-)* présentent également des défauts d'organisation de l'actine : les câbles d'actine ne sont plus complètement parallèles, ils se regroupent et semblent parfois discontinus. Pour mieux caractériser ces défauts observés avec un microscope « spinning-disk », j'ai effectué une analyse de texture développée dans l'équipe avec l'aide de notre ingénieure, Teresa Ferraro. Nous avons analysé des images d'embryons anesthésiés à différents stades («1,7-fold», «2-fold» et «3-fold») pour obtenir une résolution plus élevée de l'actine. L'analyse du signal de fluorescence associé aux filaments d'actine dans l'épiderme dorso-ventral a révélé davantage de discontinuité dans les embryons *spc-1(-) pak-1(-)* par rapport aux témoins ; de plus, leur degré d'anisotropie par rapport à l'axe circonférentiel était anormal. Avant

que les muscles commencent à se contracter, aucune différence significative n'est visible. Dès que l'activité musculaire est établie, l'organisation de l'actine devient significativement différente entre les contrôles et les *spc-1(-) pak-1(-)* mais également entre *spc-1(ARNi)* et *spc-1(-) pak-1(-).* Dans un second temps, j'ai utilisé la microscopie à super résolution pour affiner ces observations et éventuellement accéder à des évènements de remodelage en temps réel. L'analyse de segmentation du signal de fluorescence associé aux filaments d'actine a été confirmée et même améliorée puisque nous avons pu faire une différence entre la zone de l'épiderme située juste au-dessus des muscles et celle située à côté : les défauts d'organisation sont plus prononcés au niveau des muscles, là où la tension est plus forte. Par ailleurs, l'intensité du signal entre les faisceaux d'actine adjacents était également moins nette chez les embryons *spc-1(-) pak-1(-)* et ils étaient plus souvent courbés, indiquant que les faisceaux pourraient s'être partiellement défasciculés.

Ces phénotypes apparaissent une fois que les muscles entament leur activité suggérant que les contractions musculaires contribuent au remodelage de l'actine. Pour étudier plus en détail leur rôle dans ce processus, nous avons examiné les filaments d'actine spécifiquement lors de la contraction des muscles. De manière frappante, la microscopie « spinning-disk » a révélé que les contractions musculaires sont suffisamment fortes pour courber localement des faisceaux d'actine avec un angle moyen de 57 °, ce qui induirait une cassure du filament d'actine d'après des analyses réalisées *in vitro*. Les cycles répétés d'activité musculaire pourraient avoir pour effet d'induire localement la rupture du filament d'actine épidermique, suivie de leur stabilisation. Dans les doubles mutants *spc-1(-) pak-1(-),* des contractions musculaires plus courtes pourraient faire pencher la balance entre rupture et stabilisation conduisant ainsi à leur désorganisation.

2.b. Remodelage durant l'élongation

Tous ensemble, les résultats décrits ci-dessus établissent un lien entre l'activité musculaire et désorganisation de l'actine chez les embryons *spc-1(-) pak-1(-)*. L'hypothèse la plus simple est que l'activité musculaire induit chez les embryons normaux une rupture et une stabilisation de l'actine bien contrôlée qui se détériore chez les embryons *spc-1(-) pak-1(-).* En effet, une autre analyse sur ces images a montré que la circonférence de l'embryon diminuait de 20% au cours de l'allongement, impliquant que les filaments d'actine dans les cellules dorso-ventrales doivent également se raccourcir. Pour comprendre au niveau moléculaire comment ce remodelage pourrait se produire, j'ai effectué un crible ARNi en fond sensible *spc-1(-) pak-1(-)* à la recherche d'un sauvetage du phénotype de rétraction. De manière remarquable, avec l'aide de Flora Llense, maître de conférences dans l'équipe, nous avons identifié des homologues de deux « protéines de fragmentation » de l'actine, la gelsoline et la villine suggérant que les contractions musculaires

induisent une possible rupture du filament d'actine et donc une stimulation directe ou indirecte de l'activité des protéines.

Pour aller plus loin dans cette caractérisation moléculaire, Gabriella a effectué un dernier crible ARNi en fond sensible *spc-1(-)* pour trouver d'autres partenaires potentiels permettant de reproduire le phénotype de rétraction. Nous avons identifié une protéine de « câblage », la formine atypique FHOD-1. Pour évaluer le lien entre PAK-1, SPC-1 et FHOD-1 dans le phénotype de rétraction, Flora a cloné plusieurs constructions de FHOD-1 basées sur la littérature existante. Il a en effet été démontré que FHOD-1 est initialement inactive en raison d'une interaction auto-inhibitrice entre son domaine autorégulateur en C-terminal et son domaine inhibiteur en N-terminal (DID). Des expériences *in vitro* ont montré qu'en supprimant le domaine DAD, l'auto-inhibition est levée et conduit à une forme constitutivement active de la protéine. L'objectif était de savoir si je pouvais sauver le phénotype de rétraction d'embryons *spc-1(-) pak-1(-)* en surexprimant FHOD-1. Effectivement j'ai observé que 2/3 des embryons exprimant la construction FH2/DAD ne se rétractent plus et qu'ils sont significativement plus longs que les doubles mutants *spc-1(-) pak-1(-).*

3. Modélisation de l'élongation

Pour rendre compte de l'élongation du ver à l'échelle mésoscopique, nous avons développé un modèle physique prédictif. Changer le statut d'une entité physique nécessite l'intervention d'une force (mécanique ou chimique) et l'embryon de *C. elegans* n'échappe pas à cette règle de la physique. Pendant la première phase d'élongation et jusqu'à ce que les muscles deviennent actifs, l'élongation est permise par une force active dans l'épiderme latéral et par une force passive exercée par les cellules épidermiques dorsales et ventrales suffisante pour allonger l'embryon jusqu'au stade « 2-fold ». Cependant, cette force n'est pas suffisante pour expliquer l'allongement jusqu'au stade « 4-fold », puisque les embryons avec des muscles non fonctionnels ne s'allongent pas au-delà du stade « 2-fold ». Par conséquent, les muscles fournissent une deuxième force motrice d'allongement. Considérant cela, nous avons décidé de modéliser l'embryon de *C. elegans* comme un matériau de Kelvin-Voigt soumis à deux forces actives principales : la force épidermique, qui est une force positive continue, et la force musculaire, qui est une force pulsatile puisque les muscles se contractent alternativement. En utilisant un ensemble d'équations mathématiques, nous avons pu prédire l'allongement de l'embryon en introduisant un composant viscoplastique dans le système, symbolisant le raccourcissement de l'actine. Grâce à cela, nous avons également pu modéliser la rétraction des doubles mutants *spc-1(-) pak-1(-).* Comme la continuité des filaments d'actine est modifiée chez ces mutants, leur résistance au stress provenant des cellules latérales ne serait pas maintenue et la force épidermique diminuerait progressivement, ce qui réduirait la longueur du

système. L'absence combinée de SPC-1 et de PAK-1 coïncide avec l'incapacité d'étendre plastiquement la longueur du tissu.

Globalement, nos résultats identifient deux groupes de protéines impliquées dans la stabilisation de la forme des cellules dans un épiderme soumis à un stress répété : SPC-1, PAK-1 et FHOD-1 qui stabilisent les câbles d'actine lors du remodelage, GSNL-1 et VILN-1 qui les sectionnent pour les aider à raccourcir. Ce réseau cellulaire confère une plasticité mécanique (en termes physiques, il implique une déformation irréversible sous contrainte) stabilisant la forme des cellules pendant la morphogenèse. Comprendre comment les cellules s'adaptent à un stimulus mécanique est essentiel et pourrait aider à élucider les dernières étapes de la morphogenèse chez *C. elegans.* Dans un contexte plus médical, la dérégulation de PAK-1 et des spectrines a été décrite dans de nombreuses pathologies. PAK-1 apparaît surexprimée dans de multiples formes de cancers humains tels que le cancer du pancréas, de la prostate, du sein ou encore les mélanomes. De nombreuses études ont montré que la capacité à détecter une entrée mécanique, sa transduction dans la cellule et sa réponse sont défectueuses dans les cellules cancéreuses. *In fine*, nos résultats pourraient aider à mieux comprendre la dérégulation de la réponse à un stress mécanique lors de maladies.

Méthodes : - Les méthodes suivantes ont été utilisées dans le cadre de ce travail.
Analyse génétique, ARN interférent pour inhiber l'expression de gènes, Construction de plasmides, Édition du génome par CRISPR-Cas9, Microscopie super-résolutive, Microscopie à disque rotatif, Microscopie à lapse de temps, Micro-injection, Analyse d'images, Modélisation mathématique

Publications et Conférences :

Alicia Lardennois*, Gabriella Pásti*, Teresa Ferraro, Flora Llense, Pierre Mahou, Julien Pontabry, David Rodriguez, Samantha Kim, Emmanuel Beaurepaire, Christelle Gally, Michel Labouesse. An actin-based viscoplastic lock ensures progressive body axis elongation. **Nature**.

Communications orales :

European Worm Meeting (EWM), Juin 2016, MDC, Berlin
Séminaire de restitution PHC Maimonide, Novembre 2017, Jérusalem
VerMidi XXI, Janvier 2018, CIML, Marseille
European Worm Meeting (EWM), Juin 2018, Barcelone
Building The Cell, Septembre 2018, Institut Pasteur, Paris – Prix du Meilleur Flask Talk
International Worm Meeting (IWM), Juin 2019, UCLA, Los Angeles

Posters :

Retraite de l'école doctorale, ED 515, October 2016, Roscoff
VerMidi XX, Janvier 2017, ENS Lyon
Journée Boris Ephrussi, Avril 2017, Institut Pasteur, Paris
International Worm Meeting (IWM), Juin 2017, UCLA, Los Angeles
Building The Cell, Septembre 2018, Institut Pasteur, Paris
Journée Boris Ephrussi, Avril 2019, ENS (Campus Jourdan), Paris

INTRODUCTION

INTRODUCTION

The range of animal forms is immense, both in terms of obvious external appearances and in terms of the internal anatomies of organs and tissues. Observing the vast number of different shapes, we can wonder how does this diversity arise? Morphogenesis means the generation of form, and usually in the context of developmental biology it means the generation of tissue organization and shape in animal and plant embryos. It is one of three fundamental aspects of developmental biology along with the spatio-temporal control of cell growth and cellular differentiation. The process controls the organized spatial distribution of cells during the embryonic development of an organism. Morphogenesis can also take place in a mature organism, in cell culture or inside tumor cell masses.

Some of the earliest ideas and mathematical descriptions on how physical processes and constraints affect biological growth, and hence natural patterns such as the spirals of phyllotaxis, were written by D'Arcy Wentworth Thompson (Thompson, 1917; Montell, 2008) and Alan Turing (Turing, 1952). Thompson explained animal body shapes as being created by varying rates of growth in different directions, for instance to create the spiral shell of a snail. Turing correctly predicted a mechanism of morphogenesis, the diffusion of two different chemical signals, one activating and one deactivating growth, to set up patterns of development, decades before the formation of such patterns was observed (Hiscock and Megason, 2015). The first major approach to investigating morphogenesis was to look at the intrinsic morphogenetic properties of cells. It showed that randomized aggregates of cells from a mix of amphibian embryonic tissues would not only sort themselves out into their cell types but also generate some structure (Townes and Holtfreter, 1955). They demonstrated that the cells themselves had morphogenetic properties that they could use and stimulated a great deal of work in the '60 '70s and '80s on the morphogenetic abilities of cells. A second approach was to analyze cell behavior in tissues that that will develop in culture where they can be experimentally manipulated. As chick and amphibian embryos are large and accessible, they have been the model species of choice for studying morphogenesis (e.g. neural crest and nerve migrations, corneal development, gastrulation, and epithelial morphogenesis) (Trelstad *et al.*, 1967; Summerbell and Wolpert, 1972; Summerbell and Wolpert, 1973; Meier, 1981; Heasman *et al.*, 1984; Weliky *et al.*, 1991). The mouse *Mus musculus*, the zebrafish *Brachidanio rerio*, the fruitfly *Drosophila melanogaster* and the roundworm *Caenorhabditis elegans* have also supplied continuous and extensive insights into cellular and molecular aspects of morphogenesis (Knust and Müller, 1998; Chisholm and Hardin, 2005; Ellertsdóttir *et al.*, 2010; Rivera-Pérez and Hadjantonakis, 2014).

Morphogenesis was a major area of research in the 70s and early '80s, but activity then declined as the focus of research in development moved to discovering and studying the genes involved in networks that regulate differentiation. However the discovery of molecules controlling tissue organization and the development of transgenic animals led to an enormous amount of work in the first decade of the 21st century that has explained much about the molecular basics of morphogenesis, but less is known about how these are integrated at the cellular level.

For decades, the morphogenesis of epithelial tissues has fascinated scientists at the interface of cell, developmental, and molecular biology. Epithelial morphogenesis includes the various processes by which epithelia contribute to organ formation and body shape. During embryonic development, definitive epithelial organs often arise from preexisting epithelial tissues. Indeed, epithelia form transient structures, such as the neural tube, somites, and the precardiac epithelium, that serve as progenitors for the development of more complex organs (Affolter *et al.*, 2003; Mango, 2007; Bryant and Mostov, 2008). Different epithelia acquire diverse morphological forms appropriate for their specific functions, such as the kidney tubules or the complex branching structures found in the lung for example (Miura, 2015; Marciano, 2017). Recently, the characterization of some of the molecular mechanisms involved in epithelial morphogenesis has provided an abundance of new information on the role and regulation of the cytoskeleton, cell-cell adhesion, and cell-matrix adhesion in these processes (Ding *et al.*, 2004; Blankenship *et al.*, 2006; Armenti and Nance, 2012; Bosveld *et al.*, 2012, Chauhan et al, 2015).

Here I will first discuss the epithelia as layers of cells and their cellular characteristics. Then I will detail the dramatic change they undergo to drive morphogenetic processes, such as shape changes, increase in number, or rearrangements. Finally, I will talk about the mechanical forces, generated by acto-myosin and transmitted by adhesive junctions, driving most of these changes.

I. Epithelia in morphogenesis

Maintaining the homeostasis of a multicellular organism requires compartmentalization of the internal environment of the external environment. In metazoans, the epithelial tissues fulfill this function. These tissues consist of epithelial cells that line the entire body and cavities of the body. In addition, these cells are histologically compact and rest on a basal lamina. Nevertheless, the epithelium denomination includes tissues with vastly different forms and functions within the same organism. Thus, the different epithelia can first be classified empirically according to the overall morphology of their cells (squamous morphology, cubic or cylindrical). Epithelia can also be distinguished by the number of layers of the tissue: layered epithelia consisting of several stacked cell layers (eg. skin epithelium), pseudo-stratified epithelia (eg. tracheal epithelium) and simple epithelia, consisting of a single layer of epithelial cells light (ex: epithelium of the jejunum) (Marieb, 1995; Guillot and Lecuit, 2013).

Biologically, epithelia support the structures of organs and protect the body from the outside pathogens. They separate the interior from the exterior environment as a barrier or control the substance exchange across the plasma membrane as a regulated barrier. They also take part in sensing the environment, repairing wounds, contributing to various steps of development, and playing a pivotal role in shaping organs. To fulfill these roles, the epithelial cells can present additional specific structures, such as microvilli (eg intestinal epithelium), vibratile eyelashes (eg bronchial epithelium) or stereocilia (eg inner ear cells). However, despite this morphological and functional diversity, epithelial cells have a set of molecular characteristics that define them. They have an apico-basal polarity that allows polarized secretion, communication, and uptake of material from extracellular sources. This epithelial polarity is central in the biology of epithelia (Munro *et al.*, 2004; Houk *et al.*, 2012; Von Stetina and Mango, 2015) (Fig. 1). Indeed, its implementation precedes and is required for the morphogenesis of epithelial tissues and the maintenance of their homeostasis.

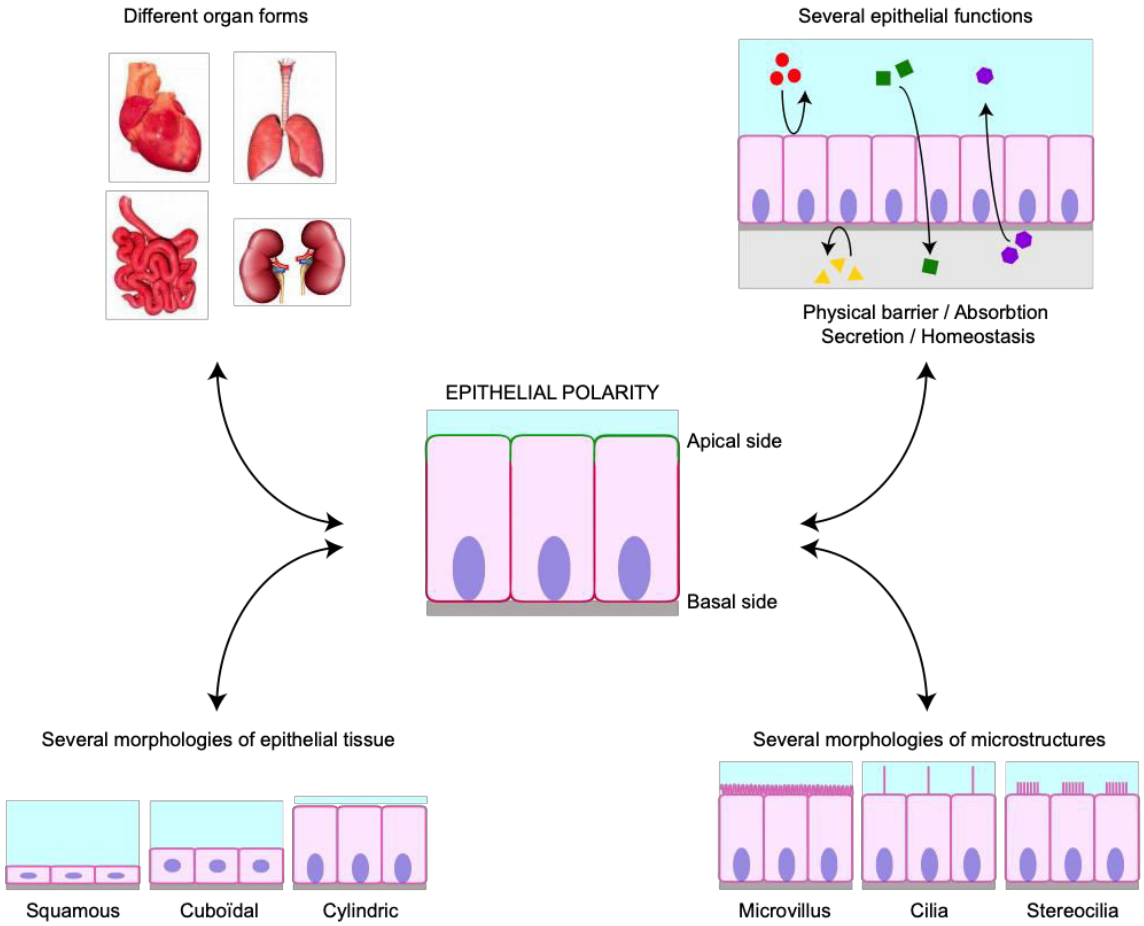

Figure 1: Morphological and functional diversity of epithelia.
Epithelial cells can form tissues of very different shapes and functions within the same organism. Nevertheless, their apico-basal polarization is required for morphogenesis to take place.
Adapted from Kévin Sollier's thesis.

In addition, they also have several cytoskeletal elements with distinct functions that allow both their shape maintenance and force generation. Finally, they have multiple sets of junctions and attachment structures that allow them to form layers with each other and to set up connection with neighboring tissues. These contacts do not solely serve structural and barrier functions: they allow intra- and inter-tissular communication in two ways. One is the classical, chemical signaling. The other one involves physical forces generated in one cell or tissue, which are transmitted and turned into biochemical signals in another cell or tissue. This way of communication is termed as mechanotransduction that is a well-characterized process in sensory mechanisms. On the other hand, a relatively new and dynamically developing research field establishes its role in various developmental processes, as for instance epithelial morphogenesis. This crossing point of epithelial morphogenesis and mechanotransduction stands in the very center of our research limelight.

I.1. General characteristics and function of the epithelia

Epithelia, along with the connective, the muscle, and the nervous tissue, are one of the four basic animal tissue types. Epithelia are continuous sheets of cells (one or more layers thick) that cover the exterior surfaces of the body, line internal closed cavities and body tubes that communicate with the outside environment (the alimentary, respiratory and genitourinary tracts), make up the secretory portions of glands and their ducts, and are found in the sensory receptive regions of certain sensory organs (e.g. ear & nose). Epithelia cover and lining surfaces (e.g. skin), take part in absorption (e.g. the intestine), secretion (e.g. glands), can be sensory (e.g. neuroepithelium) or contractile (e.g. myoepithelial cells). They secrete a basement membrane which supplies a site of attachment for the epithelium, and acts as a selective filtration barrier. There is little intercellular material. Epithelia do not have their own blood supply (avascular), they rely on diffusion for exchange of oxygen and metabolites. Epithelia hold specialized cell-cell junctions that bind adjacent cells to each other. They also have communicating junctions (gap junctions) that allow communication between adjacent cells. Cells in epithelia show a polarity along the axis between the external and internal environment, called apical-basal polarity. When organized in epithelial sheets, they can also exhibit a planar polarity, defined as polarity in a plane other than the apicobasal axis. All the three germ layers, the endoderm, mesoderm, and ectoderm can give rise to epithelial tissues.

The main functions of an epithelial tissue are:

- to protect the tissues that lie beneath from radiation, desiccation, toxins, invasion by pathogens, and physical trauma
- the regulation and exchange of chemicals between the underlying tissues and a body cavity
- the secretion of hormones into the circulatory system, as well as the secretion of sweat, mucus, enzymes, and other products that are delivered by ducts (Quitin *et al.*, 2016)
- to provide sensation (Takeichi, 2014)

Beyond that, the epithelium oversees the formation of the invertebrate exoskeleton as well (e.g. cuticle in worms and arthropods, mineralized shell in molluscs). The role of the exoskeleton is isolation and protection. But it also serves as an insertion for the muscles that enables the active movements and displacement of these animals (Wolpert *et al.*, 1998). In vertebrates the epidermis can be keratinized and can form various structures like hair, nails and claws or protective structures (like spines, scales, or carapaces).

I.2. The organization of an epithelial cell

Epithelial cells have evolutionary conserved features at the level of their structural organization. First, they have an apicobasal polarization that enables polarized secretion, helps to better fulfill their barrier function, and allows polarized communication with their environment (Johnston and Ahringer, 2010). This polarization divides the epithelial cells into an apical side that is most commonly in contact with the environment and could have various surface structures (membrane protrusions, microvilli or sensory structures) and a basolateral side that is in contact with the internal environment, with the neighboring tissues and it also secretes the basal lamina (Fig. 2).

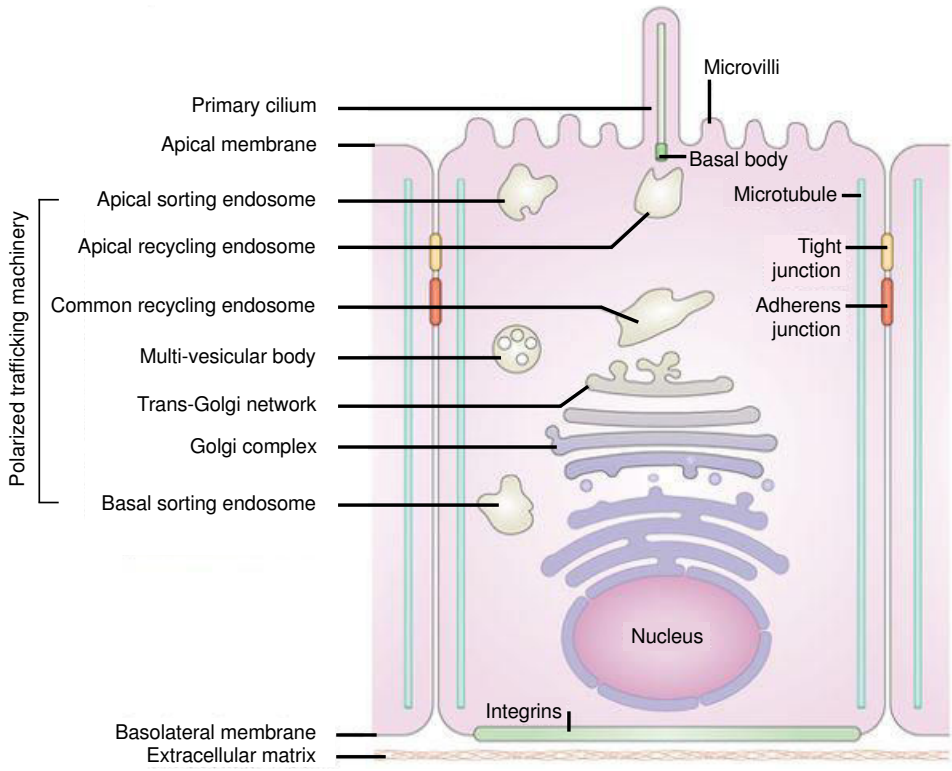

Figure 2: Features of the polarized epithelial phenotype.
A typical vertebrate epithelial cell is shown with components of the polarized vesicle sorting machinery and the apical junctional complex depicted. Note that invertebrate (for example in *Drosophila*) epithelial cells lack primary cilia and the junctional complex is organized differently with adherens junctions (AJs) located more apically than the sealing junction (named septate junction instead of tight junction). In *C. elegans*, AJs and sealing junctions are combined into a single structure.
Adapted from Rodriguez-Boulan and Macara, 2014.

Second, epithelial cells have multiple sets of cell junctions that are relatively conserved in form and to some extent also in function throughout the evolution. They set the barrier between the apical and the basolateral side of the cell, this way promoting polarity maintenance. Furthermore, they are the elements that hold together the epithelial cells. They are important in resisting and

transmitting forces within an epithelial sheet, which is pivotal during the different morphogenetic processes (Lecuit and Yap, 2015).

Epithelial cells also possess four main interconnected cytoskeletal systems. Microtubules (MTs), intermediate filaments (IFs), and actin are the commonly discussed "classical" cytoskeletal networks, shared by all animal cells. Although there is a fourth skeletal network, the spectrin skeleton. It has been initially characterized and extensively studied in red blood cells and its role was little understood in non-erythroid cells for long. Nevertheless, recent research efforts started to recognize the impact of non-erythroid spectrins that seem to be just as important as the first three cytoskeletal entities (Machnicka *et al.*, 2012).

I.2.1. Epithelial junctions

Epithelial cells are tightly connected to form a sheet. This tight connection is achieved through specialized junctions. They interconnect the membrane of adjoining cells, or between a cell and the extracellular matrix (ECM). They also build up the paracellular barrier. The primary function of cell-cell junctions is to resist the external forces that pull cells apart. For instance, epithelial cells must remain tightly linked when they are stretched and pinched. These junctions are dynamic to accommodate the changes in cellular environment such as growth and remodeling.

In epithelia, junctions can be divided into six distinct types, tight junctions, adherens junctions (AJs), desmosomes, gap junctions, hemidesmosomes (HDs), and focal adhesions (FAs) (Fig. 3). At the apical pole, some types of junctions can even combine to form junction complexes.

The apical-most junction in vertebrates is the tight junction or zonula occludens, responsible of the paracellular gating function (Hartsock and Nelson, 2008; Meng and Takeichi, 2009). The intercellular space where tight junction happens is very narrow and filled with this dense junction material. Therefore, the passage of substances between epithelial cells is impossible because the intercellular space is sealed (Sullivan-Brown and Goldstein, 2012). Its analogous structure in *Drosophila* is the septate junction (Hall and Ward, 2016), while in *C. elegans* the paracellular gating is established through different mechanisms and the zonula occludens ortholog protein functions differently (Labouesse, 2006).

Below the tight junction can be found the cadherin-catenin-based AJs: ubiquitous type of linkage between epithelial cells, responsible for maintaining cell-cell adhesions. These junctions employ cadherins and catenins to link the cytoskeleton of one cell to that of its neighbor, in the presence of calcium (Lecuit and Yap 2015). In *C. elegans,* AJ are composed of two complexes commonly referred to as the *C. elegans* Apical Junction (CeAJ) (Labouesse, 2006). First, the cadherin-catenin complex (CCC) is the most apical within the CeAJ (Koppen *et al.*, 2001; McMahon *et al.*, 2001). It is analogous in composition and to a large extent in function to the cadherin-catenin complex found in flies and vertebrates (Costa *et al.*, 1998). Second, the DLG-1/AJM-1 complex (DAC) is formed by two membrane-associated proteins: a Drosophila Discs-large homologue (DLG-1), and a coiled-coil protein AJM-1 (Bossinger *et al.*, 2001; Firestein and Rongo, 2001; Koppen *et al.*, 2001; McMahon *et al.*, 2001). They are mutually dependent on each other for proper localization *in vivo* (Koppen *et al.*, 2001; McMahon *et al.*, 2001; Segbert *et al.*, 2004).

Another complex has a key role in resisting shear stress, the desmosomes. Like AJs, they are attached to cytoskeleton IFs and allow the transmission of tensile forces between epithelial cells (Delva *et al.*, 2009). However, the desmosomes do not form a continuous belt, but circular patches randomly arranged on the lateral side of the cells, to increase the stress resistance of the intra-epithelial attachments (Wolpert *et al.* 1998). They are also located more basally compared to AJs: they are distributed over the lateral membranes, with an up limit of AJs. Desmosomes are absent in *Drosophila* and in *C. elegans*.

Unlike all other types of junctions, gap junctions connect the cytoplasm of two neighboring cells directly. As implied in its name, a gap junction allows the direct pass of various molecules, ions, and electrical impulses between two cells. One gap junction includes two connections, also called hemichannels, to form a homodimer in the intercellular space. The homodimer of connections can undergo a conformational change between close and open in different conditions and thus functions as a regulating gate between cells. Gap junctions are found in many tissues, especially in neurons and nerves, where they are called an electrical synapse (Kelsell *et al.*, 2001; Willecke *et al.*, 2002).

Focal adhesions (FAs) serve as the mechanical linkages to the ECM, and as a biochemical-signaling hub to concentrate and direct numerous signaling proteins at sites of integrin binding and clustering. Within the cell, the intracellular domain of integrin binds to the cytoskeleton via adapter proteins such as talin, α-actinin, filamin, vinculin and tensin. Other intracellular signalling proteins, such as focal adhesion kinase, also bind to and associate with this integrin-adapter protein-cytoskeleton complex. FAs are highly dynamic structures that grow or shrink due to the turnover of

their component proteins in response to changing mechanical stresses (e.g. actomyosin-generated forces, external forces exerted by or through the surrounding matrix)(Zamir *et al.*, 2000; Ballestrem *et al.*, 2001; Rid *et al.*, 2005; Holt *et al.*, 2008). For example, new adhesions are formed at the leading edge of migrating cells and grow and mature as the cells move over them (Partridge and Marcantonio, 20006). In stationary cells, they serve as anchorage devices that maintain the cell morphology. In *Drosophila* embryos FAs mediate surface-rigidity dependent development (Brown *et al.* 2000; Delon and Brown, 2006). *C. elegans* present dense bodies similar to vertebrate focal adhesions but only in muscles cells not in the epithelia (Cox and Hardin, 2004).

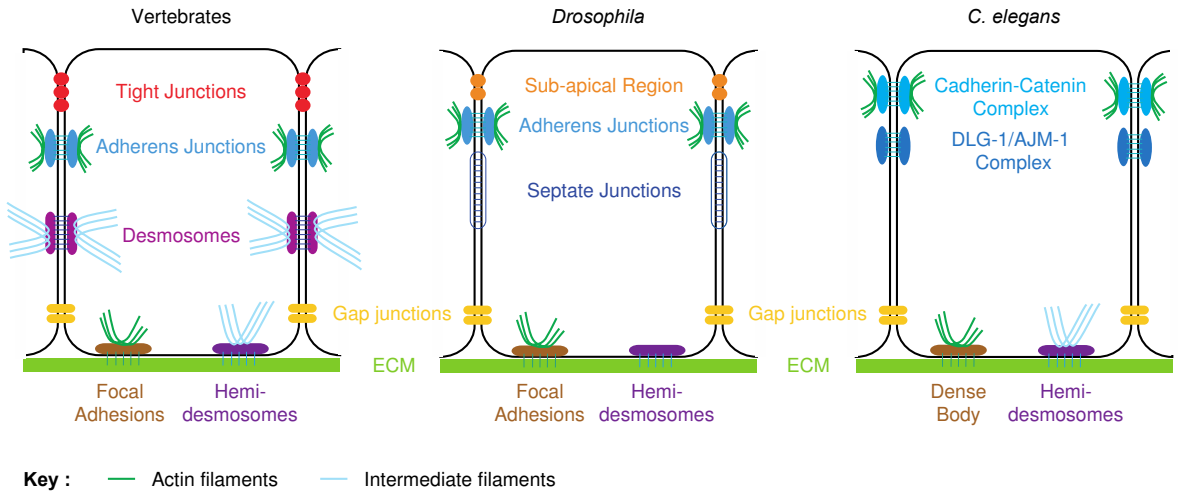

Figure 3: Epithelial junctions in vertebrates, *Drosophila* and *C. elegans*.
Schematic representation of the several types of epithelial junctions. Vertebrates present all six types of junctions: tight junctions, adherens junctions, desmosomes, gap junctions, hemidesmosomes and focal adhesions. *Drosophila* does not have tight junctions but instead present a sub-apical region and septate junctions. *C. elegans* only has adherens junctions-like complexes (CCC and DAC), gap junctions and hemidesmosomes.

Finally, the HDs are the most basal junctions. Under the electron microscope, they have a similar structure as desmosomes. However, while desmosome links two epithelial cells together, HDs link the cell to the ECM. HDs are asymmetric as they connect the basal face of the cell to the basal lamina. They include two rivet-like plaques. The plaques and the anchoring fibrils and filaments are collectively called HD-stable adhesion complex. The HD-stable adhesion complex forms a continuous link between the epithelia and the underlying basement membrane zone (Bornslaeger *et al.*, 1996; Walko *et al.*, 2015). Therefore, HDs can transmit the forces between them, like the AJs.

I.2.2. Extracellular matrix (ECM)

The extracellular matrix is an evolutionary conserved, ancient structure present in all the metazoans. The ECM participates in keeping tissues separated, providing structural support or providing a structure for cells to migrate on. It is a complex network of macromolecules (collagen, laminin, and fibronectin, among others) that are secreted locally and assembled into sheets, fibers, and gels. Multi-subunit transmembrane receptors called integrins are used to bind to the ECM. Integrins bind extracellularly to fibronectin, laminin, or other ECM components, and intracellularly to microfilament-binding proteins α-actinin and talin to link the cytoskeleton with the outside. Integrins also serve as receptors to trigger signal transduction cascades when binding to the ECM (Frantz *et al.*, 2010; Theocharis *et al.*, 2016). Different organisms have evolved different macromolecules for ECM, yet they are not so different in their functions. For instance, ECM related integrins have roles during neural development of *Drosophila* such as axonal growth and synapse formation (Broadie *et al.*, 2011). Another example is the *Drosophila* zona pellucida (ZP) domain protein, dumpy, located in the apical ECM of epithelial cells. It has been shown to interact with numerous proteins notably during embryonic tracheal development and wing development (Prout *et al.*, 1997; Walsh and Brown, 1998; Carmon *et al.*, 2010). In *C. elegans*, the apical ECM promotes elongation. The ZP domain proteins NOAH-1 and NOAH-2 are important for muscle anchoring and mechanical input from muscle contractions, which are essential for elongation (Vuong-Brender *et al.*, 2017). The matrix can also become calcified and hard as rock in case of bones and teeth or produce carapace as in turtles.

I.2.3. Cytoskeleton

The cytoskeleton is present in all type of cells in the body. It organizes cells in space and helps cells to interact mechanically with each other and with the environment. It is a complex network in a remarkable system of filaments that extend throughout the cytoplasm, from the plasma membrane to the nucleus (Fisher and Fowler, 2015). The structure, function, and dynamics of cytoskeleton can vary. They depend on the behavior of three families of filaments: intermediate filaments (IFs), actin filaments, and microtubules (MTs). Each type differs in their composition, biological role, dynamics, and mechanical properties. Actin filaments determine the shape of the cell's surface and are necessary for whole-cell locomotion and cell membrane pinching during cell division. MTs determine the positions of the membrane bound organelles, direct intracellular transport, form and orient the mitotic spindle that segregates the chromosomes. IFs supply the mechanical strength.

A network of proteins regulates the cytoskeleton. Accessory proteins, which include a variety of motor proteins such as myosins or kinesins control the assembly of cytoskeletal filaments in specific locations. (Howard, 1997; Fehon *et al.*, 2010).

I.2.3.1. Actin and myosin

Actin is a family of globular multi-functional proteins that form microfilaments. It is found in essentially all eukaryotic cells. Its mass is about 42-kDa, with a diameter of 4 to 7 nm. An actin protein is the monomeric subunit of two types of filaments in cells: microfilaments, one of the three major components of the cytoskeleton, and thin filaments, part of the contractile apparatus in muscle cells. It can be present as either a free monomer called G-actin (globular) or as part of a linear polymer microfilament called F-actin (filamentous), both of which are essential for cellular functions (Alberts, 2002, Amon, 2012). F-actin is a semi-flexible polymer with a bending stiffness much greater than that of flexible biopolymers such as DNA, but significantly more flexible than rigid rod-like macromolecules such as MTs. It has very high compressive strength however actin binding proteins (ABPs) decrease this and allow bending. These physical properties suggest that F-actin itself may function as a highly dynamic tension sensor (Galkin *et al.*, 2012). Its interaction with various ABPs allow the actin cytoskeleton to promptly adapt to intracellular and extracellular mechanical forces affecting its structure and dynamics (Harris et al, 2018).

While providing mechanical support to the cells, the actin network is also connected to trans-membrane adhesion proteins (Doherty and McMahon, 2008). This connection eases the transduction of intracellular and extracellular mechanical signals, which allow cells to detect and respond to both chemical and mechanical signals from their extra-cellular environment. Indeed, the actin skeleton conducts a broad range of functions in epithelial cells, including muscle contraction, cell motility, cell division and cytokinesis, vesicle and organelle movement, cell signaling, and the establishment and maintenance of cell junctions and cell shape (Huber *et al.*, 2013; Xu *et al.*, 2013; Suraneni *et al.*, 2015; Tsopoulidis, *et al.* 2019).

In vertebrates, three main groups of actin isoforms, α, β, and γ have been identified. The α-actins, found in muscle tissues, are a major constituent of the contractile apparatus. The β and γ actins coexist in most cell types as components of the cytoskeleton, and as mediators of internal cell motility. Although the amino acid sequences and *in vitro* properties of the isoforms are highly similar, these isoforms cannot completely substitute for one another *in vivo* (Khaitlina, 2001). Actin has been one of the most highly conserved proteins throughout evolution because it interacts with a large number of other proteins. It has 80.2% sequence conservation at the gene level between *Homo sapiens* and *Saccharomyces cerevisiae*, and 95% conservation of the primary structure of the protein product (Gunning *et al.*, 2015).

Although the monomers of actin assemble the helical rope-like filaments, these filaments are modified by and interact with other proteins to carry essential cellular functions (Sackman, 2015). This process is called actin remodeling. It is a cyclic pattern allowing the dynamic alterations of cellular organization (Fig. 4). During the remodeling process, actin monomers polymerize in response to signaling cascades that stem from environmental cues (Stossel *et al.*, 2006). The cell's signaling pathways cause actin to affect intracellular organization of the cytoskeleton and often, the cell membrane. Over the course of the cycle, actin begins as a monomer, elongates into a polymer with the help of attached actin-binding-proteins, and disassembles back into a monomer so the remodeling cycle may commence again (Stossel *et al.*, 2006; Rottner and Stradal, 2011). The dynamic function of actin remodeling is directly correlated to the immense variability of cell shape, structure, and behavior. First, there is uncapping of the barbed end by the removal of barbed end capping proteins and ABPs that sever actin filaments (Stossel *et al.*, 2006). This step is followed by de novo nucleation of new actin microfilaments from the existing sides of F-actin by the Arp2/3 complex and formins (Begg et al, 1978). It is helped by polymerization promoters and barbed end capping inhibitory proteins. The elongation phase begins when the concentration of short, F-actin polymers is significantly larger than at equilibrium. At this point, both termini accept the addition of new monomers (although primarily at the barbed end) and the actin microfilament lengthens (Kuhn and Pollard, 2005). It results in the overall stabilization of the actin filament network.

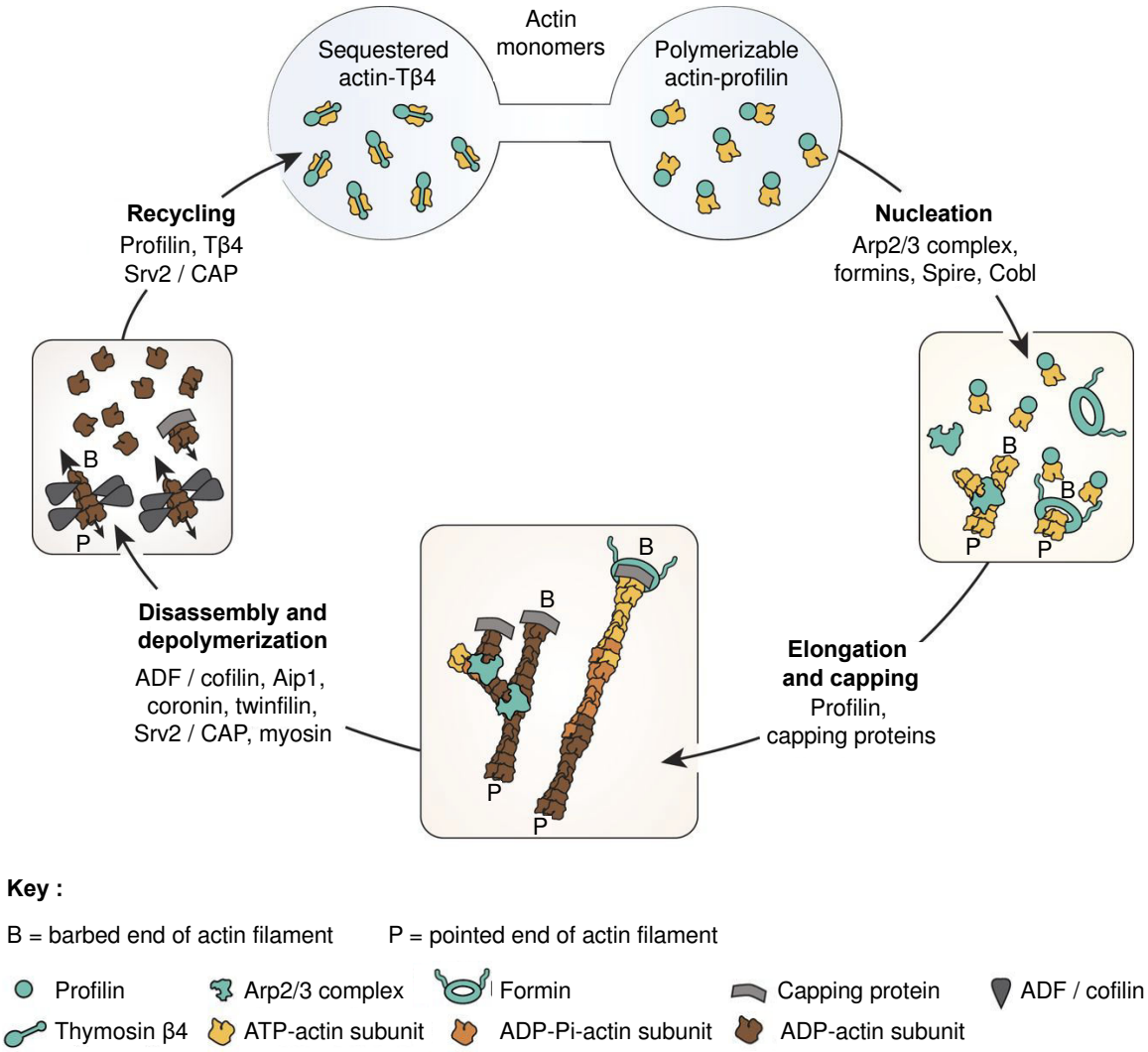

Figure 4: The dynamic steady state of actin.
The minimal steps needed to reach a dynamic steady state of different actin architectures are illustrated. Sequestered and polymerizable actin represent the pool of actin monomers. Nucleation is the formation of actin dimers or trimers. Elongation and capping modulate controlled growth of the different forms of actin organization (branched networks that are generated by the Arp2/3 complex or bundles generated by formins). Disassembly and depolymerization results in the breakdown of actin structures to monomer subunits. Recycling renews the pool of actin monomers that are charged with ATP. The different nucleotide states of actin barbed and pointed ends and different proteins, or complexes are represented by the indicated symbols. The arrows at barbed (B) and pointed (P) ends indicate depolymerization, with larger arrows representing faster dissociation. Adapted from Plastino and Blanchoin, 2018.

The cell uses crosslinking proteins of diverse sizes to carry out different means of stability within the binding network. Small ABP's such as scruin, fimbrin, and espin function by solidifying actin filament bundles (Stossel *et al.*, 2006). Larger ABPs that exhibit coil-like qualities such as filamin function in the promotion of orthogonal organization. Actin crosslinking provides a framework for which the cell may transport signaling intermediates needed for other steps within the actin remodeling cycle (Begg et al, 1978; dos Remedios, 2003; Winder and Ayscough, 2005; Lappalainen, 2016).

After a while, the immobilization by interpenetration of actin filaments results from two distinct ABP families. The gelsolin protein family is believed to be the most efficient in the disruption of actin filaments and is considered a strong severing protein. These proteins respond to an increase in Ca^{2+} and cap the barbed end of the recently severed F-actin (Kalwat and Thurmond, 2013). The increased level of Ca^{2+} may also destabilize the actin-filament network by interfering with the binding of crosslinking proteins (Nicholson-Dykstra et al, 2005). The ADF/cofilin protein family also serves to severe actin-filament networks through the weak severing of actin networks. This form of weak severing does not tightly cap the barbed ends but does allow for the disassociation of actin monomers and thus the disassembly of F-actin (Begg et al, 1978). Finally, thymosin and profilin prevent the spontaneous nucleation of new actin trimers. Actin filaments break back down into monomers and the cycle is completed. Despite its complexity, actin remodeling may result in complete cytoskeletal reorganization in under a minute (Lodish *et al.*, 2013).

Apart of the actin remodeling proteins, other regulators can also contribute to actin dynamics. Indeed, in the epithelial cells the internal force generation occurs through an actomyosin contractile system, with the contribution of non-muscle myosins: molecular motors that convert chemical energy by ATP hydrolysis into mechanical force generation. To note, several non-muscle myosins, like non-muscle myosin I and VI could also contribute to epithelial contractility (Dai *et al.*, 1999; Biro *et al.*, 2013), but the most relevant force generator is non-muscle myosin II.

Non-muscle myosin II is composed of a pair of heavy chains (MHC), a pair of essential light chains (MLC) and a pair of regulatory light chains (RLC). The MLC contain calcium-binding EF-hand domains, interacting with the neck region of the MHC (Fig. 5a). The MLC are responsible for the structural integrity of the motor domain, while the regulatory light chains regulate the myosin II ATPase activity (Ruff *et al.*, 2001). Together they form an hexameric protein complex so-called positive end motor: its progressive movement is directed towards the plus end of the actin filament (Fig. 5b). The motor part of the protein is situated in the N-terminal globular head domain of the MHC, containing the actin- and ATP-binding sites, required for motor activity. ATP-binding and hydrolysis causes conformational changes in the head domain which results in displacement. Myosin II motors by their own are unipolar and hardly processive, they do not perform a contractile activity. But following their activation, they form bipolar complexes, consisting of several NMYII hexamers in an antiparallel organization, interacting through the MHC tails. In this arrangement NMYII mini-filaments become highly processive, their motor domains associate with oppositely oriented, antiparallel actin filaments and pull them together. The attachment and detachment of NMYII and actin happens in a cyclic manner and is coupled to the ATPase activity of NMYII. The phosphate

release upon ATP hydrolysis produces the energy for the conformational change, which triggers the actin movement. At the end of the movement ATP replaces ADP at the motor domain and NMYII detaches from actin. This mechanism is the heart of the actomyosin contractility that creates cortical tension in the epithelial cells (Krendel and Mooseker, 2005; Levayer and Lecuit, 2012).

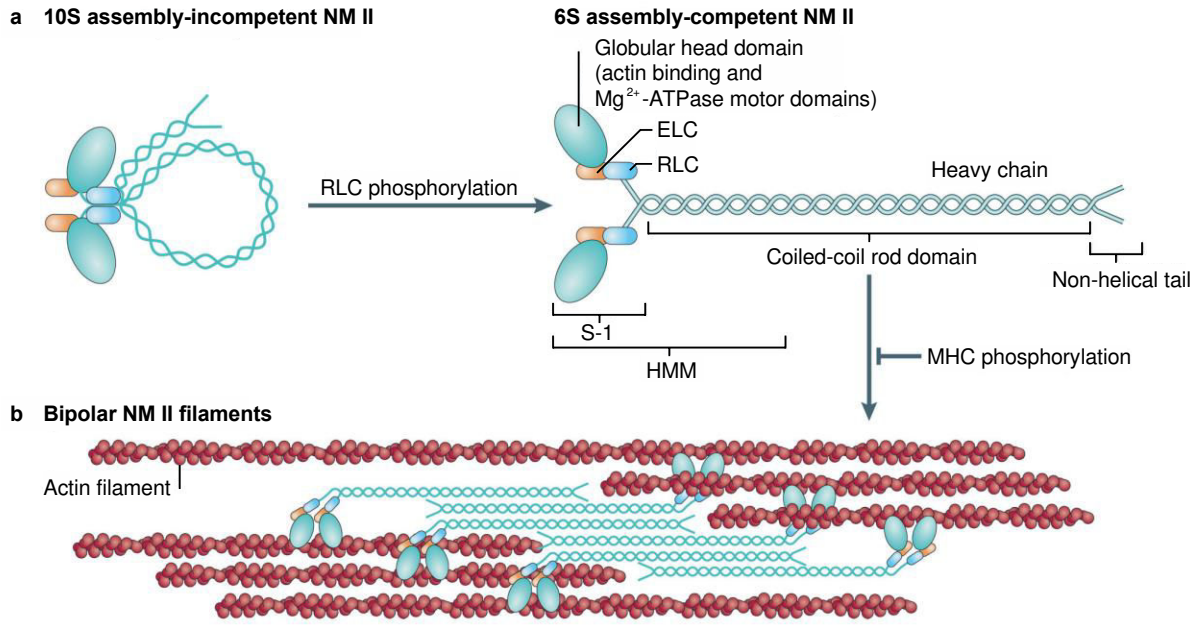

Figure 5: Domain structure of NM II.
(a) The subunit and domain structure of NM II forms a dimer through interactions between the α-helical coiled-coil rod domains. The globular head domain contains the actin-binding regions and the enzymatic Mg^{2+}-ATPase motor domains. The ELCs and the RLCs bind to the heavy chains at the lever arms that link the head and rod domains. In the absence of RLC phosphorylation, NM II forms a compact molecule through a head to tail interaction. This results in an assembly in competent form (10S; left) that is unable to associate with other NM II dimers. On RLC phosphorylation, the 10S structure unfolds and becomes an assembly-competent form (6S). S-1 is a fragment of NM II that contains the motor domain and neck but lacks the rod domain and is unable to dimerize. Heavy meromyosin (HMM) is a fragment that contains the motor domain, neck and enough of the rod to effect dimerization. (**b)** NM II molecules assemble into bipolar filaments through interactions between their rod domains. These filaments bind to actin through their head domains and the ATPase activity of the head enables a conformational change that moves actin filaments in an anti-parallel manner. Bipolar myosin filaments link actin filaments together in thick bundles that form cellular structures such as stress fibers.
Adapted from Vicente-Manzanares, M. *et al.*, 2009.

In *Drosophila*, a single gene encodes for each subunit: zipper for MHC, spaghetti squash (sqh) for MLC and mlc-c essential light chain (Yamashita *et al.*, 2000). *C. elegans* has two MHC genes (*nmy-1, nmy-2*), a single MLC gene (*mlc-4*) and a single essential MLC gene (*mlc-5*) (Chisholm and Hardin, 2005; Gally *et al.*, 2009). In vertebrates at least one regulatory light chain (MRLC2) and three MHC isoforms can be found: NMHC-IIA-C (Conti and Adelstein, 2008).

Actin forms contractile structures with myosin motor proteins to form cross-links and to slide compared to one another. As epithelial cells do not need to generate a high amount of contractile tension compared to muscle cells, they only have a small amount of actomyosin II bundles. The regulation of these contractile bundles' activity is through the phosphorylation of myosin light chain. One important function of these contractile bundles is to provide mechanical support for cells. Actomyosin bundles can assemble into cortical stress fibers to connect epithelial cells to adjoining cells or ECM through AJs (Sackman, 2015). Also, acto-myosin can generate forces inside epithelial cells for their remodeling, as well as the regulation of cell adhesion and migration during morphogenesis (Zelenka, 2004; Blaser *et al.*, 2006; Wirshing and Cram, 2017).

I.2.3.2. Microtubules (MTs)

MTs are complex and highly dynamic cytoskeletal components. The subunits of MTs are tubulins, which are heterodimers formed by two closely related globular proteins: α- and β- tubulins. Assembly of tubulins forms hollow, helical tubes of MTs, which can grow up to 50µm long tubes of 24nm in diameter (Weisenberg, 1972; Pilhofer *et al.*, 2011). These tubes are assembled of short (8nm long) protofilaments. Thirteen such protofilaments line up side by side to close a concentric tube, but the neighboring filaments are not completely aligned: there is a 0.9 nm shift between them, which gives the tube a spiral structure. MTs exist in a dynamic instability and are quasi constantly remodeled: there is a fast-growing plus end, where filament polarization and depolymerization happen, and a minus end often anchored to the centrosome or the microtubule organizing center (MTOC) (Desai and Mitchison, 1997; Marshall and Rosenbaum, 1999). The dynamics instability that MTs undergo is profoundly influenced by the binding and hydrolysis of GTP. The dynamics and organization of MTs are also modulated by the polymer-stabilizing/destabilizing drugs and MT-binding proteins (Weisenberg, 1972; Weisenberg, *et al.*, 1976). Apart of α and β tubulins, γ units also exist, but they do not contribute to such tube formation. These units are acting as nucleators that cap the minus end of the tubes. They are found at the highest concentration in the nucleus, but they are present within the whole cell architecture, at several nucleation sites of the MTs network.

A major function of MTs is to enable motor proteins to transport cargos within the cells. Two families of MT-based motors, kinesins, and dyneins move along MTs to transport vesicles and even organelles during interphase (Berg *et al.*, 2002). This MT-mediated transport is an essential element of various cellular processes and it plays a significant role during cellular movements and shape changes as well (Alberts *et al.*, 2002). It is well established that MTs are central components of cell

mechanics during tissue morphogenesis (Kirschner and Mitchison, 1986; Mathur and Hülskam, 2002; Cearns *et al.*, 2016; Singh *et al.*, 2018). Our lab has recently discovered that MTs also contribute to the process of embryonic morphogenesis as transport machinery (Quitin *et al.*, 2016). Another example is the neuronal morphogenesis in the developing brain. The MT cytoskeleton provides physical support to shape the fine structure of neuronal processes. MT-based motors play important roles in nucleokinesis and centrosomal positioning (Sakakibara *et al.*, 2013). The centrosome, as major organizer of MTs, also has essential functions in regulating cell shape, polarity, cilia formation as well as the position of cellular structures, including the mitotic spindle. Therefore, centrosomes and MTs have important roles during morphogenesis by controlling cell fate decision during tissue and organ development (Tang and Marshall, 2012). However, MTs still play key roles in development even when they are not centrosomally organized. For example, during early *Drosophila* wing epithelium development, individual cells are mechanically autonomous. They contain a polarized apical non-centrosomal MT cytoskeleton that bears compressive forces. In these cells, the Fat planar cell polarity signaling pathway couples MTs at AJs and patterns MT-based forces across a tissue via polarized transcellular stability. These results provide a physical basis to explain how global patterning of MTs controls cell mechanics to coordinate collective cell behavior during tissue remodeling (Singh *et al.*, 2018).

Despite of their obvious importance, there is still a lot left to understand about the role of MTs at the level of complex epithelial behavior, which serves as an interesting future research direction in cell biology.

I.2.3.3. Intermediate filaments (IFs)

Unlike actin and tubulin, IFs are not present in all eukaryotic cells. In the most exposed epithelia, such as the skin, and the cells undertaking mechanical stress, IFs are chemically modified and fill the cell in a massive amount. This implies that IFs endure mechanical tension, provide mechanical stability to the cells and tissues and maintain their integrity (Kolega, 1986; Loranger *et al.*, 1997; Hesse *et al.*, 2000; Fisher and Fowler, 2015). IFs are flexible and extensible structures. Most types of IFs (like neurofilaments, keratins or desmins) are cytoplasmic but nuclear IFs (lamins) also exist. They assemble into filaments of 8-12nm in diameter. These filaments assemble in antiparallel tetramers, combination of two dimers with a tripartite structure: flexible N- and C-terminal domains that flank a central coiled coil domain. The functions of IFs include organizing the internal structure of epithelial cells and maintaining the cell shape by bearing mechanical tensions (Kolega, 1986;

Bornslaeger *et al.*, 1996). They are proposed to be able to resist a significantly higher level of longitudinal strain than actin or MTs (Kreplak and Fudge, 2007). Their ability to rapidly change their organization in response to injury is a crucial part in tissue repair. Instead of treadmilling like actin and MTs, their dynamic structural changes are achieved through post-translational modifications, like phosphorylation or sumoylation (DePianto and Coulombe, 2004; Pásti and Labouesse, 2014). As mentioned in the paragraph about junctions, IFs also take part in cell-cell desmosomes and cell-matrix HDs. Therefore, they also play a role in tension transmission between epithelial cells and contribute to shear stress resistance (Hahn and Labouesse 2001). They are important during development as well: in the elongating *C. elegans* embryo their phosphorylation is at the final step of a mechanotransduction pathway and it leads to HDs remodeling, needed for the proper completion of the *C. elegans* embryonic development (Zhang *et al.*, 2011).

In this section, I reviewed the general characteristics and structure of the epithelia. Epithelial cells by their own are already very smartly designed small entities, possessing a series of useful molecular features that help their cellular functions, enable self-organization and a dynamic crosstalk with their environment. These functions and crosstalk imply to a large extent mechanical forces that can already drive cell shape changes in a single cell. But if cells cope up at a higher level through tissue interplay, it can lead to morphological changes that are crucial in development and in various other biological processes. The upcoming section aims to summarize the mechanisms underlying cell shape changes and epithelial morphogenesis, with an outlook on mechanotransduction as it is a key mechanism in this PhD work.

II. Epithelia remodeling during morphogenesis

Tissue organization arises from cells showing a set of well-defined morphogenetic behaviors that include movement, shape change, differential growth, and apoptosis. Morphogenetic events extend from the organization of subcellular structures through migration of single cells to the coordinated activity of the thousands of cells that achieves the complex folding. Collective and coordinated epithelial cell shape changes have been reported in numerous biological processes. The classical examples are crucial developmental processes like gastrulation (studied extensively in Ascidians, *Drosophila*, zebrafish or *Xenopus*), primitive gut tube formation in *Xenopus* formation (Reed *et al.*, 2009) and several organogenetic aspects (neural tube formation, mammary gland, kidney or lung tubulogenesis) (Colas and Schoenwolf, 2001; Rogers *et al.*, 2003; Ewald *et al.*, 2008; Davidson, 2012). Recent research also explores new models, where not the entire organ, but some parts of it have an epithelial origin and therefore contribute to morphogenesis. Such systems are for instance teeth morphogenesis in zebrafish (Verstraeten *et al.*, 2010) or eye morphogenesis in mice (Chauhan *et al.*, 2015), but the impact of epithelial pouches and clefts that contribute to the patterning of the vertebrate face are also subjects of intense research (Choe and Crump, 2015).

At a tissue level, morphogenesis arises because of cellular proliferation and motility. Detailed analyses of morphogenetic events in a variety of animals suggests that most morphogenetic events are in fact driven by only few basic cellular mechanisms, used in different combinations and sequences. For example, cell proliferation is driven by cell division, giving rise to two daughter cells, while apoptosis results in the disappearance of the dying cell. Changes in cell position are brought about by either cell migration or cellular rearrangements, such as cell intercalations and neighbor exchanges. Tissue separation can also occur via more dramatic cellular differentiation events during which epithelial cells become mesenchymal. Mesenchymal cells typically leave the epithelial tissue because of changes in cell adhesive and contractile properties and migrate away from the epithelium to associate with other similar cells in a new location (Yu and Elble, 2016). Coordinated changes in position of individual cells can trigger tissue rotations, spatially controlled cell proliferation, cell division orientation and cell death within multicellular tissues can give rise to global changes in tissue shape (Heisenberg and Bellaiche 2013).

However there is another of central importance for tissue morphogenesis during development: shape changes. Cell shape is the product of a cell's material and active properties balanced by external forces. Control of cell shape, therefore, relies on both tight regulation of intracellular mechanics and the cell's physical interaction with its environment. Indeed, throughout the lifespan of an organism, shape changes are necessary for cells to carry out their essential functions. Nowhere is this more dramatic than embryonic development, when cell shape changes drive large-scale rearrangements in tissue architecture to establish the body plan of the organism. A longstanding question for both cell and developmental biologists has been how are forces generated to change cell shape?

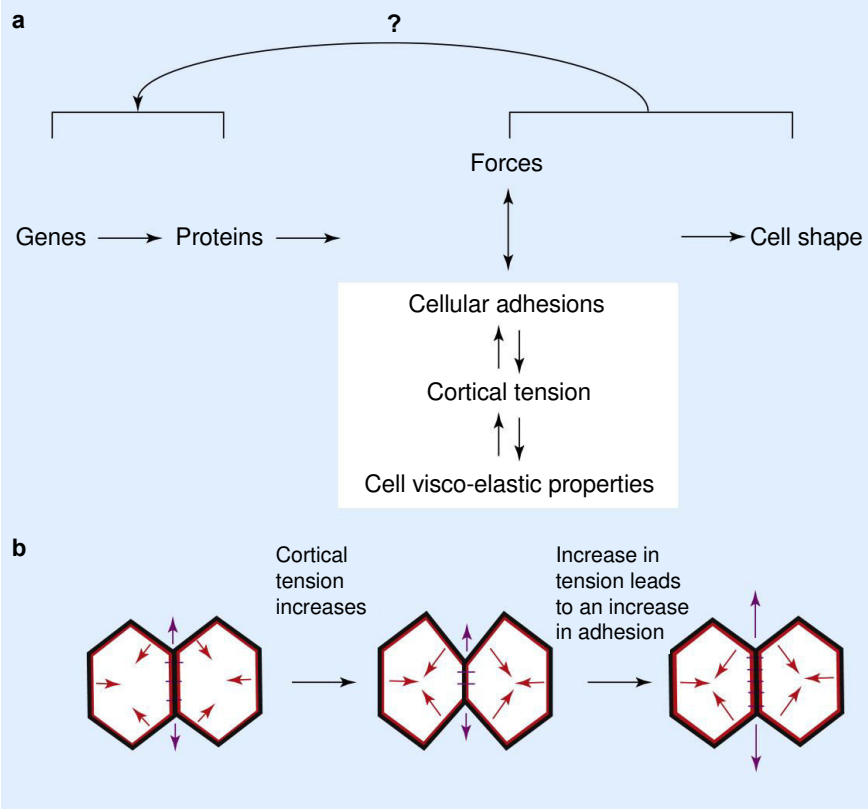

Figure 6: Regulation of cell shape.
(a) Cell shape is the result of the mechanical forces exerted on the cell surface. These forces can also be described by a set of interrelated physical properties, which include cellular adhesion, cortical tension and the cell's rheological properties. Physical properties are regulated at the protein level and are likely to feedback on protein activity and/or gene expression. **(b)** Example of the interaction between cortical tension and cellular adhesion during the formation of cell–cell contacts. Red lines, cortical cytoskeleton; black lines, plasma membrane; purple rods, adhesion sites; arrows, direction of forces.
Adapted from Paluch and Heisenberg, 2009.

Two principal factors contribute to cellular deformation and mechanical stresses that are experienced by cells and influence cell behavior in early development—the mechanical stiffness of the local tissue environment (extrinsic force) and the contractile activity of the cells pulling on that environment (intrinsic force). Extrinsic forces are applied on cells by the neighboring tissues or by other external factors, often by force transmission through the ECM (Engler *et al.*, 2006). But epithelial cells are also able to deform autonomously, by intrinsic force generation through actomyosin contractility, without any application of external stress (Murrell *et al.*, 2015). Cell deformation triggered by extrinsic forces is more like a passive response, while internal force generation can be considered as an active process. A proper balance between extrinsic and intrinsic forces is a key component of finely controlled cell shape changes and needs to be strictly regulated, both by cellular mechanical properties and by biochemical signaling (Paluch and Heisenberg, 2009). In development, understanding the interplay between cellular contractile activity, stiffness of surrounding tissues, and the resultant deformations and mechanical stresses is critical for refining model of embryogenesis (Fig. 6).

II.1. Contractility and intrinsic forces

Various internal forces also contribute to mechanical stresses during embryogenesis. These internal forces refer to contractile forces generated internally by the actomyosin cytoskeleton. There are several strategies to develop tissue dynamics. Such as cortical tension or basolateral protrusions, as reported in the case of gut organogenesis, notochord formation in ascidians, amphibians and fish, or dorsal intercalation in *C. elegans* embryos (Pilot and Lecuit 2005).

II.1.1. Apical constriction

In epithelial sheets, the mechanical coupling of cells via AJs allows individual cell behaviors to propagate change across the tissue, leading to tissue morphogenesis. A common epithelial cell shape change that participates in morphogenetic events throughout development is apical constriction (Sawyer *et al.*, 2009; Martin and Goldstein, 2014; An *et al.*, 2017). Apical constriction reduces the apical surface area of the epithelial cell, which contains AJs, and often expands at the basal end, transforming a columnar-shaped cell to a wedge or cone shape (Fig. 7). Due to the symmetrical constriction of actomyosin, the apical side of epithelial cells contracts resulting in cells taking on a wedged shape (Takeichi, 2014).

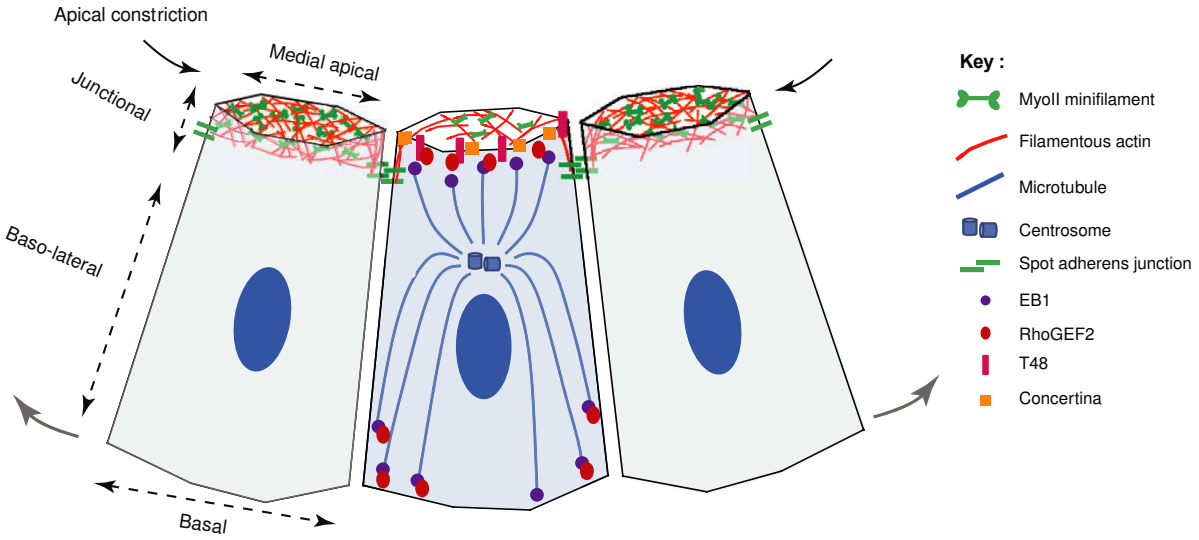

Figure 7: Steady state control of contractility during *Drosophila* epithelial morphogenesis.
Schematic of *Drosophila* mesoderm cells undergoing apical constriction and the pathway regulating RhoGEF2 delivery at the medial apical site of the cell.
Adapted from Levayer and Lecuit, 2012.

Gastrulation or neurulation for instance are spectacular examples of it. For example, mesoderm invagination during gastrulation in *Drosophila* is driven by the coordinated apical constriction of mesodermal cells. Myosin spots and fibers are formed at the apical cortex of invaginating mesodermal cells, which results in apical constriction. The myosin structures increase in intensity and move towards the center of cell apex, resulting in pulsatile centripetal actin-myosin flows. Actin-myosin network coupling to apical junctions leads to myosin organizing into a supra-cellular network that connects each cell to transmit forces across the tissue (Martin *et al.*, 2010; Bosveld *et al.*, 2012; Heisenberg and Bellaiche, 2013).

Apical constriction and Myo-II contraction in mesoderm cells are not continuous but occur as a series of constriction pulses that are often asynchronous in neighboring cells (Martin *et al.*, 2009). Individual cells undergo three to five pulses before invagination that exhibit a periodicity of about 90 seconds. Importantly, mesoderm cells maintain their contracted state between contraction pulses, which allows these cells to rapidly (5–10 min) reduce their apical area by 75% in an incremental manner (Mason and Martin, 2011). This stabilization of the contracted state between pulses occurs despite the fact that apical constriction generates levels of tension along the length of the furrow that are high enough to influence the directionality of the cell shape change (Martin *et al.*, 2010). Thus, it appears that apical constriction also occurs in a ratchet-like manner: pulses of actomyosin contraction drive apical area reduction and cell shape is stabilized between pulses to prevent apical relaxation (Fig. 8). (Mason and Martin, 2011).

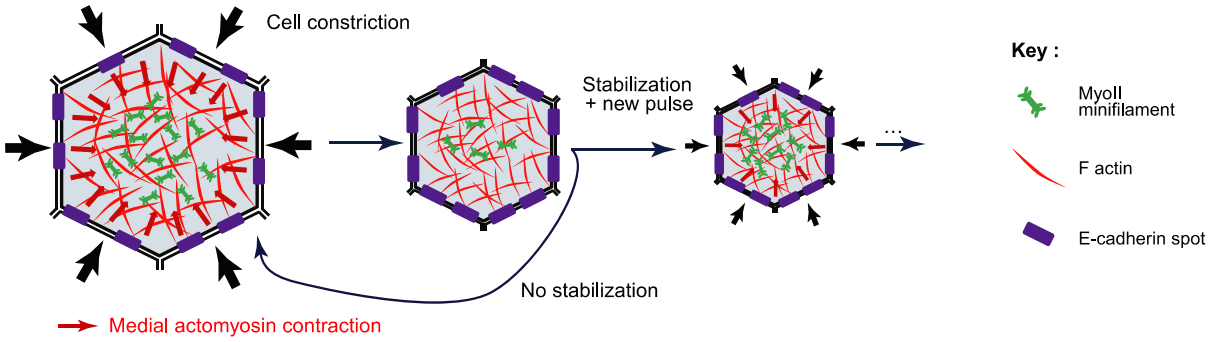

Figure 8: Ratchet mechanism and MyoII pulses during apical constriction of epithelial cells.
Top view of an epithelial cell undergoing apical constriction. The accumulation of MyoII pulls on actin filaments (centripetal red arrow) and constricts the cell apical surface (black arrows). Contraction is either stabilized (further MyoII pulses lead to an incremental decrease of cell surface) or unstabilized (the cell returns to its initial conformation).
Adapted from Levayer and Lecuit, 2012.

II.1.2. Cell migration

Cell migration is critical to the development of most animals, being responsible for the dispersal of cells from one place to others (eg cells originating in the neural crest that disperse to form melanocytes, some neural tissue and much of the face, or primordial germ cells that migrate to the developing gonads) and also being responsible for the extension of neural axons and dendrites to their targets. Cell migration is driven mainly by organization of a motile leading edge (lamellipodium) in one part of the cell, this leading edge being based on polymerization of F-actin filaments, mostly oriented with their growing (plus or barbed) ends facing the plasma membrane (Svitkina and Borisy, 1999; Pollard and Borisy, 2003; Ponti *et al.*, 2004; Koestler *et al.*, 2008). They are controlled by ARP2/3 complexes themselves regulated, via proteins such as WASP, by small GTPases such as Rac and cdc42. Contractile forces are generated by a Myo-II-containing network of longer oriented actin filaments behind the lamellipodium, called the lamella, and by actomyosin bundles called stress fibers (Verhovsky *et al.*, 1995; Svitkina *et al.*, 1997; Koestler *et al.*, 2008; Aratyn-Schaus *et al.*, 2011). The range of the periodic contractions of Myo-II can vary from about 25 seconds to several minutes (Giannone *et al.*, 2004; Giannone *et al.*, 2007; Vicente-Manzanares *et al.*, 2007; Meili *et al.*, 2010; Burnette *et al.*, 2011).

Cell motility is possible because actin filaments are semi-flexible polymers that, in conjunction with the molecular motor myosin, can act as biological active springs or "dashpots" able to exert or resist against force in a cellular environment (Blanchoin *et al.*, 2014). To modulate their

mechanical properties, actin filaments can organize into a variety of architectures generating a diversity of cellular organizations including branched or crosslinked networks in the lamellipodium, parallel bundles in filopodia, and antiparallel structures in contractile fibers. These different architectures can be envisioned as a series of interconnected active springs and dashpots that act as mechanical elements to drive cell shape changes and motility (Fig. 9) (Blanchoin *et al.*, 2014).

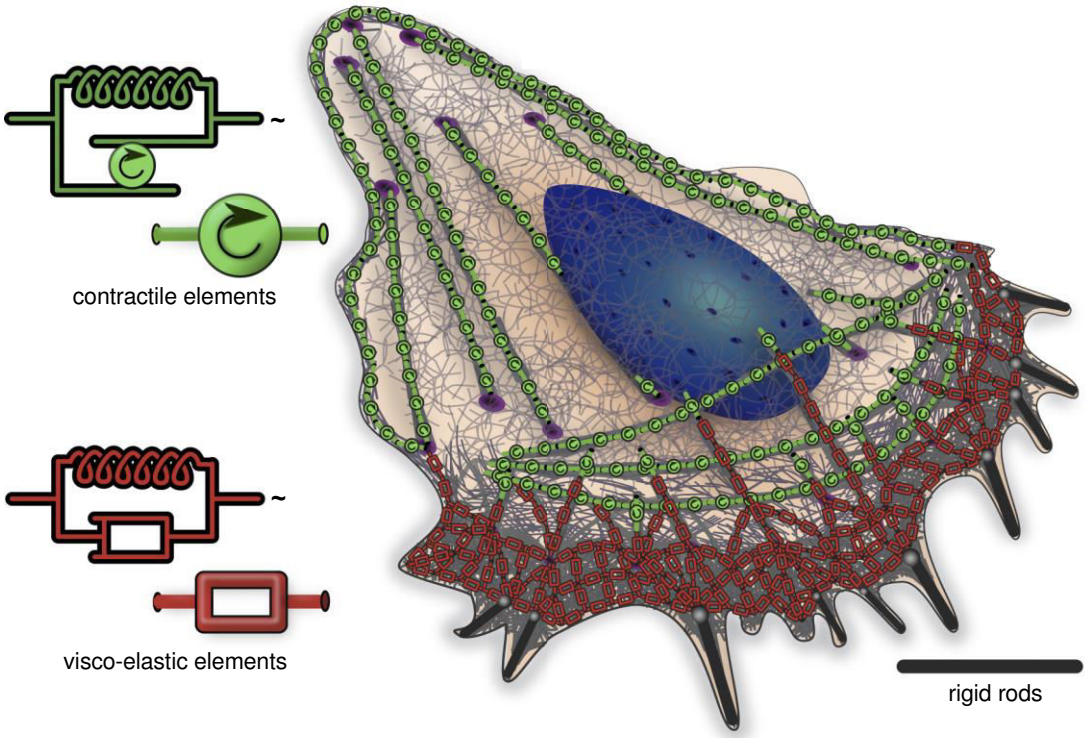

Figure 9: Schematic representation of mechanical elements driving cell shape changes.
Overlay of the actin architecture and its mechanical profile. The red rectangles are the shock absorbers (dashpots) that represent the actin network, while the green circles are active springs due to myosin motor activity.
Adapted from Blanchoin *et al.*, 2014.

Signal transduction cascades can regulate the activity of these proteins allowing cells to be guided by gradients of attractive or repulsive extracellular molecules, in a process called chemotaxis. The migration of cells can also be controlled by differences in substrate adhesion, generally choosing more adhesive surfaces when presented with a choice, for biophysical reasons (Lautscham *et al.*, 2014; Simsek *et al.*, 2019). Adhesion to substrates depends on the ECM molecules within the substrate and the repertoire of matrix receptors (for example, integrins) expressed by the cells themselves. Different cells express different combinations of integrins, and therefore can respond in a cell type-specific manner to the same ECM cues of a substrate. This coupling to the underlying substrate via adhesions allows the F-actin network to adapt and modulate cell shape. It is locally regulated and has been characterized as a molecular 'clutch' (Gardel *et al.* 2010; Stricker *et al.*, 2010).

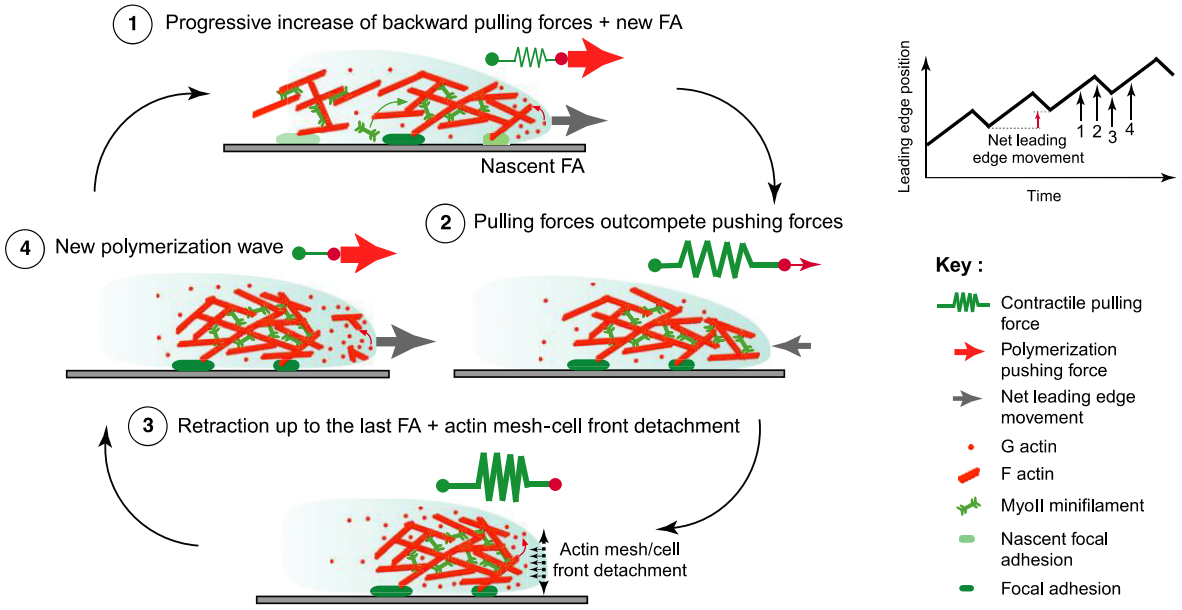

Figure 10: Oscillatory behavior of the cell leading edge and ratchet-like movement.
The leading edge alternates between phases of protrusion (3–4–1) and retraction (2–3). Phase 1: polymerization of actin generates the pushing force (red arrow) that drives leading-edge progression (grey arrow). At the same time, MyoII is progressively recruited in the mesh concomitantly with new focal adhesion point creation. Phase 2: backward-pulling forces, generated by MyoII and its anchorage to distal focal adhesions, progressively increase (green spring) while the actin polymerization rate decreases. Once the backward-pulling force overtakes the polymerization pushing force, the cell edge starts to retract (grey arrow). Phase 3: retraction is limited by focal adhesions (ratchet-like mechanism). Concomitantly, the high pulling-force breaks the actin mesh–cell-front connection. This could be reinforced by MyoII-induced actin depolymerization. Phase 4: actin mesh–cell-front detachment leaves space for a new wave of actin polymerization. The backward-pulling force is close to zero. (Bottom graph) Progression of the leading edge over time. Displacement is higher during protrusion phases compared to retraction phases, hence allowing net movement of the cell.
Adapted from Levayer and Lecuit, 2012.

Indeed, on one hand Myo-II contractile force causes the leading edge of the migrating cell to periodically retract, while on the other hand coupling of actin arcs with focal adhesions prevents further retraction by stopping the retrograde flow of actin arcs and functioning as the 'clutch' to anchor arcs relative to the substrate (Burnette *et al.*, 2011). The hypothesis is that leading edge advance acts in a cyclical and ratchet-like manner: membrane extension initiates new focal adhesions that engage actin arcs and establish a new base for membrane protrusion (Fig. 10). A proper balance between contractility and cell-substrate adhesion is required for optimal cell migration. Indeed, cells require traction to move, but too much adhesion results in drag forces that resist actomyosin contraction (Gupton and Waterman-Storer, 2006, Mason and Martin, 2011).

II.1.3. Convergent extension

Convergent extension is a mechanism that allows a structure to become long and thin without any net increase in cell volume or number. This process plays a crucial role in shaping the body plan during embryogenesis and occurs during gastrulation, neurulation, axis elongation, and organogenesis in both vertebrate and invertebrate embryos (Keller *et al.*, 1985; Shih and Keller, 1992; Topczewski *et al.*, 2001; Keys *et al.*, 2002; Munro and Odell, 2002; Williams *et al.*, 2014; Shindo, 2018). *Xenopus* gastrulation serves as an excellent example of the role of convergent extension in embryogenesis. The driving force of convergent extension is the morphogenic activity of the presumptive dorsal mesodermal cells (Keller *et al.*, 2008). If the convergent extension is interrupted or incomplete, the resulting organism will have a short anteroposterior axis, wide notochord, and broad, open neural tube (Wallingford *et al.*, 2002).

In *Drosophila*, after the initial infolding of gastrulation, the ventral region of the embryo undergoes a rapid elongation called germband extension. This elongation is produced by intercalation of the more lateral cells as they move toward the ventral midline (Fig. 11). The cells achieve convergent extension movements by treating their boundaries differently. Boundaries that lie within the plane of the epithelium but perpendicular to the axis of elongation shorten, under the action of acto-myosin contraction. In many respects, the process is very similar to the convergent extension, which occurs during amphibian gastrulation (Wieschaus *et al.*, 1991; Irvine and Wieschaus, 1994; da Silva and Vincent, 2007; Collinet *et al.*, 2017; Kong *et al.*, 2017; Siang *et al.*, 2018).

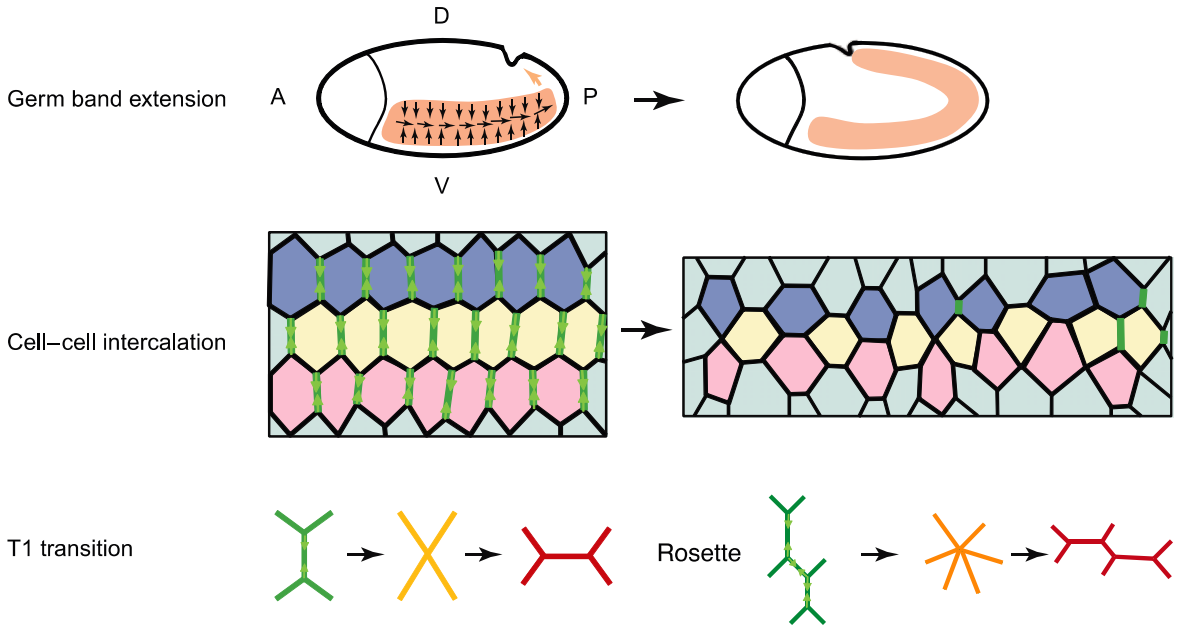

Figure 11: *Drosophila* germ band extension.
(Top) Schematic view of an early *Drosophila* embryo during germ band extension. The germ band (orange) elongates by convergent extension (black arrows). A, anterior; P, posterior; D, dorsal; V, ventral. (Middle) Convergent extension is induced by cell–cell intercalation along the dorso-ventral (D/V) axis. Blue labeled cells will form new contacts with pink labeled cells, whereas the number of junctions shared by yellow cells will be reduced. Green lines symbolize the polarized enrichment of MyoII and the resulting high contractility. (Bottom) Cell–cell intercalation is driven by polarized junction remodeling, including T1 transitions (left) and rosette formation (right). D/V junctions (green) shrink, give rise to four-way vertices (yellow) and resolve irreversibly into a new AP junction (red). Rosette formation is induced by the shrinkage of multiple DV junctions.
Adapted from Levayer and Lecuit, 2012.

Although anisotropic tension itself could explain cell rearrangements observed during germband extension (Rauzi *et al.*, 2008), live imaging of Myo-II revealed that pulsatile contractions are also present in the medial network spanning the apical surface (Rauzi *et al.*, 2010; Fernandez-Gonzalez and Zallen, 2011; Sawyer *et al.*, 2011). The shrinkage of dorsal-ventral-oriented junctions during germband extension is known to require planar polarized junctional contractility by Myosin II (Bertet *et al.*, 2004; Blankenship *et al.*, 2006; Rauzi *et al.*, 2008; Fernandez-Gonzales *et al.*, 2009). However, junctional Myosin II itself does not produce this shrinkage, but the polarized flow of medial actomyosin pulses towards vertical junctions does. Therefore, the proposed mechanism is the following: the Myo-II cable along interfaces serves as the 'catch' in a ratchet-like mechanism that incrementally shrinks interfaces of a given orientation, resulting in cell rearrangements (Fig. 12). Importantly, tension promotes the formation of multicellular Myo-II cables during rosette formation, suggesting that mechanical feedback regulates this activity to coordinate cellular behavior and generate tissue-level forces (Fernandez-Gonzalez *et al.*, 2009, Mason and Martin, 2011).

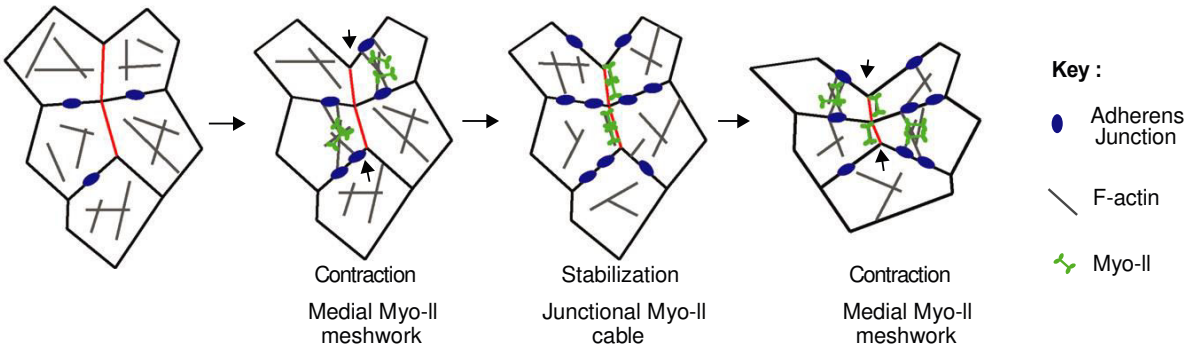

Figure 12: Cell–cell intercalation and junction remodeling induced by polarized MyoII flow and stabilization of junction shrinkage.
Ratchet model for cell interaction. Actomyosin contractions on the medial apical surface reduce apical area and shrink vertical interfaces (red edges). Flow of Myo-II into the vertical junctions increases Myo-II intensity in the junctional cable. This stabilizes the interface by preventing it from lengthening. The process repeats to incrementally bring cells closer along the dorsal–ventral axis.
Adapted from Mason and Martin, 2011.

The conservation of the ratchet-like behavior observed during cell migration, constriction and intercalation establishes the importance of this molecular machine. However, many questions still remain about this mechanism. While it is clear that dynamic and stable actomyosin networks are important for inducing and sustaining cell shape change, the connections between these distinct types of networks is still unclear.

II.2. Extrinsic forces – Mechanotransduction

As living organisms, we interact with our world through our senses. We are continuously exposed to mechanical cues and so are our cells. They can sense their physical environment by translating mechanical forces and deformations into biochemical signals such as changes in intracellular calcium concentration or activation of diverse signaling pathways. In turn, these signals can adjust cellular and extracellular structures. This process is called mechanotransduction and it is responsible for several senses and physiological processes in the body, including proprioception, touch, balance, and hearing. It is a multistep process that includes (1) mechano-coupling (transduction of mechanical forces into signals sensed by sensor cells), (2) biochemical coupling (conversion of mechanical signal into a biochemical signal to elicit a cellular response such as gene activation), (3) transfer of a signal from sensor to effector cells, and (4) the effector cell response. Mechanosensitivity in one form or another appears to be a property shared by all cells of the body and by all phyla from mammals to bacteria.

II.2.1. Matrix control of stem cell fate

Mechanotransduction has been found to occur in all corners of the biological realm and with an extremely rich and diverse set of mechanisms (Jansen *et al.*, 2015). Some of these mechanisms are very similar across all domains of life, as in the case of the mechanosensitive channels that allow physical stimuli on or across membranes to control the flow of molecules across these membranes: flow that can in turn release osmotic pressure or trigger another signaling pathway (Kloda and Martinac, 2001; Martinac, 2008). Some are more specific to a given subset of cells, like the response of mammalian cells' cytoskeletons.

Mechanotransduction is intimately associated to cell adhesion processes targeting primarily cell-matrix and cell-cell contacts. The traction forces developed and transmitted via integrins by cells toward the extracellular matrix and substratum have high incidence on cell shape, migration and differentiation. A very well-studied example is the variable differentiation of mesenchymal stem cells (MSCs). Young MSCs differentiate in response to the stiffness of the underlying matrix. Softer matrices lead to the differentiation of MSC's into neuronal cells, i.e. brain, and are neurogenic, stiffer matrices that mimic muscles lead the MSC's to differentiate into muscles and are therefore myogenic, whereas rigid matrices that mimic bones differentiate the MSC's into osteocytes and are eventually osteogenic. (Flanagan *et al.*, 2002; Neuhuber *et al.*, 2004; Garcia and Reyes, 2005; Engler *et al.*, 2006) (Fig. 13).

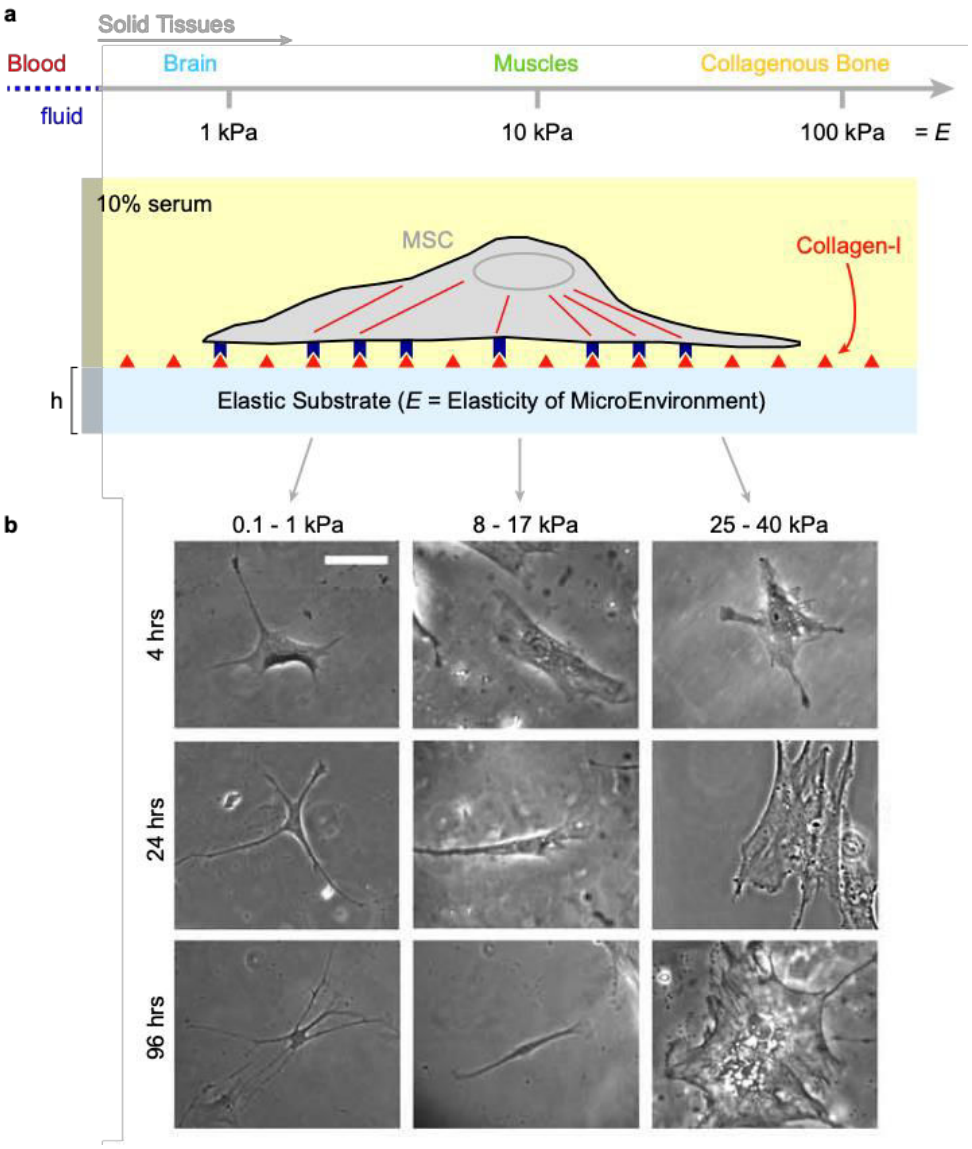

Figure 13: Tissue elasticity and differentiation of naive MSCs.
(a) Solid tissues exhibit a range of stiffness, as measured by the elastic modulus, E**. (b)** The *in vitro* gel system allows for control of E through crosslinking, control of cell adhesion by covalent attachment of collagen-I, and control of thickness, h. Naive MSCs of a standard expression phenotype are initially small and round but develop increasingly branched, spindle, or polygonal shapes when grown on matrices respectively in the range typical of E_{brain} (0.1–1 kPa), E_{muscle} (8–17 kPa), or stiff crosslinked-collagen matrices (25–40 kPa). Scale bar, 20mm.
Adapted from Engler *et al.*, 2006.

Other work also showed that decreasing substrate stiffness appears to dramatically alter cell structure in many cell types, reducing cell spreading against the substrate, the formation of focal adhesions, and stress fibers (Pelham and Wang, 1997). Indeed, cytoskeletal filaments can propagate stresses over long distances (Ingber, 2005; Wang and Suo, 2005), while structures such as focal adhesions, desmosomes and junctions provide both tensile strength and effective transmission of stress.

II.2.2. Role of cytoskeleton in mechanotransduction

The role of the mammalian cell cytoskeleton in responding to physical cues such as the rigidity of its environment is one of the most studied examples of mechanotransduction (Johnson *et al.*, 2007). Thanks to their cytoskeleton, mammalian cells can easily exert forces in the nanoNewton range on their surroundings and sense the mechanics of cells or substrates around them (du Roure *et al.*, 2005). For mammalian cells, physical forces play a direct role in important biological choices such as stem cell differentiation, motility or tumor formation (Weaver *et al.*, 1997; Engler *et al.*, 2006; Vogel and Sheetz, 2009, Paluch *et al.*, 2015).

Cytoskeletal filaments are proposed as a means to focus force upon molecules that can transmit mechanotransduction (Chen, 2008). The way mechanical stimuli are transmitted into the cell depends on the coordinated activity of mechanosensors, influenced by resting tension levels within the cell, which are set by the cytoskeletal system (Chen *et al.*, 2003; Polte *et al.*, 2004, Ingber, 2006). The adaptive cytoskeleton deforms through assembly and disassemby of its filaments in response to an applied force. ABPs also help to dynamically organize F-actin into many different structural forms such as lamellipodia, stress fibers, filopodia, podosomes, actin asters, vortices, and stars (Fritzche *et al.*, 2017; Wang, 2017; Harris *et al.*, 2018). These different architectures serve specialized roles in the cell's multiplex response to mechanical stimulation.

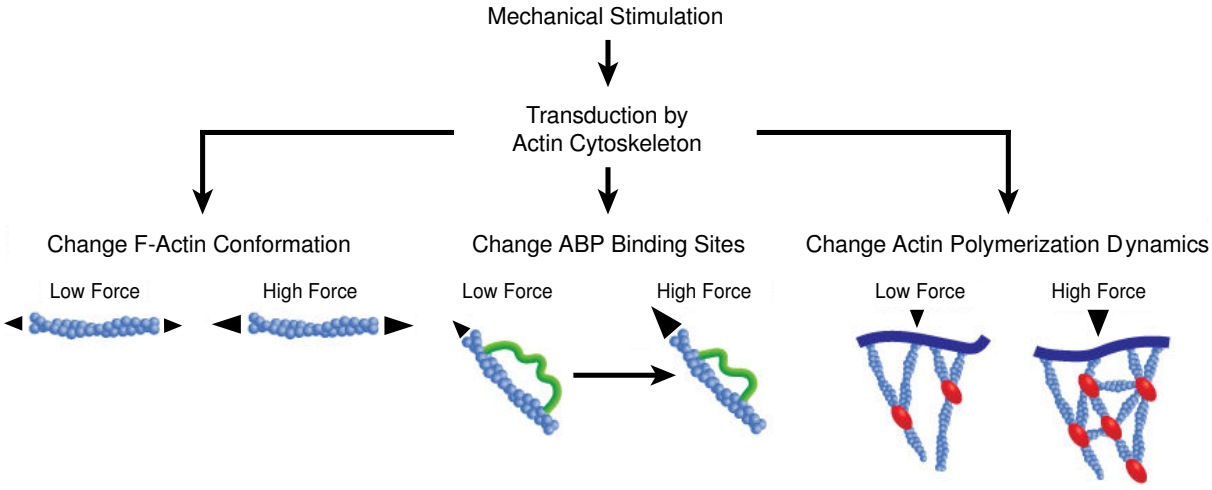

Figure 14: Actin cytoskeleton and transduction of mechanical forces.
Mechanical loads induce a: 1. Conformational change in F-actin (left schematic); 2. Conformational change in ABPs that uncovers previously concealed binding sites (middle schematic); and 3. Alterations in ABP-mediated actin polymerization dynamics (right schematic).
Adapted from Cytoskeleton Newsletter, News from Cytoskeleton inc., 2018.

FRET, AFM microscopy and optical traps experiments revealed that actin filaments in the various actin-based structures bear a mechanical load (per filament) (Wang and Kanchanawong, 2016; Wang, 2017). These different actin structures are associated with specific mechanical loading that are optimized for the structure's specialized cellular functions. Mechanical loading (increased tension) of filaments alters their conformation (Shimozawa and Ishiwata, 2009), and how ABPs bind and affect filaments (Harris *et al.*, 2018) (Fig. 14).

In the case of cofilin, a F-actin severing protein, changes in filament length affect its binding and function. Tensile forces that stretch a cell correspondingly increase the length of filaments parallel to the direction of the stretch. Under these conditions, the binding affinity of cofilin is reduced and that of myosin II is increased (Hayakawa *et al.*, 2011; Uyeda et al, 2011; Hayakawa *et al.*, 2014). This mechanical-induced change in F-actin length and binding partners results in stabilized F-actin which can more easily form stress fibers, an essential part of a cell's mechanotransduction processes (McGough *et al.*, 1997; Hayakawa *et al.*, 2011; Uyeda et al, 2011; Hayakawa *et al.*, 2014; Ohashi *et al.*, 2017) (Fig. 14). Tension-induced changes in actin structural dynamics also affect the binding of actin-nucleating proteins such as Arp2/320 (Risca *et al.*, 2012). Mechanically induced changes in actin-based structures can also affect gene expression in at least some cell types. As more stress fibers form during mechanical stimulation, the transcriptional coactivator YAP translocates to the nucleus where it is activated. YAP is integral in Hippo signaling and mediates increased expression of genes involved in cell proliferation and differentiation. Thus, the response of the actin cytoskeleton to extracellular mechanical forces can result in processes that have both physiological and pathophysiological relevance (Dupont *et al.*, 2011; Halder *et al.*, 2012; Ohashi *et al.*, 2017).

II.2.3. Protein unfolding under force: *in vitro* example, spectrin

Similar to F-actin, ABPs and other actin-associated proteins directly respond to mechanical stresses. Common responses include conformational changes, which expose previously concealed protein binding sites. Indeed, in many contexts, mechanosensory molecules have a broad set of structural regions or motifs that can be altered over a range of mechanical forces (Weaver *et al.*, 1997; Maritnac *et al.*, 2008; Vogel and Sheetz, 2009). Such proteins link the integrins or IFs of the structure to cytoskeleton. These proteins consist of tandem-repeat sequences such as spectrin-family members (α-actinin, dystrophin), talin, titin, fibronectin and cadherins. Forces can either unravel a domain or hinder the movement of a specific domain, both resulting in change of the ligand binding topology (Rohs *et al.*, 1999; Adhikari *et al.*, 2018).

How proteins sense forces and cellular geometry to create the correct morphology is not understood in detail but protein unfolding appears to be a major component in force and displacement sensing. Thus, the crystallographic structure of a protein domain provides only a starting point to then analyze what will be the effects of physiological forces through domain unfolding or catch-bond formation (Yan *et al.*, 1993; Anthis *et al.*, 2009; Elliott *et al.*, 2010; Yogesha.*et al.*, 2012).

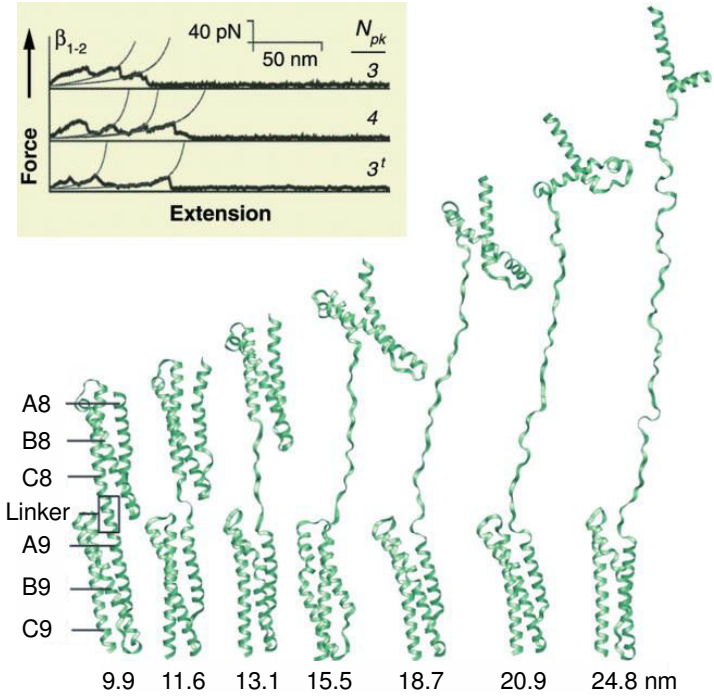

Figure 15: Linker-mediated elasticity of spectrin.
Mechanical unfolding of a double-repeat b spectrin from human erythrocytes (adapted from Paramore and Voth, 2006). Each spectrin repeat (labeled 8 and 9) is made of three α-helices denoted as A, B, and C. The unfolding sequence shows how the linker region unfolds first. (Inset) Force extension curves for a β-beta spectrin repeat construct (adapted from Law *et al.*, 2003). The bottom trace shows cooperative unfolding. Mutations weakening the linker region of spectrin have been shown to cause hereditary spherocytosis (Johnson *et al.*, 2007).
Adapted from Sotomayor and Schulten, 2007.

A well-known example is the spectrin. The erythrocytes are able to rapidly adapt to wide arteries and narrow capillaries thanks to their discoidal shape and mechanical properties. Diseases, such as hereditary spherocytosis and elliptocytosis, causing hemolytic anemia are associated with a lack of an elastic, adaptable shape are caused by mutations affecting the red blood cell cytoskeletal network made of spectrin, ankyrin, and associated proteins (Bennett and Baines, 2001; Discher and

Carl, 2001; Johnson *et al.*, 2007). Crystal structures of spectrin revealed building blocks made of three-helix bundles repeated in series and forming part of heterotetrameric assemblies arranged in elongated filaments (Bennett and Baines, 2001; Kusunoki *et al.*, 2004). The structures also revealed an α-helical linker. Moreover, AFM experiments suggested that spectrin repeats mechanically unfold predominantly one by one in an independent, all-or-none fashion (Rief *et al.*, 1999) (Fig. 15). Force peaks were found to be substantially smaller than those observed for other proteins made of β strands instead of α helices.

Further AFM experiments confirmed the relative weakness of spectrin and the one-by-one unfolding pathway but also revealed that different sets of spectrin repeats may exhibit intermediates and cooperative unfolding events involving more than one repeat (Altmann *et al.*, 2002; Law *et al.*, 2003; Randles *et al.* 2007) (Fig. 14, inset). In addition, recent work identified mutations at the linker regions of spectrin causing disease, thereby corroborating the relevance of linkers in the mechanical response of this protein as indicated by simulations (Johnson *et al.*, 2007).

Single-molecule force experiments *in vitro* enable the characterization of the mechanical response of biological matter at the nanometer scale but they do not reveal the molecular mechanisms underlying mechanical function. *in silico* experiments, despite their limitations, have resolved the molecular mechanisms underlying the elastic response of biomolecules. However, as force sensing and generation at the tissue and cellular scale is central to many biological events, there is a growing interest in modern cell biology for methods enabling force measurements *in vivo.* Fortunately, the development of new single molecule and super-resolution imaging methods enable the analysis of single molecule mechanics in physiologically relevant conditions (Jun *et al.*, 2014; Backholm *et al.*, 2019).

II.2.4. Protein unfolding under force: *in vivo* example, talin

In the few cases where single molecule mechanics are studied under physiological conditions such, as titin and talin, there are rapid cycles of stretch-relaxation that produce mechanosensing signals. Talin is one of the best-studied FA adaptor proteins. In addition to FAs, talin has been reported in podosomes, invasive structures, immunological synapses, cytotoxic synapses and so forth (Nolz *et al.*, 2007; Ham *et al.*, 2013). In FAs, talin is under tension and work as direct bridges between actin and integrin and as recruiters for other FA proteins (Kumar *et al.*, 2016). It is composed of an N-terminal globular head, a flexible rod domain and C-terminal helices (Martino *et al.*, 2018) (Fig. 16a).

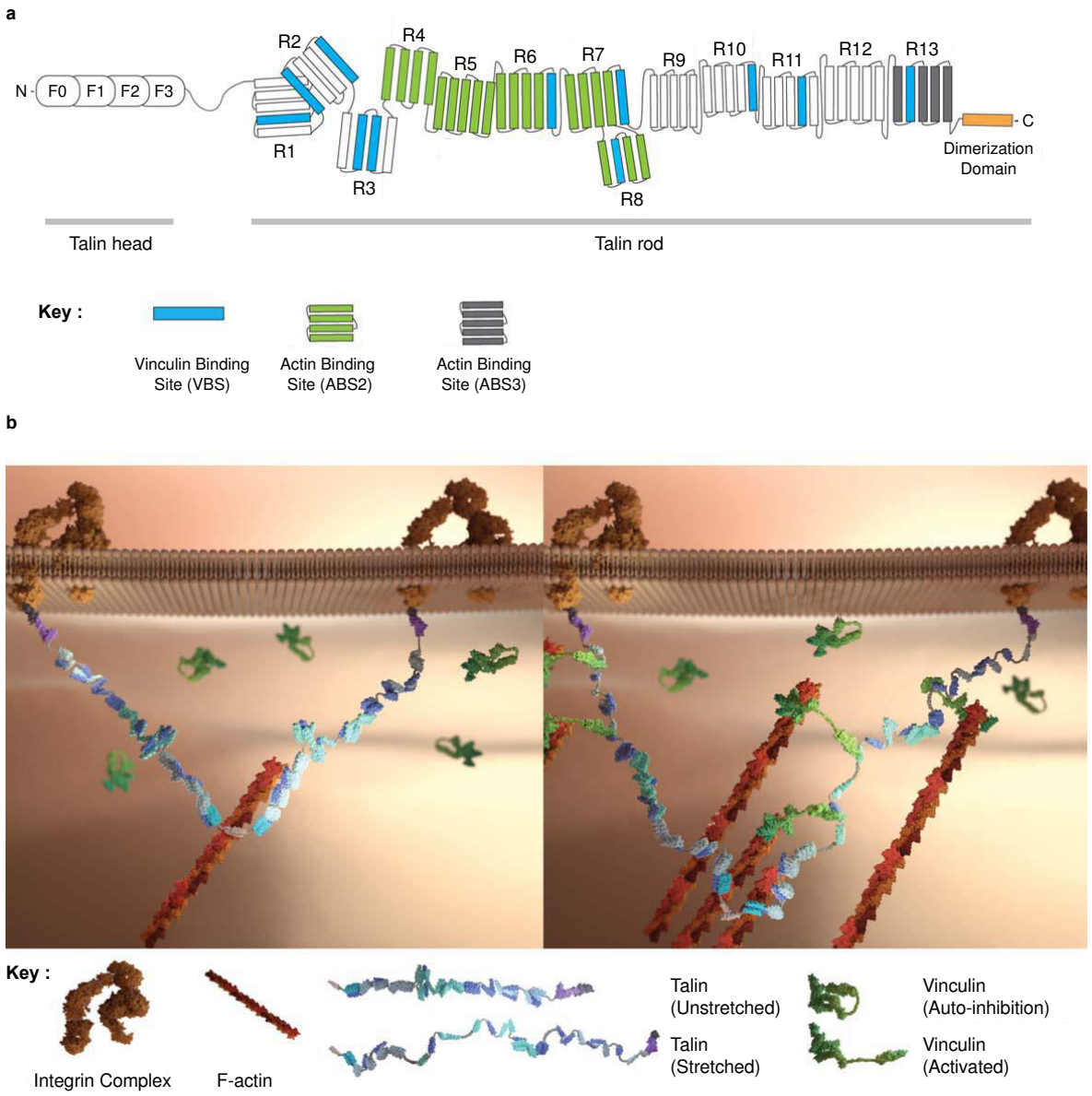

Figure 16: Talin-vinculin mechanosensitivity.
(a) Illustration of the domain structure of full-length talin. The talin head domain contains a FERM domain, followed by a flexible "neck" which connects the head domain to its C-terminal rod domain. The rod domain contains 11 cryptic VBS (drawn in blue). The dimerization domain is a single helix that sits at the end of the rod. **(b)** Schematics of the talin structure and interaction of the talin dimer with vinculin in cells. (left) In the initial stage of FA formation, the talin dimer binds to actin and integrin. At this stage, the cryptic VBSs remain buried among the α-helical bundles. (right) As the actin filament starts to pull on talin, the formerly buried VBS are revealed to allow vinculin binding and cause more actin filament recruitment.
Adapted from Hu *et al.*, 2017.

Talin rod contains an additional binding site for integrin, and two sites for actin, as well as several binding sites for vinculin, its main partner at the FA site (Gingras *et al.*, 2005; Gingras *et al.*, 2009). When forces are applied to talin, it unfolds to expose cryptic hydrophobic binding sites to host vinculin head (del Rio *et al.*, 2009; Hirata *et al.*, 2014; Maki *et al.*, 2017; Rahikainen *et al.*, 2017). Talin

has been shown to displays stepwise unfolding dynamics due to the characteristic transition kinetics of its mechanosensitive rod subdomains. In the absence of force, talin rod remains fully structured, and no vinculin binding sites (VBS) are available. Under low-force regimes, only the weakest bundle unfolds revealing its VBS. This activates one vinculin molecule, releasing it from its autoinhibited state. As the force applied to talin increases, more bundles are unfolded, revealing more VBSs and thus activating an increasing number of vinculin molecules (Haining *et al.*, 2016). Moreover, FRET experiments have shown the increase of tension on talin by vinculin depends mainly on actin-binding site 2 (ABS2) within the middle of the rod domain, rather than ABS3 at the far C terminus (Kumar *et al.*, 2016). This process is called talin-vinculin mechanosensitivity (Fig. 16b). The successful binding of vinculin to talin is considered essential to stabilize talin-F-actin interaction and thus transfer the mechanical signal inward (Humphries *et al.*, 2007).

II.2.5. The plasma membrane as a tension sensor

The physical tension of the plasma membrane can also play a role as an orchestrator of many cellular events. By forming a physical boundary between cells and their environment that is also a biochemical platform, the plasma membrane is a key interface mediating both cellular response to mechanical stimuli, and subsequent biochemical responses. Its physical state and integrity are crucial for cell survival, and one of its major functions is to preserve its integrity and enable changes in cell shape. These changes occur in response not only to cell processes such as division, migration or spreading, but also to the constant external mechanical forces present in physiological scenarios. In this context, the membrane constitutes a crucial interface, since mechanical forces will result in a change of its state. Accordingly, extensive work has addressed how membrane tension interplays with the actin cytoskeleton to regulate cell shape (Chugh *et al.*, 2017; Pontes *et al.*, 2017; Simon *et al.*, 2018), motility (Gauthier *et al.*, 2011; Lieber *et al.*, 2013; Lieber *et al.*, 2015; Hetmanski *et al.*, 2018) and polarity (Houk *et al.*, 2012; Tsujita *et al.*, 2015), as well as the feedback between membrane mechanical properties, cytoskeleton organization and cell dynamics (Keren, 2011; Gauthier *et al.*, 2012; Diz-Muñoz *et al.*, 2013; Calrk *et al.*, 2014; Sens and Plastino, 2015; Pontes *et al.*, 2017; Diz- Muñoz *et al.*, 2018; Saha *et al.*, 2018).

For example, fibroblasts employ membrane tension as a global master regulator of overall shape by ‘sensing’ tension changes and adjusting the actomyosin cytoskeleton and membrane trafficking accordingly (Parton and Simons, 2007; Gauthier *et al.*, 2011; Hamada *et al.*, 2011; Simon *et al.*, 2018) (Fig. 17). Considering a cell contacting a new substrate, first, the rounded up cell shows

weak cell–substrate attachment but higher membrane tension than interphase cell (Fig. 17a). Then the cell goes through a rapid and non-contractile phase of spreading. In this phase, membrane tension is at a high but constant level compared with the interphase cell (Fig. 17b). Once the membrane reservoirs of the cell are totally unfolded, it give rise to an increase in membrane tension due to area limitation. This is followed almost immediately by activation of exocytosis and myosin II-mediated contraction. The cell enters the contractile spreading phase (Fig 17c). As the cell spread, the leading edge becomes more heterogeneous with alternating protrusive and retractile regions along the boundary. Activation of contraction enables stable adhesions to mature and global remodeling of the cytoskeleton with formation of actin bundles. The cell starts to exert strong forces onto the substrate at this point. As a consequence of exocytosis and further spreading, the membrane area progressively increases whereas membrane tension progressively decreases (Fig. 17d). When the cell is fully spread, alternating protrusive and retractile activities reduce drastically. Meanwhile actin bundles have matured into strong and clearly identifiable stress fibers linking focal adhesions. Endocytosis and exocytosis balance maintains a constant membrane area. The membrane tension is now at its low resting level (Fig. 17e). Finally, the cell polarizes. Lamellipodia protrude on one side of the cell, whereas the other side of the cell shrinks. Due to protrusion, membrane tension increases and the higher tension seems to help to maintain polarity (Fig. 17f).

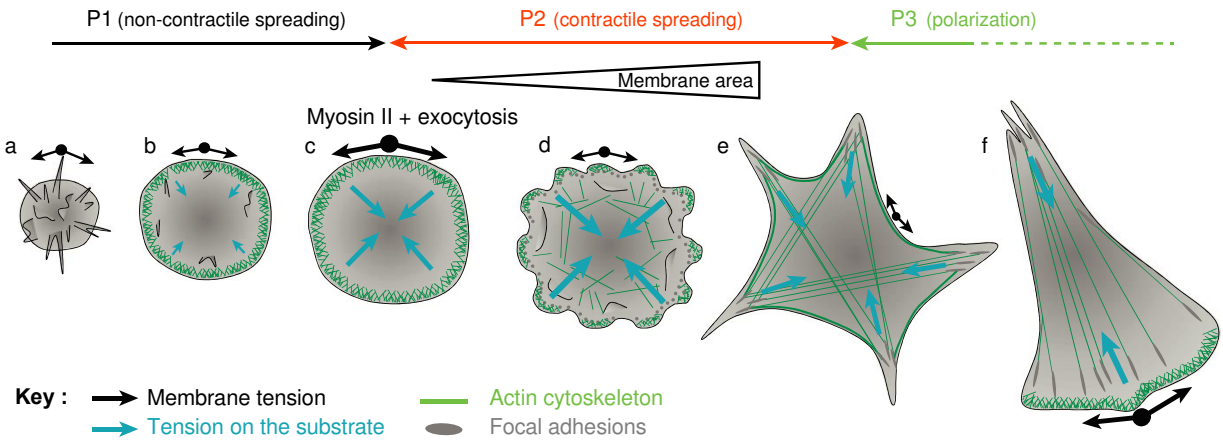

Figure 17: Model of cell spreading and polarization.
When encountering a new substrate, the cell will go from round shape with weak cell–substrate attachment to a polarized shape in several steps. It will increase tension on the substrate, as it membrane sense and adapt to the substrate, while cytoskeleton remodel.
Adapted from Gauthier *et al.*, 2012.

II.2.6. Importance of stiffness during morphogenesis

Mechanotransduction has been extensively studied in cells and tissues in culture but it has also become increasingly clear that mechanosensation and transduction play important roles in many developmental and disease-related processes, such as embryo morphogenesis and cell spreading during metastasis (Jaalouk and Lammerding, 2009; Chanet and Martin, 2014).

In vivo there is also evidence that stiffness is important during embryogenesis. For example, during *Xenopus laevis* gastrulation, convergence and extension movements can only occur if the mesoderm and notochord remain stiff enough to resist buckling (Adams *et al.*, 1990; Keller and Jansa, 1992). In addition, during this same process, the involuting marginal zone actively stiffens so that this tissue does not collapse or deform during gastrulation (Moore *et al.*, 1995). Tissue stiffness may arise from several different factors such as the stiffness of the cells, usually regulated by the cytoskeleton (Pasternak *et al.*, 1989), the strength of cell-ECM or cell-cell contacts, the biochemical identity of ECM proteins, and ECM organization and maturation. It is proposed that during convergence and extension movements in *X. laevis*, stiffness arises primarily from changes in the cytoskeleton and the ECM (Moore *et al.*, 1995). Considering the dramatic changes in cell-cell and cell-matrix adhesion occurring during this complex rearrangement of cells, it is likely that changes in adhesion also contribute to tissue stiffness.

However, because experiments targeting either cytoskeleton, cell adhesions, or ECM often affect all three, it has been difficult to develop an appropriate *in vivo* model for how these numerous factors independently contribute to a tissue's stiffness. Similarly, because of the technical challenges of accurately measuring mechanical parameters *in vivo*, only a few studies have directly measured embryo stiffness (Vuong-Brender *et al.*, 2017). Nevertheless, laser ablations are a good technique to give insight into the forces required for embryogenesis (Priess and Hirsh, 1986; Hardin, 1988; Williams-Masson *et al.*, 1997; Kiehart et al, 2000; Hutson et al, 2003; Davidson and Keller, 2007; Peralta et al, 2007). In *C. elegans* and *Drosophila melanogaster*, it helped reporting changes in global movements that are too fast to be explained by signal transduction cascades, suggesting such movements are mechanical in nature (Hardin, 1988; Suppato *et al.*, 2005; Peralta et al, 2007).

For example, recent work from our lab showed that myosin-II-dependent force anisotropy within the lateral epidermis of *C. elegans* embryos, and stiffness anisotropy within the fiber-reinforced dorso-ventral (D/V) epidermis are critical in driving their elongation. By measuring the opening shape of the epidermal actin cortex after laser nano-ablation, we assessed the spatiotemporal changes of actomyosin-dependent force and stiffness along the antero-posterior and D/V axis. We proved that the actomyosin cortex preferentially squeezes the embryo circumferentially, and that the stress anisotropy is tightly linked to the geometry of the embryo (Vuong-Brender *et al.*, 2017). This work showed that tissue elongation relies on two fundamental physical quantities (mechanical stress and tissue stiffness), and provided the most advanced mesoscopic understanding to date of the mechanics at work during the first steps of *C. elegans* embryonic elongation (Fig. 18).

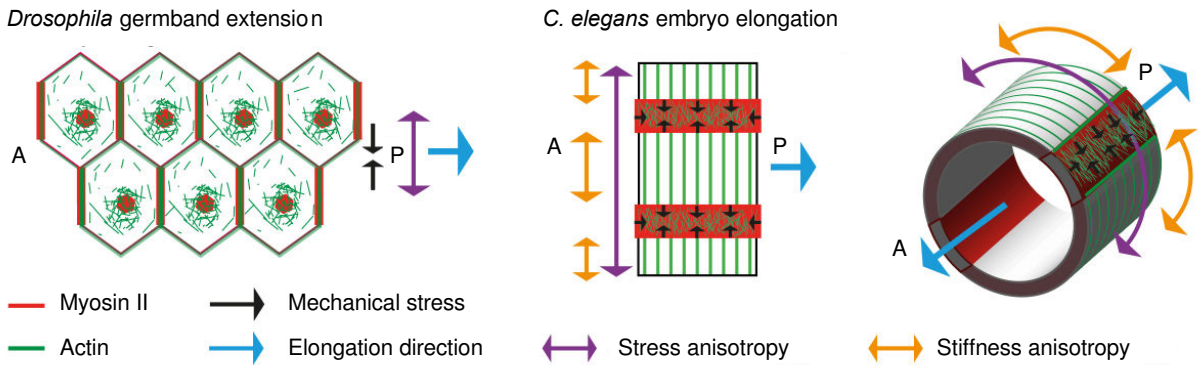

Figure 18: Actin filament organization correlation with stress and stiffness anisotropy pattern.
(Left) The anisotropy of mechanical stress generated by the polarized actomyosin network and medial myosin pulses promote *Drosophila* germband extension. (Right) The interplay of stress anisotropy (generated in seam cells - red) and stiffness anisotropy (DV cells – white) promote *C. elegans* embryo elongation. Note that, although myosin II does not display a polarized distribution within individual *C. elegans* epidermal cells as it does in *Drosophila* germband epithelial cells, its enrichment in seam cells along the circumference is reminiscent of the localized myosin II enrichment at vertical junctions in *Drosophila*. A, anterior; P, posterior. Adapted from Vuong-Brender *et al.*, 2017.

Epithelial tissues define the boundary that separates our bodies from of our world. They protect us from microbial pathogens and secrete proteins that help to digest our food and feed our young. Epithelia absorb nutrients from what we consume and excrete waste to detoxify our bloodstream. Therefore, epithelial cells are one of the most important cell types in organ and body. The reshape and rearrangement of epithelial cells at the cell-scale and the tissue-scale drive the process of morphogenesis. Cellular components such as the cytoskeleton and the adhesion complex can trigger and regulate the morphogenetic process by generating intercellular forces and transmitting them among cells. Actomyosin contractions at tissue-scale morphogenetic processes are complex, characterized by pulses and flows. Certainly, if a contractile system would only pulse back and forth, no developmental progress could be achieved. To progress in development cell shape also needs to be maintained between consecutive contractile cycles. Such questions around cell shape maintenance allowed the discovery of morphogenetic ratchet mechanisms that are interesting new research perspectives in developmental biology and biophysics. Moreover, it is now well established that mechanical cues—either extrinsic from the cell environment or intrinsic from cellular structures—can also be control cell and tissue migration, proliferation, differentiation, homeostasis and by extend play important roles in many developmental processes, such as embryo morphogenesis. Overall, understanding how mechanical forces remodel epithelia, as well as how they contribute to large-scale tissue shape change are essential to understand embryonic morphogenesis in development.

To tackle such questions during my PhD, I focused on a specific step of *C. elegans* morphogenesis, its embryonic elongation. But before describing the details of this process, I will first introduce *C. elegans* as a model system in biology.

III. Introduction to our model: the nematode *Caenorhabditis elegans*

C. elegans is small free-living soil nematode. In 1963, Sydney Brenner proposed research into *C. elegans* primarily in neuronal development. In 1974, he began research into the molecular and developmental biology of *C. elegans*, which has since been extensively used as a model organism (Brenner, 1974). This pioneer work has been rewarded by two Nobel Prizes in physiology and medicine. The first was awarded to Sydney Brenner, John Sulston and Robert Horvitz for genetics and organ development and programmed cell death, in 2002. The second went to Craig Mello and Andrew Fire for describing the mechanism of RNA interference, in 2006. A Nobel Prize in chemistry for discovery and development of green fluorescent protein is also associated to *C. elegans* – one of the laureates, Martin Chalfie, used *C. elegans* to conduct his research. Since then *C. elegans* became one of the most popular model organisms in the field of genetics, cell and developmental biology, host-parasitic interactions, evolution, and ageing.

C. elegans worms are multicellular eukaryotic organisms, that have a quick generation time including embryonic development, four larval stages and adulthood. Newly hatched larvae are 0.25 mm long and adults are 1 mm long. Numerous evolutionary conserved cellular and molecular processes (metabolism, organelle structure and function, gene regulation) can be studied in these little roundworms. They are easy to handle and breed under laboratory conditions. They easily grow on NGM (nematode growth media) plates, fed with Escherichia coli – OP50 (Brenner, 1974). Their growth can be controlled, either by incubating it at 12 or 15°C which slows the development or accelerating the growth at 25°C. In the lack of food, larvae can get arrested in development and enter in a protective state (called dauer), which enables them to survive even for several months. The L1 larvae of the organism can be frozen, just like bacteria at -80°C and stored for long-term (Brenner, 1974). It is possible to synchronize the animals and grow them in bulk in liquid medium, which enables large-scale biochemistry and screenings. They also have a large brood size, and a rapid development. In favorable environments, *C. elegans* undergoes reproductive development and progresses rapidly from embryo to adult in 3–5 days (15°C–20°C). The embryogenesis takes about 16 hours and the embryo grows from a comma stage to 2-fold and then 4-fold before hatching (see Fig. 28, will be detailed later). The newly hatched larva develops through four larval stages (L1-L4). Adults then live another 2–3 weeks. Moreover, their transparent body that eases *in vivo* microscopy with little dissection.

C. elegans was the first multicellular organism to have its whole genome sequenced, allowing genetic manipulations and offering a wide array of mutants, and as of 2012, is the only organism to have its connectome completed (White *et al.*, 1986; White *et al.*, 2013; Cook *et al.*, 2019). It is also reassuring that *C. elegans*, unlike several other Nematodes, is benign to humans and no *C. elegans*-related allergic reactions have been documented. Another advantage is that adult worms are self-fertilizing hermaphrodites, but males also occur naturally in 0.1-0.2% of the total progeny. Strains can be kept as hermaphrodites but building new strains through genetic crossing is also possible. *C. elegans* strains follow the Mendelian segregation rules. The developmental fate of every single somatic cell (959 in the adult hermaphrodite; 1031 in the adult male) has been mapped (Sulston and Horvitz, 1977; Kimble and Hirsh, 1979, Long *et al.*, 2009; Giurumescu and Chisholm, 2015). These patterns of cell lineage are invariant between individuals, whereas in mammals, cell development is more dependent on cellular cues from the embryo. *C. elegans* has five pairs of autosomes and one pair of sex chromosomes. The worms display sexual dimorphism and X0 sex determination: self-fertilizing hermaphrodites, which are XX and males, which are X0. Males are rare and only 0.1-0.2 % of the progeny, which is a result of a rare meiotic non-disjunction of the X chromosome (Hodgkin *et al.*, 1978). The percentage of males can be increased by starving the plates or by temperature shock. As all systems, *C. elegans* also has its drawbacks: some experiments can be challenging due to its small size, not all metazoan genes are present in *C. elegans* and few cell culture lines are available.

III.1. *C. elegans* general anatomy

C. elegans is an unsegmented roundworm and bilaterally symmetrical that belongs to the Nematoda phylum, a phylogenic group assembling early evolved and simple metazoans. Despite its simplicity, *C. elegans* has almost all the main tissues that higher multicellular organisms have. It has a cuticle (a tough outer covering, as an exoskeleton), an epidermis secreting the cuticle (also called hypodermis), four rows of muscle cells, and a fluid-filled pseudocoelom (body cavity). It also has some of the same organ systems as larger animals. Its basic anatomy includes a mouth, pharynx, intestine, gonad, and collagenous cuticle. Like all nematodes, they have neither a circulatory nor a respiratory system. The four bands of muscles that run the length of the body are connected to a small but complex neural system that allows the muscles to move the animal's body only as dorsal bending or ventral bending, but not left or right, except for the head, where the four muscle quadrants are wired independently from one another (Corsi *et al.*, 2015) (Fig. 19).

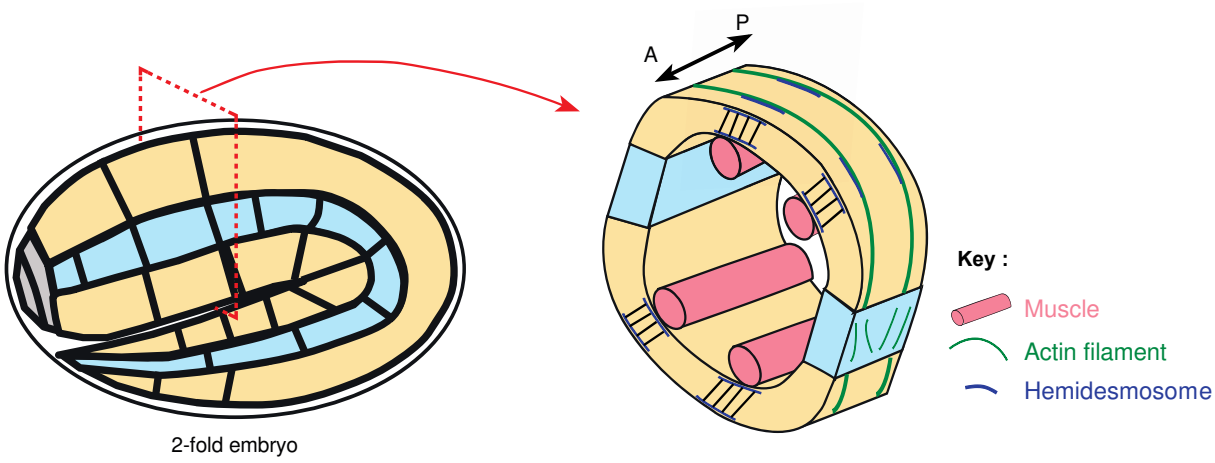

Figure 19: Schematic representation of the 2-fold embryo
On the left: 2-fold embryo represented from a side view. The red dotted rectangle represents the transversal cut through the embryo. On the right: open section of the embryo. In yellow, D/V epidermis. In blue, lateral cells also called seam cells. In pink are represented the four quadrants of muscles tightly connected to the D/V epidermis through the *C. elegans* hemidesmosomes (CeHDs), in dark blue. Running from one lateral junction to the other, the actin bundles are represented in green. A/P, Anterior/Posterior.

In the following sections, I will first describe in more details the internal organization of the embryo, the different tissues and the molecular players involved, with a special focus on the cytoskeleton as it will be of main interest in the results. Then I will discuss the different step of *C. elegans* embryonic elongation.

III.2. *C. elegans* muscles

As found in most of the animals, muscles exist in the simple invertebrate *C. elegans*. Its 95 somatic muscle cells are particular, they are striated but mono-nucleated, having multiple sarcomeres per cell (Sulston and Horvitz, 1977; Waterston, 1988, Bird and Bird, 1991). The most abundant are the body wall muscles that are responsible for locomotion and contribute to a fully accomplished embryonic elongation. They are arranged in four quadrants, two dorsally and two ventrally, beneath the D/V epidermal cells, along the full length of the body. Each quadrant is a double row of muscle cells (Moerman and Fire, 1997). Muscle cells in each longitudinal quadrant are separated from epidermal cells by a basal lamina. Their innervation is peculiar, it plays a role only during the post-embryonic life, since mutations affecting neuronal function do not affect muscles during embryogenesis (Saifee *et al.*, 1998). The muscle fibers consist of myofibrils that primarily contain actin filaments and myosin. They generate contractions that may change their length or/and their shape or maintain their shapes against extrinsic tensions. To establish coordinated movements

in the full body, the force generated by muscle contractions must be transmitted both between the neighboring muscle cells and between the muscle and the epidermis. The muscle-muscle adhesion plaques link the neighboring cells together (Francis and Waterston, 1991; Coutu Hresko *et al.*, 1994). Two muscle-epidermal structures, the dense bodies and the M-lines, connect the actin filaments and myosin filaments, respectively, to the epidermis through the muscle plasma membrane and then the basal lamina to transmit the contractile forces out from muscle cells (Barstead *et al.*, 1991). The force passes first from the actin filaments of the dense bodies, through cytoskeletal adaptor proteins into extracellular receptors, PAT-2/PAT-3 integrins (Gettner *et al.*, 1995), which then transmit the force into the ECM between the muscles and the epidermis. The complex of UNC-112/Kindlin, PAT-4/ILK and PAT-6/actopaxin is another important component of the muscle attachment assembly, as it bridges the muscular actin filaments with the PAT-3 integrin: the lack of any of these proteins prevents the proper recruitment of actin to the muscle membrane (Rogalski *et al.*, 2000; Mackinnon *et al.*, 2002; Lin *et al.*, 2003). Muscle membranes connect to the cuticle through the epidermis via cell basement membrane junction called fibrous organelle (FO) (Waterston, 1988; Francis and Waterston, 1991; Moerman and Fire, 1997; Coutu Hresko *et al.*, 1999; Hahn and Labouesse, 2001; Cox and Hardin, 2004).

Myoblasts are born after the end of gastrulation. At this stage, muscle cells lie in two lateral rows next to the seam cells, and some muscle cells have not yet undergone their terminal divisions. Around 1.5-fold stage, they migrate dorsally and ventrally to contact the ventral and dorsal epidermis. All muscle cells finish their divisions before assuming their final positions. Around the 2-fold stage they become flattened and their attachment to the epidermis begins (Hresko *et al.*, 1994; Williams and Waterston, 1994; Moerman and Williams, 2006). Therefore, the alternated contractions and relaxations of the opposing dorsal and ventral muscle quadrants can start. This contraction pattern provides the sinusoidal movement of the worms after hatching.

III.3. *C. elegans* epidermis

The morphogenesis of the *C. elegans* embryo is controlled by the development of the epidermis (also known as the hypodermis) a single epithelial layer that surrounds the animal. In wild-type embryos, epidermal cells are generated on the dorsal side of the embryo (Chisholm and Hardin, 2005). A hierarchy of transcription factors regulates specification of epidermal fate. After specification, dorsal epidermal cells rearrange, a process known as dorsal intercalation (Sulston *et al.*, 1983; Williams-Masson *et al.*, 1998). Then ventral epidermis undergoes epiboly to enclose the rest of

the embryo in a process known as ventral enclosure. Following enclosure, the epidermis elongates, and most epidermal cells fuse to generate a multi-nucleated syncytial tissue, consisting of polarized epithelial cells (Podbilewicz, 2000). It enables communication with the external environment and bridges the cuticle (that the epidermis secretes apically to serve for protection and as an exoskeleton) and the muscles. The epidermis and the muscles are tightly coupled, though separated by the basal lamina, secreted also by the epidermis (Francis and Waterston, 1991; Hresko *et al.*, 1994). Morphogenesis of the epidermis involves both autonomously generated changes in epidermal cell shape and position, and interactions with internal tissues, including the developing nervous system and body wall muscles. Molecules required for epidermal morphogenesis thus include components of the epidermal cytoskeleton, MTs, IFs, epidermal cellular junctions, cell signaling pathways running between the epidermal cells and underlying tissues, and of the ECM (Priess and Hirsh, 1986; Costa *et al.*, 1997; Costa *et al.*, 1998; Williams-Masson *et al.*, 1997; Williams-Masson *et al.*, 1998; Antoshechkin and Han, 2002).

III.3.1. *C. elegans* Adherens Junctions (CeAJs)

Adherens junctions (AJs) in vertebrates and invertebrates are essential for cell adhesion. By the onset of embryonic elongation, the epidermis organizes into three zones: one dorsal cell row and one ventral cell raw, connected on both sides by one lateral cell rows, also called seam cells. These cells are connected to each other through AJ-like, referred to as *C. elegans* apical junctions (CeAJs). *C. elegans* epithelia only has this type of apical junction (Podbilewicz and White, 1994; Costa *et al.*, 1998; Mohler *et al.*, 1998; Raich *et al.*, 1999, Armenti and Nance, 2012). They have been shown to be key components of the embryonic development from several aspects (Hardin and Lockwood 2004). They not only seal the epidermal layer and maintain its integrity but also provide a mechanical link between cells. They help to transmit forces between the individual cells. Therefore, they orchestrate the epidermal morphogenetic movements. At the same time, they provide mechanical stability and resistance against forces, generated by actomyosin contractility, muscles or other factors, like hydrostatic pressure.

As in vertebrates and *Drosophila,* CeAJs contains two sets of proteins, the cadherin/catenin complex (CCC) (Costa *et al.*, 1998) and the DLG-1/AJM-1 (DAC) complexe (Priess and Hirsh, 1986; Francis and Waterston, 1991; Podbilewicz and White, 1994; Mohler *et al.*, 1998). They have been reported to localize to CeAJs, based on their subapical localization and analogy with other systems. The apically localized polarity proteins PAR-3 and PAR-6 mediate formation and maturation of

junctions, while the basolaterally-localized regulator LET-413/Scribble ensures that junctions remain apically positioned (Legouis *et al.*, 2000; Armenti and Nance, 2012). PAR-6 is also essential for epithelial polarization (Von Stetina and Mango, 2015). In contrast to vertebrates, CeAJ proteins are not essential for general cell adhesion or for epithelial cell polarization.

III.3.2. *C. elegans* hemidesmosomes (CeHDs)

The intra-epidermal junctions are not the only epithelial attachments. Another key element of proper muscle-epidermis attachment is the *C. elegans* hemidesmosomes (CeHD). They connect the dorsal and ventral (but not the lateral) epidermal cells to the underlying muscles basally and to the cuticular exoskeleton apically. The CeHDs are electron dense plaques that resemble ultra-structurally, functionally and molecularly to vertebrate HDs, epidermis-ECM attachment structures (Nievers *et al.*, 1999; Litjens *et al.*, 2006; Zhang and Labouesse, 2010). They are also interconnected by the IFs, forming trans-epidermal attachment structures called fibrous organelles (FOs). FOs function as tendon-like structures, bridging between the muscles and the cuticle exoskeleton through the epidermis (Cox and Hardin, 2004, Francis and Waterston, 1985; Francis and Waterston, 1991). The IFs IFB-1/IFA-3 and IFB-1/IFA-2 are a principal component of the CeHD (Bosher at al., 2003; Sonnenberg and Liem, 2007). IFs provide extra strength to cells, which experience a lot of tension. They are predicted to be anchored to CeHDs through a core protein: VAB-10A (Fig. 20). It is a plakin homologous to vertebrate plectin and BPAG1e. In its absence all the other components disperse, aggregate, detach or form ectopic bundles (Bosher *et al.*, 2003; Zhang and Labouesse, 2010; Zhang *et al.*, 2011). As it will be of importance in the results section, I will shortly discuss the spectraplakin in *C. elegans.*

Spectraplakins are enormous multi-domain cytoskeletal proteins named after their features resembling both the spectrin and the plakin family. *C. elegans* possesses two categories of spectraplakin isoforms encoded by a single locus: *vab-10 (*Variable ABnormal morphology) (Roper at al., 2002; Bosher *et al.*, 2003; Suozzi *et al.*, 2012). VAB-10A and VAB-10B share a common region with a pair of calponin-homology (CH) domains and nine spectrin repeats (SRs) forming a plakin domain (Suman *et al.*, BioRxiv). When fused to GFP, The N-terminal CH-domain region of VAB-10 co-localizes nicely with actin filaments *in vivo* and can be used as a fluorescent probe to visualize actin organization (Gally *et al.*, 2009). It means that the two CH domains serve as an actin-binding domain (ABD) in VAB-10. The second CH domain expressed in epidermis also appears to be localized in the CeHDs (Kim *et al.*, 2011). Among these SRs, the SR5 of VAB-10 contains a Src Homology 3 (SH3)

domain like the SR5 of vertebrate plectin, which is a feature shared by all plakin members (Sonnenberg *et al.*, 2007; Ortega *et al.*, 2011; Gally *et al.*, 2016, Suman *et al.*, BioRxiv). It was proposed that the accessibility of the SH3 embedded in a SR domain is determined by intramolecular interaction with other SR domains, indicating complex regulation of protein interactions within these domains (Hermann and Wiche, 1987; Ortega *et al.*, 2011; Valencia *et al.*, 2013). The VAB-10A-specific region contains sixteen plectin repeats (PRs) following a small coiled-coil domain (Bosher at al., 2003; Gally *et al.*, 2016). The VAB-10B-specific domains contain 20 SRs, an EF-Hand domain and a MT−binding domain called Growth-arrest specific protein 2 (GAS2)-related homology (Fig. 20). Therefore, the predicted function of VAB-10A might be to crosslink actin and IFs cytoskeletons, while VAB-10B might mediate interaction between actin and MTs.

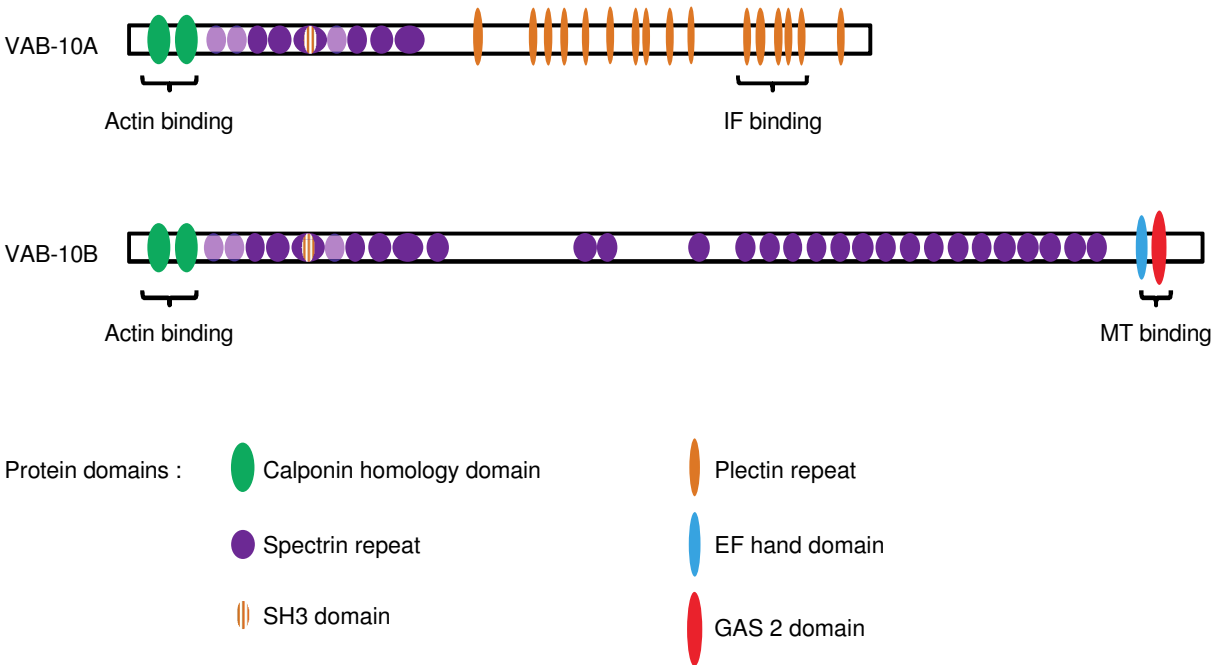

Figure 20: Schematic diagrams of *C. elegans* VAB-10 isoforms.
VAB-10A and VAB-10B each possesses a pair of calponin homology domains (CH1 and CH2) specialized for actin binding. Recent work from our lab updated the number of spectrins domains in *C. elegans* VAB-10 by homology to Human plectin plakin domain (Suman *et al.*, BioRxiv). They are situated right after the CH domains (two light purple domains). Therefore, VAB-10A and VAB-10B share a plakin domain including nine SRs (SR1-8), among which the fifth SR also contains a SH3 domain. The PR 11–15 of VAB-10A is predicted for IFs binding. The GAS2-related homology domain of VAB-10B binds to MTs.
Adapted from Fu *et al.*, 2017.

Along with VAB-10A, a series of other adhesion molecules contribute to proper CeHD maintenance. Apically there are MUA-3 and MUP-4, two homologs, essential for embryonic epithelial morphogenesis and maintenance of muscle position (Gatewood and Bucher, 1997; Bercher *et al.*,

2001; Hong *et al.*, 2001). *mua-3* shares high homology with human FBN1. It is predicted to have collagen binding activity and IF binding activity. Similarly, *mup-4*, shares high homology with human MATN4 (matrilin 4), and encodes a transmembrane protein required for attachments between the apical epithelial surface and the cuticular matrix (Fig. 21). Basally, there is LET-805/myotactin, a single transmembrane protein connecting the CeHDs to muscles and helping relay the contractile information of muscles to epidermis (Hresko *et al.*, 1999; Bercher *et al.*, 2001; Hong *et al.*, 2001). LET-805 is functional anal, although molecularly different, to the mammalian α6β4-integrin. Muscle detachment is observed in myotactin mutants, once muscles become active. Other associated molecules are found around the CeHDs, like the nematode-specific coiled-coil protein PAT-12A, which might contribute to the apical stabilization of IFs and VAB-10A (Hetherington *et al.*, 2010), or tumor suppressor Kank-homolog VAB-19, which contains C-terminal ankyrin repeats. *vab-19* mutants show muscle detachment and display aberrant actin organization. Lastly, GIT-1, a scaffolding and GTPase associated protein (GAP), recruits other proteins such as PAK-1 and PIX-1. It is maintained at the level of CeHDs once muscles become active (Zhang *et al.*, 2011). The initial recruitment of these CeHD components happens independently from each other, but they help each other in their fine patterning at the muscle - epidermis interface (Zhang and Labouesse, 2010).

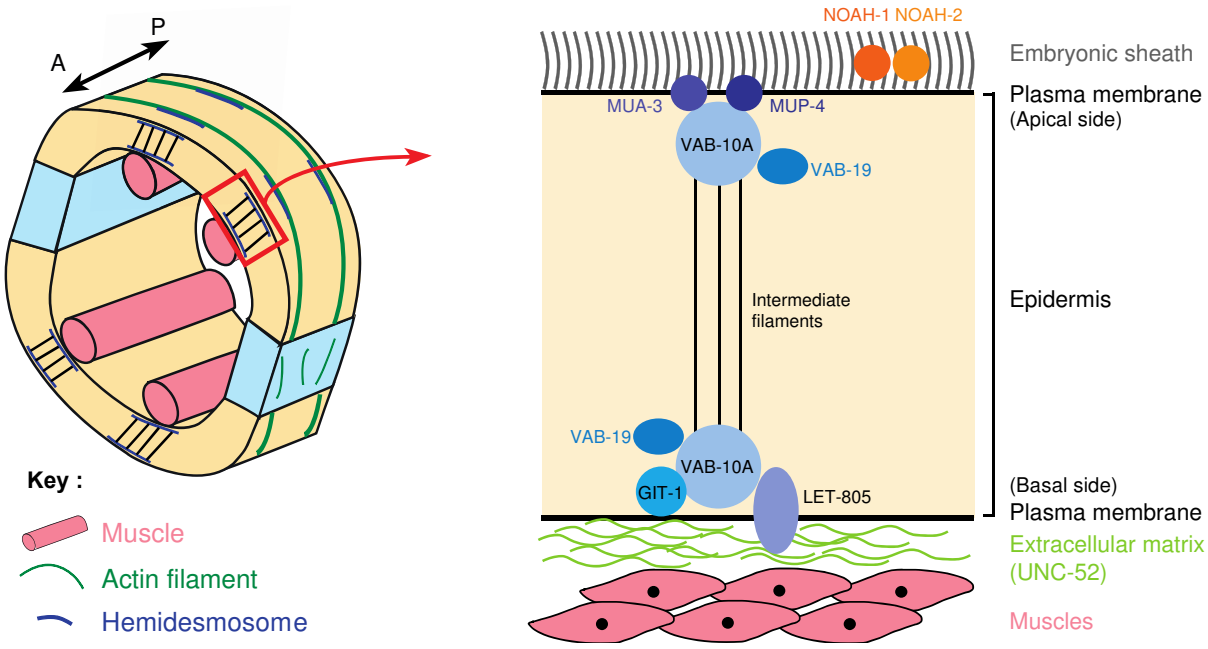

Figure 21: Schematic representation of the *C. elegans* hemidesmosomes (CeHDs)
On the left: open section of the embryo. The red rectangle highlights two CeHDs, one on the apical side and one on the basal side. On the right: structure of the CeHDs connecting muscles to epidermis. NOAH-1 and NOAH-2 are proteins of the embryonic sheath that will become the cuticule in the larva. MUA-3 and MUP-4 are at the apical side of the CeHD. VAB-10 and VAB-19 are present at both apical and basal sides, while IFs hold the structure. LET-805 is localized at the basal side. A/P, Anterior/Posterior.
Adapted from Zahreddine *et al.*, 2010 and Saurabh Tak's thesis.

The CeHDs start to assemble as foci at the apical and basal membranes prior to elongation and progressively start to form circumferential bundles above the muscles during elongation. The process depends on the presence of the underlying muscle precursors, and muscles also play a significant role in their maturation during elongation. Indeed, muscle contractions induce a mechanotransduction pathway that triggers the phosphorylation of IFs and therefore promotes the further elongation of embryos beyond 2-fold (Zhang *et al.*, 2011).

III.3.3. *C. elegans* extracellular matrix

As muscle contractions are essential for the elongation, they need to be properly transmitted to the epidermis. This depends partially on the ECM, apically and basally, between the two tissues. Therefore, the ECM can also affect elongation, especially through coordinating shape changes between the muscles and the epidermis (Labouesse, 2012). Some ECM components influence elongation indirectly, through affecting muscle sarcomere assembly. Other act more directly: for instance, even a slight reduction of UNC-52 perlecan, coupled to weakened CeHDs affects the fibrous organelle structure (Zahreddine *et al.*, 2010). To conduct a normal embryonic development, not only proper ECM composition is important, but also the proper attachment of the epidermis and the muscles to the ECM. The tissues connect to the basement membrane through ECM receptors, integrins. The muscle-specific perlecan receptors presumed to be PAT-2/PAT-3 and their lack causes a pat phenotype. (In *C. elegans,* only two α- (INA-1, PAT-2) and one β-integrin chain (PAT-3) are present). The supposed epidermal perlecan receptor is LET-805/myotactin, which can also severely compromise elongation, when disrupted (Williams and Waterston, 1994; Hresko *et al.*, 1994; Rogalski *et al.*, 1995; Hresko *et al.*, 1999; Moerman and Williams, 2006; Zahreddine *et al.*, 2010). Recent work from our lab showed another key role of the apical ECM embryonic morphogenesis. It helps preserving the integrity of the embryos and distributes tension throughout the embryo during elongation. The leucine-rich repeat (LRR) proteins SYM-1, EGG-6 and LET-4, and the zona pellucida (ZP) domain protein FBN-1/Fibrillin have already been proposed to be part of the embryonic sheath. They line the outer part of the embryo and/or are secreted in the extra-embryonic space. SYM-1, EGG-6 and LET-4 were shown essential to organize the apical extracellular matrix and maintain epithelial junction integrity (Mancuso *et al.*, 2012). In addition, FBN-1 mediates pharynx attachment and resistance of the epidermis to mechanical deformation during *C. elegans* embryogenesis (Kelley *et al.*, 2015). SYM-1 might also help attach muscles to the cuticle (Davies *et al.*, 1999). Recently, along with these already described players, we identified two ZP proteins, NOAH-1 and NOAH-2, acting in

the same pathway, and in parallel to SYM-1, LET-4 and FBN-1/Fibrillin. NOAH-1 and NOAH-2 preserve the embryonic integrity together with the p21-activated kinase PAK-1 via maintaining and relaying the actomyosin contractile tension before muscle contraction. Also, during late elongation, these ECM proteins are essential for muscle-epidermis anchorage and the input of muscle contraction transduction to epithelia (Vuong-Brender *et al.*, 2017).

III.4. Cytoskeleton

C. elegans has all the main cytoskeletal networks (actin, MTs, IFs, spectrins) and junctional components that higher organisms have. IFs can be found at the level of CeHDs, establishing the trans-epithelial connection between the apical and the basolateral CeHDs structures. Actin forms a meshwork near the epidermal cortex that rearranges to form circumferential, parallel bundles first in the D/V cells, followed by its rearrangement in the lateral cells (Priess and Hirsh, 1986; Costa *et al.*, 1997; Costa *et al.*, 1998). As they will be of major interest in the results of this thesis, I will specify what is inferred by bundles. They correspond to the cortical actin filaments that bias the growth of the epithelial cell membranes and coincide with the pattern of circumferentially oriented, parallel furrows on the cuticle of the first larval stage (Costa *et al.*, 1997). They are constituted of several actin filaments, as it will be discussed later.

The organization of MTs before, during and after elongation is very similar that of actin, they are even intermingled, though MTs are still a little less regular than actin bundles (Priess and Hirsh, 1986; Quintin et al, 2016). The spectrin cytoskeleton attaches to the actin network and to the cell membrane, to which it is apically and basolaterally linked. It is this organization that we will depict in the following sections.

III.4.1. Actin

Actin is well conserved among different eukaryotes (Elzinga, 1973). Small differences in actin sequences can lead to changes in their function. The actin network consists of filamentous or F-actin. The actin filaments are righthanded helical polymers of the protein G-actin. The monomers of G-actin are 375-amino acid polypeptides. They are single units allowing the formation of flexible structures of diameter 4-7nm that have the capacity to organize into anything from a simple filament to a 3-dimensional sheet (Reisler, 1993; Graceffa and Dominguez, 2003).

The F-actin polymer has a structural polarity: the end that possesses an actin subunit that has its ATP binding site exposed is called the (-) end or pointed end, while the opposite end where the cleft is directed at a different adjacent monomer is called the (+) end or barbed end (Lodish *et al.*, 2013). Although polymerization and depolymerization can also occur at both ends, in general there is a dynamic equilibrium between the two poles and the faster growing end is the barbed end, while the actin monomers can dissociate mostly at the pointed end in an ATP-dependent manner (Begg, 1978, Hollenbeck *et al.*, 1989; Jarhaus *et al.*, 2001). Actin dynamics are influenced by the availability of actin monomers and remodeling proteins. This group contains various proteins such as nucleating factors which accelerate actin polymerization and are responsible for branched filaments, filament stabilizing proteins such as capping proteins, severing proteins such as gelsolin and depolymerization factors as cofilin (Kovar *et al.*, 2005, Nomura and Ono, 2013). Therefore, the structural organization of different actin networks such as bundles, dendritic networks and web like structures depends on specialized accessory proteins. These proteins also control the interactions of other proteins such as myosin with actin filaments. Some of these proteins will be discussed in the next paragraph. Due to its dynamics, actin becomes a central player in various biological processes related to dynamic cellular movements and shape changes: endocytosis, cytokinesis, organelle transport or cellular motility (e.g. filopodia at the leading edge of lamellipodia in migrating cells) (Pollard and Cooper, 2009).

C. elegans has five closely related actins (ACT-1-5). They contribute to an apically organized actin skeleton essential for cell shape changes and for shape maintenance during morphogenesis (Priess and Hirsh, 1986; Costa *et al.*, 1997). The contribution of actin to embryonic morphogenesis has been reported from the end of gastrulation (Marston and Goldstein, 2006). Starting at the 1.5-fold stage, the cortical actin network reorganizes dramatically and forms parallel bundles of 5-10 filaments (Labouesse, 2006). The bundles are present all over the embryonic epidermis, having a more regular organization in the D/V cells. They are associated with non-muscle myosin II, closely attached to the membrane, below the furrows of the embryonic sheath and they have strong attachment to CeAJs in DV cells (Priess and Hirsh, 1986). The non-muscle myosin II subunits include the heavy chains NMY-1 and NMY-2, the regulatory light chain MLC-4 and the essential light chain MLC-5 (Fyrberg, *et al.*, 1994; Shelton *et al.*, 1999; Piekny, *et al.*, 2003; Gally, *et al.*, 2009). The phosphorylation of MLC-4^{S18} and MLC-4^{T19} control the activity of myosin II in epidermal cells of *C. elegans* (Gally, *et al.*, 2009). During elongation, the number of bundles does not change, but the spacing between them increases (Priess and Hirsh, 1986; Costa *et al.*, 1997). Such an epidermal actin skeleton becomes the guiding structure of *C. elegans* early embryonic elongation, until the start of muscle contractions at mid-elongation, (Shelton *et al.*, 1999; Piekny *et al.*, 2003; Gally *et al.*, 2009).

Though we increased greatly our knowledge about the role of the actin cytoskeleton and actomyosin contractility during *C. elegans* development, several poorly understood issues about the organization of this network remain. Within the dorsal and ventral epidermal cells, the specific molecular composition, the organization, and the polarity of filaments within bundles has not been established. It is not known whether actin polymerizes as long filaments running from one dorsal-seam CeAJ to the other, whether they run from one CeAJ to a CeHDs, or whether they make several short-intermingled filaments of similar or opposite polarity. The occurrence of apparent actin bundle discontinuities at the level of CeHDs in some backgrounds could indicate that CeHDs represent an intermediate anchoring structure between CeAJs. Another important question is the nature of the cues that trigger the formation and orientation of these bundles. As they are present in the entire epidermis, their organizing factors must include common features in all epidermal cells. Both polarity and mechanical cues have been suspected to be such possible factors.

III.4.2. Actin remodeling proteins

Actin cytoskeleton is essential for a wide variety of cellular functions, such as cell motility, phagocytosis, cell division, and muscle contraction. A tremendous number of molecules regulate the function of actin cytoskeleton. Regulation of polymerization and depolymerization of actin is crucial for the function of the actin cytoskeleton.

III.4.2.1. Formin

Nucleation of actin is the rate-limiting step of actin filament assembly (Cherasone *et al.*, 2010; Sit and Manser, 2011;). Members of the formin family nucleate unbranched microfilaments. Formins stabilize the first actin dimer, recruit profilin, an actin monomer binding protein and then remain bound to the growing (+) end of the filament and prevent capping proteins from terminating filament extension. The resultant long, unbranched actin filaments can be bundled into stress fibers (Taniguchi *et al.*, 2009; Iskratsch *et al.*, 2010; Kan-O *et al.*, 2012; Breitsprecher and Goode, 2013; Bechtold *et al.*, 2014). Formins participate in multiple cellular processes (Goode and Eck, 2007; Cherasone *et al.*, 2010) including cytokinesis, cell movement and changes in cell shape. The mammalian genome encodes fifteen formins while in *C. elegans* there are seven formins.

cyk-1 acts during embryonic cytokinesis and in the excretory cell (Severson *et al.*, 2002; Mi-Mi *et al.*, 2012; Shaye and Greenwald, 2016). *daam-1* and *frl-1* participate in Wnt-mediated cell polarity of the B cell (Wu and Herman, 2006). *fozi-1* encodes a divergent formin required in cell fate specification of muscles and neurons (Johnston *et al.*, 2006; Amin *et al.*, 2007). In addition to the spermatheca, *exc-6* functions in the excretory cell, as does the second inverted formin, *inft-2* (Shaye and Greenwald, 2015; Hegsted *et al.*, 2016; Shaye and Greenwald, 2016). And *fhod-1* encodes the only *C. elegans* member of the FHOD subfamily of formins and is related to the human and mouse FHOD1 and FHOD3 (Mi-Mi *et al.*, 2012; Pruyne, 2016). It has a characteristic proline-rich formin homology FH1 domain, recruiting profilin-bound actin. The FH2 domain engages in formin dimerization, forming a ring that is involved in the nucleation/processive capping of actin. Like many formins, it is initially inactive due to an autoinhibitory interaction between the formin's C-terminal diaphanous autoregulatory domain (DAD) with the N-terminal diaphanous inhibitory domain (DID, sometimes referred to as FH3). FHOD1 also contains an N-terminal GTPase-binding domain (GBD). A coiled-coil domain is found between the FH1 and FH3 domains (Vanneste *et al.*, 2013) (Fig. 22). It can be activated by binding a Rac GTPase in a nucleotide-independent manner or by phosphorylation of the DAD domain by Rho-binding kinase, although the latter does not appear to be essential in *C. elegans* (Vanneste *et al.*, 2013).

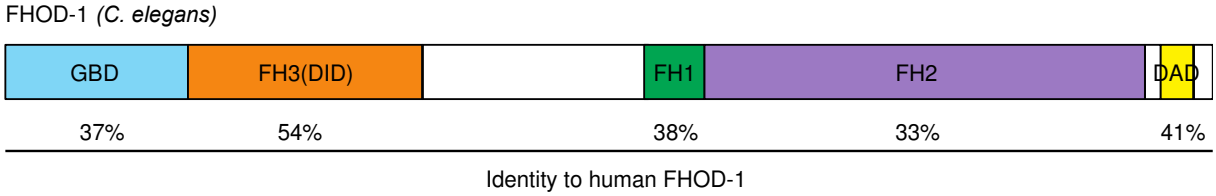

Figure 22: Schematic diagram of *C. elegans* FHOD-1.
Domain assignments are based on those of Schulte *et al.*, 2008, for human FHOD1. Amino acid similarities to corresponding domains of human FHOD1 are indicated.
Adapted from Vanneste *et al.*, 2013.

FHOD-1 has nucleating (Patel *et al.*, 2017) and bundling functions (Schönichen *et al.*, 2013; Kutscheidt *et al.*, 2014) and may also contribute to lateral vs. dorsal/ventral differences. FHOD-1 also functions in *C. elegans* muscle, where it is partially redundant with CYK-1 for formation of striated body wall sarcomeres (Mi-Mi *et al.*, 2012; Mi-Mi and Pruyne, 2015). FHOD-1 is localized near the Z lines within the contractile lattice, and along the edges of growing body wall muscle cells. Actin thin filaments still form in *fhod-1* mutants, but muscles are narrower and further apart, and Z lines attachments are defective.

III.4.2.2. Gelsolin

Gelsolin-related proteins and actin depolymerizing factor (ADF)2/cofilin are the two major classes of actin filament-severing proteins that enhance actin filament turnover by severing and depolymerizing actin filaments and take part in several cell biological processes. The gelsolin family of proteins is a major class of actin regulatory proteins that sever, cap, and nucleate actin filaments in a calcium-dependent manner (Yu *et al.*, 1992) and are involved in various cellular processes (Becker *et al.* 2003; Feldt *et al.*, 2019). Typically, gelsolin-related proteins exhibit three to six repeats of homologous domains of 100–120 amino acids, which are designated as gelsolin-like (G) domains and each domain plays a distinct role in severing, capping, and nucleation (Sun *et al.*, 1999; Ghoshdastider, 2013; Feldt *et al.*, 2019).

In *C. elegans* there are three genes encoding for gelsolin-related proteins: *gsnl-1*, *fli-1* and *viln-1. fli-1* encodes a homolog of Flightless-1 (Goshima *et al.*, 1999). FLI-1 is widely expressed in many tissues, and *fli-1* mutations cause several developmental defects (Deng *et al.*, 2007). Little is known about *viln-1*.

gsnl-1 (gelsolin-like protein-1) encodes an unconventional gelsolin-related protein. It is ortholog of several human genes including AVIL (advillin), GSN (gelsolin), and VIL1 (villin 1). It has four gelsolin-like (G) domains (G1-G4), unlike typical gelsolin-related proteins with three or six G domains. It has been shown that G1 and the linker between G1 and G2 were sufficient for actin filament severing, whereas G1 and G2 were required for barbed end capping. A PIP2-sensitive domain was mapped to G1 and G2. At least two actin-binding sites were detected: a calcium-dependent G-actin-binding site in G1 and a calcium-independent G- and F-actin-binding site in G3 and G4. (Liu *et al.*, 2010) (Fig. 23). Sequence alignment suggests that GSNL-1 lacks two G domains that are equivalent to fourth and fifth G domains of gelsolin. *In vitro*, GSNL-1 severed actin filaments and capped the barbed end in a calcium-dependent manner (Pardee and Spudich, 1982; Choe *et al.*, 2002; Klaavuniemi *et al.*, 2008), like gelsolin. However, unlike gelsolin, GSNL-1 stays bound to the side of F-actin with a submicromolar affinity and did not nucleate actin polymerization, although it bound to G-actin with high affinity (Klaavuniemi *et al.*, 2008). It localizes to the actin cytoskeleton and striated muscle dense body and is expressed in the epidermis.

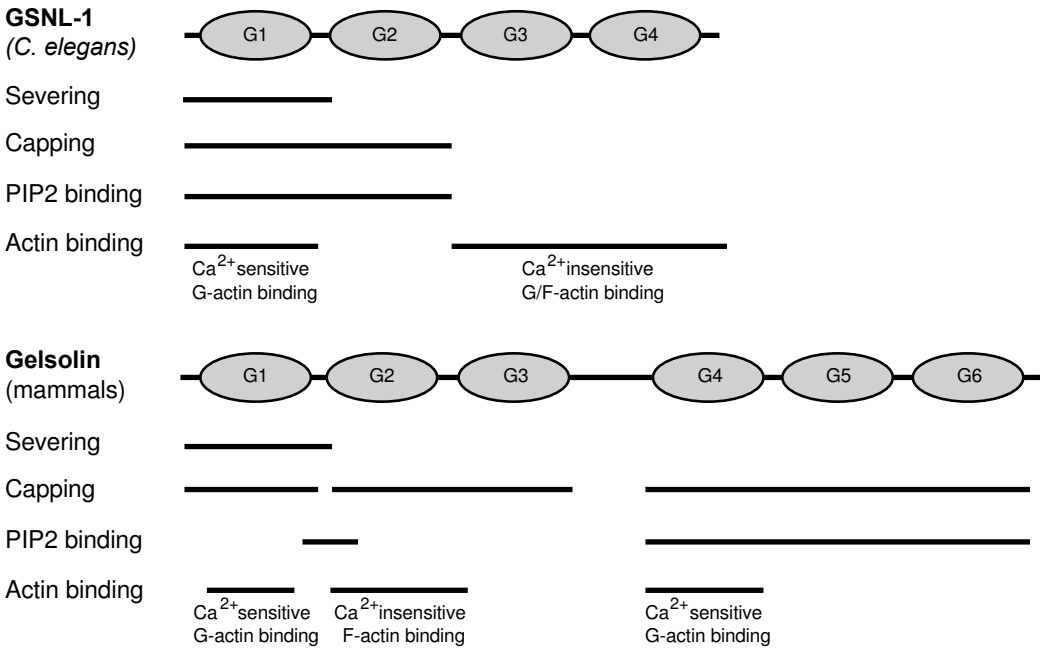

Figure 23: Schematic diagrams of *C. elegans* GSNL-1 and mammalian gelsolin.
Gelsolin-like (G) domains are numbered from G1 to G6 in the order of appearance from the N-termini but not necessarily representing sequence homology. Indeed, G4 of GSNL-1 is most closely related to G6 of gelsolin. Functional domains of *C. elegans* GSNL-1 were adapted from Klaavuniemi *et al.*, 2008 and Liu *et al.*, 2010. Functional domains of mammalian gelsolin were adapted by Liu *et al.*, 2010, from Sun *et al.*, 1999, with modifications based on the following references: severing (Kwiatkowski *et al.*, 1989), capping (Weber *et al.*, 1991 ; Sun *et al.*, 1994), PIP2 binding (Janmey *et al.*, 1992 ; Yu *et al.*, 1992 ; Feng *et al.*, 2001), calcium-sensitive G-actin binding in G1 (Way *et al.*, 1990), calcium-insensitive F-actin binding in G2 (Sun *et al.*, 1994), and calcium-sensitive G-actin binding in G4 (Pope *et al.*, 1995).

III.4.2.3. Vilin

viln-1 is an ortholog of human SVIL (supervillin) (Pope *et al.*, 1998; Liu *et al.*, 2010). Supervillin is a 205-kDa F-actin binding protein, tightly associated with both actin filaments and plasma membranes, suggesting that it forms a high-affinity link between the actin cytoskeleton and the membrane (Pestonjamasp *et al.*, 1997; Ghoshdastider *et al.*, 2013). *C. elegans viln-1* is predicted to also have actin filament binding activity. *viln-1* encodes a villin-like protein with six G domains and a C-terminal villin headpiece. It has a NH2-terminal region with one putative nuclear targeting region, three potential protein kinase A phosphorylation sites. Its vilin-like conserved COOH-terminal domain contains also one putative nuclear targeting region, three potential F-actin binding sites and one potential tyrosine phosphorylation (Pope *et al.*, 1998; Liu *et al.*, 2010) (Fig. 24). *viln-1* function is still unknown but at the adult stage, it is expressed in the head and the tail (McKay *et al.*, 2003; Hunt-Newbury *et al.*, 2007).

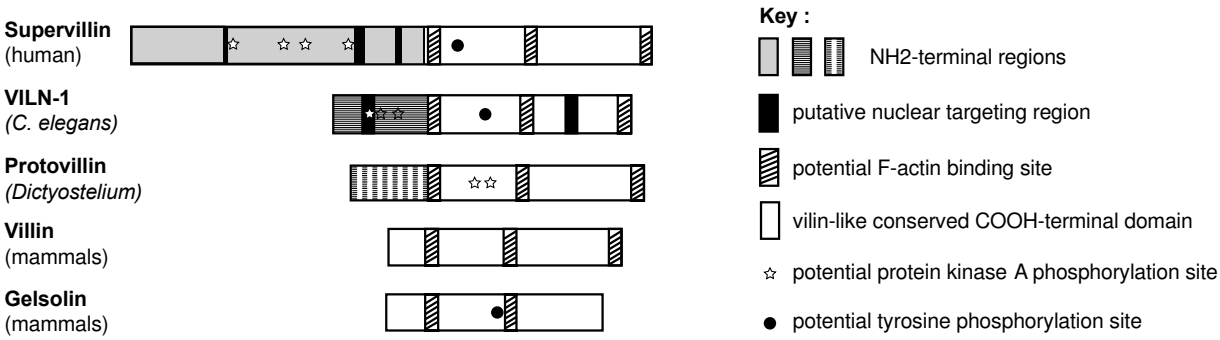

Figure 24: Schematic diagrams of the villin superfamily.
Representation of the domains structure for human supervillin, *C. elegans* VILN-1, *Dictyostelium* protovillin, and mammalian villin and gelsolin.
Adapted from Pope *et al.*, 1998, and Liu *et al.*, 2010.

III.4.3. Microtubules

MTs are known to form structures such as cilia and flagella, the motile and sensory whips, or sensory devices on the surface of the cell (Haimo and Rosenbaum, 1981; Lodish *et al.*, 2000). They can organize themselves as tracks for the transport of materials in the cell. They are long hollow cylinders made of protein tubulin. The outer diameter is 25 nm and these structures are rigid compared to actin microfilaments and are more complex than actin. MTs are long with often one end attached to a MTOC (Desai and Mitchison, 1997; Marshall and Rosenbaum, 1999). The roles of MTs are diverse and comparatively more dynamic than actin.

The nematode *C. elegans* has 20 kinesins. Most kinesins walk towards the plus end of the MTs. Some isoforms of kinesins walk towards minus end, while some do not move and depolymerize MTs (Vale *et al.*, 1985). MTs are circumferentially oriented in D/V cells in epidermis. They have been proposed to provide a passive response to help elongation in the dorsal and ventral epidermis (Priess and Hirsch, 1986; Ciarletta *et al.*, 2009). However, recent work has indicated that MTs are more likely to function as a transport key structure to favor the morphogenesis process (Quintin *et al.*, 2006). Before elongation, they are found in complex cytoplasmic networks in interphase cells or associated with the spindle apparatus in mitotic cells. In the DV cells, they undergo a remarkable transition in pattern at the start of elongation in *C. elegans* embryo and become circumferentially oriented (Priess and Hirsh, 1986). They might be intermingled with actin microfilament bundles. In the lateral epidermis, they remain less well-organized during the whole elongation. In DV cells they appear to be attached to MTOC linked to membranes while the ones in seam cells are distributed throughout their cytoplasm (Feldman and Priess, 2012). MTs function during embryogenesis and elongation was

assessed using drugs preventing mitosis: colcemid and griseofulvin. These embryos developed abnormalities such as depressions and constrictions and could not elongate fully. The microfilament pattern was not affected (Priess and Hirsh, 1986). Recent data from our lab showed that during *C. elegans* embryogenesis, MTs promote elongation process in parallel to the actomyosin activation pathway LET502/ ROCK (Quintin *et al.*, 2016). MTs are shown to be essential for elongation in a LET-502/ROCK partially impaired background. MTs promote the transport of E-cadherin and LET-805 to CeAJs.

III.4.4. Spectrin cytoskeleton

Spectrin denotes the family of α-helical, high molecular weight, multifunctional ABPs, usually found in association with the plasma membrane of mature cells (Marchesi and Steers, 1968; Hartwig, 1995). They are ubiquitous cytoskeletal proteins, forming two dimensional networks under the membrane as α-β heterotetramers (Isparo *et al.*, 2010; Brown *et al.*, 2015). They are part of the spectrin superfamily along with α-actinin or dystrophin (Broderick and Winder, 2005). The main characteristic they share is the presence of SRs. Some special domains allow to distinguish some of them such as actin binding CH domains, EF hand domains, SH3 domain or proline-rich regions, which are potential platforms for protein interactions (Broderick and Winder 2005; Gushchina *et al.*, 2011). Spectrins have been first and so far, best described in red blood cells (Stokke *et al.*, 1986; Greenquist *et al.*, 1978; Bodine *et al.*, 1984; Bennett and Baines, 2001; Lux, 2016). They are concentrated just beneath the plasma membrane, forming a 2-dimensional structure held together by actin filaments and interacting with several membrane-bound proteins. This network provides elasticity to the cell cortex and red blood cells can spring back to their original size after passing through a capillary. However, for the past 10-15 years, we have started to better understand their role in non-erythroid contexts as well. The function of spectrins in non-erythrocyte cells was unclear to a large extent for long, but recent research highlighted their many roles in various processes, like mitotic spindle orientation, DNA repair, cell signalling, or protein trafficking (De Matteis and Morrow, 2000, Phillips and Thomas, 2006; Johansson *et al.*, 2007; Kizhatil *et al.*, 2007; Machnicka *et al.*, 2012; Fletcher *et al.*, 2015).

However, one of the most evident roles of spectrins is related to membrane organization and stabilizing membrane proteins at their right place. Spectrins are helping ion channel and cell adhesion molecule recruitment in the endoplasmic reticulum, in the cell, Golgi and muscle membrane or also in the nervous system. Defects in this membrane organization can lead to

neurodegenerative diseases like spinocerebellar ataxia type 5 (Lorenzo *et al.* 2010; Stankewich *et al.* 2010), hearing loss with mislocalized voltage-gated channels at the Ranvier node in mice (Parkinson *et al.* 2001; Komada and Soriano 2002) or loss of Na+ K+-ATPase from the basolateral domain in *Drosophila* epithelium (Dubreuil *et al.* 2000).

The impact of spectrins in the mechanical stabilization of cells or tissues is also among their most important functions. This role is evident and pivotal in erythrocytes, but growing evidence shows that it is just as important in epithelia. For instance, mammalian βII spectrin is needed to maintain the proper separation between the apical and basolateral sides of epithelial cells (Kizhatil *et al.* 2007). In *Drosophila* βH-spectrin contributes to eye morphogenesis through mediating the interaction between cadherin junctions and the cell adhesion molecule Roughest (Lee *et al.* 2010). Recent work showed that the scaffold big bang (Bbg) binds to β-heavy–Spectrin/Karst subunit at the apical cortex and promotes Yorkie activity, F-actin enrichment, and the phosphorylation of the myosin II regulatory light chain Spaghetti squash. They proposed a model in which the spectrin cytoskeleton recruits Bbg to the cortex, where Bbg promotes actomyosin contractility to regulate epithelial tissue growth of *Drosophila* wing discs (Forest *et al.*, 2018). Another example is the *Drosophila* photoreceptor morphogenesis, during which Spectrins are required to control the process through the modulations of cell membrane domains (Chen *et al.*, 2009).

Finally, spectrins are also important during *C. elegans* embryonic morphogenesis and I will detail it in the following section.

C. elegans contains three spectrins, each of them encoded by a single gene: βG-spectrin (*unc-70*), βH-spectrin (*sma-1*) and α-spectrin (*spc-1*). All these three spectrins have been shown to be essential for morphogenesis and/or muscular and neuron formation. βG and βH-spectrin probably have distinct roles and can't substitute for each other's activity as neither their spatiotemporal expression, nor their subcellular localization overlap. However, the localization of α-spectrin overlaps with both and they form α-β heterotetramers. SPC-1 loss displays the strongest phenotype and it can be recapitulated by the joint loss of UNC-70 and SMA-1 (Norman and Moerman, 2002; Praitis *et al.*, 2005). It suggests that SPC-1 is present everywhere as a crucial element when UNC-70 and SMA-1 have different spatiotemporal functions. Yet, the presence of an intact α-β-spectrin heterotetramer skeleton, having all the three spectrins is necessary to accomplish its full function.

III.4.4.1. βG-spectrin/UNC-70

βG-spectrin/UNC-70 is a 262kDa protein, 54,2% identical to human SPTBN1. It is the *C. elegans* ortholog of the conventional non-erythrocyte β-spectrin in vertebrates and in *Drosophila* (Hu *et al.*, 1992; Hammarlund *et al.*, 2000). UNC-70 includes 17 SRs onsisting of 106 amino acids, a conserved region in the first two SRs (possible adducin and/or ankyrin binding motif), two N-terminal CH domains and a C-terminal plectrin homology (PH) domain (Hammarlund *et al.*, 2000; Moorthy *et al.*, 2000) (Fig. 25). SRs are flexible rod domains consisting of triple α-helices (one parallel and two non-parallels) that are attached through flexible linker regions. The helices are stabilized by interactions between hydrophobic residues and are folded in a coiled coil structure. They are supposed to be the key components in the molecular flexibility and elasticity within the entire spectrin superfamily and they have a special characteristic to fulfill this role. CH-domains are responsible for the actin binding ability of the protein. A PH domain allows the interaction with phospholipids; therefore, it provides a direct attachment to the cell membrane (Broderick and Winder 2005).

UNC-70 is expressed in all tissues, including the lateral membrane of the epidermis, starting in early embryos (Moorthy *et al.*, 2000). Strong *unc-70* mutants show that larvae cannot survive beyond the L1 stage and present an uncoordinated coiling, which severely harm the mobility of the larvae (Hammarlund *et al.*, 2000). The defects of moving ability in *unc-70* larva are due to the progressive disorganization of myofilaments and the discontinuities in the dense bodies. In body wall muscles, a reduction or loss of the sarcoplasmic reticulum is also observed. *unc-70* larvae are lethal at the L1 stage, but the embryos complete the development process and hatch, meaning that UNC-70 is dispensable for embryogenesis. UNC-70 has also been shown important for neuron formation (Sönnichsen *et al.*, 2005; Hammarlund *et al.*, 2007, Schmitz *et al.*, 2007). Depletion of UNC-70 in early larvae leads to multiple defects in nervous system. Abnormally enlarged neuronal bodies, apparent vacuolation in amphid neurons, abnormal axon outgrowth and ectopic displacement of neuronal bodies can be observed in these larvae (Hammarlund *et al.*, 2007). *unc-70* mutants lose the ability to develop sensory neurons under stress in moving larvae. Atomic force spectroscopy experiments on isolated neurons, *in vivo* laser axotomy and fluorescence resonance energy transfer (FRET) imaging, showed that UNC-70 is held under continuous tension, to transmit the pre-stress to touch receptor neurons. Genetic manipulations that decrease such spectrin-dependent tension also selectively impair touch sensation, suggesting that such pre-tension is essential for efficient responses to external mechanical stimuli (Hammarlund *et al.*, 2000; Moorthy *et al.*, 2000; Krieg *et al.*, 2014, Krieg *et al.*, 2017).

III.4.4.2. βH-spectrin/SMA-1

βH-spectrin/SMA-1 is a 470kDa protein, *C. elegans* ortholog of *Drosophila* βH-spectrin. SMA-1 contains 30 SRs, two CH domains, a SH3 domain and a C-terminal PH domain (McKeown *et al.*, 1998) (Fig. 25). SH3 domains have been characterized in the protein Src and are widely known for their contribution to signal transduction and for acting as protein interaction platforms. The SH3 domain of SMA-1 is buried within a loop between two α-helices of the SR and they acquire a folding transition state that can be switched when mechanical force is applied on it (Martinez and Serrano, 1999; Jagannathan *et al.*, 2012). SMA-1 also shows an ankyrin-binding sequence present in β-spectrin (Dubreuil *et al.*, 1990; Thomas and Kiehart, 1997) and resembles more to *Drosophila* βH-spectrin at the level of homology (McKeown *et al.*, 1998).

SMA-1 has not been reported to impact on muscle structure or neuronal morphology. Its role is related to epithelial cell shape changes that the epidermis, gut, pharynx, pharyngeal gland and excretory canal cell undergo (McKeown *et al.*, 1998; Buechner *et al.*, 1999; Norman and Moerman, 2002; Praitis *et al.*, 2005; Raharjo *et al.*, 2011). *sma-1(ru18)* null mutants elongate at a lower rate resulting in shorter larva with round heads (McKeown *et al.*, 1998; Praitis *et al.*, 2005). SMA-1 is expressed from the early embryos, at the apical part of epithelial tissues, and is required to determine cell shape in multiple epithelial tissues during morphogenesis (McKeown *et al.*, 1998). SMA-1 apical localization does not require the presence of its tetramerizing partner SPC-1, though its organization becomes weaker and more punctate in *spc-1* mutants (Praitis *et al.* 2005). As an actin-binding cytoskeletal protein, SMA-1 plays a role in actin organization: in its absence the actin remains intact at the cell boundaries and apically at the early embryonic stages but its association to the apical membrane gets disrupted during elongation (Praitis *et al.*, 2005). Another defect of *sma-1* mutants is the expanded distribution of muscle bands, basement membrane and CeHDs structures (Norman and Moerman 2002). Although *sma-1* is clearly required for normal morphogenesis, it is not an essential gene. It was hypothesized that SMA-1 might be a downstream target of regulatory interactions affected by the muscle-epidermis interaction or serve as a cytoskeletal binding site for signal transduction molecules (McKeown *et al.*, 1998).

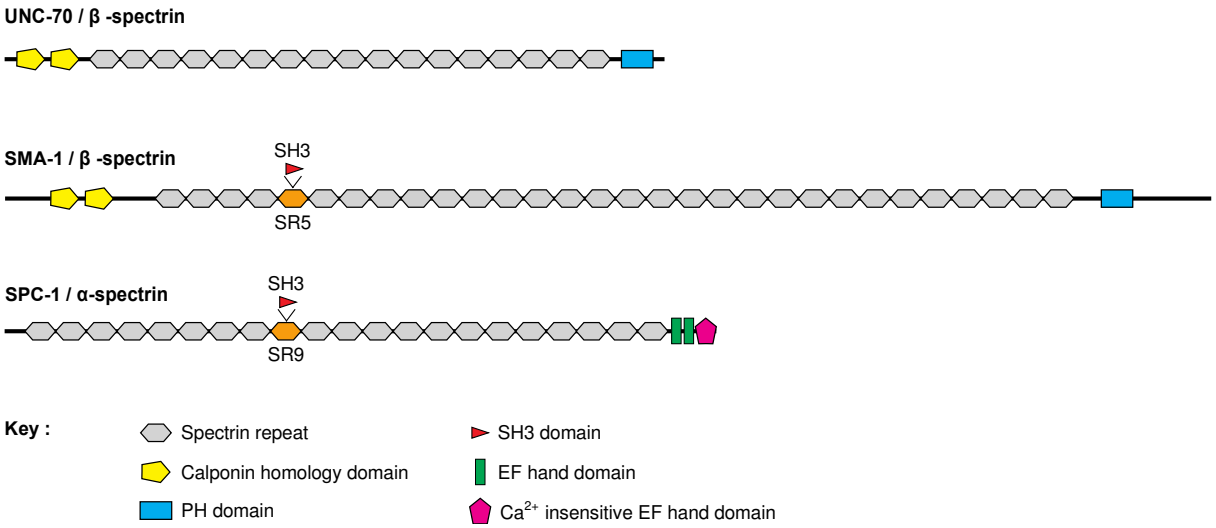

Figure 25: Schematic diagrams of the three *C. elegans* spectrins.
Domain structure of UNC-70, SMA-1 and SPC-1.
Adapted from SMART (a Simple Modular Architecture Research Tool, http://smart.embl-heidelberg.de/) website.

III.4.4.3. α-spectrin/SPC-1

The single α-spectrin in *C. elegans* is a 240kDa protein, SPC-1. It shows 61% identity and 76% similarity to *Drosophila* α-spectrin, while it is 57% identical and 72% similar to human non-erythroid α-spectrin SPTAN (Norman and Moerman, 2002). SPC-1 consists of 21 SRs, an SH3 domain and two C-terminal EF hand domains, one domain being calcium-dependent, the other one calcium-independent (Fig. 25).

SPC-1 is ubiquitously expressed all over the life cycle and it is recruited to the cell membrane. Animals lacking functional spectrin do not complete embryonic elongation and die just after hatching. Proper differentiation of the body wall muscles is also affected, myofilaments of muscles are oriented abnormally from the longitudinal anterior/posterior (A/P) direction of the embryo, and the width of the CeHDs is increased (Norman and Moerman, 2002). During embryogenesis, SPC-1 localizes to the cell membrane in most if not all cells, starting at the first cell stage. In epithelia, SPC-1 is localized both apically like SMA-1 and basolaterally, overlapping with UNC-70. When SPC-1 is absent, SMA-1 localization itself is normal. On the other hand, SPC-1 localization is dependent on UNC-70 but not SMA-1 (Norman and Moerman, 2002). *spc-1* mutants also have defects in the organization of the epidermal apical actin cytoskeleton that is needed for elongation.

Therefore, it seems that the SPC-1/SMA-1 heterotetramers are required for a proper actin organization in the embryonic epidermis. Overall, these reports on the role of the spectrin skeleton in *C. elegans* embryonic elongation suggest that spectrins could have an important role in development, in the maintenance of cellular structures and probably such properties as elasticity in non-erythroid cells as well.

III.4.4.4. The spectrin heterotetramers

Spectrins do not fulfill their role as single molecules. They form α-β heterotetramers, assembling laterally aside each other to form a dimer first. This lateral association is highly conserved. The α- and β-spectrins show high affinity to each other and to date, no independently existing α- or β-spectrins have been reported yet. The head to head assembly occurs through the partial triple-helical repeats at the C-terminus of the β-spectrin and the N-terminal part of the α-spectrin, resembling to the assembly between triple helices within a SR. In this assembly, the EF-hand domain of the α-spectrin and the CH-domains of the β-spectrin are juxtaposed to each other. Actin binding of the heterotetramers happens through β-spectrins. No actin binding activity has been reported in α-spectrins, though they are required to support their β partners, possibly to promote their proper activity (Norman and Moerman 2002). Such a heterotetramer is about 3-6nm in diameter, 55-65nm at its resting length but it can reach 200-260nm when stretched (Bennett and Baines, 2001; Machnicka *et al.*, 2012).

Recent work tried to answer how such a three to five-fold extension could be achieved with the maintenance of the heterotetramer's structural integrity. They modeled how the spectrin heterotetramer could function (Brown *et al.*, 2015). Their model has been based on recent knowledge on spectrin heterotetramers and proposes that it can undergo a seamless threefold extension under forces and can stay linear because it functions like a Chinese finger trap (Fig. 26).

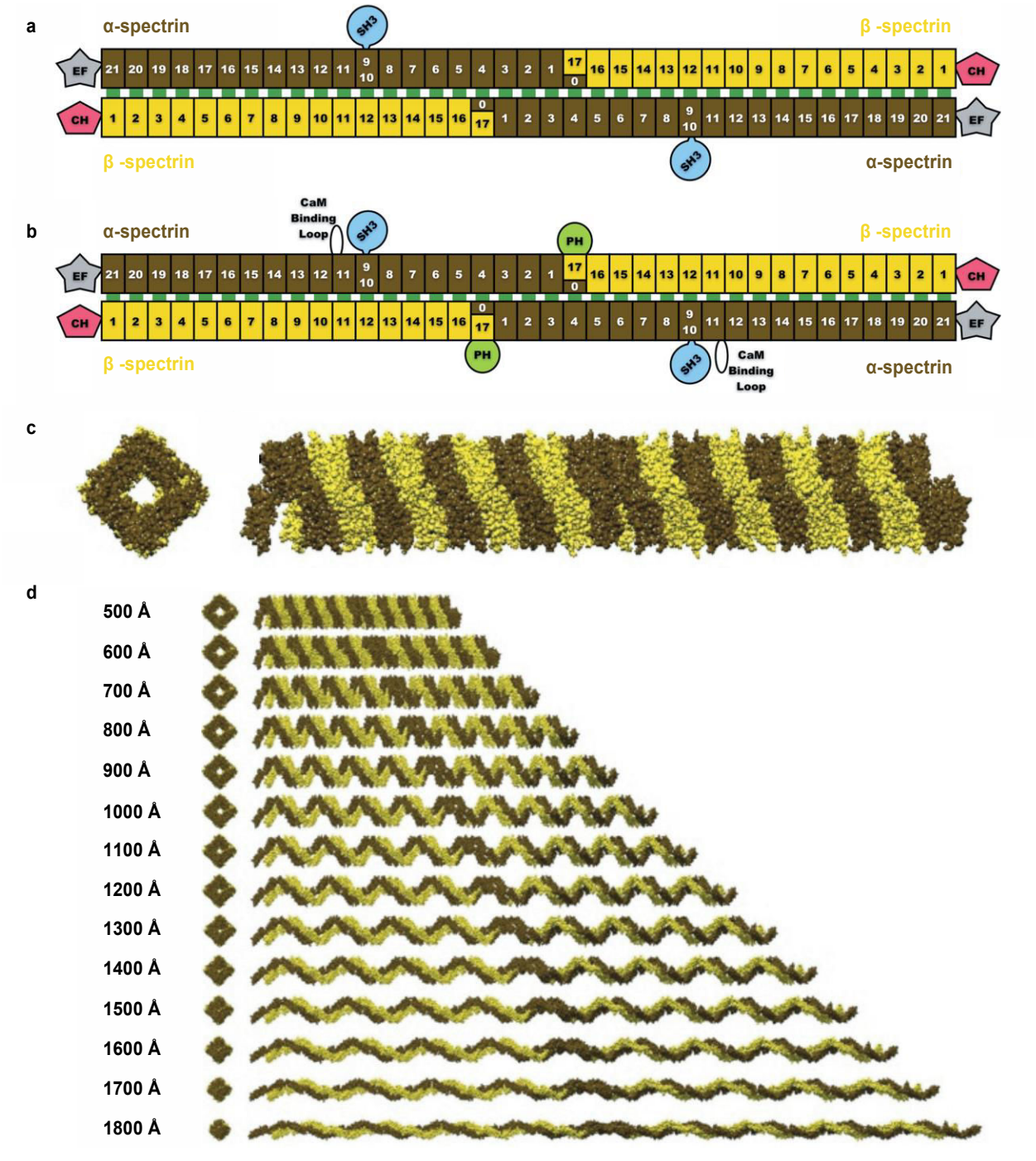

Figure 26: The "Chinese Finger Trap" model of spectrin.
Cartoon representation depicting the domain organization of **(a)** erythroid and **(b)** nonerythroid spectrin tetramers (α-spectrin—brown SRs; β-spectrin—yellow SRs). The pink pentagons labeled CH are the actin binding domains other known spectrin domains are labeled EF, SH3 and PH. **(c)** End and side views of the SRs that comprise each tetramer are arranged in a similar fashion to the geometry reported by McGough & Josephs, 1990. **(d)** The proposed mechanism by which spectrin can undergo a threefold extension, while remaining a linear filamentous polymer.
Adapted from Brown *et al.*, 2015.

At its shorter “resting” state, the heterotetramer forms a hollow cylinder. During its extension in length, the pitch of the SRs increases and the internal diameter of the cylinder decreases (Brown *et al.*, 2015). Apart of modeling, the authors confirmed their hypothesis with experimentally supported data: by the crystal structure of chicken α-spectrin tandem SRs, by structural mass spectroscopy and by electron micrographs of the full spectrin dimers and heterotetramers from erythrocytes (Yan *et al.*, 1993; Pascual *et al.*, 1997; Isparo *et al.*, 2010; Mehboob *et al.*, 2010). Nevertheless, this model still leaves unanswered questions behind. For instance, it is not based on a native, full heterotetramer and it does not address either the alternative SR-SH3 conformations in α- or βH-spectrins. However, it proposes an interesting alternative that could help to reach a more detailed understanding on the complexity of the spectrin skeleton.

III.5. *C. elegans* life cycle and its embryonic development

The life cycle of *C. elegans* consists of the embryonic stage, four larval stages (L1-L4) and adulthood (Fig. 27). *C. elegans* embryogenesis takes places after ventral enclosure and lasts for 12-16 hours at 20°C. The L1 larva hatches with 558 nuclei and many immature tissues (Sulston and Horvitz, 1977; von Ehrenstein and Schierenberg, 1980; Sulston et al, 1983; Bird, and Bird, 1991). At this point the L1 larva will begin postembryonic development where it will grow five-fold in length and ten-fold in breadth before achieving adulthood (Slack and Ruvkun, 1997, Ambros, 2000). The L1 larval stage lasts for 16h, each of the following three stages (L2-L4) last for 10-12h. Each larval stage is separated by a molting event, where the larva forms a new cuticle (apolysis) and sheds the old cuticle (ecdysis). 12h after molting from L4, young adults start egg production that they continue for 2-3 days (until they run out of the self-produced sperm). After their fertile period they can live for several more weeks before their senescence and death. In case of challenging conditions (crowd or starvation) *C. elegans* can activate an alternative life cycle: L2 molts into an alternative L3 larva called “dauer”, that has a completely sealed cuticle with enhanced resistance against external perturbation until conditions get optimized (Cassada and Russell, 1975). Then they shed the dauer cuticle and continue as slightly different L4 larvae (Corsi *et al.*, 2015).

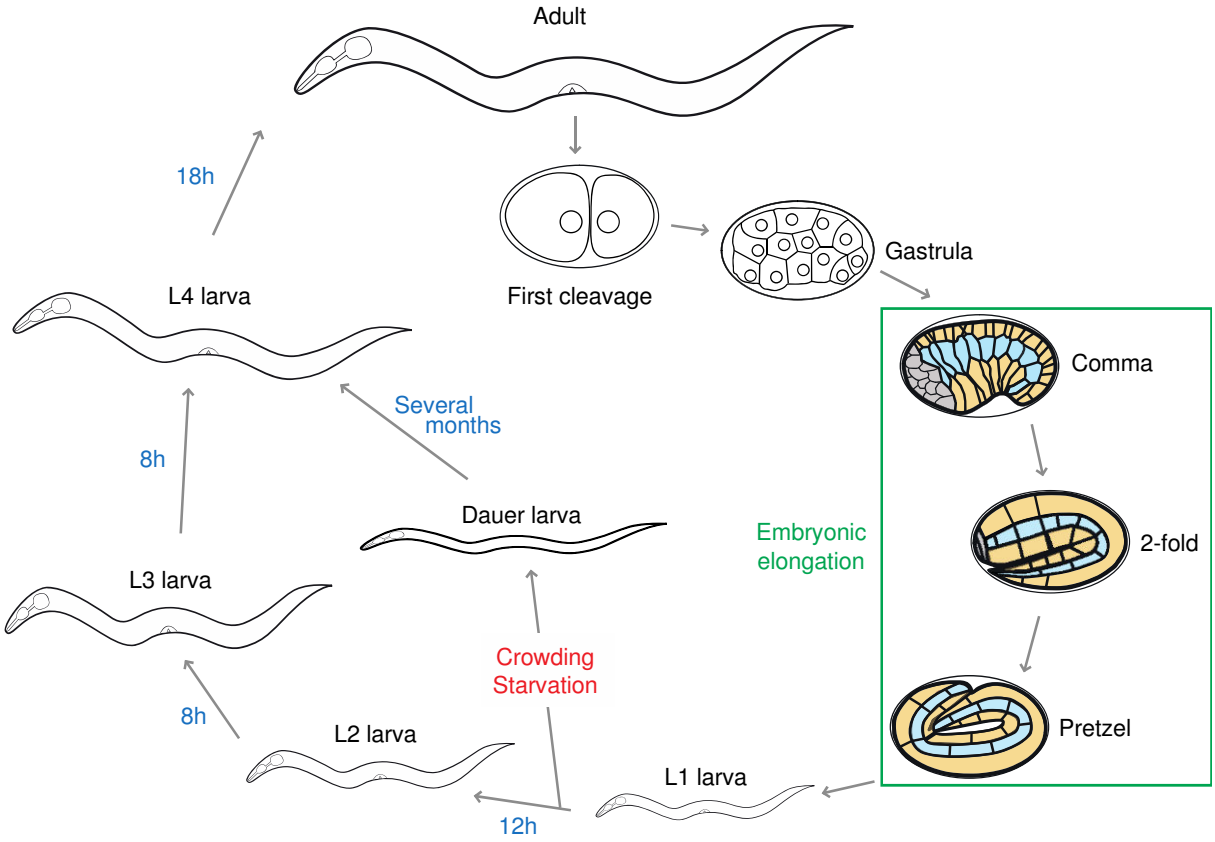

Figure 27: Schematic representation of the life cycle of *C. elegans* at 20°C.
C. elegans life cycle starts with fertilization and numerous cell divisions. First cleavage occurs at about 40 min. post-fertilization. Eggs are laid outside at about 150 min post-fertilization and during the gastrula stage. The embryonic elongation is highlighted in green, as it will be of main interest for the following work. After hatching, the larva goes through four larval stages before becoming an adult. Numbers in blue along the arrows indicate the length of time the animal spends at a certain stage.
Adapted from WormAtlas (wormatlas.org).

C. elegans embryogenesis is divided into, first, a proliferative phase (350 minutes), which covers formation of embryonic founder cells and gastrulation and second, the organogenesis/morphogenesis (490 minutes) during which the embryo gains a vermiform shape (Schierenberg *et al.*, 1980; Sulston *et al.*, 1983). I will first briefly describe the proliferative phase and then focus in more details on the elongation phase.

After fertilization, the single cell embryo begins a series of highly stereotyped cell divisions (Sulston *et al.*, 1983). Proliferation events take place within the uterus and then continue in later stages, including gastrulation and morphogenesis after the embryo is laid.

The *C. elegans* epidermis consists of 71 major and 11 minor epidermal cells, rising after the 9th and 10th round of cell divisions, respectively. Minor epidermal cells form the extreme head and tail epidermis; major ones form most of the epidermis (Gendreau *et al.*, 1994; Page *et al.*, 1997; Page and Johnstone, 2007). Terminal divisions of the epidermis precursors lead to the following organization: dorsally two rows of ten cells, along the antero-posterior axis; flanking both sides of the dorsal cells one row of lateral or "seam" cells; and two rows of ventral epidermal cells at the very lateral edges. Only 10 minutes after these divisions of epidermal precursors, the two rows of dorsal epidermal cells also undergo a morphogenetic event, called dorsal intercalation, to line up in a single row. They develop pointed basolateral protrusions towards the midline, intercalate with their contralateral neighbors and elongate until they reach the seam cells of the opposite side (Sulston *et al.* 1983; Williams-Masson *et al.*, 1998). Shortly after the beginning of dorsal intercalation, at the 30 cells stage, the ventral epidermal cells on both edges also start their morphogenetic process, called ventral enclosure. Ingressing cells become internalized and create a depression, called the ventral cleft that needs to disappear to enable further development. They migrate into the center of the embryonic mass to eventually create separate ectodermal, endodermal, and mesodermal compartments. Surrounding ventral neuroblasts move therefore towards the ventral midline after 230-290 minutes after the first cleavage, to close the ventral cleft. About an hour following ventral cleft closure, early epidermal morphogenesis can start (Chisholm and Hardin 2005).

III.5.1. Overview of the embryonic elongation

The beginning of morphogenesis overlaps with the end of gastrulation, when most cells have ended proliferation and are joining tissue subgroups. Cells become structurally specialized to adopt shapes and cell contents that reflect their eventual cell fates within specialized tissue compartments (Ding *et al.*, 2004; Chisholm and Hardin, 2005). Most epidermal cells begin to form multinucleated syncytia, with the disappearance of intervening cell membranes (Podbilewicz, 2000). Epidermal cell fusions normally follow a well-defined order and timing, though it can vary (Mohler *et al.*, 1998). Once the embryo's developing tissues begin to form a longer worm-like shape, they become folded within the eggshell. Early elongation events begin around 350 min after the first cleavage and involve both microfilaments and MTs. Moving through the comma, two-fold and finally the three-fold stage, the embryo increases its length along the A/P axis by four times and decreases its circumference by three times until it is ready for hatching (Fig. 28).

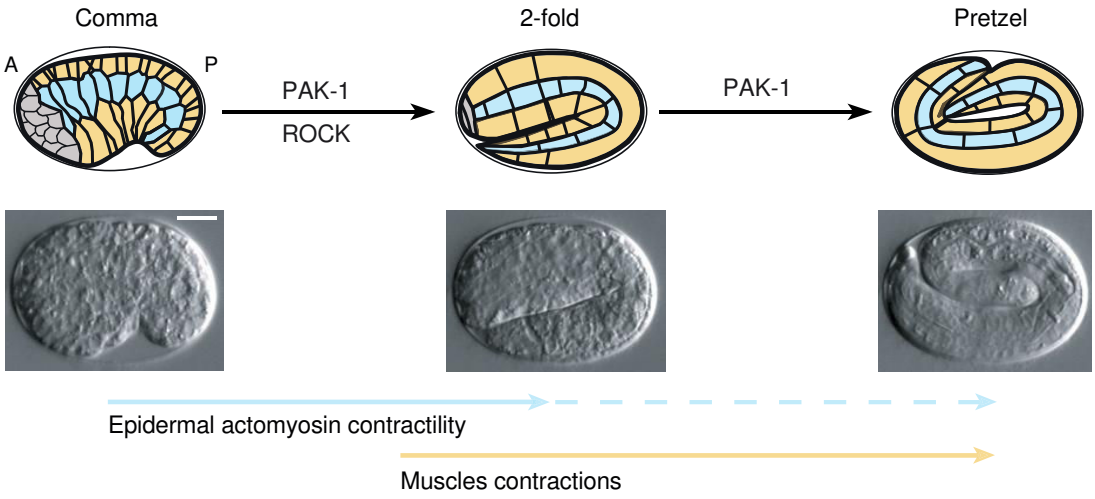

Figure 28: Schematic representation of the embryonic elongation of *C. elegans.*
During its embryonic elongation, the length of the embryo is multiplied by a factor 4 and its circumference is reduced by a factor 2.5. This 3-hour process is affected only by cell shape changes and not by the division or intercalation of cells. The first phase (or early elongation) depends on a ROCK-promoted actomyosin force in seam cells (blue) and actin-promoted stiffness in D/V cells (yellow). The second phase then requires repeated muscle contractions (yellow arrow), which induce a PAK-1-dependent mechanotransduction pathway. A/P, Anterior/Posterior.

It is important to mention that, unlike in *Drosophila* and zebrafish embryonic development, there is no cell division, cell intercalation nor cell migration (Sulston *et al.*, 1983) but only cell shape changes of the D/V and lateral epidermis. These changes are allowed by two main driving forces of *C. elegans* embryonic elongation: the epidermal actomyosin contractility in the lateral cells throughout the entire process and muscle activity beneath the epidermis observed at 475 min after fertilization (around 1.7-fold stage) (Aridel *et al.*, 2017; Gieseler *et al.*, 2017). The elongation can thus be divided into two phases: the early elongation – before muscles become active and the late elongation – after muscles become active (Chisholm, 2015) (Fig. 28). Thus, it requires the interplay of not only epithelial cell groups, but also of different tissue layers. Terminal differentiation occurs without many additional cell divisions ((Sulston *et al.*, 1983). In rare cases, specific cells undergo a delayed apoptotic cell death in the embryo or in the L1 larva after fulfilling their role in tissue morphogenesis.

III.5.2. Early elongation

Early elongation refers to the period between comma and 2-fold stages before muscles become active. During early elongation, the epidermis starts to go through shape changes, as can be most easily observed in the lateral epidermis: they shorten themselves along the dorsal/ventral (D/V) direction and lengthen themselves along the A/P direction. However, the perimeter of these lateral epidermal cells stays the same during early elongation (Vuong-Brender *et al.*, 2017). Genetic and pharmacological studies have shown that epidermal actomyosin contractility is crucial for elongation since the beginning of this process. The actin filaments and the MTs start to organize into more and more regular, circumferential, parallel bundles in the DV cells, associated to the membrane (Priess and Hirsh, 1986; Costa *et al.*, 1997; Williams-Masson *et al.*, 1997; Costa *et al.*, 1998;). This organization also happens in the lateral cells but with a slight delay and to a less regular extent. Interestingly, epidermal actomyosin contractility is mostly needed in the lateral cells, the DV cells seem to passively accommodate to the early embryonic lengthening (Chisholm and Hardin, 2005; Diogon *et al.*, 2007). Epidermal actomyosin contractility driving this first phase of elongation is regulated by the Rho kinase, LET-502, and the serine/threonine p21 activated kinase PAK-1. An evolutionary conserved, actin microfilament associated Rho-GAP/RGA-2 behaves as a negative regulator of LET-502/ROCK. RGA-2 is needed only in the D/V cells and co-localizes with the circumferential actin bundles. Its lack unleashes myosin contractions in the DV cells, which exert pulling forces on the circumferential bundles and indirectly on the CeAJs as well. This effect can be clearly seen on hypercontracted *rga-2* mutants. The small GTPase RHO-1 is the preferred target of RGA-2 *in vitro*, and acts between RGA-2 and LET-502 *in vivo* (Diogon *et al.*, 2007). Moreover, the assembly of myosin II filaments, but not actin microfilaments, depends on the myosin regulatory light chain (MLC-4) and essential light chain MLC-5. Earlier work showed that phosphorylation of two evolutionary conserved MLC-4 serine and threonine residues is important for myosin II activity and organization. Myosin II filaments can be inactivated through their dephosphorylation by the myosin phosphatase, MEL-11. Additionally, the joint loss of ROCK-PAK, or ROCK-MRCK, completely prevented embryonic elongation. It suggests that ROCK and MRCK regulate MLC-4 (Wissmann *et al.*, 1999; Piekny *et al.*, 2003; Gally *et al.*, 2009). The presence of both these regulators is vital for proper elongation: *let-502* null mutants fail to elongate, while *mel-11* mutation causes a “hypercontracted” phenotype with bulges and rupture. On the other hand, simultaneous lack of *let-502* and *mel-11* suppress each other, showing that they are antagonists and argue, for the need for another kinase activity in parallel to ROCK (Wissmann *et al.*, 1997; Wissmann *et al.*, 1999). In vertebrate smooth muscle, this redundant pathway is activated by Calmodulin and myosin light chain kinase (Somlyo and Somlyo, 2000). However, in *C. elegans*, there is no obvious myosin light chain kinase homolog

(Batchelder *et al.*, 2007). The *C. elegans* redundant also pathway includes FEM-2 (PP2c phosphatase). Indeed, *fem-2* mutations genetically enhance and suppress mutations of *let-502* and *mel-11*, respectively. Although *fem-2* mutations alone show only weak elongation defects, no elongation occurs in *let-502; mel-11; fem-2* triple mutants because both redundant pathways are inactive (Piekny *et al.*, 2000).

Overall, *C. elegans* embryonic epidermal cells to undergo a smooth muscle-like actin/myosin-based contraction redundantly controlled by LET- 502/Rho kinase and MEL-11/myosin phosphatase in one pathway and FEM-2/PP2c phosphatase and PAK-1/p21-activated kinase in a parallel pathway(s). In addition, it has also been shown that early elongation can be regulated, not only through myosin, but also through the remodeling of actin filaments. Although actin microfilaments surround the embryo, the force for contraction is generated mainly in the lateral epidermal cells whose actin microfilaments appear qualitatively different from those in their dorsal/ventral neighbors. The actin nucleator FHOD-1, a formin homologue, has been shown to be specifically involved in organizing actin filaments in the contractile lateral cells (Vanneste *et al.*, 2013, Refai *et al.*, 2018). Indeed, *fhod-1* mutants show microfilament defects in these cells. *fhod-1* also genetically interacts with *let-502, mel-11, fem-2* and *pak-1*. However, *fhod-1* regulation of microfilaments preferentially acts with *let-502* and *mel-11*, and in parallel to *fem-2* and *pak-1*. Thus, FHOD-1 may contribute to the qualitative differences in microfilaments found in the contractile lateral epidermal cells and their non-contractile dorsal and ventral neighbors (Vanneste *et al.*, 2013). In mammalian systems, autoinhibition of FHOD1 is relieved by Rho kinase, after which the FHOD1-nucleated actin filaments, in turn, respond to Rho kinase-mediated contraction (Gasteier *et al.*, 2003; Hannemann *et al.*, 2008; Takeya *et al.*, 2008; Iskratsch *et al.*, 2013). However, since *fhod-1*-like actin defects are absent in *let-502/*Rho kinase mutants (Norman and Moerman, 2002; Piekny *et al.*, 2003, Gally *et al.*, 2009). *C. elegans* FHOD-1 appears not to require Rho kinase activation during elongation.

III.5.3. Late elongation

When *C. elegans* embryos reach 1.7-fold to 1.8-fold, muscles located beneath the dorsal and ventral epidermis start to become active. The actomyosin contractility is still present but is thought to become less important for elongation (Diogon *et al.*, 2007). The epidermis, the ECM and muscles form a feedback network that controls embryonic elongation. In this network CeHDs are well positioned to integrate multiple signals and influence other cellular processes. Previous work from our laboratory unraveled a mechanotransduction pathway in which muscle contractions indeed

trigger the elongation beyond the 2-fold stage. It transforms the mechanical input, provided by muscle contractions into a biochemical signaling pathway acting in the D/V epidermis that leads to CeHD remodeling (Zhang *et al.*, 2011). Muscles strongly contract and stretch the epidermis, exerting longitudinal stress upon it. In turn, the epidermis senses this mechanical input by a yet unidentified molecular component that induces the recruitment of GIT-1 adaptor protein, which in turn activates its binding partner guanine-nucleotide exchange factor PIX-1, CED-10 and PAK-1 to the CeHDs. As a result, PAK-1, as a terminal effector of the pathway phosphorylates the IFs, which promotes CeHD remodeling. PAK-1 is a particularly important player in our system. It is one of the three PAK proteins found in *C. elegans* that are CePAK1 (PAK-1, related to the mammalian group I PAKs), CePAK2 (PAK-2, related to the mammalian group II PAKs) and MAX-2 (related to *Drosophila* DPAK3). Among them PAK-1 is the best studied. It has a highly conserved, catalytic C-terminal kinase domain and a prolin-rich N-terminal regulatory domain, also called GTPase-binding CRIB domain or p21-binding domain (PBD). As already mentioned, PAK-1 forms a signaling module along with PIX-1 (PAK interacting exchange factor) and GIT-1 (G protein-coupled receptor kinase interactor). Within this complex, PAK-1 is most commonly activated in a GTPase-dependent way by CED-10 (*C. elegans* RAC1 homolog) and CDC-42. Its localization near the junctions and the muscle attachment sites positions PAK-1 at the very center of force transmission within the *C. elegans* embryonic epidermis, where this highly conserved kinase functions as a terminal effector of elongation in multiple pathways (Gally *et al.* 2009; Zhang *et al.* 2011). As it regulates embryonic elongation relying both on chemical and physical signals, PAK-1 is an ideal starting point to understand the interplay of epithelial morphogenesis and mechanotransduction in development. Therefore, the idea to gain a better view on the molecular landscape around PAK-1 during *C. elegans* embryonic elongation became the initial motivation of this project. Indeed, while muscle defective mutants with no effective tension on the epidermis arrest midway through elongation at the two-fold stage (paralyzed at two-fold stage or Pat phenotype), *git-1, pix-1* and *pak-1* mutants are viable, suggesting that parallel pathways must also exist for this regulation. It is these parallel pathways that I investigated during my PhD.

IV. Aim of this thesis

Our understanding of *C. elegans* embryonic elongation largely increased in the past twenty years. Muscle activity is a key player for *C. elegans* morphogenesis during late elongation, however how it promotes embryo elongation is not entirely understood yet. Our laboratory identified a mechanotransduction pathway downstream of muscle input but also investigated redundant signaling pathways that could contribute to late elongation. As PAK-1, effector kinase, is an important regulator of both early and late elongation, it became the starting point of our interaction tests. The work of Gabriella Pasti, former PhD student, identified SPC-1, the α-spectrin as a strong interactor of PAK-1. The joined loss of function of the two genes leads to a drastic phenotype of elongation failure that we qualified as « retraction ». Thus, this interaction became the starting point of my PhD project aiming to answer:

- How do SPC-1 and PAK-1 interact to the “lock” the elongation?
- Are there other players involved in this process?

As it is also well described that actin cytoskeleton plays a key role cell shape changes and that the ratchet mechanism emerged as a general feature of epithelial mechanics, we wondered if it could be applicable to our system. Therefore, I also tried to answer:

- To which extend is the actin cytoskeleton important for elongation?
- How do actin cables get remodeled over time?
- Can we model the progressive elongation of the embryo to understand how the forces contribute to the remodeling of the actin?

MATERIAL AND METHODS

Animal strains, conditions of maintenance

The list of strains used is presented in Table 5. Animals were propagated on NGM agar plates as described previously (Brenner, 1974). Animals were held at a standard 20°C temperature except for the measurements of hatchlings implicating *sma-1(ru18)*, in which case L4 animals were shifted to 15°C before egg laying and measures were performed on their offsprings. However, the growth curves of *sma-1(ru18)* were performed at 20°C. The *gsnl-1(tm2730)* and *viln-1(2413)* were outcrossed three times.

Yeast Two Hybrid Screening

Yeast two-hybrid screening was performed by Hybrygenics Services (Paris, France). The bait component was the N-terminal 294 amino acids of PAK-1 (including the regulatory region of the protein) fused as a C-terminal fusion to LexA. The construct was used as a bait to screen at saturation a highly complex, random-primed *C.elegans* embryo cDNA library (Gomes *et al.*, 2013). Screening involved a mating approach on a medium lacking Trp, Leu and His, supplemented with 0.5 mM 3-aminotriazole (Fromont-Racine, Rain and Legrain, 1997). The strongest hits of the screen can be found in Supplementary Table 1. Reciprocal screens using the spectrin repeat #9 or the SH3 domains of SPC-1 as baits identified PAK-1 region 160-206, and no other meaningful prey in the context of the present study.

RNAi screens

A RNAi screen was performed in the *pak-1(tm403)* mutant along with a wild-type control. A collection of 356 essential genes from the Ahringer RNAi library (Kamath *et al.*, 2003), including adhesion proteins, signaling proteins, phosphatases, kinases, cytoskeleton-associated proteins and proteins important in epithelial morphogenesis, was assembled (Table 1), based on a previous screen performed in the *git-1(tm1962)* background (C. Gally and M. Labouesse, unpublished). The screen was performed in liquid culture on 96-well plates and RNAi knockdown was induced by feeding as described (Gally, Zhang and Labouesse, 2015). The primary screen was based on enhanced lethality and body morphology defects; the secondary screen focused on very short larvae and elongation defects. Gabriella Pàsti, former PhD student, took DIC images for body length measurements and performed DIC time-lapse imaging for the strongest candidates. She and I performed two additional RNAi screens. First, she used a *spc-1(ra409)* mutant carrying an unstable extrachromosomal rescuing *spc-1::gfp* marker to look for potential enhancers of the *spc-1(ra409)* elongation defects. She selected for this enhancer screen genes that had given the strongest defects in the initial screen with

356 genes (Table 4). In both cases, young L1 hatchlings were inspected for the presence/absence of a fluoresent *spc-1::GFP* signal and photographed using either a Leica DMI4000 (1st screen) or Leica DM6000 (2nd screen) microscope. Length of the young larvae was measured using the ImageJ software. Second, with the help of Flora Llense, associate professor in the team, I likewise used a *spc-1(ra409) pak-1(tm403)* strain carrying an unstable extrachromosomal rescuing *spc-1::gfp* marker to look for potential suppressors of the retraction phenotype. I selected 13 actin related proteins from the Ahringer RNAi library (Kamath *et al.*, 2003), including that were recently reported to modulate actin remodelling in the early embryo (Naganathan *et al.*, 2018) (Table 3). RNAi was induced by RNAi feeding on L4 larvae maintained at 20°C, and the progeny was analyzed 20h to 30h post-feeding; for early acting essential genes (*cyk-1, pfn-1, unc-60*), animals were maintained at 15°C, and the progeny was analyzed 16h to 20h post-feeding still inducing more than 14% early embryonic defects.

For specific genes (*spc-1*, *pak-1*, *fhod-1*, *vab-10b, unc-112*), RNAi was induced by injection after preparing the double-stranded RNA (dsRNA) with the Ambion mMessage mMachine® Kit and purifying the dsRNA with the Qiagen RNeasy® MinElute® Cleanup Kit (Bosher *et al.*, 2003). The embryos were analyzed from 24h to 48h post-injection. In one case, experiments involving the strain *spc-1(ra409) pak-1(tm403); mcEx1016[spc-1(+)::GFP; Pmyo-2::RFP]* (displayed in Figs.), RNAi against *unc-112* was induced by feeding because the strain barely survived the regular microinjection procedure.

Fluorescent translational reporter constructs

SPC-1::GFP and PAK-1::mKate

A 12633 bp genomic sequence including the *spc-1* coding sequence and a 3 kb promoter was inserted in frame with the GFP coding sequence present in the pPD95.75 vector (Addgene, Cambridge USA). To create the *Ppak-1::pak-1::mKate* reporter construct, first an mKate-containing backbone was created by exchanging the GFP-coding sequence of the pML1572, P*lin-26::vab-10(ABD)::GFP* plasmid (Gally *et al.*, 2009). In a following cloning step a 8204 bp genomic sequence, including the *pak-1* coding sequence and a 4.5 kb promoter was inserted in frame with the mKate coding sequence present in the vector.

To test if SPC-1::GFP could rescue the function of SPC-1, Gabriella and I first crossed the different transgenic animals of a wild-type background with *mnDp33; spc-1(ra409)* animals (strain DM3409), and F1 transgenic males again with DM3409 to establish *mnDp33; spc-1(ra409); Ex[spc-1::GFP]*. Rescuing transgenes were recognized because all viable progeny was GFP-positive and all (or most)

non-viable progeny was GFP-negative, reflecting the loss of the *mnDp33* balancer. To attempt *mnDp33* segregation, she repeatedly transferred single GFP-positive mothers over four generations and examined their progeny, starting from at least two independent extrachromosomal arrays per construct. Thereby, she successfully obtained viable *spc-1(ra409); Ex[Pspc-1::spc-1(+)::gfp]* animals, and then viable *spc-1(ra409) pak-1(tm403); Ex[Pspc-1$_1$::spc-1(+)::gfp]* animals through crossing and meiotic recombination, which segregated very short retracted GFP-negative embryos.

FHOD-1 full length and alternative constructs

For the FHOD-1 constitutively active construct, Flora deleted part of the FH2 domain and the DAD domain of a 8283 bp genomic sequence of *fhod-1* (gift from David Pruyne, (Mi-Mi *et al.*, 2012)) and inserted it under the control of the epidermis-specific 432 bp *dpy-7* promoter. Deletion of the DAD alone was obtained by inserting back the FH2 domain in the FH2/DAD deleted construct using Hifi DNA assembly cloning Kit (New England Biolabs); the FH1/FH2 deleted construct was obtained by deleting the FH1 domain using the Q5® site directed mutagenesis Kit protocol (New England Biolabs). All cloning steps relied on the use of the Phusion High-Fidelity DNA Polymerase reaction Kit (Fisher Thermo-Scientific); the constructs were subsequently verified by sequencing. The constructs were injected at 10 ng/µl plasmid construct, with 150 ng/µl pBSK + 5 ng/µl pCFJ90 (P$_{myo-2}$*::mcherry*) as co-injection markers for the *spc-1::gfp* constructs, or 100 ng/µl pRF4 (rol) co-injection marker for *pak-1::mKate*.

LifeAct::mMaple3 photoconvertible construct

For *LifeAct::mMaple3*, I amplified LifeAct from the pML36 plasmid (*Pdpy-7::LifeAct::GFP* generated by a previous post-doc of the lab, Thanh Vuong-Brender) and mMaple3 from the pCU97 plasmid (which was codon optimized for *C. elegans* by Saurabh Tak, a former PhD student of the lab). Both fragments were assembled by Gibson technique (Gibson *et al.*, 2009 ; Gibson, 2011) using the NEBuilder® HiFi DNA Assembly Gibson Cloning Kit and then were purified using Qiaprep® Spin Miniprep Kit. The sequence was verified by GATC sequencing. First I wanted to use this construct to generate a transgenic line by mos1-mediated Single Copy Insertion (mosSCI), a method to insert a single copy of a transgene into a well-defined location in the *C. elegans* genome. (Frøkjær-Jensen *et al.*, 2008; Frøkjær-Jensen *et al.*, 2014). However I decided to use a more recent approch, derived from the classical CRISPR-Cas9 system, that allows to produce integrations from extra- chromosomal arrays (Yoshina *et al.*, 2015). The first injection mixture consisted of 10ng/µl of the template, 100ng/µl of pBSK, and 50ng/µL of pFR60 (dpy-10 repair template, courtesy of the Robin Lab) and was

injected into N2 hermaphrodites. After a few days, Flora proceeded to a second injection into the progeny deriving from the first injection. The second injection mixture consisted of 70ng/µl of pDD162, 100ng/µL of pFR61 (*dpy-10* sgRNA, courtesy of the Robin Lab) and 100ng/µl of pPRF4 (roller). Then she screened for roller worms and separated this F1 them in single plates. She finally screened the F2 for plates where Dpy/Roller worms could be spotted and single cultured these worms. We succesfully obatined the desired strain, unfortunately its level of expression turned out to be too low to be used.

ACT-1::GFP overexpression

To build an extrachromosomal *Pdpy-7::ACT-1::linker::GFP* construct, I amplified multiple fragments separatly first and assembled them in two steps. First, pJET, *Pdpy-7*, *act-1* and linker::GFP have been amplified by PCR respectively from pJET blunt (NEB), pML36, genomic DNA and the plasmid *act-1::linker::GFP* (that will be described in the next paragraph). Then, pJET, *Pdpy-7* and *act-1* were assembled first and a second Gibson inserted linker ::GFP in the previously obtained plasmid. All constructs were purified using Qiaprep® Spin Miniprep Kit. I chose to use a linker as it was shown that small flexible linker contribute not only to the expression efficiency of the protein, but also to the correct folding and corresponding biological activities, especially for polymerizing proteins such as actin (Zhang *et al.*, 2009; Klein *et al.*, 2014). The small linker comes from the GFP::ACT-1 from Erin's Cram lab (Dixon and Roy, 2005; Wirshing and Cram, 2018). This linker is 17 aa long and is about 50% GS. Gs and Ss are usually added to linker to give them better flexibility. The full construction was injected in the worms at a concentration of 10ng/µL with the co-injection markers PRF4 (roller) at 100ng/µl and pCFJ90 (red pharynx) at 2.5ng/µl. The strain obtained was viable but very difficult to work with due to the low transmission of the extrachromosomal array. It was again injected at a concentration of 1ng/µL but we were not able to amplify the strain.

Pdpy-7::GFP overexpression

To build an extrachromosomal *Pdpy-7::GFP* construct, I amplified the desired portion from *Pdpy-7::ACT-1::linker::GFP* described just above by using Q5 technique and Q5® Site-Directed Mutagenesis Kit. The construct has been purified using Qiaprep® Spin Miniprep Kit and its sequence verified by GATC sequencing. Then Flora injected it in the young hermaphrodites in the following concentrations: 5ng/µl of *Pdpy-7::GFP*, 100ng/µl of pRF4 (roller) and 2.5ng/µl of pCFJ90 (red pharynx). We easily amplified the strain by picking the bright green worms at the fluorescent dissecting microscope.

CRISPR/Cas9 fluorescent knock-in transgenic worm generation

For the following constructs, Saurabh designed some of the different templates needed. Flora, cloned and injected for SMA-1::GFP. And Loan Bourdon, technician of the lab, injected the mixes in the worms for the other constructs.

I followed the established protocols for genome editing by use of CRISPR/Cas9.

ACT-1 / SMA-1 / SPC-1

I first used the method described in (Dickinson *et al.*, 2013). We used the Megawhop or Gibson techniques (Miyazaki and Takenouchi, 2002; Gibson *et al.*, 2009; Gibson, 2011) to build the homology repair template. I first amplified a 2 kb segment on the Carboxy-terminus or the Amino-terminus of the target gene from genomic DNA and cloned it into the pJET1.2 vector (from Thermo Fisher Scientific). I then inserted the fluorescent tag sequence (GFP, mMaple, mCherry or wrmScarlet) in a way that 1500 bp are before it and 500 bp are after it for a construction in C-terminal or the reverse for a construction in N-terminal. These 1500 bp and 500 bp segments function as homology arms. Additionally, I inserted the same small linker as mentioned above between the target gene sequence and the fluorescent tag sequence for ACT-1 and SPC-1. The small linker was amplified from the GFP::ACT-1 from Erin's Cram lab (Dixon and Roy, 2005; Wirshing and Cram, 2018) and then was cloned into the repair template plasmids by Gibson with the NEBuilder® HiFi DNA Assembly Gibson Cloning Kit. As the linker was extremely small (51bp) compared to the plasmid (between 5.5kb and 8kb) I tried to insert it into; I had to adjust several times the Gibson mix. I used www.crispr.mit.edu to select a Protospacer Adjacent Motif (PAM) site. PAM site in the template was mutated (without changing the protein sequence) to prevent the plasmid and the repaired genomic locus from being cleaved by Cas9. For the synthesis of single guide RNA (sgRNA), two strategies were used. Either I cloned the sgRNA sequence in pDD162 plasmid (that also encodes Cas9 under a germline promoter) by Gibson cloning. Or I cloned the sgRNA sequence in the pML2840 plasmid and used the pDD162 expressing the Cas9. pML2840 was derived from PIK198 (from AddGene), Shashi Kumar Suman, a post-doc from the lab, modified it so it would be compatible to easily insert the sgRNA sequence by PCR. This second strategy allowed me tune the sgRNA concentration (especially decrease it when it seems that it is toxic) in the injection mix without changing the Cas9 concentration (Katic, Xu and Ciosk, 2015). All constructs were purified using Invitrogen Purelink™ Quick Plasmid miniprep Kit or Qiaprep® Spin Miniprep Kit. The injection mixture consisted of 50-100ng/µl of the repair template, 25-50ng/µl of the sgRNA-Cas9, the injection markers 100ng/µl of pRF4 (roller) and 2.5ng/µl of pCFJ90 (red pharynx). When they were synthetized

separated, the sgRNA was injected at 25ng/µL and the Cas9 at 50ng/µL. Young adults were then injected into both gonades with this mixture and kept at 20°C. The F1 progeny was screened for roller and/or red pharynx, which were separated and genotyped by PCR to look for positive insertions after egg laying. A positive hit was defined by the specific band amplified from a fluorescent marker internal primer and a primer outside of the repair template. GATC sequencing of the transgenic lines was performed to confirm the CRISPR events. The CRISPR generated strains were further tested for fluorescence using dissecting microscope.

Sequence of the linker: TGCCCGGGGGATCGGTGGAGCTCCACCGGTGGCGGCCGCTCTAGAACTAGT

UNC-70

I also used the method based on Self-excising drug selection cassette (Dickinson *et al.*, 2015). I amplified 700 bp arms flanking the site of insertion from genomic DNA by using Thermo Scientific Phusion High-Fidelity DNA polymerase. The plasmids pJJR82 and pJJR83 were predigested with AvrII and SpeI for Carboxy terminal insertion and with ClaI and SpeI for Amino terminal insertion. The left and right arm were assembled with the digested plasmid by using NEBuilder® HiFi DNA Assembly Gibson Cloning Kit. As for the first strategy, I used www.crispr.mit.edu to select a PAM site and then mutate it. I synthetized the sgRNA by cloning its sequence into the pDD162 plasmid. The resulting plasmids were then injected in the gonads of young adult worms. The F1 progeny was screened specifically for rollers with no red pharynx. Screening in the F2 generation allowed to separate the homozygotes rollers. They were then given a temperature shock at 32°C for 4-5 hours to excise the cassette. The insertion of the fluorescent tag was confirmed by GATC sequencing.

Table recapitulating the different strategies used

	CRISPR strategy	Repair template successfully cloned	sgRNA	Injected in the worms	CRISPRs events in worms
ACT-1::GFP	Homology-directed repair	Yes	Yes, in pDD162	Yes	Yes but the worms never showed any fluorescence
ACT-1::linker::GFP	Homology-directed repair	Yes	Yes, in pDD162	Yes	Yes but the worms never showed any fluorescence
GFP::ACT-1	Homology-directed repair	No	Yes, in pDD162	No	
GFP::linker::ACT-1	Homology-directed repair	Yes	Yes, in pDD162 and pML2840	Yes	Yes but the worms never showed any fluorescence
ACT-1::mMaple3	Homology-directed repair	Yes	Yes, in pDD162	Yes	No
ACT-1::linker::mMaple3	Homology-directed repair	Yes	Yes, in pDD162	No	
mMaple3::ACT-1	Homology-directed repair	Yes	Yes, in pDD162	No	
mMaple3::linker::ACT-1	Homology-directed repair	Yes	Yes, in pDD162	No	
SMA-1::GFP	Homology-directed repair	Yes	Yes, in pDD162	Yes	Yes. Strain viable and working well
SPC-1::GFP	Homology-directed repair	Yes	Yes, in pML2840	No	
SPC-1::mCherry	Homology-directed repair	Yes	Yes, in pML2840	No	
SPC-1::wrmScarlet	Homology-directed repair	Yes	Yes, in pML2840	Yes	Yes, but wrmScarlet is not fluorescent in the embryo
UNC-70::mCherry	Self-excising drug selection cassette	Yes	Yes, in pDD162	Yes	No, due to screening errors

Fluorescence imaging

DIC images for time-lapse videos were obtained using a Leica DM6000 microscope with a Leica LAS-AF software, using a Leica DMRXA2 upright microscope equipped with a Peltier platform. Observations were done under a 40X oil immersion objective. Mothers were cut up to gain early-staged embryos, which were then transferred onto thin 5% soft agarose pads in a drop of M9. Z stack image series with a 1,5 µm Z step distance were taken in every 5 minutes during 6 to 10 hours. ImageJ software was used to quantify the embryonic length from the end of ventral enclosure/onset of elongation, by taking a "segmented line" through the midline of the embryos from head to tail. To image the coupling between actin bundles displacement in the epidermis and muscle contractions, Gabriella used a double reporter strain carrying the epidermal *Pdpy-7::LifeAct::GFP* and muscle *Pmyo-3::his-24::mCherry* transgenes (ML2113, see Table 5), and a spinning-disk DMI6000 Leica microscope equipped with an Andor software (experiments for Fig. 1). Series of five Z planes (1 epidermal + 4 muscle) were imaged continuously for 5 min, with 0,5 µm Z steps and no averaging. The time interval between two Z series was 360 ms. I measured the actin displacement according to the same strategy, using a CSUX1-A1 spinning-disk mounted on a Zeiss Axio Observer Z1 inverted microscope with a Roper Evolve camera controlled by the Metamorph software, and a 100x oil immersion objective (experiments for Fig. S9). A Z-stack of 4 focal planes with 0,5 µm step size was acquired using a streaming acquisition mode. The time between two acquisitions was 0.41 second during 300 time frames. To synchronize embryos, mothers were put on an empty NGM agar plate to lay eggs for a short time window, and embryos were left to develop until the stage of interest. (For the analyse of the contraction see next section on **Image analysis.** To analyse the *in vivo* o-localisation between PAK-1::mKate, ABD::mcherry and SPC-1::GFP, Gabriella used the Zeiss/Roper spinning-disk microscope under a 100X oil immersion objective, keeping the laser intensity at a constant level throughout the experiments. Image processing and computing the co-localisation coefficient was done using the Volocity software.

TIRF-SIM imaging

Embryos were mounted between 22 mm square cover glasses (thickness of 0.170±05 µm, Carl Zeiss Microscopy GmbH, Jena, Germany) and 25×75 mm teflon-coated glass slides with three depression wells. Embryos were embedded in 2 µl water containing Polybeads® acrylate microspheres of 15.4±1.43 µm diameter (Polysciences, Inc). Wild-type embryos were at 1.8 to 2-fold stage; *spc-1(RNAi) pak-1(tm403)* embryos were aged between 2-fold and 3-fold equivalent for a control embryo. TIRF-SIM images (Gustafsson, 2000; Kner *et al.*, 2009) were acquired on a DeltaVision OMX SR imaging system from GE Healthcare Life Sciences equipped with a 60× oil

immersion objective from Olympus (PlanApo N 60x 1.42 NA). To minimize spherical aberrations, Pierre and I used Cargille labs immersion oil with a n_D at 25°C (5893 Å) = 1.5140 ± 0.0002. Imaging was performed using the excitation at 488 nm with laser transmission ranging from 75 to 100% and integration time ranging from 2 to 3 ms. For each embryo, time series of 50 to 100 TIRF-SIM images of 256 x 256 pixels (pixel size of 80 nm) were acquired. Each TIRF-SIM image corresponds to a set of 9 images (3 phases at 3 angles) acquired within 90.6 to 99.6 ms. Reconstruction of TIRF-SIM images (final pixel size after reconstruction is 40nm) were performed with the softWoRx software (Applied Precision, Inc) which in turn enables a resolution enhancement by a factor of 2 leading to a final lateral resolution in the order of 100 nm.

Image analysis and quantification of actin filament contraction, continuity and orientation

The analysis of mechanical displacement in the epidermis was performed on the movies of the dorso-ventral actin layer by measuring the distance over time between two landmarks across the region of contraction. The landmarks were set manually on a frame showing relaxed tissue and tracked all over the contraction till the subsequent relaxed state. Landmarks tracking was performed using a statistical template matching approach (Mathhews, Ishikawa and Baker, 2004). The method was implemented as an ImageJ plugin (http://sites.imagej.net/Julienpontabry/), giving as output the landmarks locations, their distance across time and the Kymographs. The curves show a pre-contraction state, a minimum (the maximal contraction point) and an ending part where the distance progressively increases again (see Fig. 1B'' and Fig. S9). After a smoothing and interpolation of the curves, the starting, ending and maximal contraction points were extracted by studying the time derivative of the distance and by setting a threshold on the distance itself. Finally the contraction time was computed as the difference between the ending time and the initial time. The quantification of bending angles was done using a similar strategy; the angles were measured on single bundles at the frame of maximal deformation in a contraction cycle (see figure S5). The analysis of the curves and statistics were done using a MATLAB script. All images were analysed using the ImageJ (FiJi) software (NIH, Bethesda, Maryland, USA; http://rsb.info.nih.gov/ij/) and MATLAB R2015b (The MathWorks Inc., Natick, MA). To study the features of actin pattern, I imaged embryos that were put to sleep by oxygen deprivation through a high concentration of bacteria with the Zeiss/Roper spinning-disk using a 100X oil immersion objective. For each experiments, a Z-stack of 16 focal planes with 0,2 µm step size was acquired. On the original maximum z projection created by imageJ, a manual Region of Interest (ROI) was defined on the dorso-ventral cells (Fig. 2 and Fig. S3) from which a high pass filter in the Fourier space was applied to select only structures smaller than 10 pixel of diameter (Fig. 2 and Fig. S3).

Continuity: The filtered ROIs were binarized by setting to one all the pixels with a value bigger then zero and setting to zero all the other pixels. The resulting structures were then fitted by ellipses from which the length of the Major axis was extracted as a measure of the length of the actin filament. The longer actin filaments are those presenting a more uniform fluorescence along their length (showing higher continuity). By contrast, short segments result from discontinuity in the fluorescence signal. To avoid noise only segments longer than 4 pixels have been considered for the analysis.

Anisotropy of the orientation: The same filtered ROI used for continuity measurements were used to measure the distribution of cable orientation. Fast Fourier Transform (FFT) of these ROIs was computed in order to work in the frequency domain and more easily identify repetitive patterns. The resulting power spectrum of the ROIs was represented in polar coordinates in order to extract the distribution of angles of ROI pattern (Gonzalez and Woods, 2006). The method was implemented in an ImageJ plugin (http://sites.imagej.net/Julienpontabry/), giving as output the angular distribution. In order to compare the distributions coming from different images the distributions were normalized by their integral (Fig. 2 and Fig. S3). The more the pattern consists in structures oriented in a preferred direction (the more anisotropic), the highest is the peak of the distribution in that direction. In the case of an isotropic pattern, the angular distribution should show a flat behavior. As an estimate of the pattern anisotropy, the prominence of the highest peak of the angular distribution was considered (Fig. 2 and Fig. S4). The analysis of the angular distributions and statistics was performed by a MATLAB script. All images were analysed using the ImageJ (FiJi) software (NIH, Bethesda, Maryland, USA; http://rsb.info.nih.gov/ij/) and MATLAB R2015b (The MathWorks Inc., Natick, MA). All MATLAB scripts used for the present analysis are available upon request.

Straightness: For each embryo Teresa Ferraro, engineer in the team, selected an ROI containing the region above the muscles based on a contraction pattern. She selected ROIs containing about ten actin bundles, and she segmented manually seven of them for each ROI (the number of bundles that were on average well resolved). For each bundle she computed the 'Straightness' as the ratio between the length of the segmented bundle and the distance between the initial and final points of the bundle. This quantity has an upper limit equal to one for perfectly straight lines. The manual segmentation and 'Straightness' calculation were performed with a custom made MATLAB interface.

Bundle organization: For each embryo, we measured the relative contrast in the image between the regions occupied by actin filaments and those in-between as a proxy for bundle composition and organization. The reasoning was that in the extreme case where bundles defasciculate to generate individual filaments, each filament is likely to have a lower intensity than a bundle made of several filaments, and the contrast between filaments and the intervening space would be less sharp. This should result in a lower variance or standard deviation of the image intensity compared to a wild-type bundle image. To do so we divided the standard deviation by the average intensity.

Statistical Analysis

For elongation curves, standard deviation was measured. For L1 length measurement and rescue experiments I perform unpaired t-test using GraphPad Prism 5.00 (San Diego, California, USA) and Excel. For contraction time, actin continuity and orientation, Teresa and I applied for all genotypes a paired t-test using MATLAB.

RESULTS

RESULTS

I. Introduction to the results

Morphogenesis is a process determining the shape, structure of tissues, organs and developing organisms. More specifically, embryonic morphogenesis refers to changes in the shape and position of cells within the embryo, especially in the epithelium. The importance of epithelial morphogenesis has been reported in crucial developmental processes like gastrulation or neural tube formation (Chisholm and Hardin, 2005; Colas and Schoenwolf, 2001; Davidson, 2012). A primary component of morphogenesis is the actin cytoskeleton, which drives the cell shape changes, cell division or migration characterizing morphogenesis. Recent studies have emphasized the role of the mechanical forces powered by actomyosin contractility and of cortical tension in driving cell shape change (Lecuit and Lenne, 2007; Salbreux *et al.*, 2012). In other organisms, actin and myosin II filaments undergo rapid and dramatic apical flows in the minute range (Martin *et al.*, 2009; Munro *et al.*, 2004) and in different tissues (He *et al.*, 2010; Kim *et al.*, 2011; Munro *et al.*, 2004; Rauzi *et al.*, 2010; Roh-Johnson *et al.*, 2012; Solon *et al.*, 2009). The pulsatile activity of myosin II induces cell deformations because they are interspersed with phases of cell shape stabilization, in a process analogous to a mechanical ratchet (Martin *et al.*, 2009; Mason *et al.*, 2011). However, *C. elegans* elongation does not involve myosin II pulsatile flows, but instead requires the input of muscle contractions providing the necessary mechanical force (Waterston *et al.*, 1989; Williams and Waterston, 1994). Moreover, *C. elegans* muscles contract every few seconds (Zhang *et al.*, 2011), at a time scale where cells exhibit a mostly elastic behavior (Salbreux *et al.*, 2012) whereas in *Drosophila* the ratchet powered by actomyosin flows occurs every few minutes (Martin et al, 2009; Rauzi *et al.*, 2010; Solon *et al.*, 2009) at a time scale where cells mainly exhibit a viscous behavior. Together, the fact that tension changes are causes by an extrinsic factor and are rapid could mean that the mechanism involved in stabilizing epidermal cells are different from those observed in *Drosophila*.

Therefore, *C. elegans* provides an anatomically simple and integrated model to study the cellular impact of mechanical forces, which does not depend on pulsatile actomyosin flows (Vuong-Brender *et al.*, 2017) as described in other cells (Munro *et al.*, 2004; Martin *et al.*, 2009; Rauzi *et al.*, 2010; Gilmour *et al.*, 2017).

We investigated how the epidermis, an elastic material, acquires progressively its shape through cycles of muscle contractions, while extending only in the antero-posterior (A/P) direction. More precisely, we characterized how cells adapt in response to mechanical input from muscles and

how the cytoskeleton remodels during this process. Previous work of the lab had shown that these contractions promote the remodeling of the CeHDs (structures connecting the epidermis to the muscles) through a mechanotransduction pathway involving the kinase PAK-1 (Zhang *et al.*, 2011; Labouesse, 2011). Through genetic and molecular screens, we identified SPC-1, the alpha-spectrin, as a partner of PAK-1 and showed that together they stabilize the shape of the full embryo by impacting on actin remodeling through several actin-related proteins.

II. Previous work: molecular and functional screens identify SPC-1 as a potential PAK-1 partner

During *C. elegans* embryonic elongation, the length of the embryo increases while its circumference decreases. As we already discussed it in the introduction, muscular activity is crucial for the elongation to proceed beyond the 2-fold stage. Because of their tight mechanical coupling to the epidermis through the hemidesmosomes (CeHD), muscle contractions mechanically impact on the epidermis. To prove it, a former PhD student of the lab, Gabriella Pàsti, manually tracked the displacement of both actin and muscle nuclei. She chose landmarks on the two tissues that she could track for a full cycle of contraction on short spinning-disk time-lapses, at the 2-fold stage of wild-type embryos. She developed a semi-automated analysis of the recordings to generate kymographs. From this tracking she extracted the distance between landmarks and normalized it to the maximal length (relaxation state). From the curves, she extracted the starting, ending and maximal contraction. She observed that the A/P displacement of circumferentially oriented epidermal actin filaments closely mirrors that of muscle nuclei (Fig. 1a-a''). Importantly, all muscles do not contract simultaneously; when some areas of the epidermis were longitudinally compressed (red line), others were stretched (green line) before eventually relaxing (Fig. 1b-b"). The relaxation observed after each muscle contraction raises a conundrum: how can muscle activity power embryonic elongation from 100 µm to 200 µm within an hour if cell elasticity brings cells back to their initial length after each contraction. One simple hypothesis would be that some mechanism stabilizes the transient cell shape induced by muscle activity. For instance, during *Drosophila* gastrulation and germband extension actomyosin pulsatile flows are thought to modify junctions (Rauzi *et al.*, 2010; Simoes *et al.*, 2014; Vasquez *et al.*, 2014).

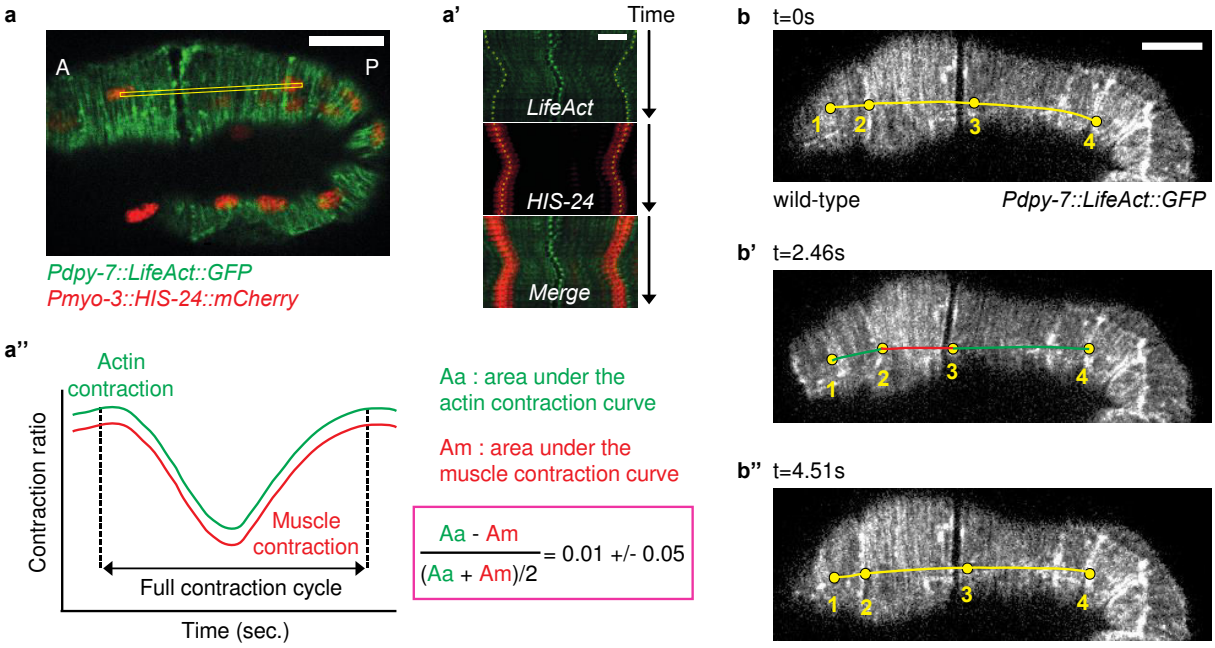

Figure 1: Muscle contractions deform the epidermis due to their mechanical coupling.
(a-a''') Spinning-disk micrograph of epidermis actin filaments (green) and muscle nuclei (red) in a wild-type 2-fold embryo. Scale bar: 10 µm. **(a')** Kymographs (yellow rectangle area in **a**) illustrate the concurrent displacement of epidermal actin and muscle nuclei. **(a'')** Quantification of the area below the resulting displacement curves (pink box) (n=11, contractions=33). **(b-b")** A muscle contraction/relaxation cycle illustrating its local impact on epidermal actin filaments in a wild-type 2-fold embryo (timing above). Yellow (relaxation), red (compression), green (stretching) distances between four landmarks (denoted 1-4): **(b)** [1-2], 7.8 µm; [2-3], 19.8 µm; [3-4], 24.6 µm. **(b')** [1-2], 9.4 µm; [2-3], 13.6 µm; [3-4], 26.2 µm. **(b")** [1-2], 8.0 µm; [2-3], 19.2 µm; [3-4], 25.0 µm.

II. 1. SPC-1 and PAK-1 loss leads to a retraction of the embryo

To uncover this mechanism, she focused on the kinase PAK-1, which mediates mechanotransduction (Zhang *et al.*, 2011) and regulates myosin II (Gally *et al.*, 2009; Vuong-Brender *et al.*, 2017; Campbell *et al.*, 2019). Two screens were performed: a feeding RNAi screen in a strong *pak-1* yet viable mutant, looking for enhanced embryonic lethality (Fig. 2a) and a yeast-two hybrid screen taking the N-terminal domain of PAK-1 as a bait (Fig. 2b). The RNAi screen identified the gene *spc-1* encoding α-spectrin as a strong *pak-1* genetic enhancer. Indeed, *spc-1 pak-1* embryos elongate up to 1.5- fold and then retract to 1-fold. These short hatchlings (~58 µm) were significantly shorter than *pak-1(tm403)* (~178 µm) or *spc-1(RNAi)* (~91 µm) hatchlings (Fig. 2c, Table 1). The yeast two-hybrid screen identified the central Src Homology 3 domain (SH3) of SPC-1, embedded within the large, 9th spectrin repeat domain (SR9), as an interactor of the N-terminal domain of PAK-1 (Fig. 2b, Table 2). Together, both screens pointed to a functional interaction between SPC-1 and PAK-1 during axis elongation.

To understand why *pak-1(tm403) spc-1(RNAi)* embryos are shorter than *spc-1(RNAi)* embryos, she examined their elongation rate using DIC microscopy. Wild-type and *pak-1(tm403)* embryos initially elongated at the same rate, while *spc-1* defective embryos elongated slower and stopped around the 2-fold stage as previously described (Norman and Moerman, 2002) (Fig. 2d). By contrast, *spc-1(ra409) pak-1(tm403)* and *spc-1(RNAi) pak-1(tm403)* embryos reached ≈65 µm at a slow rate, but then could not maintain their shape, retracting back to ≈50 µm, which neither *spc-1(ra409)* nor *pak-1(tm403)* embryos did (Fig. 2d,h, Movie 1).

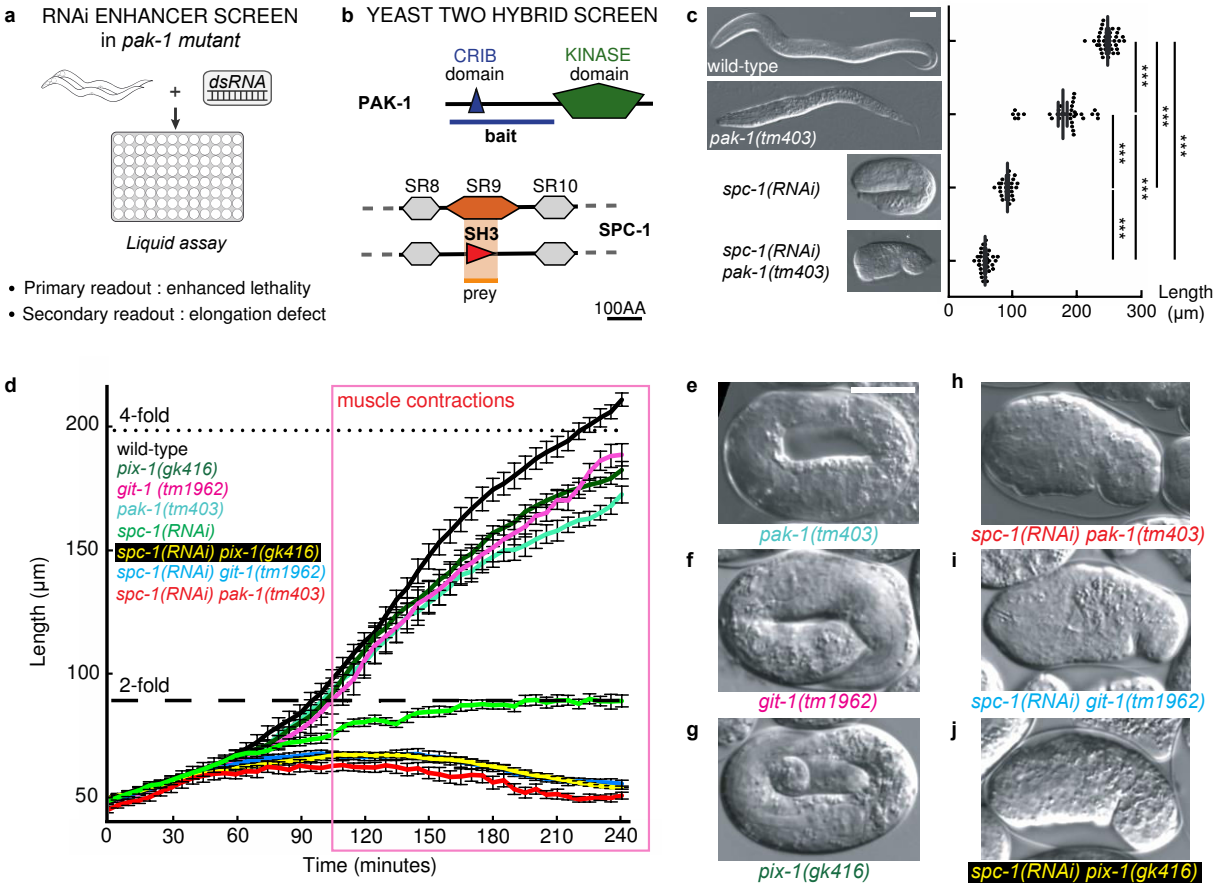

Figure 2: Combined loss of PAK-1 and SPC-1 triggers embryo retraction.
(a) RNAi screen in a *pak-1* mutant identified *spc-1* as an enhancer (Table 1). **(b)** A yeast two-hybrid screen using the PAK-1 N-term domain as a bait identified the SPC-1 SH3 domain as a prey (orange background) (Table 2). **(c)** DIC pictures and quantification of newly hatched wild-type body length (n=38), *pak-1(tm403)* (n=32), *spc-1(RNAi)* (n=26) and *spc-1(RNAi) pak-1(tm403)* (n=36). Scale bar: 25 µm (*wt and pak-1*), 10 µm (*spc-1 and spc-1 pak-1*). Data represent mean values ± SD. Two-sided paired t-test. **(d-j)** Loss of the proteins GIT-1 and PIX-1, acting upstream of PAK-1 in the mechano-transduction pathway promoted by muscle contractions, in the absence of *spc-1* also triggers a retraction phenotype. **(d)** Elongation curves and **(e-j)** terminal phenotypes of wild-type (n=12), (**e**) *pak-1(tm403)* (n=11),**(f)** *git-1(tm1962)* (n=10), (**g**) *pix-1(gk416)* (n=10), *spc-1(RNAi) (n=8),* (**h**) *spc-1(RNAi) pak-1(tm403)* (n=9), (**i**) *spc-1(RNAi) git-1(tm1962)* (n=11), (**j**) *spc-1(RNAi) pix-1(tm416)* (n=8). Pink box, period of muscle activity. Scale bar: 17 µm. Data represent mean values ± SEM.

As mentioned earlier, muscle tension is important for embryonic elongation (Williams and Waterston, 1994; Zhang *et al.*, 2011). When muscle activity is inhibited, elongation is halted, and embryos are paralyzed at 2-fold stage. Muscle tension is responsible for compressing and squeezing the epidermis laterally. As a result, epidermis experiences a tension inducing the recruitment of GIT-1 and PIX-1, acting upstream of PAK-1, to the CeHDs. Therefore, CeHD remodel via PAK-1 / PIX-1 / GIT-1 signaling promoting embryonic elongation. We could have expected mutants for these three genes to be arrested at 2-fold. However, *git-1(tm1962), pix-1(gk416)* and *pak- 1(tm403)* mutants are viable although shorter than wild-type at hatching (Fig. 2d-g) suggesting the existence of at least a parallel pathway to the one described before (Zhang, Landmann *et al.* 2011). This idea was confirmed by *spc-1* knockdown in *git-1* or *pix-1* mutants, which induced retraction phenotype as the one just described in *spc-1 pak-1* embryos (Fig. 2d-j).

II. 2. This retraction phenotype depends on the muscle input

This last observation led her to think that the retraction phenotype could be linked to muscle activity. This idea was supported by the fact that *spc-1(RNAi) pak-1(tm403)* embryos started to retract at the onset of muscle contractions in control embryos (box in Fig. 2d). To directly prove this, she abrogated muscle function in *spc-1(ra409) pak-1(tm403)* embryos by knocking-down the kindlin homolog UNC-112 (Rogalski *et al.*, 2000). When UNC-112 is absent in wild-type background, it leads to disruption of myofilament attachment structure, causing a 2-fold arrest. Strikingly, *spc-1(ra409) pak-1(tm403)* embryos defective for *unc-112* no longer retracted (Fig. 3a,f ; Movie 2). In addition, I verified that the joint loss of SPC-1 or PAK-1 along with UNC-122 would not lead to short embryos similar to a retraction phenotype due to the loss of muscle activity. Indeed, *unc-112(RNAi); pak-1(tm403)* and *unc-112(RNAi) spc-1(ra409)* behaved very similarly to *unc-112(RNAi)* (Fig. 3a,c,d); supporting the rescue of the retraction by *unc-112(RNAi)* in *spc-1 pak-1* background. We conclude that the mechanical input provided by muscles to the epidermis induces the retraction phenotype observed in *spc-1 pak-1* double mutants.

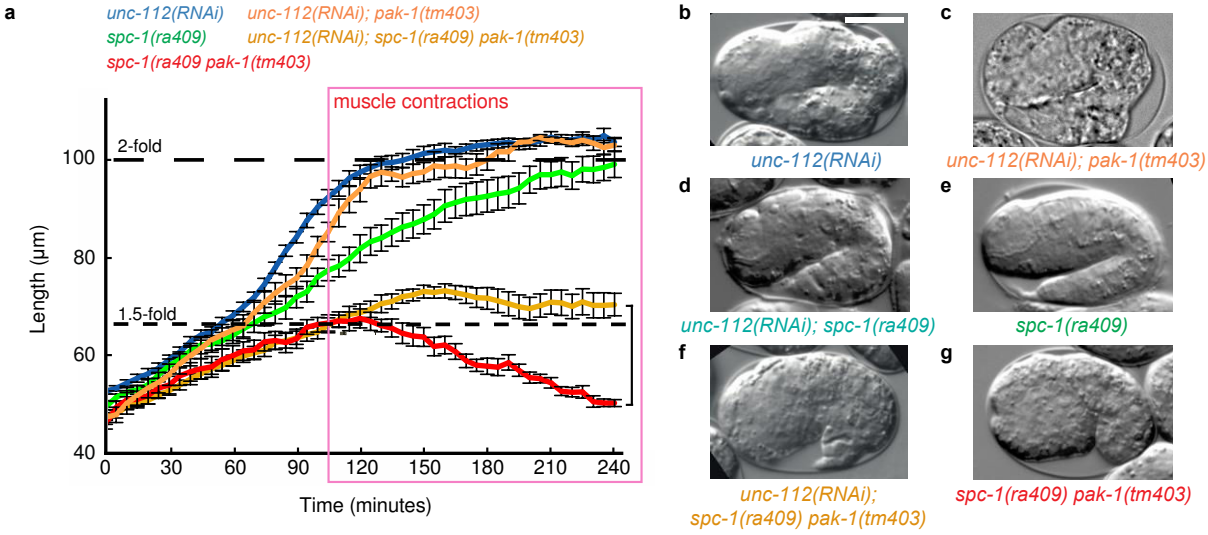

Figure 3: *spc-1 pak-1* retraction is muscle dependent.
(a) Elongation curves and **(b-g)** DIC pictures showing the terminal phenotypes of **(b)** *unc-112(RNAi)* (n=14), **(c)** *unc-112(RNAi); pak-1(tm403)* (n=8), **(d)** *unc-112(RNAi); spc-1(ra409)* (n=4), **(e)** *spc-1(ra409)* (n=8), **(f)** *unc-112(RNAi); pak-1(tm403) spc-1(ra409)* (n=7), **(g)** *spc-1(ra409) pak-1(tm403)* (n=8). Pink box, period of muscle activity; bracket, extent of retraction. **(d)** Terminal phenotype of *unc-112(RNAi); spc-1(ra409)* obtained by inducing *unc-112(RNAi)* in the strain ML2436 bearing a rescuing extrachromosomal *spc-1::gfp* array and looking for embryos having lost the array; we could only obtain a few embryos of the desired phenotype despite numerous repeats (n=4), which all had the phenotype illustrated here and is similar to that of *spc-1(ra409)* alone. Scale bar: 17 µm. Data represent mean values ± SEM.

III. PAK, SPC-1, SMA-1 co-localize with actin near the epidermal cell membrane

III. 1. PAK-1 and SPC-1 localize along the actin filaments

A previously proposed role of SPC-1 is the maintenance of proper actin distribution (Norman and Moerman, 2002). SPC-1 is supposed to ensure this role through forming heterotetramers with β-spectrins. In *C. elegans* embryos, the apical localization of βH-spectrin and the lateral localization of βG-spectrin both have been reported (Praitis *et al.*, 2005; Hammarlund *et al.*, 2000). To examine how SPC-1/PAK-1/actin physical interaction could occur in the epidermis, we first looked at the potential co-localization of these actors. New constructs of SPC-1::GFP and PAK-1::mKate have been developed by Gabriella. Her spinning-disk images of the new PAK-1::mKate reporter allowed to see a more subtle, previously less-described localization of PAK-1 near the cortex in *C. elegans* embryos (Fig. 4a). Image processing and computing the co-localization coefficient was done using the Volocity software. The XZ and YZ projections better highlighted these regions of co-localization at the level of the apical cortex. They showed a high level of *in vivo* co-localization at the uppermost apical region of the epidermis, near the cell membrane and at the level of junctions. This localization pattern was

highly reminiscent to actin expression (Fig. 4a,c). As the interaction between the spectrin and actin cytoskeleton has been reported both in erythroid and non-erythroid cells, in several model organisms (including *C. elegans* embryos) (Baines, 2009; Bennett and Baines, 2001; Korsgren and Lux, 2010; Korsgren *et al.*, 2010 ; Machnicka *et al.*, 2012), it was reasonable to suspect that PAK-1 and SPC-1 also co-localize with actin. Therefore, under the same conditions just described, she performed an *in vivo* co-localization test between our SPC-1::GFP and an ABD_{VAB-10}::mKate reporter. Although a strong intestinal and cytoplasmic expression of SPC-1::GFP on maximal Z-projection images made it difficult to observe the most apical SPC-1 localization, on the single Z merge images and on the co-localization channel a clear co-localization can be detected between SPC-1 and actin at the cortical regions, near the cell membrane and the junctions (Fig. 4b,d).

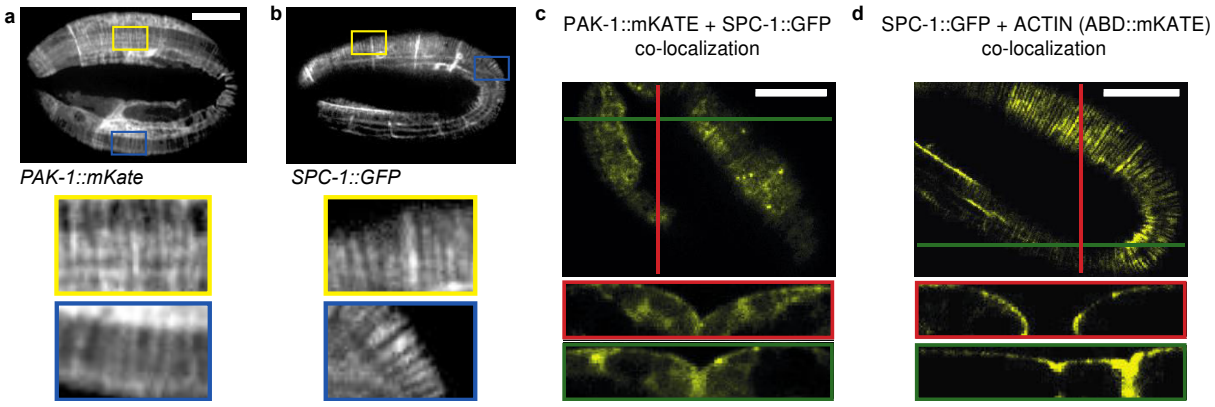

Figure 4: PAK-1 and SPC-1 colocalize with actin filaments.
(a-b) Distribution of (a) PAK-1::mKate (n=20) and (b) SPC-1::GFP (n=13) in a late embryo. Enlarged pictures of PAK-1 and SPC-1 showing a filamentous distribution in the dorso-ventral (D/V) epidermis similar to actin filaments. Scale bar: 10 µm. **(c)** Fluorescence pictures of PAK-1::mKate (red) and SPC-1::GFP (green) (n= 20): the panel shows the colocalization image for the most apical focal planes (top image), and full XZ (green panel) and YZ (red panel) projections. The level of co-localization is high based on Pearson's correlation coefficient (0.7-0.9, n=20). The highest level of co-localization is detected at the apical cortex**. (d)** Fluorescence pictures of *Plin-26::*VAB-10(ABD)::mKate (red) and SPC-1::GFP (green) (n=8): the panel shows the colocalization image for the most apical focal planes (top image), and full XZ (green panel) and YZ (red panel) projections. The level of co-localization is high based on Pearson's correlation coefficient (0.7-0.9, n=8). The co-localization is almost exclusively detected at the apical cortex. The gene *lin-26* drives expression in the epidermis; VAB-10(ABD) corresponds to the two actin-binding domains (calponin homology) of the protein VAB-10. Scale bar: 10 µm.

III. 2. Super-resolution shows precise co-localization of actin and spectrin cytoskeletons

As it has also been shown that SMA-1 maintains the association between actin and the apical membrane via interactions at its N-terminus (Praitis *et al.*, 2005), I tried to probe it further thanks to Flora Llense, associate professor in the lab, who developed a SMA-1 reporter using CRISPR-Cas9 technology. With this new reporter, I used SIM-TIRF super resolution microscopy to unravel a more detailed organization of the spectrin/actin cytoskeletons. TIRF microscopy allowed us to illuminate our embryos only at the level of the epidermis and SIM microscopy uses spatially structured illumination light in three directions. The reconstruction of TIRF-SIM images requires the acquisition of a minimum of three phase shifts per pattern rotation. Therefore, one final image corresponds to a set of 9 images (3 phases at 3 angles).

To perform the experiment I used a strain combining our SMA-1::GFP to the ABD_{VAB-10}::mKate reporter described in the previous experiment. I acquired short movies of 50 to 100 TIRF-SIM images (about 5-10 seconds) of embryos at the 2-fold stage, when their muscles start to be active. The imaging revealed to be difficult as the embryo would often move faster than the temporal resolution of the microscope. Nevertheless, I could observe colocalization of SMA-1 along actin cables, with a dotted pattern (Fig. 5b). Indeed SMA-1 did not seem to form a continuous signal along the actin cables but rather a succession of small dots.

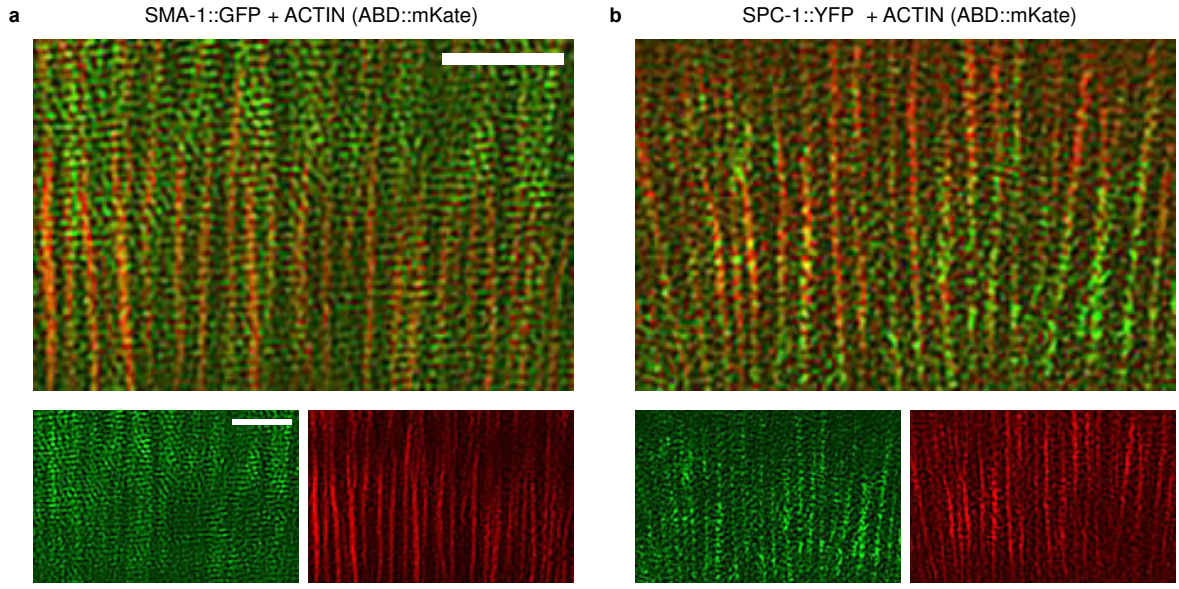

Figure 5: SPC-1 and SMA-1 colocalization with actin filaments is highlighted by TIRF-SIM microscopy.
(a-b) TIRF-SIM snapshots of grouped Z movies to emphasize the colocalization of **(a)** SMA-1 (SMA-1::GFP) (n=20) and **(b)** SPC-1 (SPC-1::YFP) (n=6) with actin bundles (ABD_{VAB-10}::mKate). Scale bar: 2 µm.

Then, I also wondered if TIRF-SIM microscopy could help refine the colocalization between actin and SPC-1 compared to spinning-disk imaging. For this experiment, I used a CRISPR strain of SPC-1 (SPC-1::YFP, ordered from SunyBiotech) instead of the extrachromosomal overexpression strain Gabriella used before. Once again, I crossed this new reporter to ABD_{VAB-10}::mKate. Unfortunately, the signal of SPC-1::YFP appeared very fuzzy and was difficult to work with (Fig. 5a). It seemed that SPC-1 still colocalized with actin but it did not significantly improve our knowledge compare to spinning-disk imaging.

By lack of time I could not perform a lot of acquisitions with these two strains, but I still want to better understand how spectrins and actin interact *in vivo*. Therefore, I am planning more acquisitions using a different approach. I would like to image anesthetized embryos by using sodium sulfite that mimics hypoxic stress (Jiang *et al.* 2011). It would allow me to image the embryos with more ease and at later stages of development (3-fold), when the actin and spectrins pattern will be sharper. I am also planning to work with other reporters. I am currently crossing another SPC-1 CRISPR strain (SPC-1::mKate, courtesy of Erin Cram's lab) to SMA-1::GFP and to *LifeAct::GFP* (another actin reporter that will extensively be discussed in the following results). By changing the reporters, I hope to obtain a better signal and maybe access to the localization of the two spectrins in respect to each other. SMA-1 appears as a succession of dots along the cables and it would be interesting to see if SPC-1 intercalate in between or if it perfectly colocalizes with SMA-1. Overall it would give us a clearer picture of the two spectrins localize and interact with actin during *C. elegans* elongation.

III. 3. Other tools have been developed to investigate actin dynamics

To better understand the interaction between actin and the spectrin cytoskeletons, I examined their localization and dynamics by *in vivo* imaging and super resolution microscopy as presented above. However, the original goal was even more ambitious: further elaborate the internal organization of these actin cables and their precise interaction with the spectrin cytoskeleton. Indeed, the circumferential actin bundles are formed of 5-10 individual filaments of about 7nm each (Priess and Hirsh, 1986; Pásti and Labouesse, 2014). However, nothing is known about the length of the individual filaments and their orientation inside the bundle. Considering data collected from *in vitro* experiments and other systems (Burlacu *et al.*, 1992; Edelstein-Keshet and Ermentrout, 1998; Cooper, 2000; Haine *et al.*, 2015), it seems unlikely that actin filaments could run uninterrupted from one side of the DV cell to the other.

Therefore, we can imagine several scenarios raising the following questions (Fig. 6):

- Are they all orientated in the same direction (either from the junction to the CeHD or the contrary)?
- Are they organized as anti-parallel filaments?
- Can the filaments run uninterrupted from the junction to the CeHD or is the bundle subdivided in more mini-filaments?

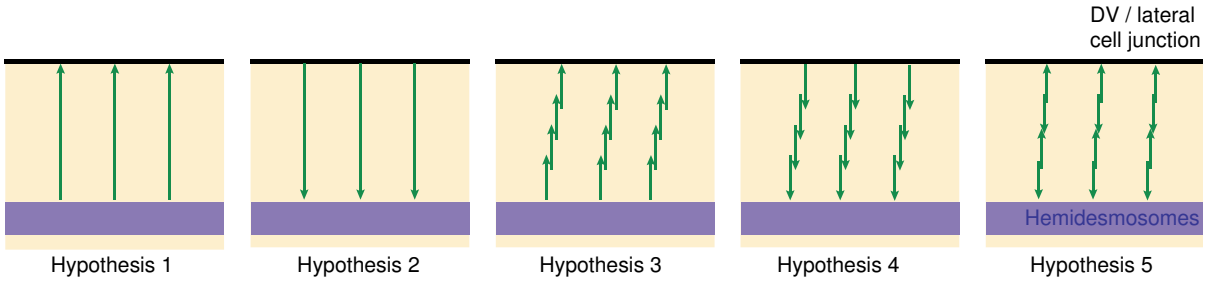

Figure 6: Schematic representations of the different hypothesis about actin organization inside a bundle. Hypothesis 1 and 2: actin bundles are constituted of long filaments going from one DV/lateral cell junction to the CeHDs. Hypothesis 3 and 4: actin bundles are constituted of several smaller filaments all orientated in the same direction. Hypothesis 5: actin bundles are constituted of several smaller filaments in anti-parallel disposition.

It was to address these questions that I initially turned to developing new reporter tools and use super resolution microscopy. To do so, I developed different strategies but most of them remained unsuccessful or unfinished. Here is an overview of what has been tried, what worked and what could be used for experiments in the future.

I tried to build fluorescent marker knock-in of actin and spectrins using CRISPR Cas-9 genome editing strategy. In *C. elegans,* there are five genes encoding for actin: *act-1, act-2, act-3* (redundant, controlling cytoplasmic microfilament function in the early embryo, expressed in the epidermis), *act-4* (expressed in body wall and vulval muscles and the spermatheca), *act-5* (expressed only in intestinal cells and in the excretory cell). Since I am interested in the localization and organization of actin in the epidermis through the embryonic elongation of the worm, I chose to work with ACT-1 to design 8 different constructions, with the help of Saurabh Tak. I started to couple ACT-1 either to GFP or to mMaple3 (photo-convertible protein) at C-terminus or at N-terminus. Once I obtained the four possible combinations, I inserted a linker between ACT-1 and the fluorescent reporter. This linker has been shown to ease the interaction of the tagged proteins as actin forms polymers (Dixon and Roy, 2005; Zhang *et al.*, 2009; Klein *et al.*, 2014; Wirshing and Cram, 2018). Then, with the help of the technician of the lab, Loan Bourdon, I proceeded to injections to obtain CRISPR events in worms. We

tried various injections mixes and although we did not get insertions for all the constructs, we did obtain many CRISPR events visible by genotyping. Unfortunately, I have never been able to spot fluorescence of the constructs in the embryos by spinning-disk imaging. I never obtained a functional tagged protein expression, probably due to the redundancy of the *act* genes. In parallel, I also worked on developing an extrachromosomal ACT-1::GFP construct, that has been successfully injected in the worms at a concentration of 10ng. The strain obtained was viable but very difficult to work with due to the low transmission of the extrachromosomal array. Therefore, with the help of Flora, we tried to generate another strain injected at a lower concentration of 1ng and this time we failed to amplify a viable strain. By lack of time I did not pursue in that direction. However, it could still be interesting to try injections again at different concentrations to generate a viable strain. Similarly, for the actin CRISPR, I did not have enough time to troubleshoot and develop alternative constructs, maybe with other types of linkers or other locations of insertions.

I also worked on building an alternative LifeAct reporter, in case no viable CRISPR strain could be generated for actin. I combined LifeAct to mMaple3, a photoconvertible protein, which turns to red from green on being illuminated by UV light (Wang, Moffitt *et al.* 2014). The goal was to use it for FRAP analysis using spinning microscopy, to get an idea of the dynamics of actin in our system. To generate this strain, with the help of Flora, we used a locus-specific integration of extrachromosomal transgene based on the CRISPR/Cas9 system (Yoshina *et al.*, 2015). We successfully obtained the strain; however, the expression level was not sufficient to perform the experiment we had planned.

In parallel, we used the same CRISPR technology with the three spectrins: the α-spectrin SPC-1 (required for body morphogenesis, formation of body wall muscles, locomotion, and larval development), the $ß_G$-spectrin UNC-70 (required for normal body curvature and shape, normal movement, and correct localization of the α-spectrin SPC-1) and the $ß_H$-spectrin SMA-1 (required for a normal rate of elongation and thus, for a wild-type body length upon hatching*)*. As mentioned above, thanks to Flora, we easily obtained a functional SMA-1::GFP, that could be used for super-resolution. For UNC-70::mCherry the cloning has been done and the plasmids are ready to be injected, if needed in the future. For SPC-1::wrmScarlet, I did obtain a viable strain nicely expressing the tagged SPC-1, but I was really disappointed to realize that wrmScarlet, although extremely bright in the larvae (El Mouridi *et al.*, 2017), is not expressed at all in the embryo. Since this strain turned out to be useless, the cloning for alternative SPC-1::mCherry and SPC-1::GFP constructs has been completed, but again by lack of time, they have not been injected in the worms and we requested the SPC-1::mKate2 strain developed by Erin Cram's lab (Wirshing and Cram, 2018), as mentioned earlier.

Overall, I tried to develop new reporters for actin and spectrin visualization. Unfortunately, most of them were unsuccessful and by lack of time I could not try other strategies. Therefore, all the work that will be discussed later, have been performed using our already existing *dpy-7::LifeAct::GFP* construct.

IV. Genetic interactions of *pak-1*, *sma-1*, *unc-70*, *vab-10b* affects elongation

In most systems, spectrins can fulfill their role only if they form α-β heterotetramers. Therefore it was important to address if, similarly to *spc-1*, *C. elegans* β-spectrin coding genes, *sma-1* (encoding for βH-spectrin, the apical partner of α-spectrin) and *unc-70* (encoding for βG-spectrin, the lateral partner of α-spectrin) could be involved in a genetic interaction with *pak-1*.

As reported previously, the loss of *unc-70* does not affect embryonic elongation; L1 larvae look almost normal (Fig. 7b). The serious larval defects due to the absence of *unc-70* develop gradually during the larval life caused by neuronal problems, adults get paralyzed and dumpy (Hammarlund *et al.* 2000). *unc-70(RNAi); pak-1(tm403)* double mutants were similar to *pak-1* single mutants (Fig. 7c,e). Similarly, to *unc-70*, *sma-1(ru18)* L1 show a 2.5-fold arrest but are viable (Fig. 7d). When *unc-70* is simultaneously downregulated with *sma-1*, they recapitulate, but do not enhance the ~1.7-2fold embryonic elongation arrest of *spc-1* single deficient embryos (Norman and Moerman 2002). And when *sma-1* and *spc-1* are both downregulated, the result is not significantly different from *spc-1* single mutants. Therefore, I wondered if I could recapitulate the retraction phenotype with ß-subunit mutants. But even the triple deficient *unc-70(RNAi) sma-1(ru18); pak-1(tm403)* arrested around the 2-fold stage and never showed a retracted phenotype as *spc-1(RNAi) pak-1(tm403)* does (Fig. 7f-k). Hence, in the absence of PAK-1, the knockdown of each ß-subunit had a milder phenotype than in the absence of SPC-1, even though the $ß_H$-spectrin SMA-1 appeared more important than the $ß_G$-spectrin UNC-70. It suggested that SPC-1 functions in interaction with PAK-1 to stabilize embryonic shape independently of ß-spectrin subunits.

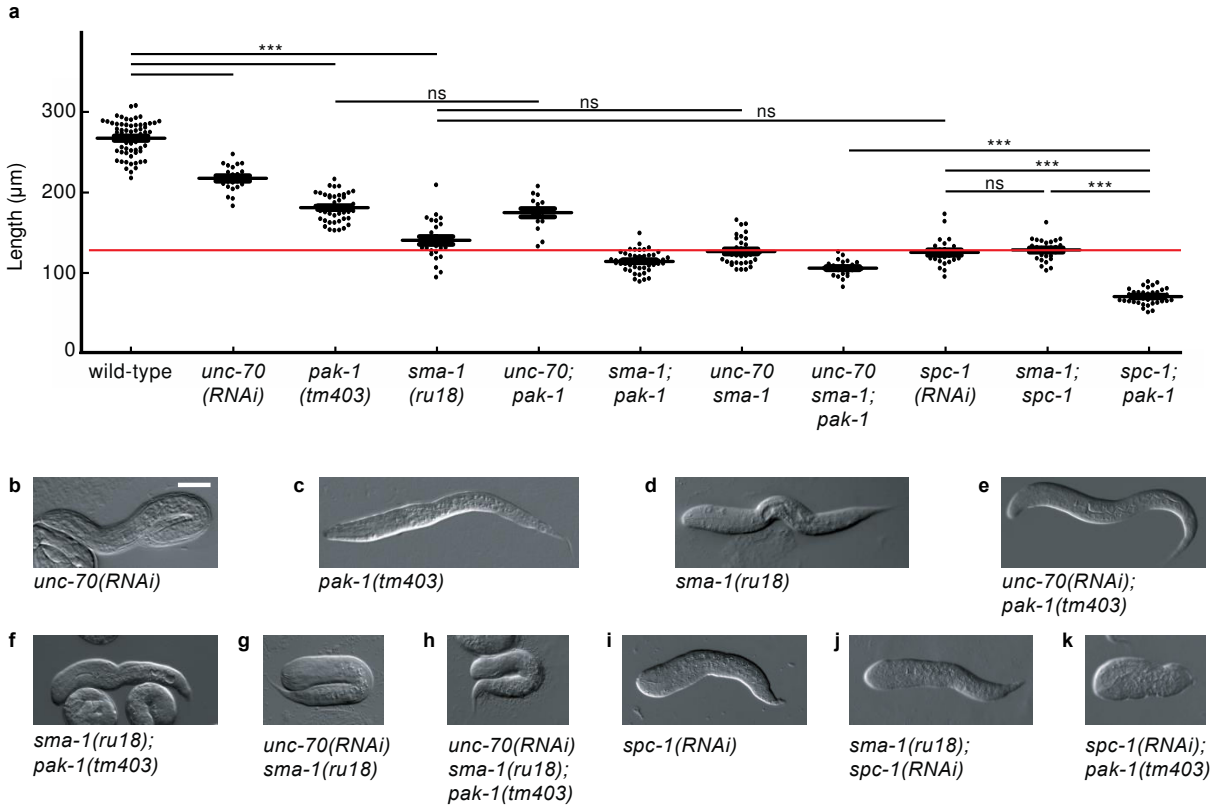

Figure 7: Genetic interactions of *pak-1, spc-1, sma-1 and unc-70* affect elongation.
(a) Quantification of L1 hatchling length and DIC pictures showing the terminal phenotypes of wild-type (n=65), *unc-70(RNAi)* (n=23) **(b)**, *pak-1(tm403)* (n=47) **(c)**, *sma-1(ru18)* (n=28) **(d)**, *unc-70(RNAi) ; pak-1(tm403)* (n=16) **(e)**, *sma-1(ru18) ; pak-1(tm403)* (n=52) **(f)**, *unc-70(RNAi) sma-1(ru18)* (n=33) **(g)**, *unc-70(RNAi) sma-1(ru18) ; pak-1(tm403)* (n=26) **(h)**, *spc-1(RNAi)* (n=27) **(i)**, *sma-1(ru18); spc-1(RNAi)* (n=28) **(j)**, *spc-1(RNAi) pak-1(tm403)* (n=) **(k)**,. Scale bar: 25 µm. Data represent mean values ± SD. Two-sided paired t-test. P-values: *<0,05; **<0,001; ***<0,0001; ns, not significant.

However, one of the isoforms of the spectraplakin VAB-10 showed a genetic interaction with both SPC-1 and SMA-1. Indeed, as seen in the introduction, *vab-10* generates isoforms related either to plectin (VAB-10A) or to microtubule actin cross-linking factor (VAB-10B) and have been reported to have specific localizations and functions in the epidermis (Bosher *et al.*, 2003). The loss of VAB-10A impairs the integrity of FOs, leading to epidermal detachment from the cuticle and muscles, while VAB-10B loss increases epidermal thickness during embryonic morphogenesis when epidermal cells change shape, suggesting that it protects cells against tension that builds up within the epidermis.

I focused on VAB-10B and I examined elongation rate of different genotypes using DIC microscopy. As previously described, *sma-1(ru18)* elongated until 2.5-fold and survived after hatching (Fig. 8a,b). *vab-10b(mc44)* also elongated but were slightly shorter and stopped around 2.3-fold (Fig. 8a,c). However, *vab-10b(RNAi); sma-1(ru18)* showed a 2-fold arrest quite similar to *spc-1(409)* embryos (Fig. 8a,d, Movie 3). In addition, *vab-10b(mc44); spc-1(RNAi)* showed two different

behaviors. About 60% of the embryos were shorter than *spc-1(ra409)* and stopped their elongation around 1.7-fold (Fig. 8a,e, Movie 3). The 40% others first elongated and could not maintain their shape when muscles started to contract. They retracted in a very similar fashion to that of *spc-1(ra409) pak-1(RNAi)* (Fig. 8a,f,g, Movie 3).

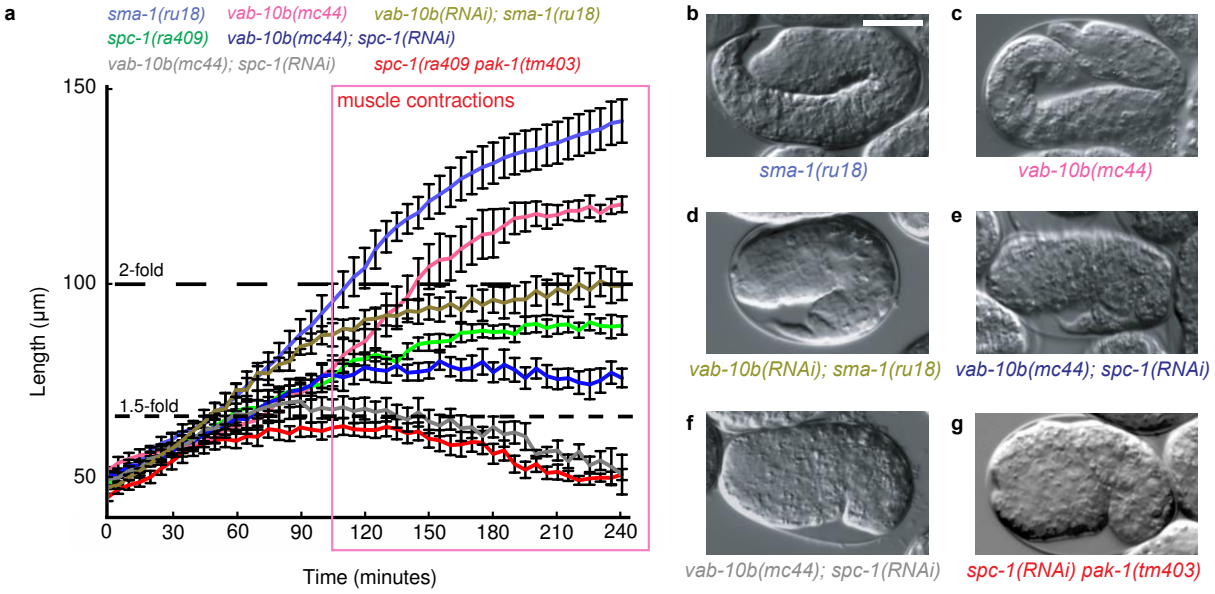

Figure 8: Combined loss of SPC-1 and VAB-10B also triggers embryo retraction.
(a) Elongation curves and **(b-g)** DIC pictures showing the terminal phenotypes of **(b)** *sma-1(ru18)* (n=8), **(c)** *vab-10b(mc44)* (n=6), **(d)** *vab-10b(mc44); sma-1(ru18)* (n=10), *spc-1(RNAi)* (n=8), **(e)** *vab-10b(mc44); spc-1(RNAi)* (n=11) that do not retract, **(f)** *vab-10b(mc44); spc-1(RNAi)* (n=8) that retract and **(g)** *spc-1(RNAi) pak-1(tm403)* (n=8). Pink box, period of muscle activity. Scale bar: 17 µm. Data represent mean values ± SEM.

These results suggested that VAB-10B may also play a role in stabilizing the shape of the embryos during elongation. Recent work from our lab showed that VAB-10 acts as a CeHDs mechanosensor and could be the molecular component that induces the recruitment of GIT-1, therefore the activation of the mechanotransduction pathway downstream of muscles (Suman *et al.*, BioRxiv). I also mentioned that although muscle defective mutants show a strong phenotype (2-fold arrest), *git-1, pix-1* and *pak-1* mutants are viable, suggesting the existence of parallel pathways for this regulation. The retraction of *spc-1 pak-1*, *git-1; spc-1* and *pix-1; spc-1* embryos confirmed this idea. The enhanced phenotypes of *vab-10b* combined to either *sma-1* or *spc-1* strengthened it even more.

V. The organization and remodeling of actin filaments is a key element of the retraction

V. 1. Spinning-disk characterization of the actin disorganization in *spc-1 pak-1* embryos

The simplest interpretation of the retraction phenotype observed in *spc-1 pak-1* embryos is that a cellular structure maintaining embryo shape fails to emerge or collapses in *spc-1 pak-1* double mutants once muscles contract. Two arguments suggest that this structure corresponds to the bundles of 3-5 actin filaments present in the dorso-ventral (D/V) epidermis (Costa *et al.*, 1997; Priess and Hirsh, 1986). First, SPC-1/α-spectrin and its binding partner SMA-1/$ß_H$-spectrin (apical) or UNC-70/ $ß_G$-spectrin (basolateral) form an actin-binding hetero-tetramer co-localizing with actin (Praitis *et al.*, 2005) and partially with PAK-1 in epidermal cells (Fig. 4). Second and foremost, treating *C. elegans* embryos with the actin-depolymerizing drug cytochalasin-D induces a retraction phenotype very similar to that presented herein (Priess and Hirsh, 1986).

Thus, with the help of Teresa Ferraro, engineer in the lab, we characterized actin filaments organization, by imaging a *LifeAct::GFP* probe expressed specifically in the epidermis under the promotor *dpy-7*. In *C. elegans*, the contribution of actin to embryonic morphogenesis has been reported from the end of gastrulation (Marston and Goldstein, 2006). Actin forms a meshwork near the epidermal cortex but prior to embryonic elongation it rearranges to form circumferential, parallel bundles first in the D/V cells, followed by its rearrangement in the lateral cells. Once the embryonic elongation is completed, the circumferential bundles disassemble (Priess and Hirsh, 1986). Thus, we first performed some texture analysis (Fig. 9a-a'') on spinning-disk images. We chose manually ROIs of a constant size in the D/V area for all genotypes. On these ROIs we performed a Fourier transform analysis with a high pass filter to select only small structures. After this treatment, the ROI were either binarized and fit by ellipses to extract the continuity of the actin filaments or directly used to measure the distribution of cable orientation (Fig. 9a'''). These analyses were done on anesthetized embryos (put to sleep by oxygen deprivation through a high concentration of bacteria) at different stages (1.7-fold, 2-fold and 3-fold) to get higher resolution of the actin compared to live imaging. Segmentation analysis of the fluorescence signal associated with actin filaments in the D/V epidermis revealed more discontinuity in *spc-1 pak-1* double deficient embryos (Fig. 9d-d''') compared to the control genotypes (Fig. 9a-c'''). Moreover, Fourier transform analysis indicated that their degree of anisotropy relative to the circumferential axis was abnormal (Fig. 9d''-d''').

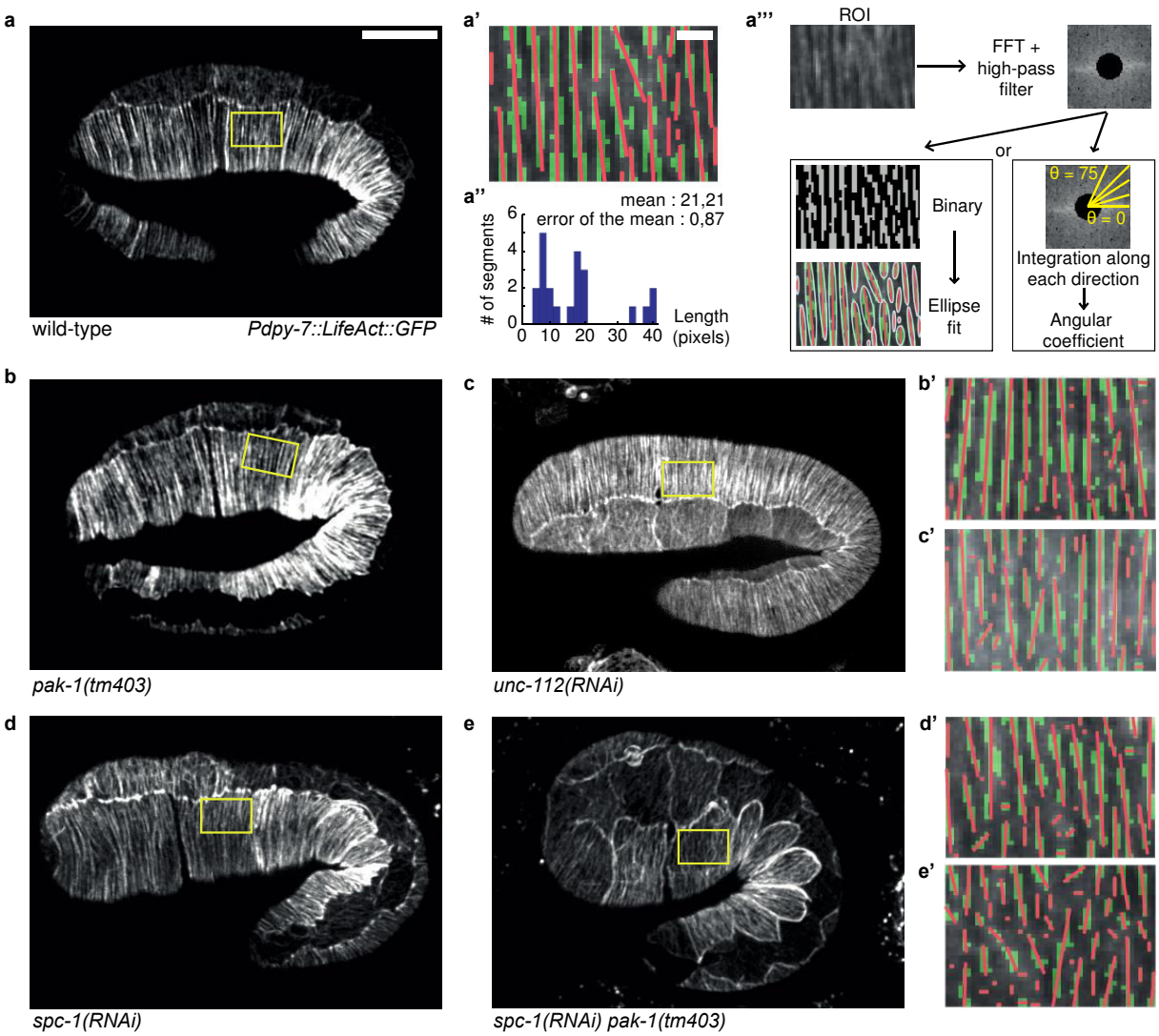

Figure 9: Actin filaments show organization defects in *spc-1 pak-1* defective embryos.
(a-e) Epidermal actin filaments visualized with the *Pdpy-7::LifeAct::GFP* reporter construct in wild-type (**a-a'**), *pak-1(tm403)* (**b-b'**), *unc-112(RNAi)* **(c-c')**, *spc-1(RNAi)* **(d-d'),** *spc-1(RNAi) pak-1(tm403)* **(e-e')** (at mid-elongation (2-fold equivalent) stage. Yellow rectangle, region of interest (ROI). **(a'-e')** ROI after binarisation (green) and major axis detection (red), based on (**a'''**) three steps of image treatment for continuity and orientation analysis. **(a'')** Actin continuity: distribution of actin segments based on their length**.** Scale bar: 10 µm **(a-e)**. Scale bar: 1 µm **(a'-e')**.

In more details, at 1.7-fold – thus before muscles start to contract – the actin is still organized as a meshwork for all genotypes. At 2-fold the actin cable anisotropy has decreased and circumferential parallel actin bundles run through the DV cells from one DV/ lateral cell junction to the other. Later, this pattern becomes even sharper and all genotypes get more organized with time, differences among them become less significant (Figs. 10-11). Overall *pak-1* and *unc-112* display similar organization through time. *spc-1* and *spc-1 pak-1* are constantly less organized than wild-type but the difference between themselves tends to disappear with time.

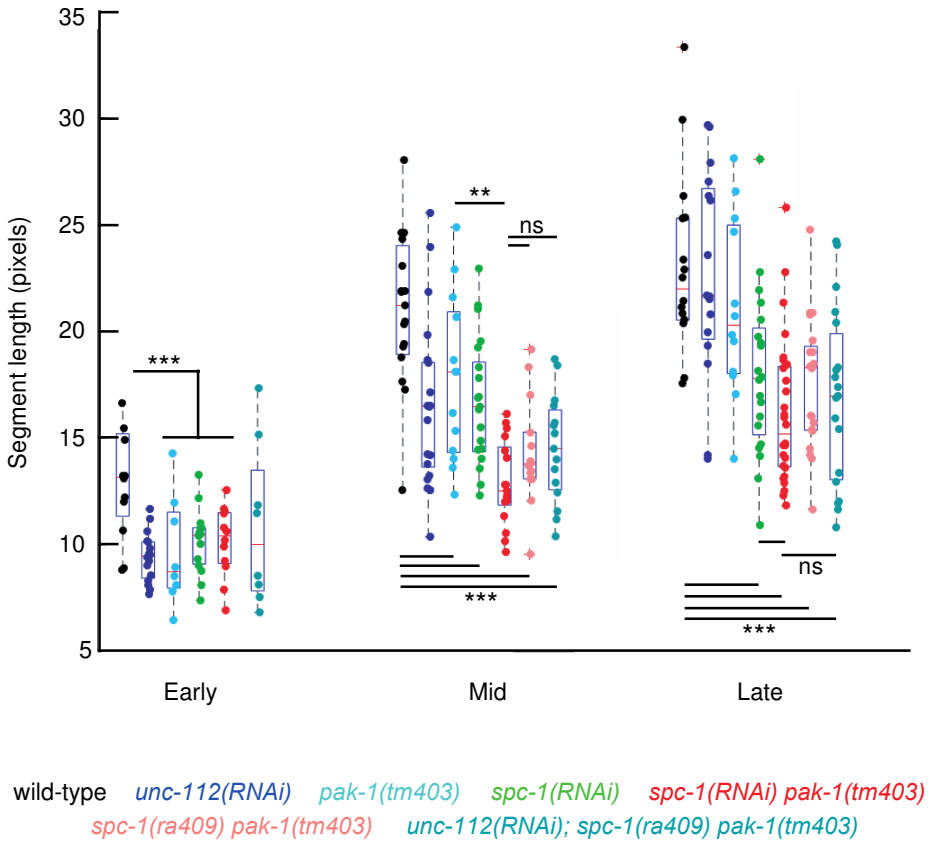

Figure 10: Actin filament continuity varies during development.

Quantification of actin filament continuity ; the graph represents the length (in pixels) along the circumferential axis of actin filaments in early, mid and late (corresponding to 1.7-fold, 2-fold and 3-fold equivalent stages in a wild-type embryo, respectively) embryos of wild-type (early n=12, mid n=19, late n=16), *pak-1(tm403)* (early n=16, mid n=21, late n=16), *spc-1(RNAi)* (early n=15, mid n=21, late n=20), *spc-1(RNAi) pak-1(tm403)* (early n=12, mid n=17, late n=26), *unc-112(RNAi)* (early n=8, mid n=13, late n=12), *spc-1(ra409) pak-1(tm403)* (mid n=14, late n=20) and unc-112(RNAi) ; *spc-1(ra409) pak-1(tm403)* (early n=8, mid n=15, late n=19) genotypes. Graphs represent median values, 25th and 75th percentiles; whiskers extend to the most extreme data points not considered outliers. Two-sided paired t-test. P-values: *<0,05; **<0,001; ***<0,0001; ns, not significant.

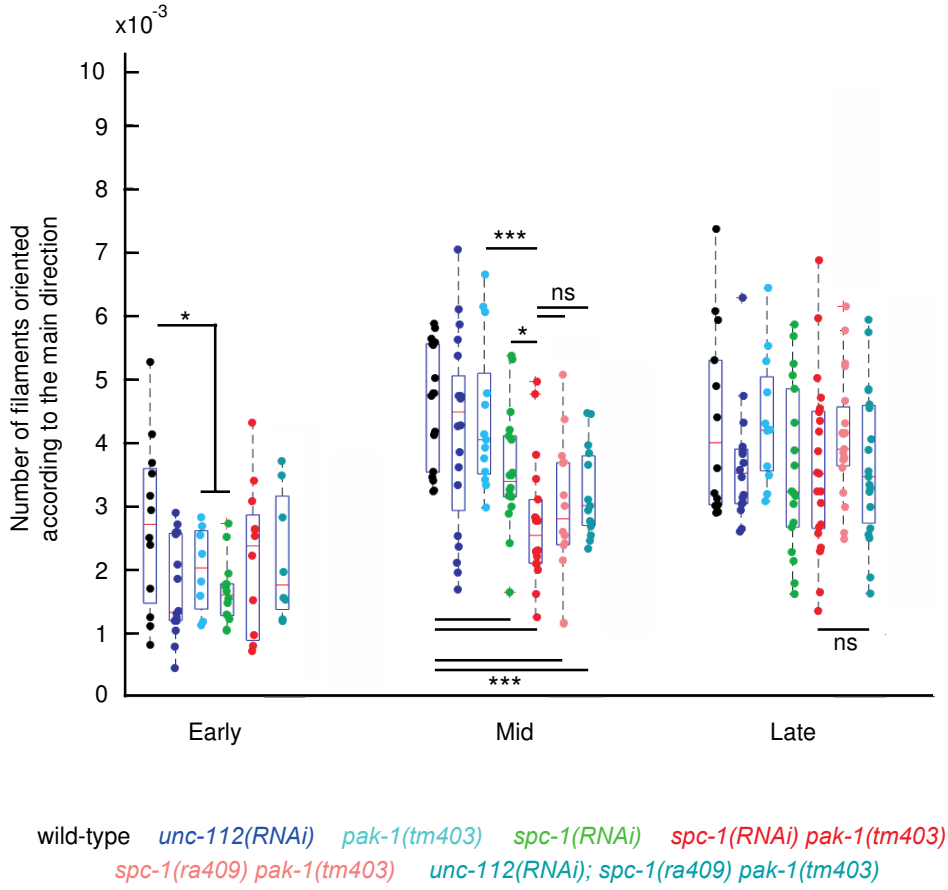

Figure 11: Actin filament orientation varies during development.

Actin filament orientation based on Fast Fourier Transform and binarisation. Wild-type (early n=12, mid n=18, late n=14), *pak-1(tm403)* (early n=16, mid n=20, late n=16), *spc-1(RNAi)* (early n=14, mid n=18, late n=18), *spc-1(RNAi) pak-1(tm403)* (early n=12, mid n=18, late n=21), *unc-112(RNAi)* (early n=8, mid n=13, late n=12), *spc-1(ra409) pak-1(tm403)* (mid n=14, late n=19) and unc-112(RNAi) ; *spc-1(ra409) pak-1(tm403)* (early n=8, mid n=15, late n=19) genotypes. Note that the characteristics of actin filaments in *spc-1(RNAi) pak-1(tm403)* embryos differ mostly at the equivalent of the two-fold stage when muscles become active. At ealier and later stages, *spc-1(RNAi)* embryos and *spc-1(RNAi) pak-1(tm403)* embryos become similar. Graphs represent median values, 25th and 75th percentiles; whiskers extend to the most extreme data points not considered outliers. Two-sided paired t-test. P-values: *<0,05; **<0,001; ***<0,0001; ns, not significant.

As we showed that *spc-1(ra409) pak-1(tm403)* embryos also defective for *unc-112* no longer retracted I wondered whether the abnormalities in filament organization observed in the *spc-1(RNAi); pak-1(tm403)* embryos only appear in the presence of muscle activity. This experiment turned out to be technically challenging. I started again by isolating a new *spc-1(ra409) pak-1(tm403)* strain maintained by an extrachromosomal *spc-1(+)::GFP* construct marked by a red pharynx marker (P*myo-2::mCherry*), which I then crossed with our integrated *LifeAct::GFP* construct, hoping that the new combination would be less stable. I succeeded and recovered about 20% embryos after segregation of the *spc-1(+)::GFP* construct tracked by loss of the red pharynx marker and absence of SPC-1::GFP fluorescence (which is significantly different from that of LifeAct). The quantifications showed that the actin defects in *unc-112(RNAi); spc-1(ra409) pak-1(tm403)* embryos were statistically comparable to those of *spc-1(ra409) pak-1(tm403)* embryos, although the bundles seemed less damaged by eye. From this experiment it is very difficult to conclude weather the actin disorganization of *spc-1 pak-1* embryos depend on muscle input or not. Most probably, we reached the limit of our analysis and we are limited by the resolution of the pictures we can obtain with spinning-disk imaging.

V. 2. Enhanced visualization of actin filament abnormalities in *spc-1 pak-1* defective embryos

As the embryo elongates, its circumference decreases, implying that the length of actin filaments in D/V cells should decrease and therefore the actin cables should remodel. To understand how this remodeling could happen, I tried to catch it live by again using TIRF-SIM super-resolution microscopy of the same *LifeAct::GFP* probe, focusing only on wild-type and *spc-1 pak-1* genotypes.

As mentioned earlier, this approach allowed me to illuminate only the cortex of the embryos and I tried to follow the actin re-organization upon muscles contractions. Although it is a significant improvement in spatial resolution compared to spinning-disk microscopy, TIRF-SIM stays challenging once the embryo starts to move as it often moves faster than the temporal resolution of the microscope. Nevertheless, super-resolution confirmed our first observations according to which actin filaments in *spc-1 pak-1* double mutants are more interrupted and do not show the same degree of anisotropy as control embryos.

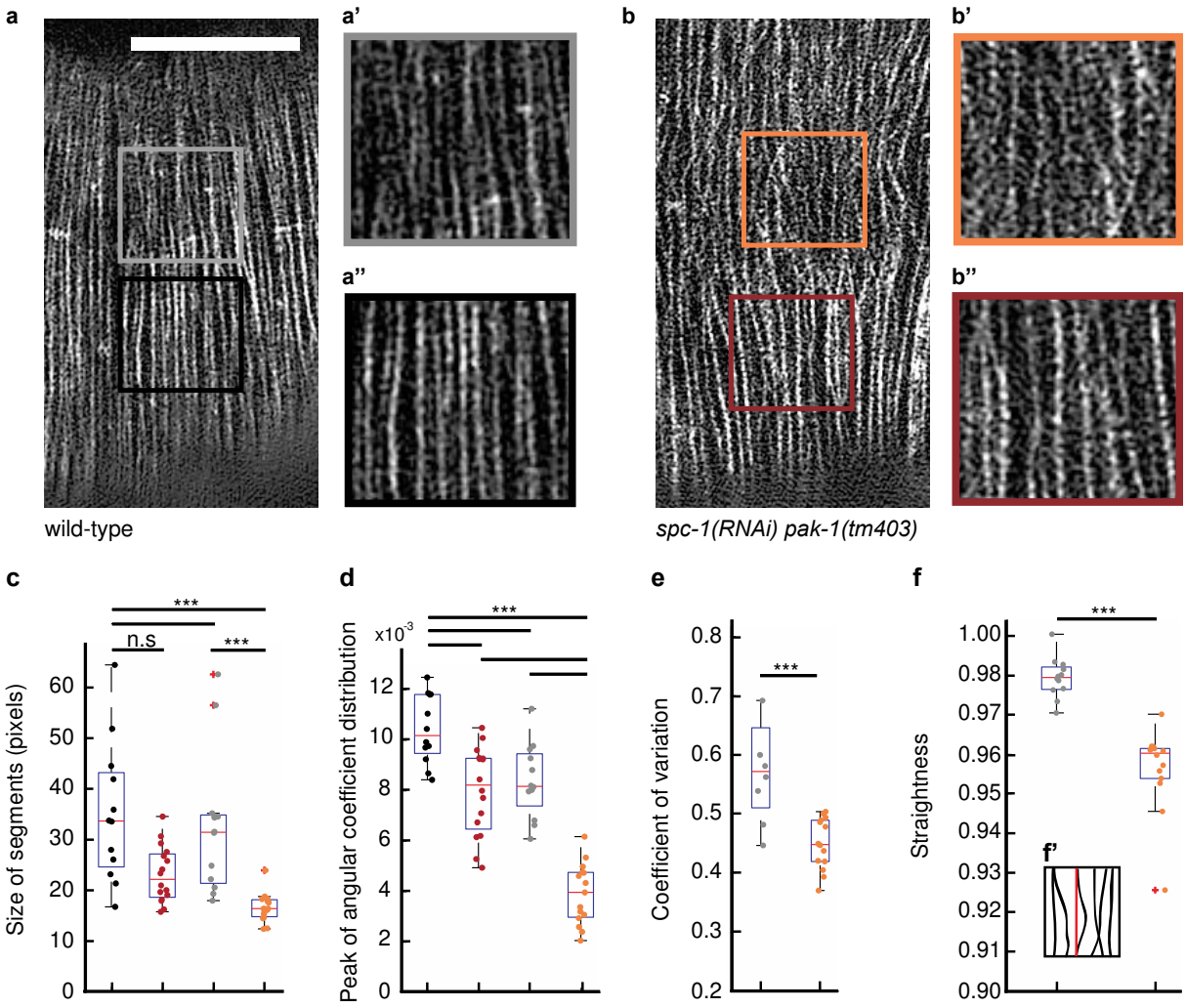

Figure 12: Actin filament abnormalities are highlighted by TIRF-SIM microscopy in *spc-1 pak-1* embryos.
TIRF-SIM super-resolution images of actin filaments (*Pdpy-7::LifeAct::GFP* reporter). **(a-a'')** Wild-type and **(b-b")** *spc-1(RNAi) pak-1(tm403)* embryos at the 2-fold stage or equivalent. Grey and orange rectangles, region of interest (ROI) above muscles (area of higher bending in time-lapse images); black and bordeaux rectangles, ROI taken elsewhere. Scale bar: 5 µm. **(c)** Actin continuity estimated as the segment length in binarised ROI images, and **(d)** peak value of the angular coefficient calculated after Fast Fourier Transformation as a proxy for actin bundle anisotropy. Defects are significantly more pronounced above muscles. **(e)** Coefficient of variation (SD/mean) of the fluorescence signal in ROIs above muscles as a proxy for actin bundle organization. **(f)** Actin bundle straightness (**f**) calculated as the ratio between the actual length of a bundle (black line in **f'**) and the shortest distance between its endpoints (red line in **f'**). Graphs represent median values, 25th and 75th percentiles; whiskers extend to the most extreme data points not considered outliers. Two-sided paired t-test. P-values: *<0,05; **<0,001; ***<0,0001; ns, not significant.

Thanks to the increased spatial resolution, we slightly adapted our earlier analysis. We distinguished two different types of ROI on the actin pattern: ROIs above muscles (area of higher bending in time-lapse images) (Fig. 12a'',b''; grey and orange rectangles) and ROIs closer to the DV/lateral cell junction (Fig. 12a',b'; black and bordeaux rectangles). It revealed that the defects are more prominent in the area that is over the muscles (putative CeHDs, Fig. 12a-d, 13a,b), which I could not detect with spinning-disk microscopy. The actin appears even more fragmented (Fig. 12c) and more disorientated (Fig. 12d) in the areas submitted to a more direct stress from muscles underneath. Moreover, by performing a line-scan intensity profile on the ROIs above muscles, the signal intensity between adjacent actin bundles appeared less sharp in *spc-1 pak-1* deficient embryos (Fig. 12e) and they were more often bent (Fig. 12f), indicating that the bundles might have partially defasciculated from the main bundle (Fig. 13a,b). Importantly these phenotypes became apparent once muscles became active, suggesting that muscle contractions contribute to actin remodeling.

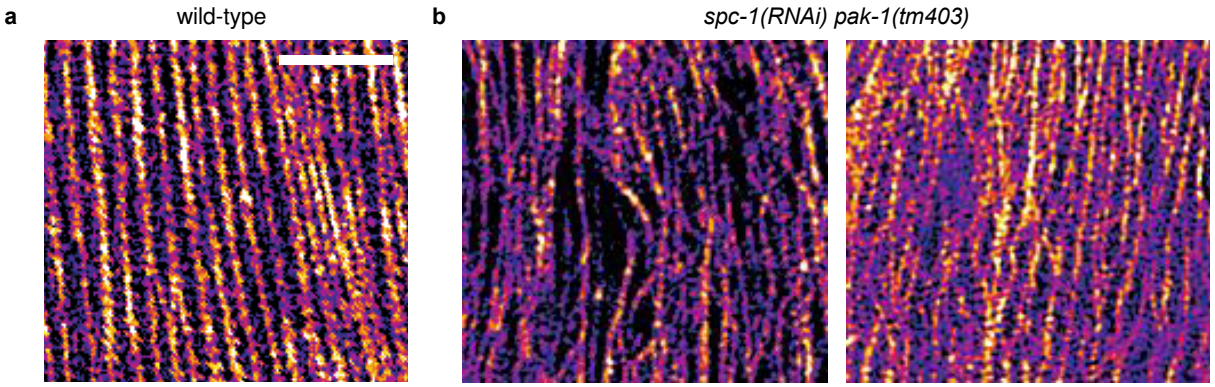

Figure 13: Actin filament abnormalities are highlighted by TIRF-SIM microscopy in *spc-1 pak-1* embryos.
(a-b) TIRF-SIM snapshots of grouped Z movies with Fire LUT to emphasize the actin bundle defects of *spc-1(RNAi) pak-1(tm403)* embryos compared to wild-type. P-values: *<0,05; **<0,001; ***<0,0001; ns, not significant.

Unfortunately, I could not use TIRF-SIM microscopy to examine more precisely the defects in *unc-112(RNAi); spc-1(ra409) pak-1(tm403)* and check if the non-significance of the analysis with the spinning-disk could be due to a lack of resolution. In fact, the spontaneous segregation of the extrachromosomal *spc-1(+)::GFP* was low (20%) making useful embryos difficult to spot. Another limitation in our experiment was the fact that the SIM-TIRF setup offered by the Beaurepaire laboratory does not come with a low magnification objective to first find embryos. These two problems combined made the experiment nearly impossible to perform, or it would have taken too much time.

Yet, we infer that after strong bending some circumferential actin filaments within bundles get severed, then probably partially depolymerized upon severing and rebundled. Indeed, we assume that criss-crossed and curved filaments observed in *spc-1 pak-1* defective embryos, but not in control embryos, could correspond to severed filaments that did not get repaired/stabilized. However, I am remaining careful on that statement, because even TIRF-SIM did not resolve how shortening events occurred. Indeed, the *LifeAct::GFP* signal, although very stable at the spinning-disk, bleached very fast due to the very high laser power used. Hence the movies acquired are short (10 seconds max). Combined with the fact that the embryo often moves faster than the temporal resolution of the microscope, very few contractions could be fully captured, and it did not allow me to clearly see live remodeling events.

V. 3. The intensity of actin varies over time in *spc-1 pak-1* defective embryos

From the spinning-disk and super-resolution microscopy results, I concluded that the disorganization of actin observed in *spc-1 pak-1* embryos could be due to the severing of filaments that did not get repaired properly. Therefore, it would mean that actin polymerization may be defective in these embryos. To investigate this hypothesis, I followed over time the intensity of actin. With the help of Teresa, we made global measurements of *Pdpy-7::LifeAct::GFP* fluorescence intensity from the spinning-disk images shown earlier. We found that whether measured on the entire embryo (Fig. 14a) or along the filaments in a small ROI (Figs. 12-13), the fluorescence in *spc-1 pak-1* defective embryos was lower than in control embryos (Fig. 14c). To ensure that this does not reflect a lower efficiency of the *dpy-7* promoter used to drive *LifeAct::GFP* in mutants, we generated transgenic lines carrying a *Pdpy-7::GFP* construct showing fluorescence in the cytoplasm and nucleus (Fig. 14b). We observed that the average fluorescence of the reporter was very similar in both genotypes over time (Fig. 14d). Comparing the intensity ratio of *Pdpy-7::GFP* to *Pdpy-7::LifeAct::GFP* fluorescence clearly indicates that the activity of the *Pdpy-7* promoter is not affected in mutants, and that the LifeAct signal was significantly lower in *spc-1 pak-1* compared to control embryos (Fig. 14e). While we know that LifeAct provides only an indirect measure to actin polymerization, we showed that the intensity variation we observed in our double mutants does not depend on the epidermal promotor, or on the stage of the embryos. Therefore, it suggests that in *spc-1 pak-1* double mutants the balance between polymerization and depolymerization is significantly tilted in favor of depolymerization.

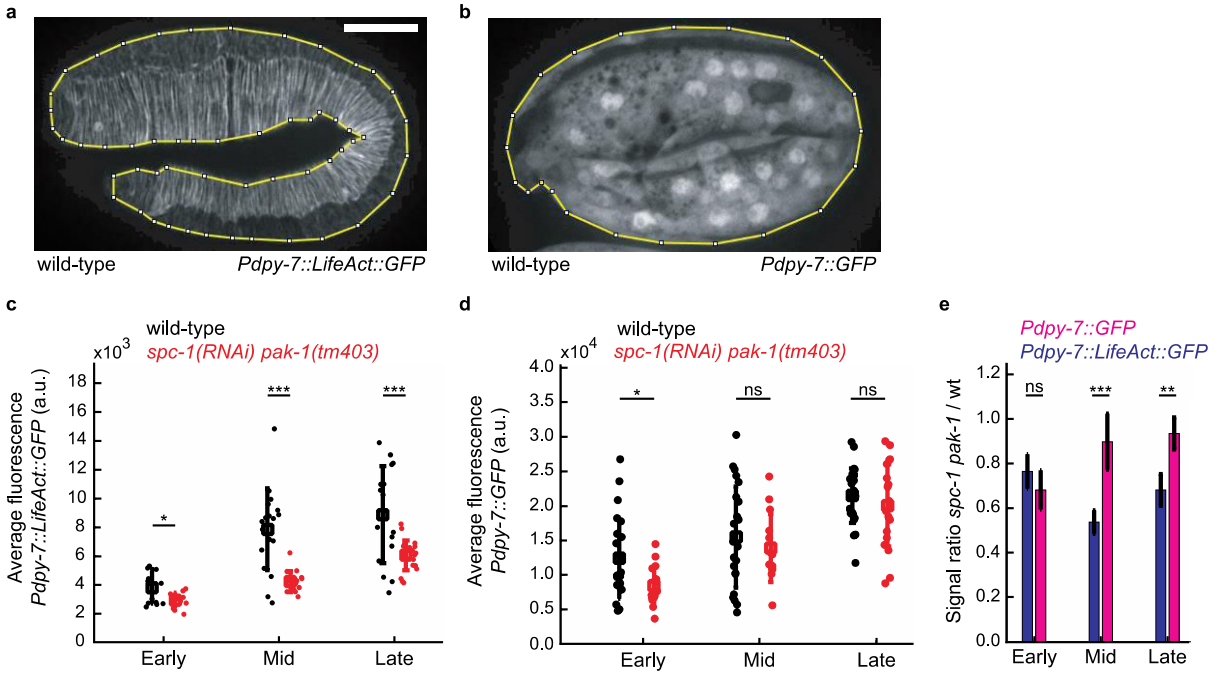

Figure 14: Variation of actin intensity over time in wild-type and *spc-1 pak-1* embryos
(a-b) Spinning-disk images of wild-type embryos expressing the *Pdpy-7*::*Lifeact::GFP* **(a)** and the *Pdpy-7::GFP* **(b)** contsructs in the epidermis at the 2-fold stage. Scale bar: 10µm. **(c-d)** Quantifications of the *Pdpy-7::LifeAct::GFP* **(c)** and the *Pdpy-7::GFP* **(d)** intensity in the entire embryo (ROI in yellow on the images) at threes stages early, middle and late (corresponding to 1.7-fold, 2-fold and 3-fold equivalent stages in a wild-type embryo, respectively) in wild-type and *spc-1(RNAi) pak-1(tm403)* embryos. Graphs represent median values, 25th and 75th percentiles; whiskers extend to the most extreme data points not considered outliers. **(e)** Ratio between the signal in *spc-1(RNAi) pak-1(tm403)* and wild-type embryos for the *Pdpy-7*::*Lifeact::GFP* and the *Pdpy-7::GFP* constructs at threes stages. Data represent mean values and SD. **(c-e)** Two-sided paired t-test. P-values: *<0,05; **<0,001; ***<0,0001; ns, not significant.

VI. The embryo diameter decreases during elongation

By using the same spinning-disk anesthetized embryos as for the texture analysis, with the help of Teresa, we also observed that as wild-type embryos lengthen, their circumference decreases by roughly 20% due to embryo volume conservation (Fig. 15a,c,d), implying that the length of actin filaments in D/V cells should decrease and therefore that the cables should remodel. In *spc-1(RNAi) pak-1(tm403)* embryos, the trend is opposite; the circumference tends to increase by about 10%, leading to longer actin cables (Fig. 15b-d). Interestingly, in *unc-112(RNAi); spc-1(ra409) pak-1(tm403)* the lateral seam cells did not become circumferentially as narrow. In this respect they behaved more like *unc-112* single mutants than *spc-1 pak-1.* Thus, although the spinning-disk quantification of the actin defects in *unc-112(RNAi); spc-1(ra409) pak-1(tm403)* did not suggest a statistical difference compared to the *spc-1(ra409) pak-1(tm403)* embryos, this result lead us to believe that their actin filaments were less damaged and significantly stiffer than in *spc-1(ra409) pak-1(tm403)* embryos.

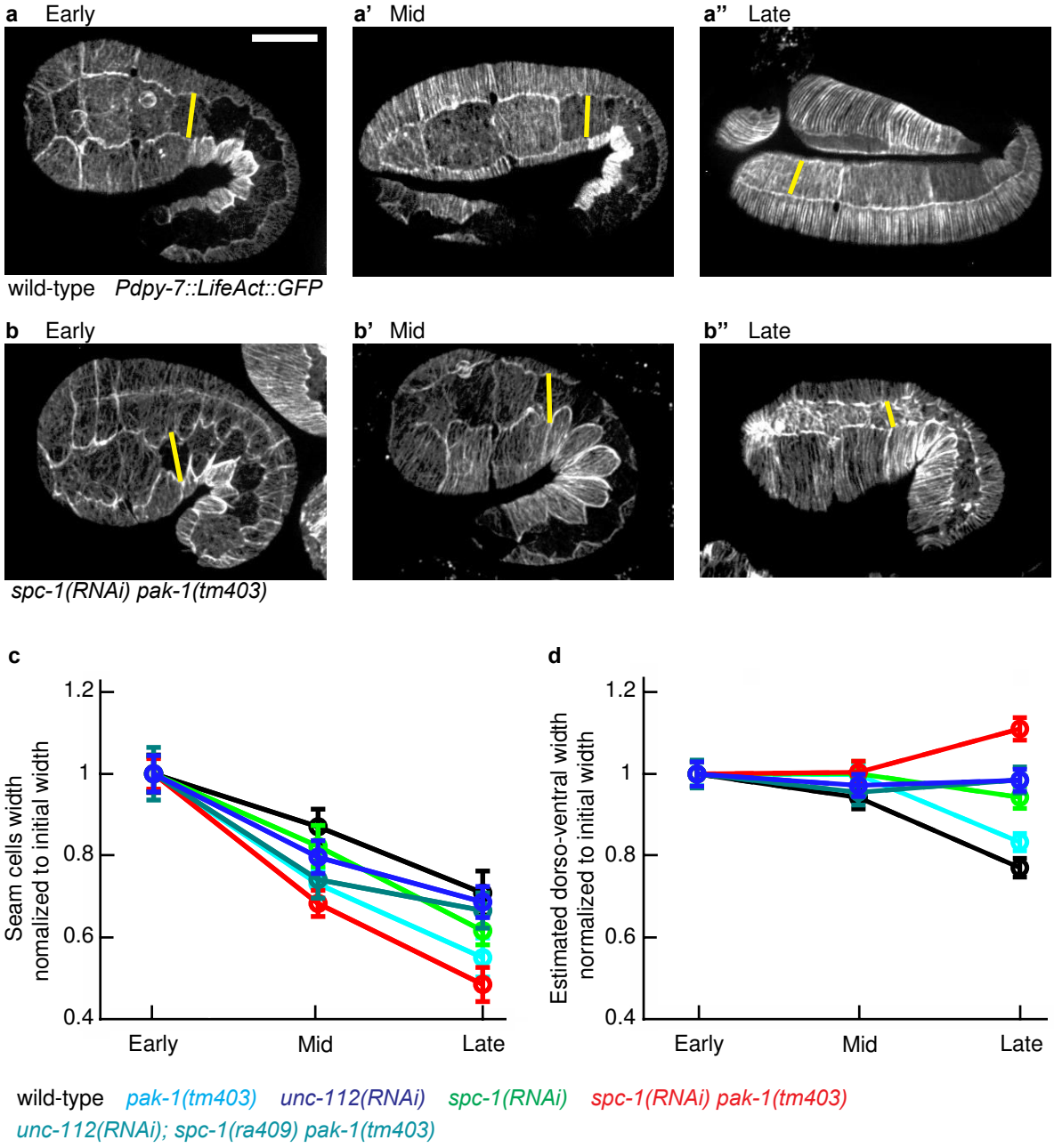

Figure 15: Embryo diameter varies during elongation.
(a-b") Spinning-disk images of embryos expressing the *Pepid*::*Lifeact*::*GFP* construct in the epidermis at three elongation stages early, middle and late (corresponding to 1.7-fold, 2-fold and 3-fold equivalent stages in a wild-type embryo, respectively) for wild-type (**a-a"**) and *spc-1(RNAi) pak-1(tm403)* embryos (**b-b"**)**.** Scale bar: 10 µm**.** The *Pepid* promoter corresponds to *Pdpy-7***.** The yellow lines correspond to the segments used to measure the D/V width of the V1 seam cell. **(c)** Quantification of the average V1 cell circumferential width normalized to the initial width during elongation, and **(d)** of the average D/V circumferential width at the level of the V1 seam cell, which was calculated using the measured embryo length and V1 cell width, taking into consideration the conservation of the total embryo volume, in wild-type (early n=38, mid n=10, late n=14), *pak-1(tm403)* (early n=26, mid n=8, late n=20), *spc-1(RNAi)* (early n=24, mid n=26, late n=18), *spc-1(RNAi) pak-1(tm403)* (early n=22, mid n=30, late n=38), *unc-112(RNAi)* (early n=8, mid n=9, late n=8), and unc-112(RNAi) ; *spc-1(ra409) pak-1(tm403)* (early n=7, mid n=12, late n=17) genotypes. Error bars, SEM. A notable feature of *spc-1(RNAi) pak-1(tm403)* embryos is that the circumferential dimension of the seam cells decreased much more than that of their DV cell, which most likely reflects the actin filament integrity defects combined with a F_{seam} force largely unchanged.

Altogether, we suggest that the circumferential actin bundles remain damaged when muscle activity is prevented in *spc-1 pak-1* double mutants due to the absence of SPC-1 and PAK-1, but less than in *spc-1 pak-1* mutants alone.

VII. Muscle contractions bend actin filaments leading to the recruitment of severing proteins

VII. 1. Actin filaments are bend at very sharp angles upon muscle input

In wild-type embryos, muscle contractions promote embryonic elongation from the 2-fold to the final 4-fold stage. During this time, junctions must lengthen along the A/P direction, while the length of the stress fiber-like actin bundles present in dorsal and ventral cells must get shorter as the embryo diameter gets reduced. The next step I took was to further understand how this remodeling of the actin cables could happen in wild-type condition and how it is impaired in *spc-1 pak-1* mutants. To do so, I acquired short spinning-disk time-lapses. With Teresa, we examined the behavior of actin filaments upon muscle contractions. Strikingly, live imaging revealed that muscle contractions are strong enough to locally bend actin bundles with an angle greater than 57° (Fig. 16a,c), which has been reported to induce actin filament severing in vitro (McCullough *et al.*, 2011). To be more specific, when muscles locally contract, we observed that they locally squeeze the embryo along the A/P axis producing an increased circumferential stress due to volume conservation. Moreover, during these contraction phases, the actin bundles get bent to angles that match the local extent of muscle contractions. This could lead to a local severing of the cables and help their shortening through the elongation in wild-type condition. Interestingly, we observed similar bending of the actin cables in the *spc-1 pak-1* embryos with angles in the same range as the wild-type (Fig. 16b,d).

This last result supports the hypothesis developed after the actin pattern analysis presented earlier. Both in control and in *spc-1 pak-1* muscles can mechanically affect the epidermis and eventually promote actin severing. In control embryos, this severing would be quickly stabilized and would help the cables shorten through elongation as its circumference decreases. In *spc-1 pak-1* embryos, the criss-crossed and curved filaments observed would be severed filaments that did not get stabilized.

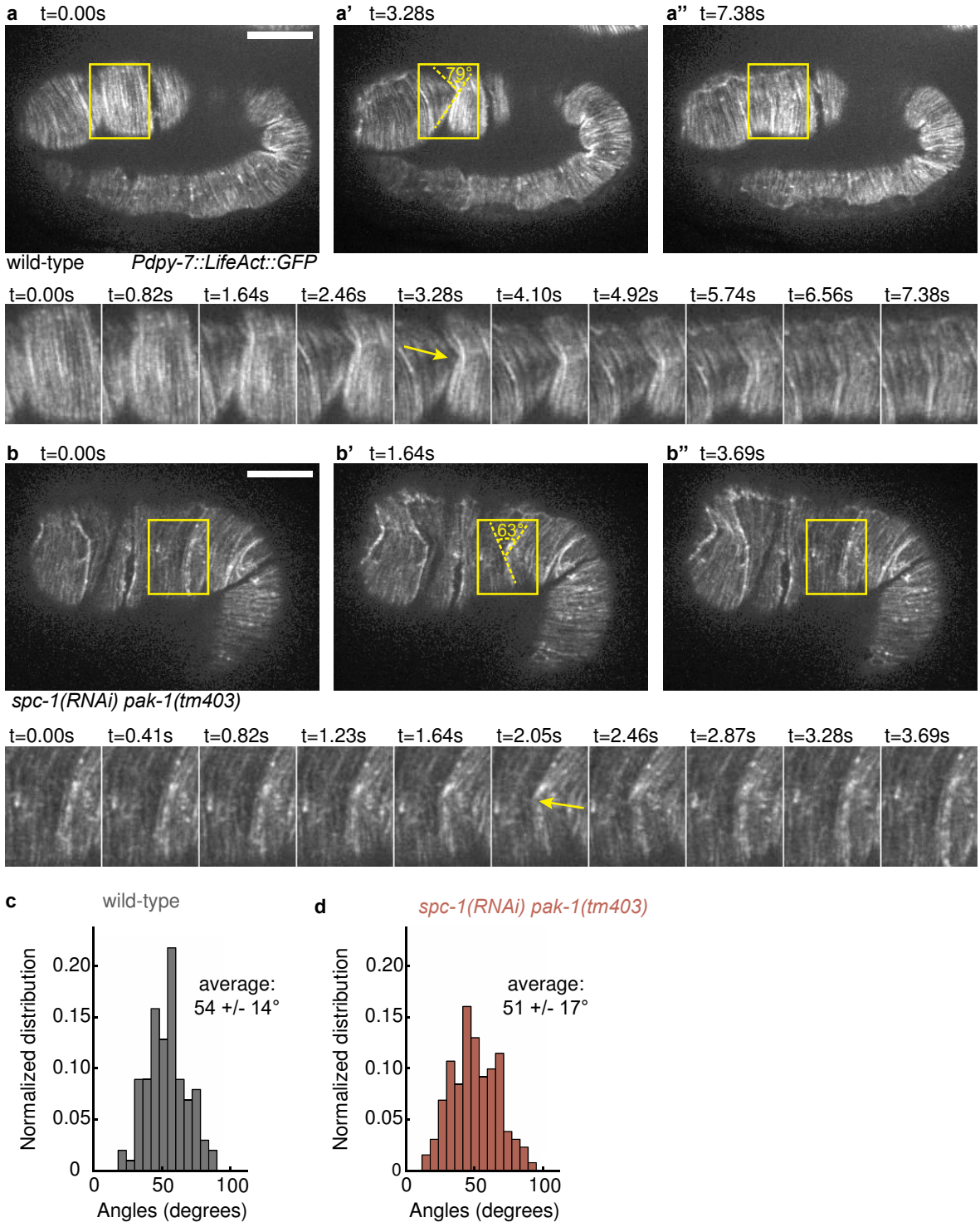

Figure 16: Actin bundles strongly bend during muscle contractions.

(a-d) Spinning-disk time-lapse images of epidermal actin filaments (*Pdpy-7::LifeAct::GFP* reporter) and quantification of their bending angles in wild-type (n=23, contractions=101) **(a, c)** and *spc-1(RNAi) pak-1(tm403)* (n=134, contractions=131) **(b, d)** embryos at mid-elongation (2-fold equivalent) stage; kymographs of the region boxed in yellow are displayed below. Scale bar: 10 µm.

VII. 2. GSNL-1 and VILN-1 are involved in the remodeling of actin in our system

Because muscles are strong enough to bend the actin cables at high angles, leading to a local severing of the cables, I investigated which proteins could be involved in this process. Therefore, I reasoned that compromising severing genetically might partially rescue the retraction of *spc-1 pak-1* defective embryos. With the help of Flora, we performed a RNAi screen using the same *spc-1(ra409) pak-1(tm403), spc-1(+)::GFP* strain as described earlier, and focused on actin-binding proteins known to modulate actin remodeling in early *C. elegans* embryos (Fig 17a). Remarkably, among thirteen genes tested (Table 3), the screen identified two proteins whose vertebrate homologs have known actin-severing activity, gelsolin and villin (Fig. 17b, Movie 4).

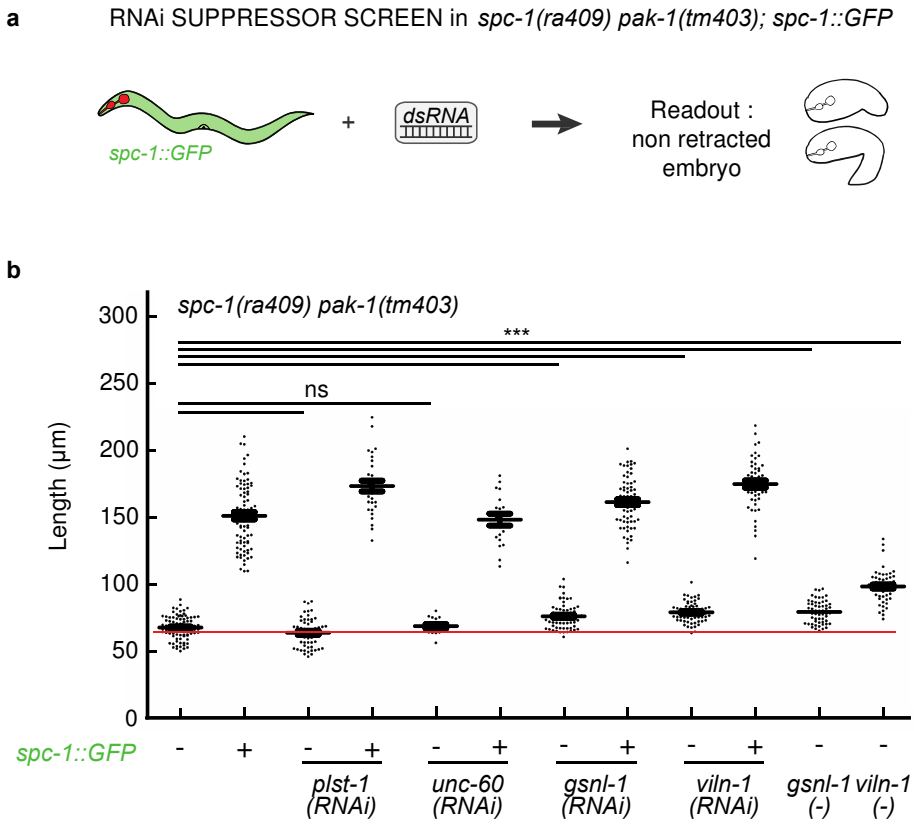

Figure 17: Identification of two severing proteins rescuing the retraction phenotype.
(a) Principle of the RNAi screen performed to identify proteins mediating actin remodeling; the recipient strain carried a rescuing but frequently lost *spc-1(+)* transgene (noted +). **(b)** Quantification of L1 hatchling length after down-regulation or mutation of the indicated genes. *spc-1(ra409) pak-1(tm403)* (n=92), *spc-1(ra409) pak-1(tm403); spc-1::GFP* (n=81), *plst-1(RNAi); spc-1(ra409) pak-1(tm403)* (n=55), *plst-1(RNAi); spc-1(ra409) pak-1(tm403); spc-1::GFP* (n=30), *unc-60(RNAi); spc-1(ra409) pak-1(tm403)* (n=16), *unc-60(RNAi); spc-1(ra409) pak-1(tm403); spc-1::GFP* (n=19), *gsnl-1(RNAi); spc-1(ra409) pak-1(tm403)* (n=64), *gsnl-1(RNAi); spc-1(ra409) pak-1(tm403); spc-1::GFP* (n=68), *viln-1(RNAi); spc-1(ra409) pak-1(tm403)* (n=69), *viln-1(RNAi); spc-1(ra409) pak-1(tm403); spc-1::GFP* (n=52), *gsnl-1(tm2730); spc-1(RNAi) pak-1(tm403)* (n=57), *viln-1(ok2413); spc-1(RNAi) pak-1(tm403) (n=55).* Control animals fed on L4440 bacteria. Data represent mean values ± SD. Two-sided paired t-test. P-values: *<0,05; **<0,001; ***<0,0001; ns, not significant.

The partial rescues observed by using gelsolin and villin RNAi were confirmed with gelsolin and villin mutation (Figs. 17b, 18a-g). As for *spc-1 pak-1* when we first observed the retraction phenotype, we examined the elongation rate of the triple deficient embryos *gsnl-1(tm2730); spc-1(ra409) pak-1(tm403)* and *viln-1(ok2413); spc-1(ra409) pak-1(tm403)* using DIC microscopy. They initially elongated at the same rate as *spc-1(RNAi) pak-1(tm403),* but once muscles started to be active, they could maintain their shape compared to the retracting embryos (Fig. 18a-g).

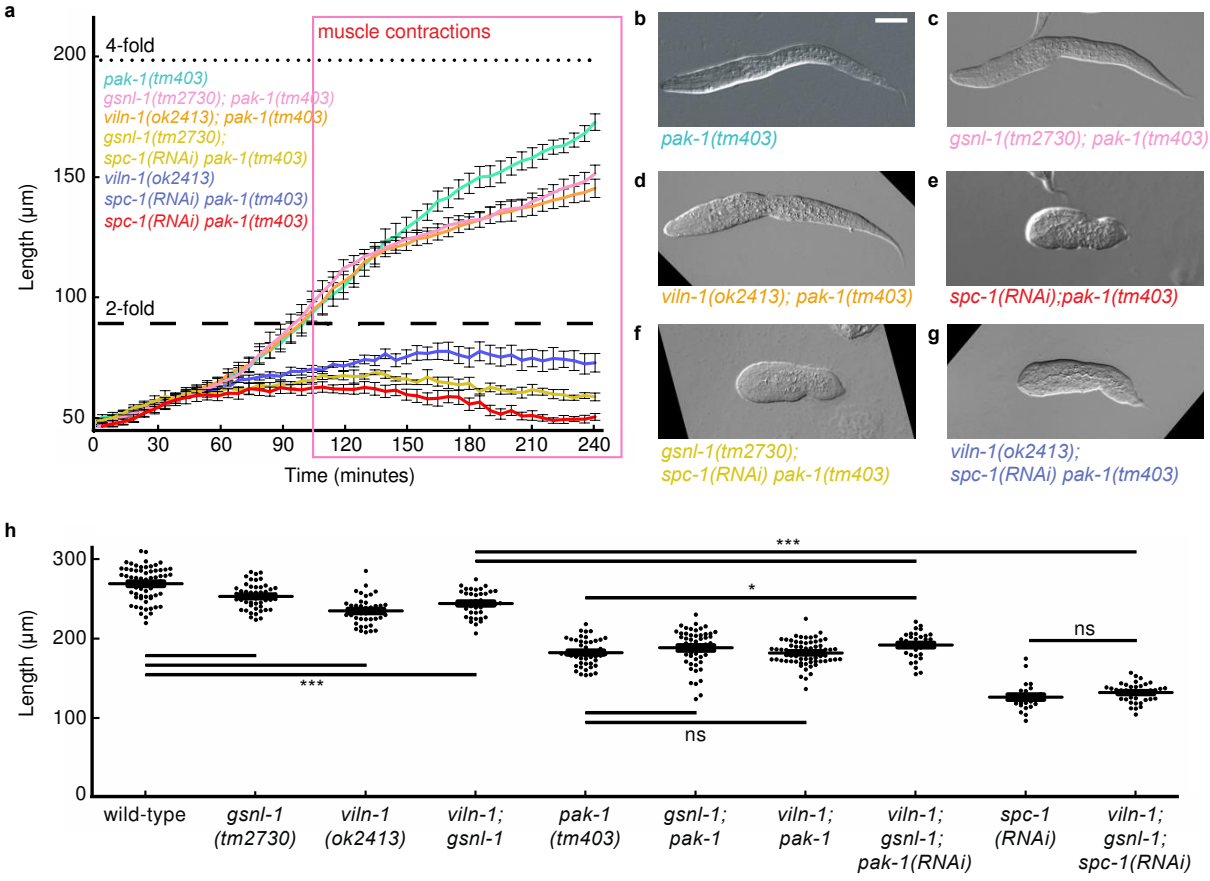

Figure 18: Combined loss of severing proteins, SPC-1 and PAK-1 rescues the retraction phenotype.
(a-g) Elongation curves and DIC pictures showing the terminal phenotypes of **(b)** *pak-1(tm403)* (n=11), **(c)** *gsnl-1(tm2730); pak-1(tm403)* (n=9), **(d)** *viln-1(ok2413); pak-1(tm403)* (n=9), **(e)** *gsnl-1(tm2730); spc-1(RNAi) pak-1(tm403) (n=5),* **(f)** *viln-1(ok2413); spc-1(RNAi) pak-1(tm403) (n=11)* and **(g)** *spc-1(RNAi) pak-1(tm403)* (n=9) (**a**). Pink box, period of muscle activity. Scale bar: 25 µm. Data represent mean values ± SEM. **(h)** Quantification of the L1 hatchling body length of *wild-type* (n=65), *gsnl-1(tm2730)* (n=52), *viln-1(ok2413)* (n=43), *viln-1(ok2413); gsnl-1(tm2730)* (n=41), *pak-1(tm403)* (n=47), *gsnl-1(tm2730); pak-1(tm403)* (n=51), *viln-1(ok2413); pak-1(tm403)* (n=70), *viln-1(ok2413); gsnl-1(tm2730); pak-1(RNAi)* (n=35), *spc-1(RNAi)* (n=27), and *viln-1(ok2413); gsnl-1(tm2730); spc-1(RNAi)* (n=41). Data represent mean values ± SD. Two-sided paired t-test. P-values: *<0,05; **<0,001; ***<0,0001; ns, not significant.

The finding that depleting GLSN-1 and VLN-1 can partially rescue elongation in *spc-1; pak-1* mutants was intriguing. Until now, I addressed their role in mediating a loss of network integrity in the absence of SPC-1/PAK-1 function, but I did not address their other possible role in the cycle of filament bending, disassembly and network remodeling that leads to shortening of circumferential filament bundles. If VLN-1 and GLSN-1 had key roles in the disassembly step, then one would predict that depleting VLN-1 and GLSN-1 or perhaps both together, in wild-type embryos, would affect elongation. To do so, we requested single and double *gsnl-1* and *viln-1* very strong or null mutations, previously characterized by Shoichiro Ono and his colleagues. I found that *gsnl-1* and *viln-1* single mutants and *gsnl-1; viln-1* embryos had an almost normal elongation, although their final length was slightly and significantly shorter than that of control embryos (Fig. 18c, d, h). Removing *pak-1* or *spc-1* in addition did not significantly modify their length compared to single *pak-1* or single *spc-1* embryos (Fig. 18c,d,h), although *gsnl-1(tm2730); pak-1(tm403)* and *viln-1(ok2413); pak-1(tm403)* did displayed a lower rate elongation compared to *pak-1(tm403)* (Fig. 18a). I concluded that the reason wild-type embryos are not more severely affected by the loss of zygotic GSNL-1 and VILN-1 activity could be that they rely on more than one process to remodel actin.

I also considered to test whether the retraction rescue provided by *viln-1* or *gsnl-1* would modify actin filament damage in *gsnl-1* or *viln-1*; *spc-1(RNAi) pak-1(tm403)* triple deficient embryos. Unfortunately, the *viln-1; Pepid::LifeAct::GFP; pak- 1(tm403)* combination was not viable for reasons that I did not explore, while the *gsnl-1* locus falls at about the same position as the *LifeAct::GFP* insertion point making a double recombination difficult to obtain.

Although spinning-disk microscopy did not reveal the precise remodeling mechanism, it suggests that muscle contractions induce actin filament bending and hence, direct or indirect stimulation of severing protein activity. Furthermore, we propose that this process goes uncontrolled in the absence of SPC-1 and PAK-1. The severing activity mediated by villin and gelsolin might act in parallel to some other process since villin gelsolin double deficient embryos show only minor elongation defects (Fig. 17h).

VIII. A Kelvin-Voigt model recapitulates the elongation of the embryos of various phenotypes

To rationalize the role of muscles in epidermal remodeling, we decided to use a mathematical model. The aim was to give a mesoscopic physical description and interpretation of embryo elongation, rather than a detailed mechanistic formulation. Thus, we described the *C. elegans* embryo under elongation as a visco-elastic body: a solid that deforms permanently when it is submitted to mechanical stress. The model that will be described now has been fully implemented by Teresa. The model is considering:

- the elongation profiles described in this work,
- the results of our previously published laser ablation experiments (Vuong-Brender et al, 2017),
- the data on the organization of the actin cytoskeleton described in this work as an indirect measure of its stiffness,
- the duration of muscle contractions described in this work.

Our model is summarized in four main equations (Fig. 19). Even if the scheme is very simple, the parameters have a strong connection with biological entities. The parameters playing a fundamental role in the equations that account for the elongation curves are:

- αDV, which is positively related to actomyosin stiffness in the D/V cells;
- β, which expresses the global activity of the remodeling factors SPC-1, PAK-1 and FHOD-1;
- γ, which represents the accumulation of cytoskeleton damage.

a $$\eta \frac{dl}{dt} = -k\,(l - \lambda) + F_{epid} + F_{muscles}$$

b $$F_{epid} = F_{seam}\,\alpha_{DV}$$

c $$\frac{d\lambda}{dt} = \beta \frac{dl}{dt} H(\alpha_{DV})\, Hill(\lambda) \quad \text{if} \begin{cases} \cdot\ \frac{dl}{dt} > 0 \\ \cdot\ 0 \leqslant \beta < 1 \\ \cdot\ l - \lambda > \frac{F_c}{k} \end{cases}$$

d $$\frac{d\alpha_{DV}}{dt} = \gamma \frac{dl}{dt} \quad \text{if} \ \frac{dl}{dt} < 0 \ \text{and} \ \alpha_{DV} > 0$$

Figure 19: Equations supporting the mechanical model.
(**a**) System equations for the viscoplastic mechanical model of embryo elongation. The embryo is represented as a Kelvin-Voigt solid (spring stiffness *k*, resting length *λ*, viscosity η) submitted to forces F_{epid} and F_{muscle}.

We chose to use a Kelvin-Voigt system represented by a spring in parallel to a dashpot, subject to two main active forces (Fig. 20). First, the epidermal force F_{epid} is a continuous positive force, allowing the embryo to elongate. The elongation will stop when the resistance of the spring will equalize the intensity of F_{epid}. Since muscle-defective mutants cannot elongate beyond 2-fold the presence of F_{epid} is tuned can capture the first phase of elongation. Second, the muscle force $F_{muscles}$ is a pulsatile force since muscles alternatively contract and relax, starting from the 1.7-fold stage. We want to stress out that while the embryo extends along its A/P axis, actin bundles shorten along the DV axis due to volume conservation. We chose to model with a resting length increase only for positive rates for two reasons: 1) it is simple in terms of modeling; 2) it captures the mechanism we hypothesize for actin shortening. The model has free parameters, but we constrained the parameter space by using the experimental observations of the different phenotypes. Based on the mechanism of elongation that we hypothesized, a resting length that responds to stretching ensures elongation. To simplify its comprehension, it will now be developed step by step.

We started with the simplest version of the model represented by a regular spring and a dashpot, only submitted to the force from the epidermis F_{epid} (Fig. 20a). In terms of physics, we represented the Kelvin-Voigt viscoelastic model in the first equation where k is the body stiffness, λ is the spring resting length and η is the coefficient of viscosity (Fig. 19a). It captures the behavior of viscoelastic solids under stress. F_{epid} is the result of an active force in the lateral epidermis (also called seam cells), and a passive force exerted by the dorsal and ventral epidermal cells (called DV cells) adjacent to the seam cells. The seam cells have a high concentration of non-muscle myosin II, which has a non-polarized distribution and does not display pulsatile flow (Vuong-Brender *et al.*, 2016; Vuong-Brender *et al.*, 2017). Therefore, the stress generated by the seam cells is anisotropic and globally oriented along the DV axis. On the other hand, the DV epidermal cells do not contribute to generate active stress, as their myosin II is kept mostly silent through the activity of the RhoGAP RGA-2 (Vuong-Brender *et al.*, 2016; Vuong-Brender *et al.*, 2017; Diogon *et al.*, 2007), but the presence of circumferential F-actin filament bundles creates a global stiffness anisotropy. Thus, we described, in a second equation, F_{epid} as the product of an active force, *Fseam*, and a passive component, αDV, resulting from actin bundle stiffness (Fig. 19b). It recapitulates the first phase of elongation before reaching a plateau that depends on αDV (Fig. 20a'). The parameter αDV is positively related to the stiffness of the cytoskeleton in the D/V cells, with its initial value, αDV being the one set at the 2-fold stage. In our model αDV can evolve in time by decreasing if there is tearing. We constrained αDV to be constant for wild-type embryos, since we observed that their actin cytoskeleton integrity and straightness is maintained over time. Likewise, we assume that αDV is constant in the muscle-defective *unc-112* background, since muscles do not exert any stress. By

contrast, we allowed αDV to change for *spc-1* single and *spc-1 pak-1* double mutants, considering that their cytoskeleton is less organized and more compliant to stress. Moreover, based on our measurements we constrained αDV (0) for all the genotypes to be inferior to the one obtained for wild-type. We would like to point out that when fitting the parameters in absence of this constraint we obtained the same results.

The second step was to introduce the force from the muscles into the system (Fig. 20b). As the muscles allow the elongation beyond the 2-fold stage, we represented $F_{muscles}$ stronger than F_{epid}. The muscles contract in a cyclic manner, so the force they deploy oscillates between positive and negative values (Fig. 20b', blue rectangle). Because of this behavior, the net contribution to elongation is null; the simulated curve obtained is very similar to the first situation, except constant oscillations when the plateau is reached.

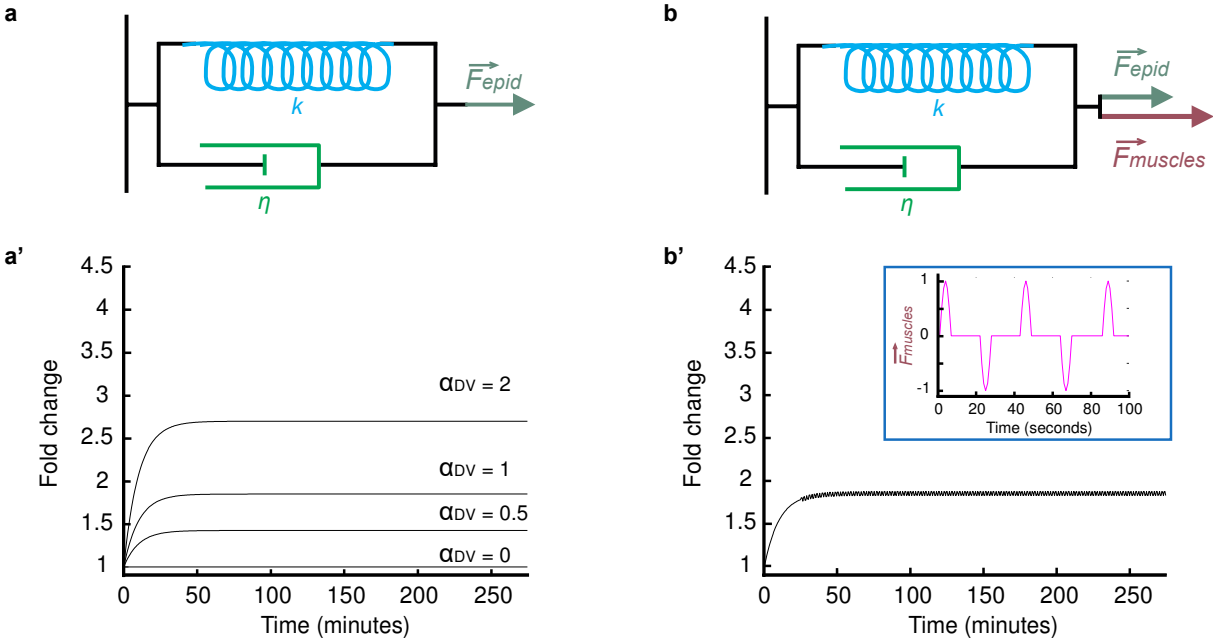

Figure 20: Time-dependent length of a Kelvin-Voigt model in different conditions.
(a-a') A generic Kelvin-Voigt system exposed to a constant force F_{epid}, and **(a')** its predicted elongation change for F_{seam} =0.85 and four different values of α_{DV} based on the equation $F_{epid} = F_{seam}\ \alpha_{DV}$. **(b-b')** A similar system exposed to two forces, F_{epid} and an oscillating force $\vec{F}_{muscles}$, and **(b')** predicted elongation change using F_{epid}=0.85 and $\vec{F}_{muscles}$ with an amplitude equal to 1 and the behavior depicted in the blue-boxed inset. For simplicity, we will refer to the amplitude of $\vec{F}_{muscles}$ by $F_{muscles}$. As the pulsatile force induces both compression and stretching (see Fig. 1c), its net input on elongation is transient and the system oscillates around the maximal value reached without $\vec{F}_{muscles}$. In all other panels (except in a), $\vec{F}_{muscles}$ was set as a periodic function with positive and negative steps of duration 6 seconds modulated by a cosine function, alternating with periods of null value of duration 15 seconds **(b'-inset).** In **(a-b')** the elastic constant of the spring is k=1, the initial resting length has the value λ(t=0)=1, and the viscosity value is η=10.

Despite having introduced the two forces submitting our system to stress, yet we could not recapitulate the elongation of the wild-type embryos as the curves rapidly reached a plateau. Thus, to introduce a positive contribution to embryo lengthening, we allowed some plasticity, in the physical sense, or ability of the system to get reorganized. In terms of biology, it corresponds to a permanent rearrangement as it has been already observed and modeled in systems undergoing stresses (Doubrovinski *et al.*, 2017; Munoz and Albo, 2013). In terms of modeling, it means adding a "plasticity factor" β to the spring and a ratchet in the system, which can be done by a simple mathematical solution: having an adjustable resting length λ described in a third equation (Figs. 19c, 21a). The simulated curves displayed an increase of the length with time. The speed of the growth (angle of the curve) can be adapted either by modulating either β or $F_{muscles}$ (Fig. 21a',a''). The "plasticity factor" β is constrained between 0 and 1, 0 corresponding to no plasticity, therefore no elongation beyond the 2-fold stage. We chose the tearing factor, β, to be null in control embryos as a mean to simplify the equations and to avoid adding a positive polymerization factor. We view the "plasticity factor" as an indirect measure of actin bundle shortening, thus of stiffness maintenance, as they are related. Our measurements show that the circumferential length of dorsal-ventral cells in *spc-1 pak-1* defective embryos is almost unchanged during the first elongation phase and increases during the second phase of elongation. We interpret this as evidence that *spc-1 pak-1* defective embryos are unable to remodel their cytoskeleton at the level of D/V cells in order to reduce the length of actin bundles and to resist the tension created by actomyosin in lateral cells. The moderate gain in length of the embryo during the first elongation phase is only due to myosin II acting in the seam epidermal cells to reduce their circumferential dimension. The result of the fit is coherent with this picture since we found the plasticity factor to be close to zero. From a cellular standpoint, having a changing resting length at each cycle of contractions means that body elasticity does not bring the embryo back to its initial shape upon muscle relaxation, enabling progressive lengthening.

Regarding the force produced by muscles, which is essential for elongation, the growth rate is predicted to be an increasing function of $F_{muscles}$. We could not directly test the behavior of an intermediate muscle force, since the available muscle mutants totally suppress muscle activity and show a Pat phenotype. To highlight the predicted effect of increasing $F_{muscles}$, we considered the length of the embryo as increasing function of the intensity of the muscle force $F_{muscles}$. To link muscles activity and cytoskeleton remodeling, we showed that they locally squeeze the embryo along the A/P axis producing an increased circumferential stress due to volume conservation. And, during these contraction phases, the actin bundles get bent to angles that match the local extent of muscle contractions. It has been demonstrated by in vitro experiments that actin can get severed

when bent at an angle distributed around 57° (McCullough et al, 2011). Interestingly, we frequently observed that muscle contractions resulted in actin bending at angles greater than 57°.

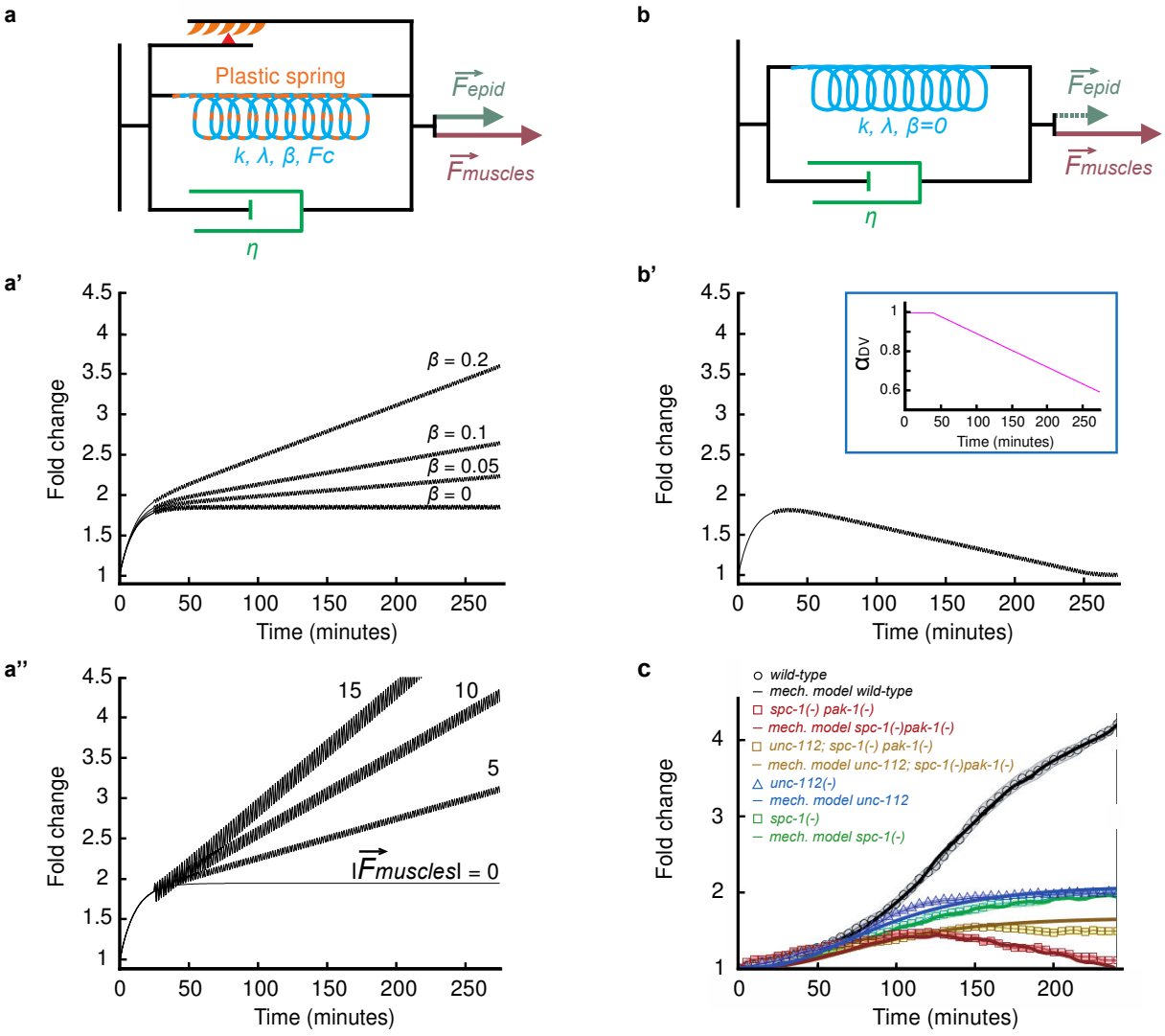

Figure 21: Time-dependent length of a Kelvin-Voigt model in different conditions.
(a-a'') A Kelvin-Voigt system with mechanical plasticity introduced according to Eqs. (1, 4, 6, 7), and **(a')** predicted elongation change using F_{epid}=0.85, F_c=0, $F_{muscles}$ =3 and four distinct values of the plasticity factor β, or **(a'')** using F_{epid}=0.85, F_c=0, β =0.10 and four distinct values of $F_{muscles}$. **(b-b')** A Kelvin-Voigt system in which the plasticity is defective (β=0), and in which there is actin tearing according to Eq. (7) inducing a progressive reduction of F_{epid}, and **(b')** predicted elongation change with an initial value of F_{epid}=0.85, the tearing factor γ=0.15 and $F_{muscles}$ =3; the blue-boxed inset **(b')** shows the behavior of $\alpha_{DV}(t)$ over time. In **(a-b'')** the elastic constant of the spring is k=1, the initial resting length has the value λ(t=0)=1, and the viscosity value is η=10. **(c)** Result of the fit for the following genotypes: *wt*, *unc-112* alone *spc-1* alone, *spc-1 pak-1* double, *unc-112; spc-1 pak* according to Eqs. (1, 4, 9-11). The values of the parameters are specified in paragraphs 1.5 and 1.6. The shallow decrease in length for the curve of *unc-112; spc-1 pak-1* after 150 minutes is due to a deformation of the embryos under the effect of *unc-112* knock-down but not to retraction, which is why the fit has been evaluated on the first 150 minutes of the curve.

After modeling the wild-type elongation, we wondered how we could reproduce the retraction of the double *spc-1 pak-1* mutant embryos. We showed that the loss of SPC-1 and PAK-1, affects the integrity of the actin cables in the DV cells, which provide stiffness and define αDV (Figs 8-13). Thus, we defined a "tearing factor" *γ* as described in the fourth equation (Fig. 19d). When *γ* is equal to 0, it corresponds to an absence of tearing, as in wild-type embryos. It leads to a decrease of αDV over time (Fig. 21b' blue rectangle) and therefore a similar decrease of *Fepid*. All these characteristics combined with a "plasticity factor" β equal to 0 generate a simulated curve that first grows and rapidly decreases; mimicking the retraction phenotype observed in the embryos.

To also further constrain the model by additional measurements we tried to follow over time the intensity of actin and its organization. Using TIRF-SIM super-resolution imaging, we could clearly observe criss-crossing occurrences in *spc-1 pak-1* deficient embryos right above muscles. Furthermore, by performing a line-scan intensity profile of adjacent actin filaments, we observed that their intensity was more irregular in those double mutants consistent with some individual filaments defasciculating from the main bundles - we are remaining careful on that statement, because even TIRF-SIM did not resolve shortening events. Accordingly, we infer that after strong bending some circumferential actin filaments within bundles get severed, then probably partially depolymerized upon severing and re-bundled. Furthermore, it suggests that the criss-crossing plus potential defasciculation of individual actin filaments in *spc-1 pak-1* defective embryos, but not in control embryos, could correspond to severed filaments that did not get repaired/stabilized.

Thanks to the developed model, we could accurately predict the elongation pattern of wild-type embryos but also of several mutant conditions, notably the retraction pattern of *spc-1 pak-1* and the triple deficient *unc-112 spc-1 pak-1* (Fig. 21c). Note that for this last mutant, the simulated curve is less accurate, mostly due to the collapsing of the worms as the muscle input is removed and their epidermis is damaged / weaker. Nevertheless, the predictions of our model are strongly connected with some experimental findings. Fitting the parameters predicts a value close to zero for the plasticity factor of *spc-1 pak-1* mutants associated with a tearing factor different from zero. It means that *spc-1 pak-1* mutants are unable to remodel their cytoskeleton to reduce the circumferential size of the actin filaments in the D/V epidermal cells. Consistent with this view, we showed that the circumferential size of *spc-1 pak-1* defective embryos increases once muscles become active, showing that the actin filaments did not shorten. The model also predicts a small plasticity factor but with a low tearing factor for single *spc-1* mutants. These mutants can slightly decrease their circumference, meaning that their actin filaments have a small ability to remodel.

To conclude on this part, we propose that SPC-1/α-spectrin and PAK-1 regulate a cellular process of mechanical plasticity. When muscles contract, they locally squeeze the embryo along the AP axis, which generates an increased circumferential stress due to volume conservation. As shown before, circumferential actin cables become bent (Fig. 16), which certainly introduces a state of increased stress along their length and induce their severing (Figs. 17-18). Overall it creates the conditions for actin filament remodeling toward filament shortening, as the embryo elongates and its circumference decreases. In *spc-1 pak-1* defective embryos, the continuing stress on weakened actin filaments leads to their disorganization and reduces their stiffness. The remodeling process becomes less efficient and does not allow the embryo to stabilize their shape.

IX. Combined loss of FHOD-1 and SPC-1 leads to the same retraction phenotype

IX. 1. *fhod-1 spc-1* retracts and their actin show the same abnormalities as *spc-1 pak-1*

Next, we wanted to mechanistically define how cell shapes are maintained at the molecular level when cells are exposed to repeated mechanical strain and further define the molecular basis of viscoplasticity. Thus, Gabriella searched for gene knockdowns inducing retraction of *spc-1(ra409)* embryos (Fig. 22a; Table 4). The screen was limited to ninety essential genes, among phosphatases, cytoskeleton/cell cortex-related and junctional/attachment-related genes, shortlisted from the initial enhancer screen mentioned earlier. It identified the atypical formin FHOD-1 (Fig. 22a,b; Movie 5), which has previously been linked to actin dynamics in the epidermis (Vanneste *et al.*, 2013). I confirmed that *fhod-1(tm2363); spc-1(RNAi)* embryos also showed a penetrant retraction phenotype (Fig. 22j).

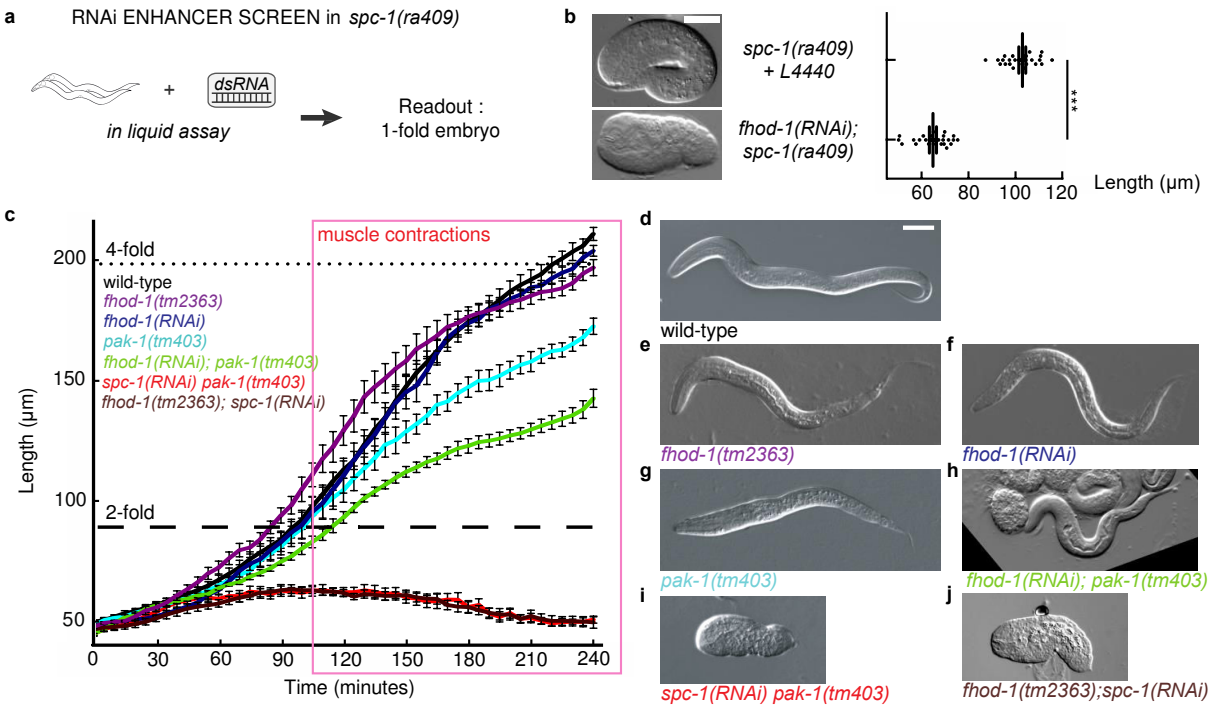

Figure 22: Combined loss of SPC-1 and PAK-1 or SPC-1 and FHOD-1 leads to comparable retraction phenotypes.
(a) A retraction screen in a *spc-1* mutant identifies *fhod-1*; **(b)** quantification of *spc-1(ra409)* L1 hatchling body length after feeding on L4440 control (n=21) or *fhod-1(RNAi)* (n=25) bacteria. Scale bar: 15 µm. Data represent mean values ± SD. Two-sided paired t-test. P-values: *<0,05; **<0,001; ***<0,0001; ns, not significant. **(c)** Elongation curves and **(d-j)** corresponding DIC pictures showing the terminal phenotypes at hatching of **(d)** wild-type (n=12), **(e)** *fhod-1(tm2363)* (n=10), **(f)** *fhod-1(RNAi)* (n=10), **(g)** *pak-1(tm403)* (n=11), **(h)** *fhod-1(RNAi); pak1(tm403)* (n=10), **(i)** *spc-1(RNAi) pak-1(tm403)* (n=8), and **(j)** *fhod-1(tm2363); spc-1(RNAi)* (n=9). Pink box, period of muscle activity. Note that the elongations curves of *spc-1(RNAi) pak-1(tm403)* and *fhod-1(tm2363); spc-1(RNAi)* completely overlap. Scale bar: 25 µm. Data represent mean values ± SEM.

Then, with Teresa, we performed the same texture analysis as described before. Again, I acquired pictures of anesthetized embryos at different stages (1.7-fold, 2-fold and 3-fold) by spinning-disk imaging (Fig.23).

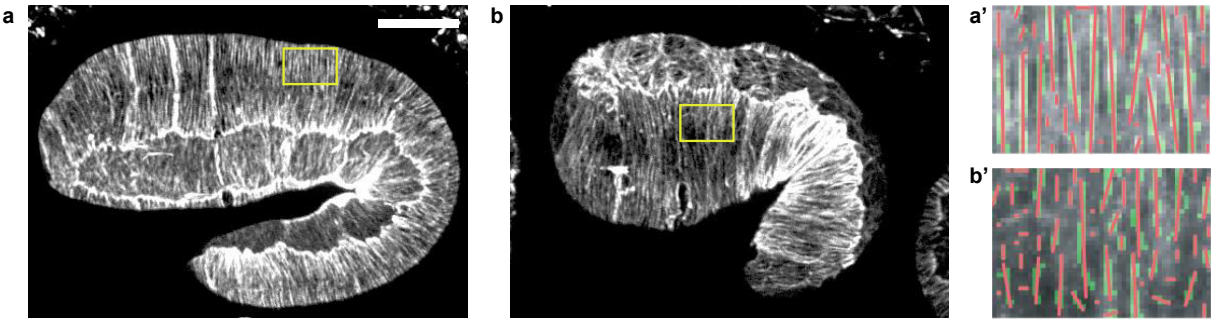

Figure 23: Actin filaments show organization defects in *fhod-1; spc-1* defective embryos.
(a,b) Epidermal actin filaments visualized with the *Pdpy-7::LifeAct::GFP* reporter construct in *fhod-1* (**a-a'**), and *fhod-1(tm2363) spc-1(RNAi)* (**b-b'**) at mid-elongation (2-fold equivalent) stage. Yellow rectangle, region of interest (ROI). Scale bar: 10 µm**. (a'-b')** ROI after binarisation (green) and major axis detection (red).

Segmentation analysis of the fluorescence signal associated with actin filaments in the D/V epidermis revealed more discontinuity in *fhod-1; spc-1* double deficient embryos compared to wild-type embryos, with no significant difference from *spc-1 pak-1* embryos (Fig. 24). Moreover, like in *spc-1 pak-1* again, Fourier transform analysis showed that the degree of anisotropy relative to the circumferential axis of *fhod-1; spc-1* was abnormal (Fig.25).

Both parameters followed the same trend over time, as described earlier. Actin cable anisotropy decreases with time and at 2-fold, the difference between the different genotypes reaches its maximum. As the embryos elongate, differences among them become less significant (Figs. 24-25). Nevertheless, *spc-1 pak-1* and *fhod-1; spc-1* show similar defects over time and are constantly less organized than wild-type.

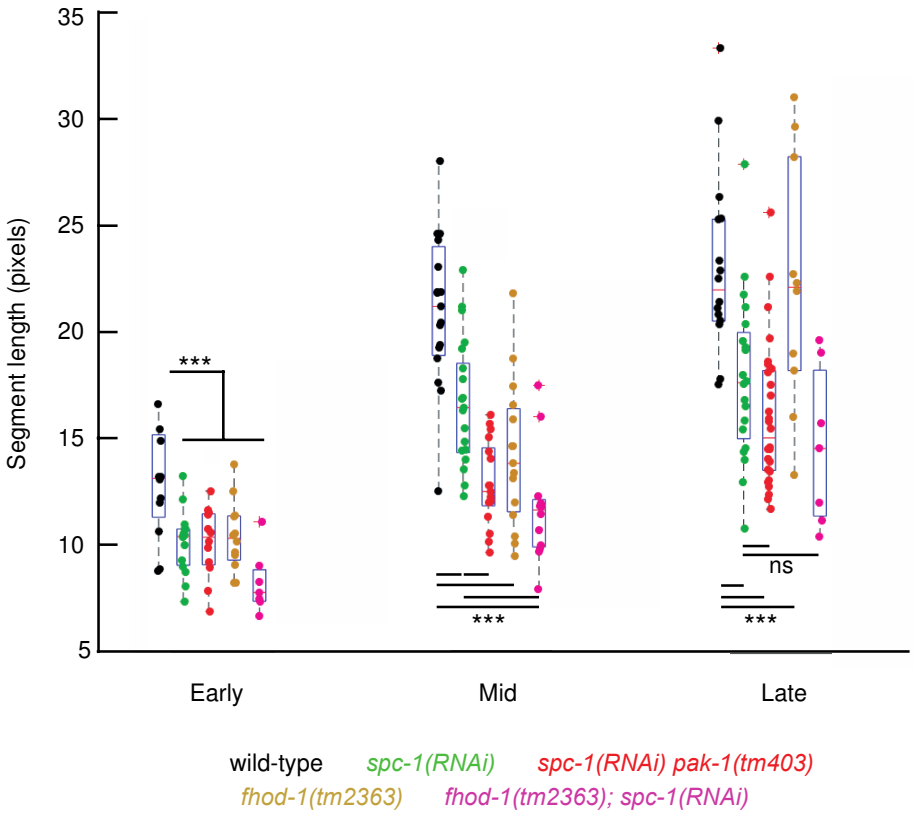

Figure 24: Actin filaments show continuity defects in *fhod-1; spc-1* defective embryos.
Quantification of actin filament continuity ; the graph represents the length (in pixels) along the circumferential axis of actin filaments in early, mid and late (corresponding to 1.7-fold, 2-fold and 3-fold equivalent stages in a wild-type embryo, respectively) embryos of wild-type (early n=12, mid n=19, late n=16), *spc-1(RNAi)* (early n=15, mid n=21, late n=20), *spc-1(RNAi) pak-1(tm403)* (early n=12, mid n=17, late n=26), *fhod-1(tm2363)* (early n=12, mid n=14, late n=10), *fhod-1(tm2363); spc-1(RNAi)* (early n=7, mid n=11, late n=8) genotypes. Graphs represent median values, 25th and 75th percentiles; whiskers extend to the most extreme data points not considered outliers. Two-sided paired t-test. P-values: *<0,05; **<0,001; ***<0,0001; ns, not significant.

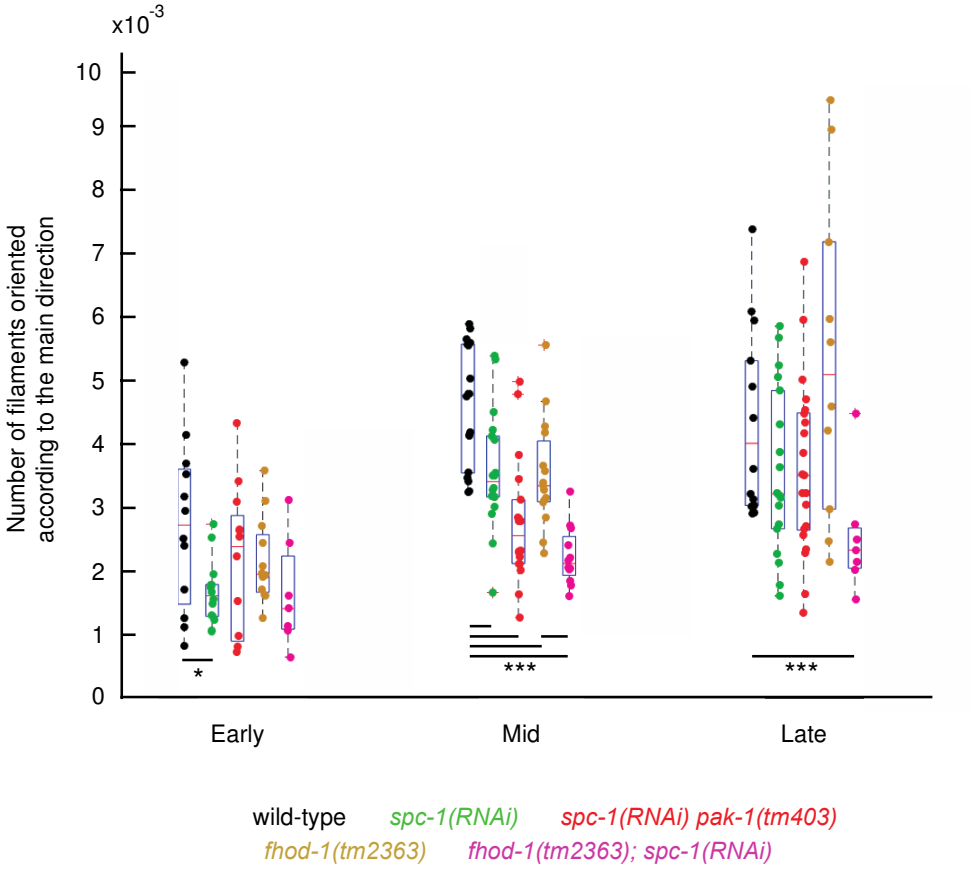

Figure 25: Actin filaments show orientation defects in *fhod-1; spc-1* defective embryos.
Actin filament orientation based on Fast Fourier Transform and binarisation. Wild-type (early n=12, mid n=18, late n=14), *spc-1(RNAi)* (early n=14, mid n=18, late n=18), *spc-1(RNAi) pak-1(tm403)* (early n=12, mid n=18, late n=21), *fhod-1(tm2363)* (early n=12, mid n=14, late n=10), *fhod-1(tm2363); spc-1(RNAi)* (early n=7, mid n=11, late n=8) genotypes. Note that the characteristics of actin filaments in *spc-1(RNAi) pak-1(tm403)* embryos differ mostly at the equivalent of the two-fold stage when muscles become active. At ealier and later stages, *spc-1(RNAi)* embryos and *spc-1(RNAi) pak-1(tm403)* embryos become similar. Graphs represent median values, 25th and 75th percentiles; whiskers extend to the most extreme data points not considered outliers. Two-sided paired t-test. P-values: *<0,05; **<0,001; ***<0,0001; ns, not significant.

IX. 2. FHOD-1 bundling activity is important for the remodeling

FHOD-1 identification was intriguing as, in addition to nucleation, vertebrate FHOD1 promotes actin capping and bundling (Schonichen *et al.*, 2013). This raised the tantalizing possibility that FHOD-1 activity stabilizes the actin cytoskeleton after severing. Furthermore, the genetic interaction suggested that FHOD-1 acts with SPC-1 and PAK-1.

To examine this possibility, Flora built several constructions of FHOD-1 based on what was known from the literature. Indeed it has been shown that the formin FHOD-1 is initially inactive due to an autoinhibitory interaction between its C-terminal diaphanous autoregulatory domain (DAD) with the N-terminal diaphanous inhibitory domain (DID)[29]. By deleting the DAD domain, the autoinhibition is removed and was shown to generate a constitutively active form of the protein in vertebrate tissue cells. I wanted to test if a similar approach would work in our system and whether FHOD-1 derivatives removing the C-terminal DAD domain could rescue the retraction phenotype of *spc-1 pak-1* deficient embryos.

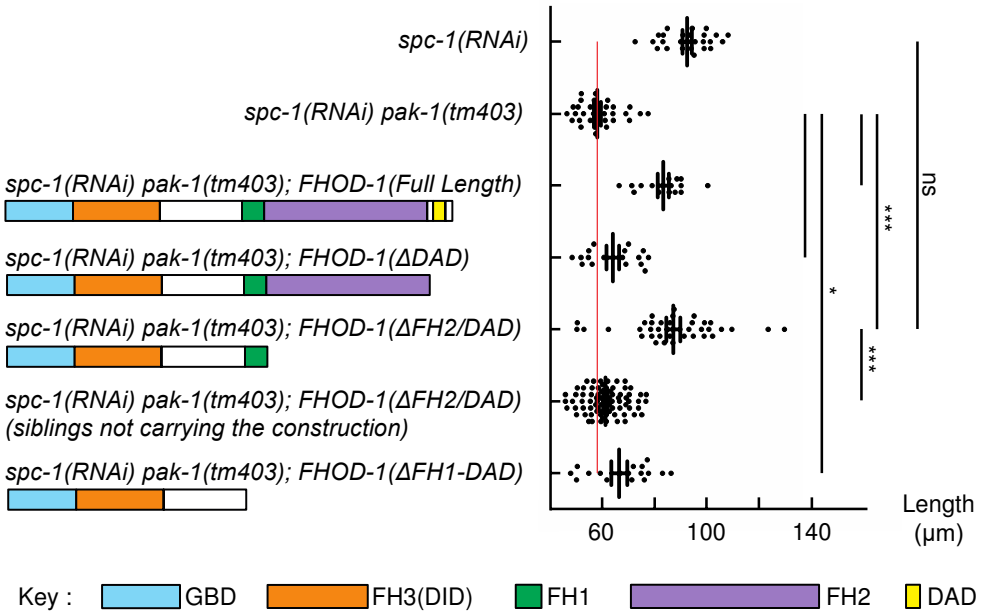

Figure 26: FHOD-1 construction lacking FH2 and DAD domains rescues the retraction phenotype.
Pdpy-7 driven epidermis expression of truncated FHOD-1 variants and terminal body length at hatching: *spc-1(RNAi)(*n=26); *spc-1(RNAi) pak-1(tm403)* with no transgene (n=36), with FHOD-1(full length) (n=16), FHOD-1(ΔDAD) (n=17), FHOD-1(ΔFH2-DAD) (n=38) transgenes or non-transgenic siblings (n=78), FHOD-1(ΔFH1-FH2-DAD) transgene (n=18). Data represent mean values ± SD. Two-sided paired t-test. P-values: *<0,05; **<0,001; ***<0,0001; ns, not significant.

Strikingly, after epidermis-specific expression of a form lacking the FH2 and DAD domains, transgenic *spc-1(RNAi) pak-1(tm403)* embryos reached the length of *spc-1* single mutants without retracting; rescue was better than with the full-length protein. By contrast, the DAD deleted construct failed to rescue, while deletion of the FH1-FH2-DAD domains and other forms marginally rescued retraction (Fig. 26), arguing that the FH2 F-actin nucleation domain is dispensable for rescue while the FH1 is not. Importantly, a mammalian FHOD1 lacking the FH2-DAD domains can still bundle actin (Schonichen *et al.*, 2013), thereby emphasizing that FHOD-1 bundling activity matters. It further suggests that he atypical formin-homologue responsible for actin capping and bundling is involved in the same regulatory pathway as PAK-1. The retraction of *spc-1 pak-1* deficient embryos could mainly result from a lack of FHOD-1 activation downstream of the muscle-induced mechanotransduction pathway. This result raises the possibility that this direct activation could be mediated by a phosphorylation of FHOD-1 by PAK-1. In conclusion, I suggest that the actin filament severing initiated by muscle contractions (Figs. 17-18) followed by FHOD-1-dependent bundling or capping (Fig. 26) represent a ratchet-like mechanism, providing a molecular basis for viscoplasticity.

IX. 3. FHOD-1 and PAK-1 localization are affected the same way by the lack of SPC-1

Several factors could contribute to alter PAK-1 and FHOD-1 activity. First, Gabriella noticed that inducing *spc-1(RNAi)* in embryos expressing PAK-1::GFP, disturbed PAK-1 localization and lead to the formation of ectopic PAK-1 aggregates (Fig. 27a,a'). Interestingly Flora observed the same defect in FHOD-1::GFP expressing embryos upon *spc-1(RNAi)* downregulation (Fig. 27b,b'). Additionally, FHOD-1 localizes at the same sites as PAK-1, SPC-1 and actin at the level or the epidermal cell cortex.

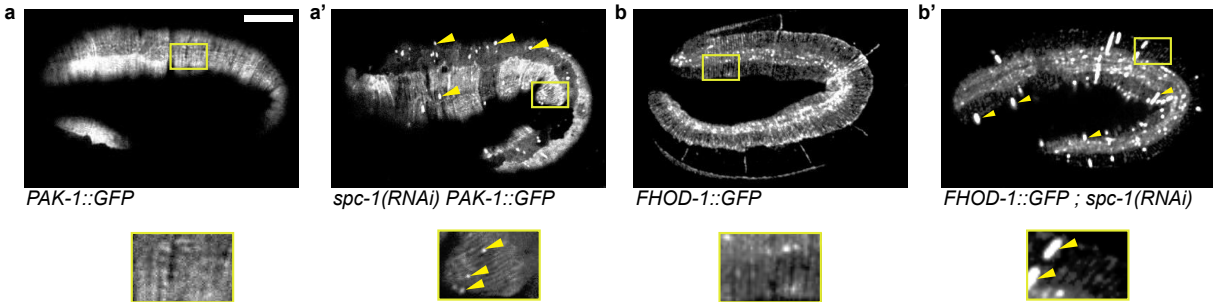

Figure 27: PAK-1 and FHOD-1 form aggregates in *spc-1(RNAi)* loss of function.
(a-a') PAK-1::GFP localisation in wild-type and *spc-1(RNAi)* embryos. Yellow box, area enlarged below the panel. Note the punctae in SPC-1 deficient embryos. (**b-b'**) FHOD-1 localization in wild-type and *spc-1(RNAi)* embryos. Note the aggregates (arrowheads). Note also that FHOD-1::GFP displayed a filamentous organization reminiscent of actin filaments. Scale bar: 10 µm.

These results strongly suggest that FHOD-1, the atypical formin, responsible for actin capping and bundling, is involved in the same regulatory pathway as PAK-1 and SPC-1 during the embryonic developmental process we characterized and SPC-1 could help recruit these proteins.

Second, by using the short spinning-disk time-lapses and tracking landmarks on the actin as described at the beginning, I found that muscle contractions in *spc-1(RNAi) pak-1(tm403)* embryos were almost twice as short as those in *pak-1(tm403)* and wild-type controls (3 sec against 5.7 sec; Fig. 28, Movie 6). Although, muscles can strongly bend actin cables even in *spc-1 pak-1*, as shown earlier, such shorter contractions might not give enough time for FHOD-1 to stabilize actin filaments.

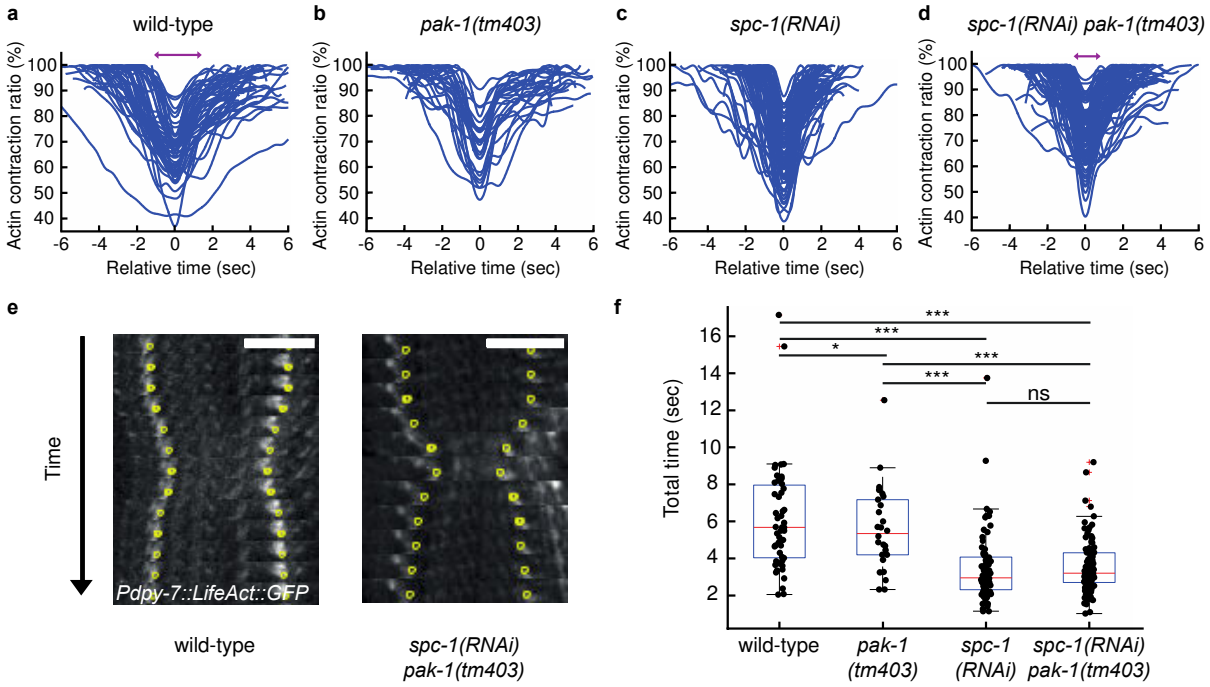

Figure 28: Tracking of the actin displacement reveals duration of the muscle contractions.
(a-d) Spinning-disk microscopy tracking of actin filaments visualized with a *Pdpy-7::Lifeact::GFP* marker specifically expressed in the epidermis. Individual displacement tracks of wild-type **(a),** *pak-1(tm403)* **(b),** *spc-1(RNAi)* **(c)** and *spc-1(RNAi) pak-1(tm403)* **(d)** embryos at a stage equivalent to 2-fold in a wild-type embryo. Scale bar: 10 µm. **(e)** Typical kymographs of the *Lifeact::GFP*–labeled actin filaments in wild-type and *spc-1(RNAi) pak-1(tm403)* embryos from which the tracks in a-d were derived. Time interval between two images is 0.41 second. Yellow dots correspond to landmarks for quantitative analysis. **(f)** Quantification of the displacement duration in (N=embryo/ n=contraction): wild-type, N=11/n=51; *pak-1(tm403)*, N=11/n=26; *spc-1(RNAi)*, N=11/n=73; *spc-1(RNAi) pak-1(tm403)*, N=11/n=89. Graphs represent median values, 25th and 75th percentiles; whiskers extend to the most extreme data points not considered outliers. Two-sided paired t-test. P-values: *<0,05; **<0,001; ***<0,0001; ns, not significant.

To conclude, we uncovered a novel machinery involving α-spectrin/SPC-1, the kinase PAK-1 and several actin remodeling proteins involved in stabilizing cell shapes in a system submitted to repeated external mechanical stress. When SPC-1 and PAK1 are both absent, the embryo starts to elongate then retracts to its initial length, A key aspect of our results is that embryonic retraction is triggered only when muscles start to contract, exposing the overlying epidermis to changes in tension every few seconds. In wild-type embryos, muscle contractions promote embryonic elongation from the 2-fold to the final 4-fold stage. As the embryo elongates and its diameter reduces, actin bundles present in D/V cells must shorten. Our data show that the molecular machinery enabling actin filament remodeling is at the heart of the defects observed in *spc-1 pak-1* deficient embryos. We propose that the progressive shortening of actin filaments under the control of these factors mediates a cellular viscoplastic process promoting axis elongation. A similar viscoplastic process might operate in vertebrate tissues comprising an epithelial layer surrounded by a contractile layer, such as our internal organs.

DISCUSSION AND PERSPECTIVES

DISCUSSION AND PERSPECTIVES

To study mechanotransduction and its importance in morphogenesis at the scale of an organism, I worked with a simple model, the nematode *C. elegans*. My thesis aimed to give a better understanding of the role of the actin cytoskeleton and its remodeling during *C. elegans* elongation as it would provide finer details of how cells adapt and respond to mechanical input. The work presented here is mostly included in a letter published in Nature. The full version of the paper including all the supplementary information is available in the annex of the thesis.

The focus of this work was directed to the second phase of *C. elegans* embryonic elongation. This process does not involve cell divisions or rearrangements and relies entirely on epidermal cell shape changes. The second phase of elongation starts at the onset of muscle contractions: from this point the epidermal cells are submitted to regular cycles of intense mechanical input. The epidermis needs to meet two requirements for the maintenance of a proper embryonic development. On the one hand, it must be able to mechanically resist to this force input that exerts cyclic physical stress on the epidermis. On the other hand, this input provides a crucial development signal at the same time: it induces a biochemical signaling pathway that promotes hemidesmosome remodeling and further elongation through a tension-induced mechanotransduction pathway. The molecular components of the epidermis need to be able to properly sense and translate this signal and execute the necessary developmental changes.

In the frame of this thesis project we extended our understanding on the molecular landscape around that complex process. We identified a novel morphogenetic ratchet mechanism that is responsible for the stabilization and remodeling not only of the epidermal cells, but also, of the entire embryonic body under cyclic stress from the second elongation phase. We equally identified the main molecular players of this morphogenetic ratchet through the interaction of PAK-1, p-21 activated kinase and SPC-1, a cytoskeletal component, important for the maintenance of cellular mechanical properties.

Through genetic and reciprocal molecular screens, we established both an *in vivo* genetic and *in vivo* physical interaction between these two players. The combined loss of SPC-1 and PAK-1 lead the embryos to first elongate and then retract to their initial shape. We considered that together SPC-1 and PAK-1 function as a locking mechanism of the elongation. When they are absent, the system is not locked and goes awry. We provided evidence that this interaction takes place in the epidermis. To characterize the defects underlying the retraction, we developed a novel approach for

the dynamic and simultaneous acquisitions of epidermal actin filaments and the underlying muscles. We developed a corresponding novel approach for image analysis and quantification of this coupling. This way we were able to establish that the two neighboring tissues, epidermis and muscles, are properly coupled, even in the *spc-1 pak-1* deficient embryos. Using different translational reporters, co-localization tests and super-resolution microscopy we showed that the physical interaction might take place between these players also *in vivo* as we established a co-localization of a PAK-1/SPC-1/actin network at the epidermal cell cortex at the level of cell junctions and the circumferential actin bundles. We also know that, at the level of the epidermal components, the retraction process does not affect the proper recruitment and localization neither of the adherens junctions nor the microtubules (data not shown, Gabriella Pasti's thesis). A key aspect of our results is that embryonic retraction is triggered only when muscles start to contract, exposing the overlying epidermis to changes in tension every few seconds. The mechanical properties of a biological material are dominated by an elastic behavior at low timescales (seconds), which allows the propagation of tension between the cells in a tissue. Hence, the retraction phenotype most likely relies on the elastic properties of the epidermis. That is why we focused our attention to the actin cytoskeleton. Indeed, we observed a muscle dependent disorganization of the actin filaments in the combined loss of PAK- and SPC-1. Super-resolution microscopy showed that epidermis circumferential actin filament bundles are discontinuous and not fully oriented perpendicular to adherens junctions in *spc-1(-) pak-1(-)* embryos. The actin defects could be best observed in the region that overlaps with the muscle attachment zone. Additionally, spinning-disk microscopy revealed that muscle contractions are strong enough to locally bend actin bundles at great angles, which has been reported to induce actin filament severing in vitro (McCullough *et al.*, 2011). We observed this strong bending of the actin cables both in *spc-1 pak-1* and wild-type embryos.

Strikingly, Priess & Hirsh (1986) found that actin depolymerization induces embryo retraction, suggesting that actin rearrangement could account for the lock counteracting elasticity. In wild-type embryos, muscle contractions promote embryonic elongation from the 2-fold to the final 4-fold stage. During this time, since the embryo diameter gets reduced, the actin bundles present in dorsal and ventral cells must get shorter, hence they need to remodel. Therefore, we reasoned that on one hand severing proteins might help breaking the actin cables, on the other hand, capping proteins should help stabilizing the cables. Two additional RNAi screens were then performed to identify which severing and capping proteins could be involved in our system. We first looked for players that might partially rescue the retraction of *spc-1 pak-1* defective embryos. Remarkably, among thirteen actin binding genes tested, the screen identified homologs of two actin-severing proteins, gelsolin and villin. Mutations in villin and to a lesser degree gelsolin confirmed this partial rescue. Second, we

searched for gene knockdowns inducing retraction of *spc-1(-)* embryos. This screen identified the atypical formin FHOD-1, which has previously been linked to actin dynamics in the epidermis. We confirmed that *fhod-1(-); spc-1(-)* embryos also showed a penetrant retraction phenotype with damaged actin. Furthermore, overexpressing in the epidermis a C-terminally truncated FHOD-1(ΔFH2/DAD) construct, predicted from vertebrate studies to only bundle actin, partially rescued the *spc-1(-) pak-1(-)* retraction phenotype. We thus suggest the following scenario in normal embryos: (1) muscle activity bends at a sharp angle actin bundles which with the help of severing proteins could break them, (2) the formin FHOD-1 with actin bundling properties blocks further actin depolymerization until the next cycle of muscle activity (Fig. 1a). We propose this goes uncontrolled in *spc-1 pak-1* double mutants (Fig. 1b). A possible molecular mechanism could be that upon the muscle-induced epidermal cell deformation SPC-1 somehow activates PAK-1 kinase activity, which in turn modulates the remodeling of actin filaments via bundling and severing proteins.

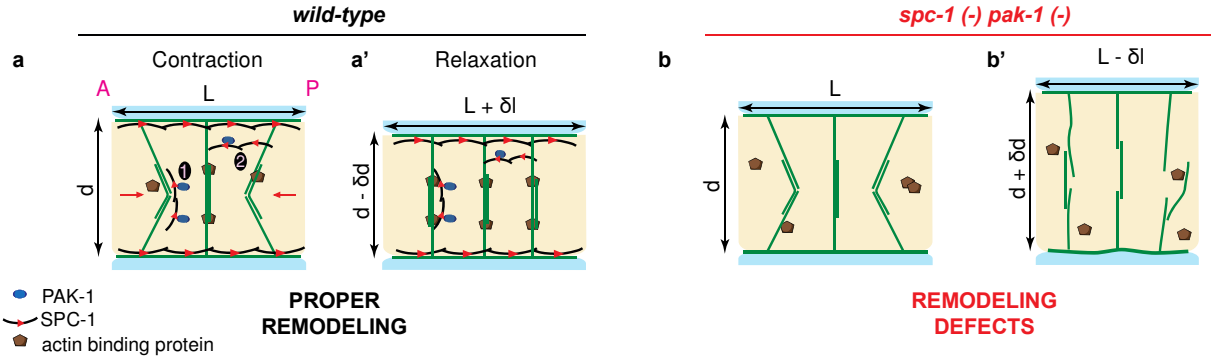

Figure 1: Cellular model of embryo elongation.
(a-b') Cellular model of embryo elongation based on volume conservation in normal embryos, in which an increase in axial length implies a decrease in circumferential length. **(a-a')** Proposed model: in control embryos, muscle contractions (red arrows) induce actin filament bending and their severing, followed by SPC-1/PAK-1-dependent stabilization; whether spectrin is found along (scenario 1) or between (scenario 2) actin filaments is unknown. **(b-b')** In *spc-1 pak-1* deficient embryos, actin remodeling goes uncontrolled**.** A-P, Anterior-Posterior.

To back our results with theory, we modeled the embryo as a Kelvin-Voigt material experiencing acto-myosin force from the epidermis plus muscle tension. We could predict embryo lengthening by introducing a viscoplastic component in the system, which we propose corresponds to actin shortening.

Altogether, we uncovered a novel machinery involving the α-spectrin SPC-1, the kinase PAK-1, an atypical formin FHOD-1 and two actin severing proteins, GSNL-1 and VILN-1, which confers mechanical plasticity to stabilize cell shapes during a ratchet morphogenetic process.

I. Identification of a novel morphogenetic ratchet

Based on our results we propose a novel morphogenetic ratchet mechanism, relying on PAK-1/spectrin/actin/actin-remodeling system that is different from previously known molecular ratchet of three reasons.

First, previously described ratchets stabilize cell shape against internally generated forces, originating from epithelial actomyosin contractions. For example, mesoderm invagination during *Drosophila* gastrulation does require a whole-body coordination of the mechanics of tissue behavior but cell shape changes of cells belonging to different tissues is driven by their apical actomyosin contractility (Rauzi *et al.*, 2010). Similarly, the *Drosophila* dorsal closure is influenced by forces generated by two different embryonic tissues: the dorsally positioned amnioserosa and the lateral epidermis (Kiehart *et al.*, 2000; Hutson *et al.*, 2003, Sawyer *et al.*, 2010). Cells at the leading edge of the dorsally migrating epidermis assemble an acto-myosin cable at the interface between these two tissues, exhibiting tension perpendicular to the direction of movement (Young *et al.*, 1991; Kiehart *et al.*, 2000; Hutson *et al.*, 2003). Thus, contractile activity of the actin-myosin cable of the epidermis could function like a supracellular purse-string that helps pull the epidermis dorsally (Edwards *et al.*, 1997; Franke *et al.*, 2005, Martin and Goldstein, 2014). During *C. elegans* elongation, acto-myosin contractility is present in lateral cells and drives the first phase of elongation until muscle become active. The mechanism we describe in this work is a stabilization occurring to answer an extrinsic force, provided by the cyclic contractility of the underlying muscle tissue.

Second, the timescale of stabilization is different. In already described ratchets in *Drosophila*, the frequency occurs in minutes. For example, prior to dorsal closure, actin-myosin networks undergo cell shape fluctuations with large amplitudes and a periodicity of about 4 min (Blanchard *et al.*, 2010; Sokolow *et al.*, 2012; Hayes and Solon, 2017). During dorsal closure, cell shape fluctuations become more frequent with a smaller amplitude. This transition is associated with increased apical myosin levels and a transition from cycles of actin-myosin network assembly and disassembly to more persistent apical actin-myosin networks (Blanchard *et al.*, 2010; David *et al.*, 2010, David *et al.*, 2013). In the process we described, the frequency is considered at the scale of seconds. Indeed, we showed that wild-type embryos contract with an average timing of 6 seconds and a considerable proportion of their contractions are even shorter. In the scenario we proposed muscle activity bends at a sharp angle actin bundles which with the help of GSNL-1 and VILN-1 could break them and FHOD-1 blocks further actin depolymerization until the next cycle of muscle activity. It means that the stabilization mechanism happens at each contraction, in a narrow time window.

Finally, the previously described ratchets used different stabilization mechanisms. For instance, during *Drosophila* embryonic germband extension, tissue elongation is driven by cell intercalation, requiring the shrinkage of dorsal-ventral-oriented junctions during this process. The polarized flow of medial actomyosin pulsing towards junctions allows the irreversible and planar polarized remodelling of epithelial cell junctions (Rauzi *et al.*, 2010; Munjal *et al.*, 2015). At the beginning of *Drosophila* dorsal closure, a supracellular actin cable that surrounds the opening provides the contractile force. Amnioserosa cells that fill the opening produce an additional critical force pulling on the surrounding epidermal tissue. As we already mentioned, this force is not gradual but pulsed and occurs long before dorsal closure starts. The actin cable function as a ratchet to counteract ventral-ward epidermis relaxation after force pulses. The dorsal closure proceeds thanks to the interplay of pulsatile actomyosin flows in one tissue and a continuous purse string constriction in the surrounding tissue (Solon *et al.*, 2009). During *Drosophila* gastrulation, cycles of Myo-II and apical Rok pulses are associated with apical constriction. The dynamic coupling of Myo-II phosphorylation to upstream signals organizes contractile Myo-II pulses in both space and time. This pulsatile nature of apical constriction is required for the stable transmission of intercellular forces during tissue morphogenesis. Additionally, the polarized localization of Rok to medioapical foci results in the persistence of medioapical actomyosin fibers stabilizing cell shape between pulses (Vasquez *et al.*, 2014).

Here, we propose that SPC-1/α-spectrin and PAK-1 regulate a cellular process of mechanical plasticity. When muscles contract, they generate a stress. Circumferential actin cables are bent which induce their severing. It creates the conditions for actin filament remodeling toward filament shortening, as the embryo elongates and its circumference decreases. This actin filament severing initiated by muscle contractions followed by FHOD-1-dependent bundling or capping represent a ratchet-like mechanism, providing a molecular basis for viscoplasticity.

II. Modelization of our ratchet mechanism

The model developed by Teresa aims to describe the embryo under elongation as a solid that deforms permanently when it is submitted to mechanical stress. It gives a mesoscopic physical description and interpretation of embryo elongation, rather than a detailed mechanistic formulation. We choose to describe the *C. elegans* embryo under elongation as a visco-elastic body: a solid that deforms permanently when it is submitted to mechanical stress. We took in account our previous and already published work, data on the organization of the actin cytoskeleton described in this work and the duration of muscle contractions also described in this work. There are three main parameters: αDV positively related to actomyosin stiffness in the D/V cells, β expressing the global activity of the remodeling factors SPC-1, PAK-1 and FHOD-1, and γ, which representing the accumulation of cytoskeleton damage.

Because the model we proposed has several free parameters, we tried to narrow it down as possible. To do so, we extracted some of them from experimental data. For example, for $F_{muscles}$, we specified its details on the basis of the measured contraction durations for embryos at the 2-fold stage. For wild-type embryos, the duration of positive and negative periods has been set to 6 seconds while for spc-1 mutants and *spc-1 pak-1* double mutants the duration of non-null activity has been set to 3 seconds. And the muscle force amplitude for *spc-1* and *spc-1 pak-1* mutants has been set to 50% of the wild-type intensity according to our experimental observations. However, it was more difficult for αDV which is related to the stiffness in the D/V cells. As mentioned in the introduction, accessing the stiffness of a tissue *in vivo* is challenging. Laser ablation experiments could have been an added value to measure the relative stress and/or stiffness in our system. However, as we model the elongation of the embryo, process enabled by muscle contractions, it would have been interesting to access the stiffness of the epidermis at 2-fold and beyond. Unfortunately performing laser ablation in a moving embryo is in our experience extremely challenging, because the embryo rotates once muscles start to twitch and reacts to the laser by stronger contractions, making it almost impossible to track the recoil process. Therefore, we used our previous work showing that prior to muscle contractions, actin bundles in D/V cells provide stiffness due to their high anisotropy in the circumferential direction, by using laser ablation (Vuong-Brender et al, 2017). It allowed us to constrain the time behavior of F_{epid} (the epidermal force introduced by the shrinking of the seam cells).

We are also aware that the general form we propose is one of some other possibilities to capture the phenomenology of the process. We know that our model leads to non-trivial consequences about the speed of the applied deformation: fast-applied deformations will induce strong plastic response and very slow deformations will leave the system almost elastic. Indeed, we did not apply our model to a large range of deformation speeds, because the average speed of deformation is of the order of ~1 µm/s for all genotypes, making the value of the deformation speed uniform across our genotypes and not crucial for their description.

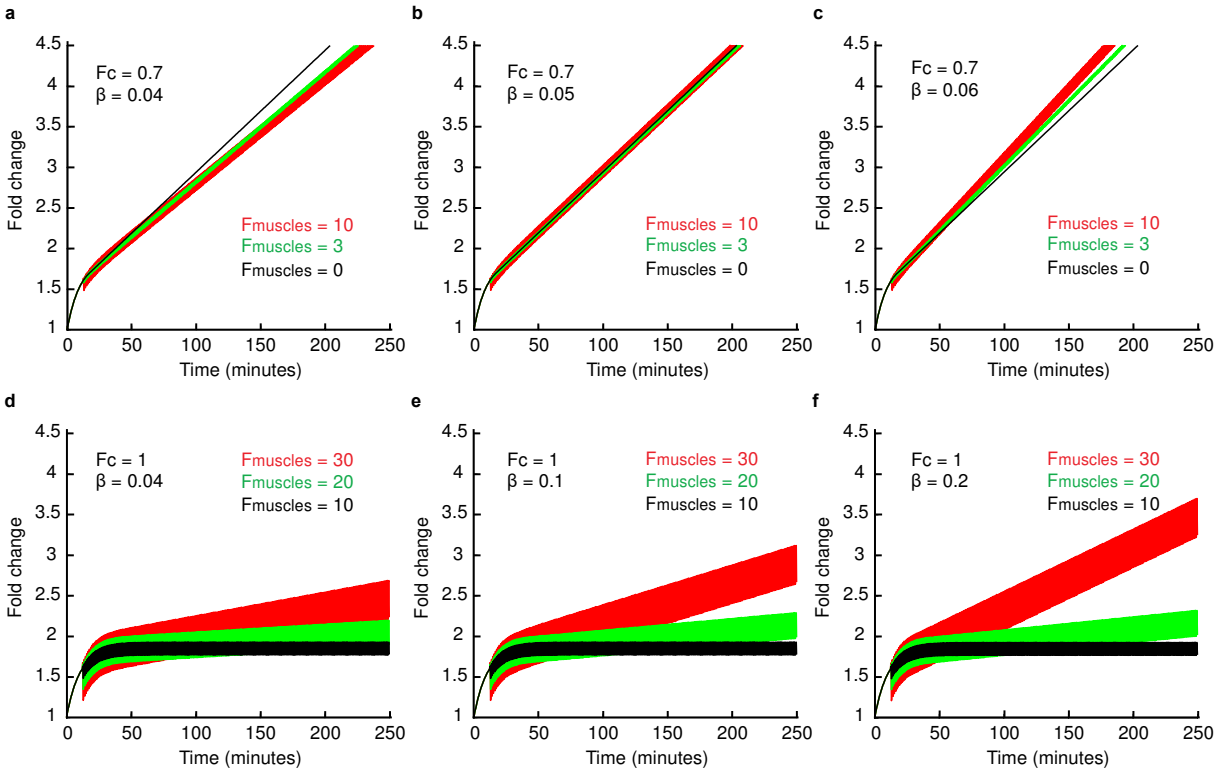

Figure 2: Time-dependent length of a Kelvin-Voigt model in different conditions.
(a-e) A Kelvin-Voigt system with mechanical plasticity introduced according to Eqs. (1, 4 discussed here, 6, 7), and predicted elongation change **(a-c)** using F_c=0.7, three distinct values of β, and three disctint values of $F_{muscles}$ for each β, or **(d-f)** three distinct values of β, and three disctint values of $F_{muscles}$ for each β.

Nevertheless, we investigated other possibilities to verify that the model we propose is the best to describe our system. A more standard way to introduce plasticity would be trough the following equation:

$$\frac{d\lambda}{dt} = \beta\,(l - \lambda)\,H(\alpha_{DV}) \quad \text{if} \quad \frac{dl}{dt} > 0 \quad \text{and} \quad l - \lambda > \frac{F_c}{k}$$

Using different values of $F_{muscles}$, the yield stress Fc and β, we observed a regime of elongation with some parameters (Fig. 2d-f), but it remains that elongation is predicted to occur when $F_{muscles}$=0 irrespective of the parameters (Fig. 2a-c), which is contradictory with the fact that Pat mutants (which have no muscle force) fail to elongate beyond the 2-fold stage. Furthermore, some curves are predicting a poor relationship between the level of $F_{muscles}$ and the speed of elongation (Fig. 2a-c), whereas some of our ongoing work point towards a direct relationship.

Overall this alternative is contradictory with the phenomenology observed in our data. In order to respect the biological phenomenology, the muscle force needs to contribute positively to elongation and elongation needs to arrest in the absence of this force even if the epidermal force is still present. On the other hand, our model properly recapitulates the elongation arrest in the absence of muscle activity. However, we do not pretend that it is easy to generalize it to other contexts, and that we are not aware of other work where it has been used. In principle, this model could be useful in a framework that requires a plastic deformation that saturates. We find it useful to rationalize a complex biological process such as the elongation of an embryo under the influence of two cooperating tissues. We think that our choice is appropriate to describe the phenomenology of the process, although we do recognize some of its limitations.

III. Unraveling the internal organization of actin

In the work, we describe a morphogenetic racthet in which actin bundles counteract the elasticity of the cells. As mentioned in the results, these circumferential actin bundles are formed of 5-10 individual filaments (Pásti and Labouesse, 2014). But nothing is known about the length of the individual filaments and their orientation inside the bundle. It does not seem too risky to rule out that they would run uninterrupted from one side of the DV cell to the other. Moreover, super resolution revealed that the actin organization defects observed in *spc-1 pak-1* were more prominent in the area over the muscles, most probably where hemidesmosomes are located. This trend was also verified in wild-type embryos where the well-organized pattern seemed less sharp in the areas submitted to a more direct stress from muscles underneath. These results may point to an important role for CeHDs probably in anchoring the actin filaments, as relay in the DV cells. However, even super resolution and the potential defasciculation of individual actin filaments in *spc-1 pak-1* defective embryos did not tell us anything about the internal organization of actin bundles.

As described in the figure 6 of the results section, we could image different scenarios. Bundles could be formed of filaments running uninterrupted from the junction to the CeHD or could be subdivided in more mini-filaments. Their orientation is also a pending question. I started to tackle this by developing new reporter tools to look at actin. I tried to obtain ACT-1 CRISPR reporters, in C-ter and N-ter, with and without linker. I also created an extrachromosomal ACT-1::GFP construct, that was viable but very difficult to work with due to the low transmission of the extrachromosomal array. And I built an alternative LifeAct::mMaple3, for FRAP analysis using spinning microscopy, which expression level was not sufficient to perform the experiment we had planned. All these approaches were focused on actin. However, to answer this big question, we could also focus on actin related proteins with specific binding to the filaments.

For example, we could imagine tagging a processive myosin motor that walk along the filament. Knowing that myosins move along the actin filament in the direction of the plus end, it would give us insight on the orientation of the filaments inside the bundle. TIRF imaging would help follow the displacement of the myosin and if the myosin stops and detach from the filament, its disappearance could indicate where the end of the filament stands. Therefore, at single molecule level, we may be able to track both the direction of the displacement and the length of the mini-filaments.

Another way to do it could be to use an optogenetic tool as it is already has been extensively used for neurobiology (Husson *et al.*, 2013; Fang-Yen *et al.*, 2015; Bergs *et al.*, 2018). We could even combine it to a new approach, the use of unnatural amino acids (Greiss and Chin, 2011; Bianco *et al.*, 2012; Elliott *et al.*, 2013; Han *et al.*, 2017; Italia *et al.* 2017; Vinson 2017). The use of unnatural amino acids had been limited to single celled systems until very recently, when it has been extended to *C. elegans* (Davis and Greiss; 2018). There are photo-caged amino acids already available for the design of light-activatable proteins. As actin is incredibly challenging to tag, we would imagine targeting actin related proteins. This would allow us to dissect their dynamic inside living cells with great precision and great temporal resolution.

IV. Interaction of actin and spectrin cytoskeleton

To better understand the interaction between actin and spectrin cytoskeletons, I examined their localization and dynamics by *in vivo* imaging and super resolution microscopy. I used CRISPR strains for SMA-1 and SPC-1 both combined to our well characterized ABD_{VAB-10}::mKate reporter. SMA-1 was present along actin cables, with a dotted pattern, while SPC-1::YFP reporter turned out to be difficult to work with. Therefore, as I already briefly mentioned in the results, I propose an alternative imaging strategy. First, I am crossing a SPC-1::mKate reporter to SMA-1::GFP and to *LifeAct::GFP*. Second, with these two new strains, I would image anesthetized embryos by using sodium sulfite that mimics hypoxic stress (Jiang *et al.* 2011). Indeed, I cannot use the same strategy as for spinning-disk imaging, put to sleep the embryos by oxygen deprivation through a high concentration of bacteria. The bacteria produce a strong autofluorescence that would interfere with the signal I would like to acquire, as with TIRF-SIM we only illuminate the plans very close to the cover slip. However, anesthetizing the embryos seem a good option because it would allow me to image the embryos with more ease and at later stages of development (3-fold), when the actin and spectrins pattern will be sharper.

Indeed, it would be interesting to see if SPC-1 intercalate in between SMA-1 or if it perfectly colocalizes with SMA-1. It has been shown that the interaction between SMA-1, actin, and the apical membrane is independent of SPC-1 (Praitis *et al.*, 2005). As actin reorganizes into parallel bundles during morphogenesis, SMA-1 is required to maintain the localization of actin at the apical membrane. When the embryo elongates, the SMA-1 network stretches to accommodate changes in cell shape. To stabilize these changes, it dynamically reorganizes, returning to its relaxed state. Therefore, the authors propose the following model. At the beginning of cell elongation, SMA-1 interacts with SPC-1 forming a tetrameric network that cross-links actin to the apical membrane. When cells elongate, the actin bundles move apart from each other (Costa *et al.*, 1997), causing the associated SMA-1 network to shift from a relaxed to a stretched state. Because SMA-1 tetramer is not sufficiently long to accommodate the maximum distance between the actin fibers (Costa *et al.*, 1997, Dubreuil *et al.*, 1990), SMA-1 tetramer would dissociate from the apical membrane and returns to a relaxed state. This association between the spectrin tetramer and the apical membrane may require SPC-1. Following this hypothesis, by super resolution microscopy, I would expect at least a partial colocalization of SPC-1 and SMA-1 along the actin bundles but also in the interspace between the bundles.

V. SPC-1 as a major player in a mechanotransduction pathway

As a crucial component of our morphogenetic locking mechanism, the spectrin cytoskeleton could play a major role in sensing the force exerted by muscles on the epidermis. It forms a ubiquitous 2D network, crosslinking the cell membrane, actin filaments and membrane-associated proteins. The contribution of spectrins to cellular mechanical properties, more precisely to cellular elasticity gained wide acceptance in multiple tissues. Recent studies showed that spectrins play a crucial role in cell morphology, protein localization, cellular motility and in the mechanical stabilization of both erythroid and non-erythroid tissues (like epithelia, neurons or other tissues exposed to mechanical stress and deformation). In this work, we provided evidence that *C. elegans* alpha-spectrin SPC-1 contributes to the elasticity of the cells during embryonic elongation. However, we did not investigate its behavior under force exertion. Special conformational changes are also in the focus of our interest as we suspect them to be important in the establishment of a PAK-1 - SPC-1 interaction.

Spectrins have been shown to form functional units only as alpha-ß heterotetramers and as such they attach to the membrane and to the actin filaments. The alpha and ß-spectrins show high affinity to each other and their lateral association is highly conserved. The heterotetramers are around 60nm at their resting length but they can reach up to a three-to-five-fold extension (Sotomayor and Schulten, 2007; Mehboob *et al.*, 2010; Brown *et al.*, 2015).

A recent model (relying on crystal structures, electron micrographs, mass spectroscopy results and modeling approaches) proposes that the heterotetramers behave like Chinese finger traps that form a hollow cylinder at their resting length and during their extension the pitch of the spectrin repeats increases while the cylinder's internal diameter decreases. This way the heterotetramers can remain linear and maintain their structural integrity. Moreover, α-spectrin and ß-spectrin heterotetramers are modular proteins including several so called spectrin-repeats (SR), which can unfold under tension (Rief *et al.*, 1998). Interestingly, they both possess an unconventional spectrin repeat domain that includes an alternative Src-homology domain-3 (SH3). Our work highlighted that this domain is a crucial element of the morphogenetic locking process we revealed. Based on our reciprocal yeast two-hybrid screens, the SH3 domain is the predicted interaction site between PAK-1 and SPC-1. It is a part of an evolutionary conserved site, located between the B and C helices of the unusually large triple α-helical SR9 spectrin repeat.

Previous work performed by Gabriella Pàsti examined whether the SH3 or the SR9 could be critical for the interaction between SPC-1 and PAK-1. In addition, she wondered whether the SH3 domain was easily accessible to interact with PAK-1, or whether it required SR9 to unfold under mechanical stress, as many spectrin repeats can do. To test these possibilities, she used *spc-1(ra409)* transgenic animals expressing alternative SPC-1::GFP constructs with either the SH3 domain alone or the SR9 domain alone. She found that the SPC-1(ΔSH3)::GFP transgene failed to rescue the elongation defects of *spc-1(ra409)* mutants. When *pak-1* was knocked down in these transgenic *spc-1(ra409)* embryos, they retracted nearly to their initial length. By contrast, the SPC-1(ΔSR9)::GFP transgene, could rescue the elongation of *spc-1(ra409).* When combined with *pak-1(RNAi),* these embryos did not retract. Instead, they arrested at 2-fold, resembling to *spc-1* single mutant animals. These results could indicate that SPC-1 might interact through its SH3 domain not only with PAK-1, but possibly with other molecular players in a molecular locking mechanism that relies behind the retraction. Therefore, the SH3 domain of SPC-1 possibly serves as an interaction site for SPC-1 binding partners and it is crucial for α-spectrin function, including the maintenance of the embryonic shape, when challenged by repeated mechanical stress.

This idea is supported by numerous studies that already proved the importance of the SH3 domain in interacting with signaling proteins (Bialkowska *et al.*, 2005; Bournier *et al.*, 2006; Machkina *et al.*, 2014; Desrochers *et al.*, 2017). Indeed, they participate in the regulation of important cellular pathways, such as cell proliferation, migration and cytoskeletal modifications. For example, Human proteome contains ∼300 different SH3 domains and many more SH3 ligand proteins, creating an enormous number of theoretically possible SH3 interactions. Therefore, knowing which of these interactions actually take place and are biologically meaningful would greatly increase our understanding about the signaling networks that regulate normal cellular behavior and become deregulated in many important diseases (Kazlauskas *et al.*, 2016). Moreover, recognition of polyproline and a number of noncanonical sequences by SH3 domains has been extensively studied by crystallography, nuclear magnetic resonance, and other methods. High-affinity peptides that bind SH3 domains are used in drug development as candidates for anticancer treatment (Kurochkina and Guha, 2013).

To probe further this hypothesis and to assess the cortical tension experienced by the epidermis once muscles are active, we developed a FRET tension sensor inserted within SPC-1. Based on the recent use of TSMod within the linker separating SR8 and SR9 of the neuronal *C. elegans* ß-spectrin UNC-70, which is neutral for function and provides a good tension sensor (Krieg *et al.*, 2014), the TSMod have been inserted at the linker regions separating adjacent SRs. Four regions have been

chosen, two before the SR9 and two after, plus one in C terminal as a negative control. More specifically, we chose the linkers located around the SR9 of SPC-1 because some of our previous data showed that the SH3 domain of SPC-1 is essential for elongation, but not the surrounding SR9. Furthermore, as SPC-1 and PAK-1 cooperate to maintain embryo shape during elongation, it raises the possibility that the SPC-1 SH3 domain defines a mechanotransduction pathway. Therefore, we started to work with this SPC-1 FRET strain. First, we obviously need to image it alone to verify that the sensor works. Then, it would be of interest to introduce it in different mutant backgrounds such as *sma-1* or *vab-10b,* to see how the cortical tension is affected.

Additionally to our first yeast two hybrid screen showing that PAK-1 interacts with the conserved SH3 embedded within the central SR domain of SPC-1 (SR9), another one showed that FHOD-1 interacts with that of the ß-spectrin SMA-1 embedded within its SR4. Furthermore, we found that epidermis expression of a truncated derivative of FHOD-1 predicted to be constitutively active fully rescues the retraction phenotype observed in defective *spc-1 pak-1* mutants, raising the possibility that FHOD-1 is the terminal player in a mechanotransduction pathway induced by muscles to bring actin remodeling. Hence, we could test whether PAK-1 phosphorylates FHOD-1 to activate it, and/or if the protein becomes properly localized by SPC-1 and PAK-1, and whether it depends on the muscle input as we previously did for CeHDs remodeling (Zhang *et al.*, 2011). SPC-1 might also act redundantly with another component during this process, as *spc-1* single mutant embryos do not retract. Such possible partners could be for instance SMA-1 or also VAB-10, with which one of our Y2H screen also yielded as a result. We started to investigate both of these possibilities.

VI. Identification of other players that could also be involved

Finally, it is important to underline that there must be several aspects that avoided our attention. It is also possible that there exist other molecular elements of the ratchet mechanism. Several lines of evidence indicate that the actin cytoskeleton is an important component of cell shape maintenance. For example, in erythrocytes the actin-spectrin-based membrane skeleton is responsible for the shape maintenance of the red blood cells. Spectrins link short actin filaments in a polygonal network to the membrane (Bennett, 1989; Pan *et al.*, 2018). Besides the attachment of the actin filaments, their stabilization is just as important. In this role adducin helps by capping the fast-growing end of actin and helps its association with spectrins. Non-muscle tropomyosin sets the length of the actin filaments within the meshwork and tropomodulin caps the slow-growing actin end to optimize actin dissociation (Bennett and Baines 2001). This actin-spectrin membrane skeleton is crucially needed in erythrocytes to ensure their flexible mechanical support in the bloodstream.

Insufficient lateral association of the spectrin-actin system, disruption of the tetramers or improper support of the membrane bilayer leads to diseases (Zhang *et al.*, 2013; Smith *et al.*, 2015).

In *C. elegans*, it has been shown that actin capping by tropomodulin, UNC-94, is important in the epithelial and intestinal lumen morphogenesis. In epithelia, UNC-94 is enriched within a HMP-1-dependent junctional actin network at epidermal adherens junctions subject to stress during morphogenesis. Loss of UNC-94 leads to discontinuity of this network, and *hmp-1; unc-94* embryos present large junctional displacements. *In vitro*, UNC-94 acts in combination with HMP-1, leading to longer actin bundles than with HMP-1 alone. It suggests that tropomodulin protect actin filaments recruited by α-catenin from minus-end subunit loss, enabling them to withstand the stresses of morphogenesis (Cox-Paulson *et al.*, 2012). In the intestine, UNC-94, localizes at the F-actin rich terminal web at the intestinal apical membrane, along with non-muscle NMY-1. In the lack of UNC-94 the F-actin amount is reduced, and the intestinal lumen is flatter, but this phenotype can be rescued by increased actomyosin contractility. This work points out that actin capping coupled to actomyosin contractility at the level of the apical cytoskeleton can influence epithelial morphogenesis and lumen shape maintenance in the *C. elegans* intestine (Cox-Paulson *et al.* 2014).

In our system, we showed that actin cables are important to stabilize cell shape changes but the mechanism of formation of actin cables during *C*. *elegans* embryonic elongation is still unknown. We wanted to probe it further and examined the contribution of other predicted *C. elegans* actin-binding proteins (formins, filamins, tropomodulin …) as described in the examples above. We used a candidate-gene approach screening for retraction phenotype and/or actin organization defects, in single *pak-1(-), spc-1(-)* and *fhod-1(-)* backgrounds. We tested thirty-three actin-binding candidates (Nishikawa *et al.*, 2017). Only seven gave phenotypes different from the wild-type (ANI-1, CYK-1, INFT-1, FLN-1, DGN-1, TMY-1 and UNC-60), and only two (DGN-1 and CYK-1) showed high embryonic lethality (greater than 20%) in a *pak-1(-)* and *fhod-1(-)* backgrounds. They are promising considering their function. CYK-1 is a formin essential for cytokinesis embryonic and cortical assembly of actin filaments independent of the Arp2/3 complex. DGN-1 is involved in the dystroglycan complex located at the cell membrane, allowing interactions between cellular components like actin filaments and extracellular matrix via laminins. Further quantification of these potential interactions would be needed. However, this screen has not been performed following a robust protocol and would need to be repeated.

To conclude, my four years of PhD lead to the identification of several proteins involved in stabilizing cell shapes in a system submitted to repeated external mechanical stress. We propose that the progressive shortening of actin filaments under the control of these factors mediates a cellular viscoplastic process promoting axis elongation. We described this ratchet mechanism both at the cellular/molecular level and in term of physics.

APPENDIX I.

Captions for movies and tables

CAPTIONS FOR MOVIES

Movie 1: Embryonic elongation and retraction profiles.
Combined DIC timelapse movie. Image acquisition was every 5 minutes in wild-type, *pak-1(tm403), spc-1(RNAi), spc-1(RNAi) pak-1(tm403)* embryos. Scale bar: 10 µm.

Movie 2: Muscle-dependence of the retraction profile.
Combined DIC timelapse movie of *unc-112(RNAi)* and *unc-112(RNAi); spc-1(RNAi) pak-1(tm403)* embryos. Scale bar: 10 µm.

Movie 3: **Elongation profile of *vab-10b; sma-1* defective embryos.**
Combined DIC timelapse movies of *vab-10b(mc44); sma-1(ru18)* embryos. Scale bar: 10 µm.

Movie 4: **Elongation profile of *vab-10b; spc-1* defective embryos.**
Combined DIC timelapse movies of the two populations of *vab-10b(mc44); spc-1(RNAi)* embryos.
Scale bar: 10 µm.

Movie 5: **Severing proteins rescuing the retraction profile.**
Combined DIC timelapse movies of *gsnl-1(tm2730); spc-1(RNAi) pak-1(tm403)* and *viln-1(ok2413); spc-1(RNAi) pak-1(tm403)* embryos. Scale bar: 10 µm.

Movie 6: Retraction profile of *fhod-1; spc-1* defective embryos.
Combined DIC timelapse movies of *spc-1(ra409)* and *fhod-1(RNAi); spc-1(ra409)* embryos. Scale bar: 10 µm.

Movie 7: Epithelial actin displacement in mutants.
Fluorescence movie showing the displacement of actin filaments labelled with *Pdpy-7::lifeact::GFP* in the epidermis in wild-type, *pak-1(tm403), spc-1(RNAi)* and *spc-1(RNAi) pak-1(tm403)* embryos. Time interval: 0.41s. Scale bar: 10 µm.

CAPTIONS FOR TABLES

Table 1: Primary enhancer RNAi screen in *pak-1(-)* background.
RNAi screen was performed in the *pak-1(tm403)* mutant along with a wild type control, testing a collection of 356 essential genes from the Ahringer RNAi library.
The table recapitulates all the genes tested and the score of their interactions for the strongest.

Table 2: Primary and secondary Yeast Two-Hybrid (Y2H) screens.
Yeast two-hybrid screening performed by Hybrygenics Services (Paris, France) using the N-terminus of PAK-1 up to the kinase domain as a bait (Primary Screen), or two different regions of the SPC-1 protein spanning the SH3 domain (Secondary Screens). The table recapitulates the strongest interactions.

Table 3: Secondary RNAi screen in *spc-1(ra409) pak-1(tm403)* mutants.
Additional RNAi screen in a *spc-1(ra409) pak-1(tm403)* mutant maintained by an exctrachromosomal *spc-1(+)::GFP* transgene of 13 actin related proteins from the Ahringer RNAi library that were recently reported to modulate actin remodeling in the early embryo (see text).

Table 4: Secondary enhancer RNAi screen in *spc-1(ra409)* mutants.
Additional RNAi screen in a *spc-1(ra409)* mutant maintained by an exctrachromosomal *spc-1(+)::GFP* transgene. Genes that gave the strongest defects in the initial RNAi screen (Supplementary Table 1) were tested again.

Table 5: List of strains used in this work.

Table 6: List of Extrachromosomal constructs and Insertions used in this work.

APPENDIX II.

Tables

Table 1 | Primary enhancer RNAi screen in *pak-1(-)* background

A Reproducible 50-100% enhanced defect* compared to wild-type
B Reproducible 20-50% enhanced defect* compared to wild-type
C Reproducible 5-20% enhanced defect* compared to wild-type

* Defect refers to lethality and body morphology defects

Targeted gene	Function	Strength of interaction
(III) ani-1	Anilin	A
(IV) cap-1	F-actin capping protein α subunit	A
(II) cap-2	β subunit of actin capping protein	A
(V) cdc-25.2	Putative homolog of Cdc25 phosphatase	A
(II) cdc-42	RHO GTPase	A
(III) dlc-1	Dynein light chain	A
(IV) epi-1	Laminin α chain	A
(I) hmp-2	β-catenin	A
(IV) lam-1	Laminin β	A
(I) let-502	Rho-binding Ser/Thr kinase	A
(III) mlc-5	Myosin II essential light chain ortholog	A
(I) pfn-1	Profilin	A
(V) sma-1	βH-spectrin	A
(X) spc-1	α-spectrin	A
(I) sur-6	Regulatory subunit of serine/threonine protein phosphatase 2A	A
(X) tni-1	Troponin	A
(II) dsh-2	Dishevelled (Dsh) homolog	B
(I) goa-1	Ortholog of the heterotrimeric G protein α subunit Go	B
(I) hmr-1	Cadherin	B
(I) kin-10	Putative regulatory (β) subunit of casein kinase II	B
(V) mom-2	Member of the Wnt family	B
(II) mpk-2	Mitogen activated protein (MAP) kinase	B
(I) pfd-3	Putative prefoldin, orthologous to human VBP1	B
(II) aakg-5	AMP kinase	C
(V) arx-2	Subunit of the actin related protein of the conserved Arp2/3 complex	C
(III) arx-3	Subunit of the actin related protein of the conserved Arp2/3 complex	C
(I) bub-1	Serine/threonine kinase	C
(V) chk-1	CHK1-like serine threonin protein kinase	C
(I) chp-1	Protein containing two CHORD domains	C
(I) csnk-1	Ortholog of human CSNK1G3, CSNK1G1 and CSNK1G2	C
(II) ect-2	Putative RHO guanine nucleotide exchange factor (RhoGEF)	C
(I) ekl-1	Ortholog of members of the human TDRD	C
(IV) fln-1	Filamin	C
(X) ifa-3	Intermediate filament protein	C
(III) klp-19	Plus-end-directed microtubule motor protein	C
(III) lit-1	Serine threonine protein kinase	C
(I) mei-2	Novel protein containing a region similar to the p80-targeting subunit of katanin	C
(V) mrck-1	Serine/threonine-protein kinase	C
(III) par-2	Protein containing a C3HC4-type RING-finger	C
(III) pfd-5	Putative prefoldin 5 subunit	C
(I) sys-1	Novel protein that contains three divergent armadillo repeats	C
(II) spv-1	Ortholog of human GMIP	C
(I) tbcd-1	Puatative β-tubulin folding cofactor D	C
(I) usp-5	Ortholog of human USP5 and USP13	C
(II) Y19D2B.1	Structural constituent of cytoskeleton	C

Table 1 | Primary enhancer RNAi screen in *pak-1(-)* background

No enhanced defect* compared to wild-type

* Defect refers to lethality and body morphology defects

(I) afd-1	*(II) aak-1*	*(III) abce-1*	*(IV) arp-11*	*(V) air-1*	*(X) aakb-1*
arx-7	*arp-1*	*abi-1*	*ced-5*	*cct-7*	*aakg-2*
aspm-1	*C27H5.4*	*arf-1.2*	*dli-1*	*F14H3.12*	*abl-1*
chs-1	*cacn-1*	*cct-5*	*dnc-1*	*gck-2*	*dyn-1*
col-53	*cal-2*	*cct-6*	*dyci-1*	*knl-3*	*efn-3*
cpn-1	*ccm-3*	*cls-1*	*eps-8*	*mig-6*	*F20B6.1*
cutl-13	*cct-1*	*cls-2*	*frk-1*	*noca-1*	*frm-9*
dhc-1	*cct-2*	*col-94*	*gex-2*	*pak-2*	*hpk-1*
dlc-6	*cct-4*	*col-97*	*gex-3*	*par-1*	*ifa-2*
eak-6	*cdc-25.4*	*cra-1*	*klp-10*	*rbx-1*	*kin-29*
egg-5	*cpn-2*	*cyk-4*	*klp-11*	*spas-1*	*lam-2*
egg-6	*dep-1*	*daf-4*	*klp-5*	*sun-1*	*lin-18*
ekl-4	*ebp-2*	*fem-2*	*let-60*	*syx-5*	*lpr-3*
erm-1	*eff-1*	*frm-2*	*let-92*	*unc-112*	*nck-1*
fhod-1	*egg-3*	*gei-4*	*M116.5*	*unc-70*	*pak-1*
gei-17	*evl-20*	*gop-3*	*nsp-1*		*pfn-2*
gfi-2	*F59A6.5*	*ina-1*	*par-5*		*pfn-3*
gsa-1	*frm-5.2*	*inft-1*	*pfd-1*		*pqn-34*
gsk-3	*glb-12*	*kin-18*	*pld-1*		*unc-97*
gsp-3	*gpb-1*	*klp-6*	*pmk-2*		
gsp-4	*klp-1 / unc-104*	*klp-7*	*pmk-3*		
kca-1	*klp-17*	*let-805*	*ptp-4*		
lim-9	*let-268*	*mpk-1*	*rac-1 / ced-10*		
mel-26	*lrr-1*	*mtm-3*	*rack-1*		
mfap-1	*max-2*	*nfm-1*	*unc-33*		
mom-5	*mel-11*	*pef-1*	*wsp-1*		
nab-1	*mig-5*	*plk-1*	*zen-4*		
ned-8	*mlt-8*	*pph-6*			
nkb-1	*nsy-1*	*ptp-1*			
nmy-2	*pfd-2*	*pxl-1*			
npp-4	*pink-1*	*rfl-1*			
ocrl-1	*pir-1*	*tbb-2*			
pes-7	*ptc-3*	*ten-1*			
pfd-6	*ptp-2*	*tlk-1*			
ppk-1	*ptp-3*	*trd-1*			
rga-2	*saps-1*	*unc-116*			
rsa-1	*scpl-2*	*wrm-1*			
smgl-1	*sds-22*				
spd-1	*spdl-1*				
tba-2	*tac-1*				
ttx-7	*tba-4*				
unc-35	*unc-52*				
unc-59	*vab-19*				
unc-73	*vab-9*				
unc-94	*vhp-1*				
vab-10	*vps-11*				
viln-1	*vps-32*				
vps-20	*W0761.1*				
wve-1	*zyg-9*				

Table 2 | Primary and secondary Y2H screens

Global Predicted Biological Score (*categories computed and established by Hybrigenics, to assess the interaction reliability)*

A Very high confidence in the interaction

B High confidence in the interaction

C Good confidence in the interaction

D Moderate confidence in the interaction
(either due to false-positive interactions or due to interactions that are hardly detectable by the Y2H technique)

Strongest candidates
(Prey library: C. elegans embryo)

Primary Yeast Two Hybrid Screen *(Bait: CePAK-1 N-terminal amino acids: 1-294)* * Positive controls (PAK-1 itself + its known interactors)			Secondary Yeast Two Hybrid Screen † *Bait I: CeSPC-1 SR8-10(aa:796-1243)* ‡ *Bait II: CeSPC-1 SH3 (aa:986-1041)* § *Common hits using Bait I and Bait II*		
Interactor candidate	Protein Function	Global PBS	Interactor candidate	Protein Function	Global PBS
SPC-1	α-spectrin	A	PAK-1 §	p21-activated kinase	A
F47B10.1	β-chain succinyl-co-A ligase	A	LIM-8 §	LIM domain muscle component	A
CHW-1	RhoU homolog	A	F44.E2.3 ‡	ARGLU1 ortholog	A
GCK-1	STE20-family kinase	A	CSN-5 ‡	COP9-subunit ortholog E3 ubiquitin ligase interactor	A
NCK-1	NCK adaptor	A	DEB-1 ‡	Vinculin	A
PIX-1 *	ARHGEF7 homolog β-Pix	A	DnaJ ‡	DNAJ/ZRF1/MPP11 ortholog ribosome-associated chaperone	B
CDC-42 *	Small GTPase	A	CYLD-1 ‡	Human CYLD1 ortholog NF-κβ signalling interactor	B
PAK-1 *	P21-activated Ser/Tre kinase (multiple hits through kinase domain)	A	VAB-3 / VAR-1 †	Homeodomain protein PAX6 ortholog	B
CED-10 *	Rac-1 / Small GTPase	B	GRL-4 ‡	Hedgehog-like protein	C
POD-2	Predicted acetyl-coA carboxylase	B	UNC-34 ‡	Enabled/VASP homolog	C
Y39E4A.3	Transketolase	B	T04F8.6 †	Human ninein and ninein-like (GSK3B interactor) ortholog	D
EEL-1	HECT-ubiquitin ligase	C	ALR-1 †	Human ARX (aristaless) ortholog homeodomain transcription factor	D
NPP-21	Nuclear pore protein	C	ATN-1 †	α-actinin homolog	D
TAG-143	Transcription factor	C	MMCM-1 †	Methylmalonyl-CoA mutase	D
UNC-44	Ankyrin	D	UNC-70 †	βG-spectrin	D
HIPR-1	SLA2 and Hip related	D	VAB-10 †	Spectraplakin	D
T05C1.4	Conserved calmodulin-binding TFs	D	F26A10.2 ‡	Zinc-finger containing protein	D
Y53F4B.13	RNA methyltransferase	D	F43C1.1 ‡	Human PHLPP1&PHLPP2 ortholog	D
PTP-3	LAR-like receptor tyr-protein phosphatase	D	ALP-1 ‡	Enigma family member ALP (α-actinin associated LIM Protein) ortholog	D
COGC-6	Conserved Oligomeric Golgi (COG) Component	D	CIT-1.2 ‡	Cyclin T ortholog	D
DAF-21	Hsp90 molecular chaperone family member	D	FLH-1 ‡	FLYWCH zinc finger transcription factor homolog	D
GCK-1 variant	STE20-family kinase	D	SHW-1 ‡	Human KCNC3 voltage-gated SHaW family potassium channel ortholog	D

Table 3 | Secondary RNAi screen in *spc-1(ra409) pak-1(tm403)* background

A Longer compared to *spc-1(-) pak-1(-)* (no retraction phenotype)
B Not longer compared to *spc-1(-) pak-1(-)* (retraction phenotype)

Targeted gene	Function	Strength of interaction
(I) viln-1	Ortholog of human SVIL (supervillin)	A
(V) gsnl-1	Gelsolin-related proteins	A
(X) tth-1	Thymosin beta ortholog	A
(I) pfn-1	Profilin	B
(II) cap-2	Beta subunit of actin capping protein	B
(III) ani-1	Anillin	B
(III) cyk-1	Formin homologous to Drosophila diaphanous and human DIAPH1	B
(III) fli-1	Orthologous to Drosophila and human Flightless I	B
(IV) cap-1	F-actin capping protein alpha subunit	B
(IV) fln-1	Ortholog of human filamin A	B
(IV) plst-1	Ortholog of human PLS1, PLS3 and LCP1	B
(V) arx-2	Subunit of the actin related protein of the conserved Arp2/3 complex	B
(V) unc-60	Actin depolymerizing factor(ADF)/cofilin	B

Table 4 | Secondary enhancer RNAi screen in *spc-1(ra409)* background

A Shorter compared to *spc-1(-)*
B Not shorter compared to *spc-1(-)*

Targeted gene	Function	Strength of interaction
(I) fhod-1	Formin	A
(I) hmr-1	Cadherin	A
(I) hmp-2	β-catenin	A
(II) cdc-42	RHO GTPase	A
(II) spdl-1	Coiled-coil protein	A
(II) vps-11	Ortholog of human VPS11	A
(III) mtm-3	Myotubularin lipid phosphatase	A
(III) mlc-5	Myosin II essential light chain ortholog	A
(IV) dnc-1	Ortholog of the dynactin complex subunit p150/GLUED/DCTN1	A
(IV) epi-1	Laminin α chain	A
(I) goa-1	Ortholog of the heterotrimeric G protein α subunit Go	B
(I) kin-10	Putative regulatory (β) subunit of casein kinase II	B
(I) mec-8	mRNA processing factor	B
(I) nmy-2	Non-muscle myosin II	B
(I) unc-94	Tropomodulin	B
(II) cap-2	β subunit of actin capping protein	B
(II) evl-20	Ortholog of human ADP-ribosylation factor-like protein 2	B
(II) spv-1	Ortholog of human GMIP	B
(II) unc-52	Perlecan	B
(III) klp-7	Ortholog of human KIF2A, 2B and 2C	B
(III) mup-4	Transmembrane protein	B
(IV) cap-1	F-actin capping protein α subunit	B
(IV) eps-8	Cell signaling adaptor protein	B
(IV) frk-1	Non-receptor tyrosine kinase	B
(IV) unc-33	Conserved member of the CRMP/TOAD/Ulip/DRP family	B

Table 5 | List of strains used in this work

Name	Genotype
DM3409	*mnDp33 (X;IV)/+ IV.; spc-1(ra409) X.*
DWP10	*fhod-1(tm2363) I.; qaIs8001 [unc-119(+) fhod-1::gfp]*
ML1694	*pix-1(gk416)X.*
ML1822	*sma-1(ru18)V.; pak-1 (tm403)X.*
ML1911	*git-1(tm1962)X.*
ML2113	*mcIs67 [dpy7p::LifeAct::GFP; unc-119(+)] V.; stIs10088[hlh-1::his-24::mCherry, unc-119(+)]*
ML2129	*pak-1(tm403) X.*
ML2200	*pak-1(tm403) X.; mcIs67 [dpy7p::LifeAct::GFP; unc-119(+)] V; stIs10088[hlh-1::his-24::mCherry, unc-119(+)]*
ML2419	*mcEx915[ppak-1::pak-1::mkate;pR4(rol);pBSK]*
ML2428	*sma-1(ru18)V.*
ML2436	*spc-1(ra409) X.; mcEx636 [spc-1p::spc-1::GFP]*
ML2446	*pak-1(tm403) X.; spc-1(ra409) X.; mcEx636 [spc-1p::spc-1::GFP]*
ML2465	*mcIs91[linc26p::ABD::mkate; myo-2p::mcherry]*
ML2537	*vab-10b(mc44) I. / hT2 [bli-(e937), let-?(q782) qIS48] III.*
ML2684	*mcEx1008 [fhod-1ΔFH2/DAD]*
ML2688	*pak-1(tm403) X.; mcEx1009 [fhod-1ΔFH2/DAD]*
ML2853	*pak-1(tm403) X.; mcEx1002 [fhod-1ΔFH1/FH2/DAD]*
ML2854	*pak-1(tm403) X.; mcEx1003 [fhod-1ΔDAD]*
ML2855	*pak-1(tm403) X.; mcEx1004 [fhod-1 full length]*
ML2856	*mcEx1005 [fhod-1ΔFH1/FH2/DAD]*
ML2857	*mcEx1006 [fhod-1ΔDAD]*
ML2858	*mcEx1007 [fhod-1 full length]*
ML2896	*mcEx1014 [dpy7p::GFP]*
ML2898	*fhod-1(tm2363) I.; mcIs67 [dpy7p::LifeAct::GFP; unc-119(+)] V.*
ML2903	*spc-1(ra409) X.; pak-1(tm403) X.; mcEx1016 [spc-1p::spc-1::GFP] line 1*
ML2904	*spc-1(ra409) X.; pak-1(tm403) X.; mcEx1016 [spc-1p::spc-1::GFP] line 3*
ML2906	*spc-1(ra409) X.; pak-1(tm403) X.; mcEx1016 [spc-1p::spc-1::GFP] line 4*
ML2907	*pak-1(tm403) X.; mcEx 1014 [dpy7p::GFP] line 1*
ML2929	*mcIs67 [dpy7p::LifeAct::GFP; unc-119(+)] V.; spc-1(ra409) X.; pak-1(tm403) X.; mcEx1016 [spc-1p::spc-1::GFP]*
ML2931	*viln-1(ok2413) I.; pak-1(tm403) X.*
ML2932	*gsnl-1(tm2730) V.; pak-1(tm403) X.*
ON204	*gsnl-1(tm2730) V.* (3x outcrossed)
ON206	*viln-1(ok2413) I.* (3x outcrossed)
ON218	*viln-1(ok2413) I.; gsnl-1(tm2730) V.*
N2	*Bristol*
XA8001	*fhod-1(tm2363) I.*

Table 6 | List of Extrachromosomal constructs and Insertions used in this work

Name	Genotype
mcEx636	*[spc-1p::spc-1::GFP]*
mcEx1002	*[fhod-1ΔFH1/FH2/DAD]*
mcEx1003	*[fhod-1ΔDAD]*
mcEx1004	*[fhod-1 full length]*
mcEx1005	*[fhod-1ΔFH1/FH2/DAD]*
mcEx1006	*[fhod-1ΔDAD]*
mcEx1007	*[fhod-1 full length]*
mcEx1008	*[fhod-1ΔFH2/DAD]*
mcEx1009	*[fhod-1ΔFH2/DAD]*
mcEx1014	*[dpy7p::GFP]*
mcEx1016	*[spc-1p::spc-1::GFP]*
mcIs55	*[pak-1::GFP;pRF4]*
mcIs67	*[dpy7p::LifeAct::GFP; unc-119(+)] V.*
mcIs91	*[lin26p::ABD::mkate; myo-2p::mcherry]*
stIs10088	*[hlh-1::his-24::mCherry, unc-119(+)]*

APPENDIX III.

An actin-based viscoplastic lock ensures progressive body axis elongation

Alicia Lardennois*, Gabriella Pásti*, Teresa Ferraro, Flora Llense, Pierre Mahou, Julien Pontabry, David Rodriguez, Samantha Kim, Shoichiro Ono, Emmanuel Beaurepaire, Christelle Gally, Michel Labouesse#

Nature

LETTER

Corrected: Publisher Correction

https://doi.org/10.1038/s41586-019-1509-4

An actin–based viscoplastic lock ensures progressive body–axis elongation

Alicia Lardennois[1,6], Gabriella Pásti[2,6], Teresa Ferraro[1], Flora Llense[1], Pierre Mahou[3], Julien Pontabry[2,4], David Rodriguez[2], Samantha Kim[2], Shoichiro Ono[5], Emmanuel Beaurepaire[3], Christelle Gally[2] & Michel Labouesse[1,2]*

Body-axis elongation constitutes a key step in animal development, laying out the final form of the entire animal. It relies on the interplay between intrinsic forces generated by molecular motors[1–3], extrinsic forces exerted by adjacent cells[4–7] and mechanical resistance forces due to tissue elasticity or friction[8–10]. Understanding how mechanical forces influence morphogenesis at the cellular and molecular level remains a challenge[1]. Recent work has outlined how small incremental steps power cell-autonomous epithelial shape changes[1–3], which suggests the existence of specific mechanisms that stabilize cell shapes and counteract cell elasticity. Beyond the twofold stage, embryonic elongation in *Caenorhabditis elegans* is dependent on both muscle activity[7] and the epidermis; the tension generated by muscle activity triggers a mechanotransduction pathway in the epidermis that promotes axis elongation[7]. Here we identify a network that stabilizes cell shapes in *C. elegans* embryos at a stage that involves non-autonomous mechanical interactions between epithelia and contractile cells. We searched for factors genetically or molecularly interacting with the p21-activating kinase homologue PAK-1 and acting in this pathway, thereby identifying the α-spectrin SPC-1. Combined absence of PAK-1 and SPC-1 induced complete axis retraction, owing to defective epidermal actin stress fibre. Modelling predicts that a mechanical viscoplastic deformation process can account for embryo shape stabilization. Molecular analysis suggests that the cellular basis for viscoplasticity originates from progressive shortening of epidermal microfilaments that are induced by muscle contractions relayed by actin-severing proteins and from formin homology 2 domain-containing protein 1 (FHOD-1) formin bundling. Our work thus identifies an essential molecular lock acting in a developmental ratchet-like process.

C. elegans provides an anatomically simple and integrated model to study the cellular effect of mechanical forces; however, unlike other such models, morphogenesis in *C. elegans* is not dependent on pulsatile actomyosin flows[1–3,10,11]. Because the muscles are tightly mechanically coupled to the epidermis through epidermal hemidesmosomes[12] (Fig. 1a, Supplementary Information), their contractions also displace the epidermis. Indeed, the anterior–posterior displacement of circumferentially oriented epidermal actin filaments closely mirrors that of muscle nuclei (Fig. 1b). Notably, the muscles do not all contract simultaneously; when some areas of the epidermis were longitudinally compressed (red line in Fig. 1c), others were stretched (green line) before eventually relaxing. The relaxation that follows each muscle contraction raises the conundrum of how muscle activity can power embryonic elongation from 100 μm to 200 μm if cell elasticity brings cells back to their initial length during relaxation. A simple hypothesis would be that some mechanism stabilizes the transient cell shapes induced by muscle activity. For instance, during *Drosophila* gastrulation and germband extension, actomyosin pulsatile flows are thought to progressively modify junctions[3,13,14]. To uncover such a mechanism, we focused on the kinase PAK-1, which mediates mechanotransduction[7] and regulates myosin II[15,16]. We first performed a feeding RNA-mediated interference (RNAi) screen in a strong but viable *pak-1* mutant, looking for enhanced embryonic lethality (Extended Data Fig. 1a). The gene *spc-1*—which encodes α-spectrin—behaved as a strong genetic enhancer of *pak-1*, producing short hatchlings (approximately 58 μm long), significantly shorter than *pak-1(tm403)* (approximately 178 μm long) or *spc-1*(RNAi) (approximately 91 μm long) hatchlings (Extended Data Fig. 1b, Supplementary Table 1). Moreover, a yeast two-hybrid screen identified the central Src homology 3 domain (SH3) of SPC-1 as an interactor with the PAK-1 N terminus (Extended Data Fig. 1c, Supplementary Table 2). Thus, both screens indicate a functional interaction between SPC-1 and PAK-1 during axis elongation.

Next, differential interference contrast (DIC) video microscopy showed that *spc-1(ra409) pak-1(tm403)* and *spc-1*(RNAi) *pak-1(tm403)* embryos could reach about 65 μm at a slow rate, but then failed to maintain their shape and retracted back to about 50 μm (Figs 1d–h, Extended Data Fig. 1d–j, Supplementary Video 1). Two observations suggest that muscle activity accounts for this phenotype. First, *spc-1* knockdown in *git-1* or *pix-1* mutants, which act upstream of *pak-1* in mediating mechanotransduction[7], also induced retraction (Extended Data Fig. 1d–j). Second, *spc-1*(RNAi) *pak-1(tm403)* embryos started to retract at the onset of muscle contractions in control embryos (Fig. 1d, Extended Data Fig. 1d). We abrogated muscle function in *spc-1(ra409) pak-1(tm403)* embryos by knocking down the kindlin homologue UNC-112[17]; the *spc-1(ra409) pak-1(tm403)* embryos defective for *unc-112* no longer retracted (Fig. 1d–n, Supplementary Video 2). Therefore, we conclude that the mechanical input provided by muscles to the epidermis induces the retraction phenotype observed in *spc-1 pak-1* double mutants.

The simplest interpretation of this retraction phenotype is that a cellular structure that maintains embryo shape fails to emerge or collapses when muscles contract. Two arguments suggest that this structure corresponds to the bundles of 3–5 actin filaments present in the dorsoventral epidermis[18,19]. First, SPC-1 and its binding partner SMA-1 (β-spectrin) form an actin-binding heterotetramer, colocalizing with actin[20] and partially with PAK-1 in epidermal cells (Extended Data Fig. 2). Second, treating *C. elegans* embryos with the actin-depolymerizing drug cytochalasin D induces a retraction phenotype very similar to the one described above[19]. We therefore characterized actin filaments using super-resolution microscopy of a LifeAct::GFP probe[10]. Segmentation analysis of the resulting images in the dorsoventral epidermis (Fig. 2a, b) revealed more discontinuity in *spc-1 pak-1* double-deficient embryos compared with control genotypes, particularly over the area in which muscles contract (putative hemidesmosomes) (Fig. 2c, Extended Data Fig. 3). Fourier transform analysis indicated that their degree of anisotropy relative to the circumferential axis was abnormal (Fig. 2d, Extended Data Fig. 3). Moreover, the signal intensity between adjacent actin bundles was less sharp in *spc-1 pak-1* deficient embryos and they

[1]CNRS UMR7622, Institut de Biologie Paris–Seine (IBPS), Sorbonne Université, Paris, France. [2]IGBMC –CNRS UMR 7104, INSERM U964, Development and Stem Cells Department, Université de Strasbourg, Illkirch, France. [3]INSERM U1182 – CNRS/ UMR7645, Laboratoire d'Optique et Biosciences, Ecole Polytechnique, Paris, France. [4]RS2D, Mundolsheim, France. [5]Departments of Pathology and Cell Biology, Winship Cancer Institute, Emory University School of Medicine, Atlanta, GA, USA. [6]These authors contributed equally: Alicia Lardennois, Gabriella Pásti. *e-mail: michel.labouesse@sorbonne-universite.fr

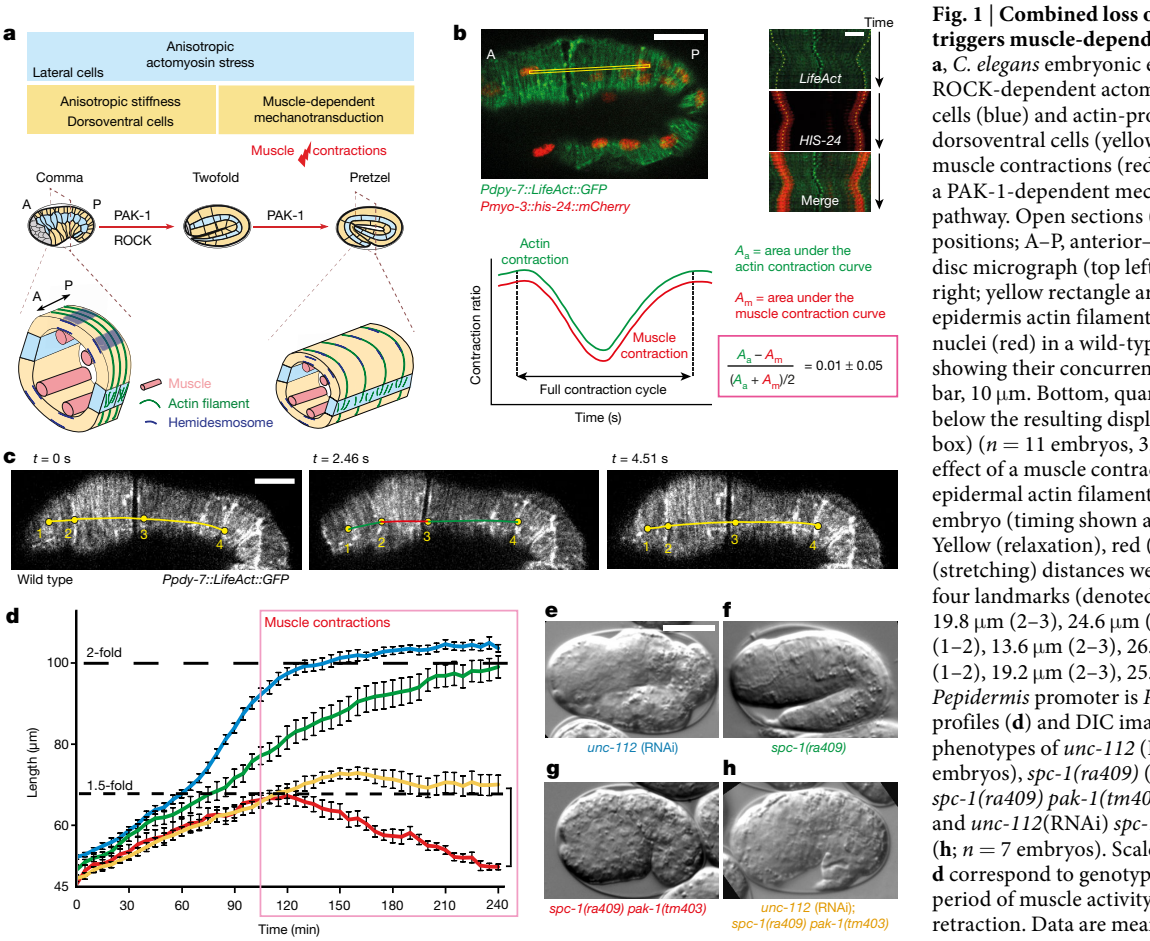

Fig. 1 | Combined loss of PAK-1 and SPC-1 triggers muscle-dependent embryo retraction. **a**, *C. elegans* embryonic elongation requires a ROCK-dependent actomyosin force in lateral cells (blue) and actin-promoted stiffness in dorsoventral cells (yellow), followed by repeated muscle contractions (red flash), which induce a PAK-1-dependent mechanotransduction pathway. Open sections (bottom), muscle positions; A–P, anterior–posterior. **b**, Spinning-disc micrograph (top left) and kymographs (top right; yellow rectangle area from top left) of epidermis actin filaments (green) and muscle nuclei (red) in a wild-type twofold embryo, showing their concurrent displacement. Scale bar, 10 µm. Bottom, quantification of the area below the resulting displacement curves (pink box) ($n = 11$ embryos, 33 contractions). **c**, Local effect of a muscle contraction–relaxation cycle on epidermal actin filaments in a wild-type twofold embryo (timing shown above each panel). Yellow (relaxation), red (compression) and green (stretching) distances were measured between four landmarks (denoted 1–4). Left, 7.8 µm (1–2), 19.8 µm (2–3), 24.6 µm (3–4); middle, 9.4 µm (1–2), 13.6 µm (2–3), 26.2 µm (3–4); right, 8.0 µm (1–2), 19.2 µm (2–3), 25.0 µm (3–4). In **b**, **c**, the *Pepidermis* promoter is *Pdpy-7*. **d**–**h**, Elongation profiles (**d**) and DIC images showing the terminal phenotypes of *unc-112* (RNAi) (**e**; $n = 14$ embryos), *spc-1(ra409)* (**f**; $n = 8$ embryos), *spc-1(ra409) pak-1(tm403)* (**g**; $n = 8$ embryos) and *unc-112*(RNAi) *spc-1(ra409) pak-1(tm403)* (**h**; $n = 7$ embryos). Scale bar, 17 µm. Colours in **d** correspond to genotypes in **f**–**h**. Pink box, period of muscle activity; bracket, extent of retraction. Data are mean ± s.e.m.

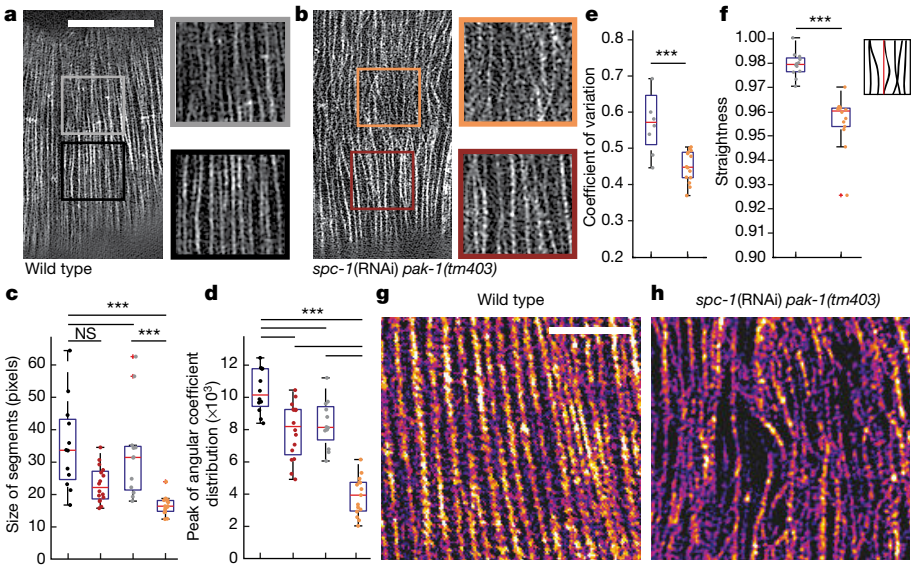

Fig. 2 | Actin-filament abnormalities in *spc-1 pak-1* defective embryos. **a**, **b**, Total internal reflection fluorescence–structured-illumination microscopy (TIRF–SIM) super-resolution images of actin filaments (*Pdpy-7::LifeAct::GFP* reporter) from wild-type (**a**) and *spc-1*(RNAi) *pak-1(tm403)* (**b**) embryos at the twofold stage or equivalent. Grey and orange rectangles, region of interest (ROI) above muscles (area of higher bending in time-lapse images); black and burgundy rectangles, ROI elsewhere. Scale bar, 5 µm. **c**, **d**, Actin continuity estimated as the segment length in binarized ROI images (**c**) and actin-bundle anisotropy calculated from the peak value of the angular coefficient after fast Fourier transformation (**d**) (Extended Data Fig. 3). Defects are more pronounced above muscles. Colours of dots correspond to those of the boxes in **a** and **b**; images are representative of a wider sampled group of images (**c** and **d**; above muscles, wild type $n = 12$, *spc-1 pak-1* $n = 15$; elsewhere, wild type $n = 12$, *spc-1 pak-1* $n = 16$; **e**: wild type $n = 8$, *spc-1 pak-1* $n = 14$; **f**: wild type $n = 12$, *spc-1 pak-1* $n = 14$). **e**, Coefficient of variation (s.d./mean) of the fluorescence signal in ROIs above muscles as a proxy for actin-bundle organization. **f**, Left, actin-bundle straightness, calculated as the ratio of the actual length of a bundle (black line in the sketch (right)) and the shortest distance between its endpoints (red line in the sketch). **g**, **h**, Snapshots of TIRF–SIM reconstructed images with Fire LUT to emphasize the actin-bundle defects of *spc-1*(RNAi) *pak-1(tm403)* embryos compared with wild-type controls. Scale bar, 2 µm. Graphs show median and 25th and 75th percentiles; whiskers extend to the most extreme data points not considered outliers. Two-sided paired *t*-test. $^*P < 0.05$; $^{**}P < 0.001$; $^{***}P < 0.0001$; NS, not significant.

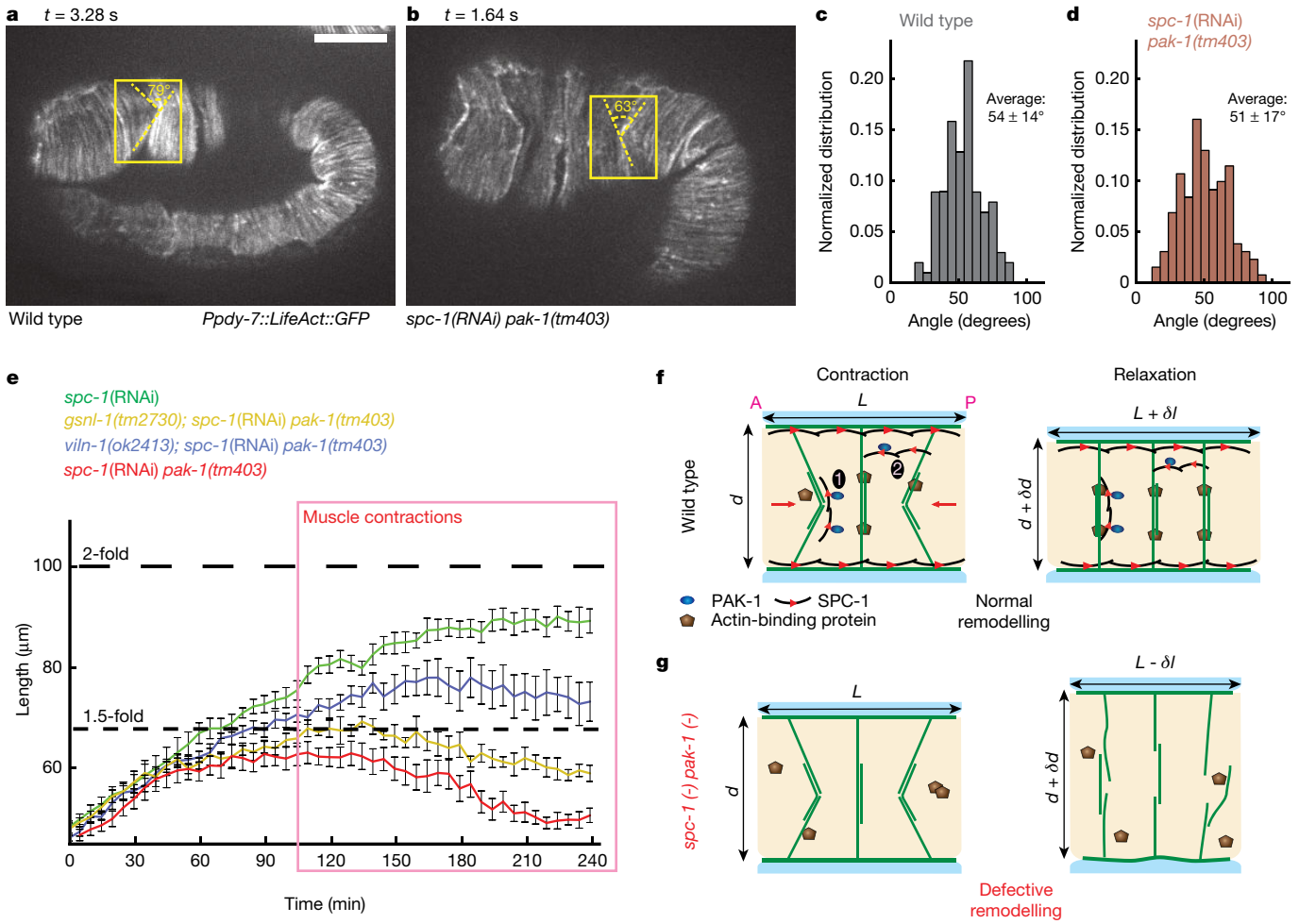

Fig. 3 | Muscle contractions are linked to severing of epidermal actin filaments. a–d, Spinning-disc images of epidermal actin filaments (*Pdpy-7::LifeAct::GFP* reporter) and quantification of bending angles in wild-type ($n = 23$ embryos, 101 contractions) (**a**, **c**) and *spc-1*(RNAi) *pak-1(tm403)* ($n = 14$ embryos, 131 contractions) (**b**, **d**) embryos at twofold-stage equivalent (kymographs in Extended Data Fig. 5). Scale bar, 10 µm. **e**, Elongation profiles of *spc-1*(RNAi) ($n = 8$ embryos), *spc-1*(RNAi) *pak-1(tm403)* ($n = 9$ embryos), *viln-1(ok2413); spc-1*(RNAi) *pak-1(tm403)* ($n = 11$ embryos) and *gsnl-1(tm2370); spc-1*(RNAi) *pak-1(tm403)* ($n = 5$ embryos). Pink box, period of muscle activity. Data are mean ± s.e.m. **f**, **g**, Cellular model of embryo elongation based on volume conservation in normal embryos, in which an increase in axial length implies a decrease in circumferential length. **f**, Proposed model. In control embryos, muscle contractions (red arrows) induce actin-filament bending and their severing, followed by SPC-1–PAK-1-dependent stabilization; whether spectrin is found along or between actin filaments is unknown. **g**, In *spc-1 pak-1* deficient embryos, actin remodelling is uncontrolled.

were more frequently bent (Fig. 2e–h), indicating that the bundles might have partially defasciculated. Of note, these phenotypes became apparent once muscles became active (Extended Data Fig. 3), which suggests that muscle contractions contribute to actin remodelling.

To further investigate this phenomenon, we examined actin filaments during muscle contraction. As wild-type embryos lengthen, their circumference decreases by roughly 20% owing to embryo-volume conservation (Extended Data Fig. 4); thus, the length of actin filaments in dorsoventral cells would be expected to decrease. Spinning-disc microscopy revealed that muscle contractions are strong enough to locally bend actin bundles with an angle greater than 54° (Fig. 3a–d, Extended Data Fig. 5a, b), which has previously been reported to induce severing of actin filaments in vitro[21]. Therefore, we reasoned that compromising severing genetically might partially rescue the retraction of defective *spc-1 pak-1* embryos (Extended Data Fig. 5c, d). Among 13 genes tested (Supplementary Table 3), our screen identified homologues of 2 actin-severing proteins, gelsolin and villin (Fig. 3e). Mutations in villin and, to a lesser degree, gelsolin confirmed this partial rescue (Fig. 3e, Extended Data Fig. 5d–l). Together, these data suggest that muscle contractions induce actin-filament bending, and directly or indirectly stimulate the activity of severing proteins. We propose that this is uncontrolled in *spc-1 pak-1* double mutants (Fig. 3f, g).

This model predicts that preventing muscle activity should improve actin organization in *spc-1 pak-1* mutants, and that *viln-1; gsnl-1* double mutants should exhibit defective elongation. First, we found that actin filaments in *spc-1 pak-1* mutants were probably stiffer when muscles were inactive, as lateral cells were wider (Extended Data Fig. 4c, d)—although continuity defects remained (Extended Data Fig. 3b, c). Second, villin–gelsolin double-deficient embryos showed only minor elongation defects (Extended Data Fig. 5l), which suggests that additional parallel processes might contribute to actin remodelling.

To rationalize the role of muscles in remodelling, we described the *C. elegans* embryo as a Kelvin–Voigt material (a spring in parallel with a dashpot) submitted to forces acting in the epidermis and muscles ($F_{\text{epidermis}}$ and F_{muscles}, respectively) (equations (1) and (2); see Supplementary Information for details).

$$\eta\frac{\mathrm{d}l}{\mathrm{d}t} = -k(l-\lambda) + F_{\text{epidermis}} + F_{\text{muscles}} \quad (1)$$

$$F_{\text{epidermis}} = F_{\text{seam}}\alpha_{\text{DV}} \quad (2)$$

Note that $F_{\text{epidermis}}$ is written as the product of an active force, F_{seam}, which corresponds to the contractile force produced by myosin-2 in

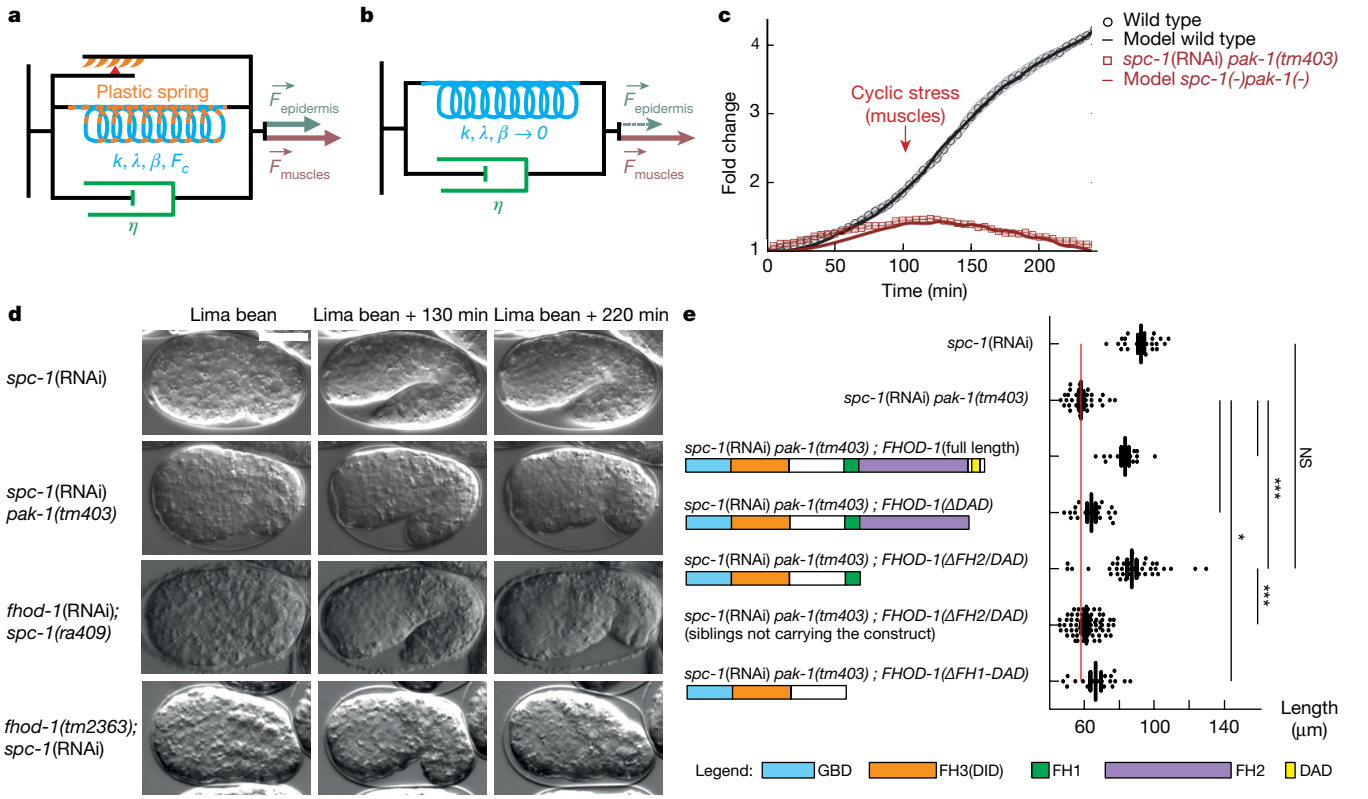

Fig. 4 | An actin-remodelling network providing mechanical plasticity ensures embryo elongation. a–c, Viscoplastic mechanical model of embryo elongation. The embryo is represented as a Kelvin–Voigt solid with spring stiffness k, resting length λ, viscosity η, submitted to forces $F_{epidermis}$ and F_{muscle}, defined by equations (1) to (4). **a**, Wild-type case. An increasing resting length during stretching phases imparts mechanical plasticity. **b**, *spc-1 pak-1* mutants. $F_{epidermis}$ progressively decreases. **c**, Comparison of experimental and predicted elongation curves using the constitutive equations (1) to (4). **d**, DIC snapshots at three time points of *spc-1* deficient embryos on control, *pak-1* or *fhod-1* backgrounds, and of a *fhod-1* mutant after *spc-1*(RNAi). **e**, *Pdpy-7*-driven epidermis expression of truncated FHOD-1 variants and terminal body length at hatching: *spc-1*(RNAi) ($n = 26$ hatchlings); *spc-1*(RNAi) *pak-1(tm403)* with no transgene ($n = 36$ hatchlings), with full-length FHOD-1 ($n = 16$ hatchlings), FHOD-1(ΔDAD) ($n = 17$) and FHOD-1(ΔFH2–DAD) ($n = 38$ hatchlings) transgenes, or non-transgenic siblings ($n = 78$ hatchlings) and FHOD-1(ΔFH1–FH2–DAD) transgene ($n = 18$ hatchlings). Data are mean ± s.d. Two-sided paired *t*-test. $^*P < 0.05$; $^{**}P < 0.001$; $^{***}P < 0.0001$; NS, not significant. Scale bars, 15 μm.

seam epidermal cells, and a passive component, α_{DV}, which results from actin-bundle stiffness in dorsal and ventral epidermal cells[10]. $F_{epidermis}$ can extend embryo length only up to twofold, as muscle-defective mutants cannot elongate more than this (Extended Data Fig. 6a, a′). The force $F_{muscles}$ should not trigger any further extension, because it oscillates between a positive and a negative input (Fig. 1b, c, Extended Data Fig. 6b, b′).

Several studies have suggested that systems exposed to a mechanical stress can undergo a permanent rearrangement that can be described as a plastic deformation[22] or as a change in the spring resting length[23,24]. Accordingly, we imposed the condition that the spring resting length λ in equation (1) changes linearly with positive elongation rates (equation (3), Fig. 4a).

$$\frac{d\lambda}{dt} = \beta \frac{dl}{dt} H(\alpha_{DV}) \mathrm{Hill}(\lambda) \quad \text{if} \begin{cases} \frac{dl}{dt} > 0 \\ 0 \le \beta < 1 \\ l - \lambda > \frac{F_C}{k} \end{cases} \tag{3}$$

Conversely, in *spc-1 pak-1* defective embryos, the continuing damage to actin filaments should reduce their stiffness (component α_{DV} in equation (2)). We accounted for this by including a tearing factor γ in the equation for stiffness (equation (4), Fig. 4b).

$$\frac{d\alpha_{DV}}{dt} = \gamma \frac{dl}{dt} \quad \text{if } \frac{dl}{dt} < 0 \text{ and } \alpha_{DV} > 0 \tag{4}$$

Using equations (1) to (4), we could accurately predict both the elongation pattern of wild-type embryos and the retraction pattern of *spc-1 pak-1* embryos (Fig. 4c, Extended Data Fig. 6d, e). Further, the model predicts that the plasticity factor of the *spc-1 pak-1* embryos is zero (Supplementary information). We propose that SPC-1 and PAK-1 regulate a cellular process of mechanical plasticity. From a cellular perspective, we suggest that elasticity does not fully bring the embryo back to its initial shape on muscle relaxation, enabling progressive lengthening.

To further define the molecular basis of viscoplasticity, we searched for gene knockdowns that induced retraction of *spc-1(ra409)* embryos (Extended Data Fig. 7a, Supplementary Table 4). This screen identified the atypical formin FHOD-1 (Fig. 4d, Extended Data Fig. 7, Supplementary Video 3), which has been linked to actin dynamics in the epidermis[25]. We confirmed that *fhod-1(tm2363) spc-1*(RNAi) embryos also showed a penetrant retraction phenotype with damaged actin (Fig. 4d, Extended Data Figs. 3, 7). Of note, vertebrate FHOD1 promotes actin capping, bundling and nucleation[26], raising the possibility that FHOD-1 activity stabilizes the actin cytoskeleton after actin severing (Fig. 3). Furthermore, the genetic interaction suggests that FHOD-1 acts with SPC-1 and PAK-1. To investigate this possibility, we tested whether FHOD-1 derivatives that lack the C-terminal diaphanous autoregulatory domain (DAD), predicted to release the autoinhibition characteristic of formins[27], could rescue the retraction phenotype of *spc-1 pak-1* deficient embryos. After epidermis-specific expression of a form that lacks the FH2 and DAD domains, transgenic *spc-1*(RNAi) *pak-1(tm403)* embryos reached 90 μm in length without retracting; this was longer than embryos that express the full-length protein. By contrast, longer FHOD-1 forms that include the FH2 domain rescued

poorly or not at all (Fig. 4e), which suggests that the FH2 F-actin nucleation domain is dispensable for the rescue. Of note, a mammalian FHOD1 lacking the FH2 and DAD domains can still bundle actin[26]. Collectively, our data underline that FHOD-1 bundling activity is key, and that the retraction phenotype mainly results from a lack of FHOD-1 activation downstream of the muscle-induced mechanotransduction pathway. We conclude that actin-filament severing initiated by muscle contractions (Fig. 3) followed by FHOD-1-dependent bundling or capping (Fig. 4) represents a ratchet-like mechanism, providing a molecular basis for viscoplasticity.

Several factors could contribute to alter PAK-1 and FHOD-1 activity. First, SPC-1 could help recruit these proteins, as FHOD-1–GFP and PAK-1–GFP formed small aggregates in SPC-1 defective embryos (Extended Data Fig. 8). Second, muscle contractions in *spc-1*(RNAi) *pak-1(tm403)* embryos were decreased in duration by almost half compared with *pak-1(tm403)* or wild-type control embryos (3 s against 5.7 s) (Extended Data Fig. 9, Supplementary Video 4). These shorter contractions may mean that there is insufficient time for FHOD-1 to stabilize actin filaments.

In sum, our results identify several proteins that are involved in stabilizing cell shapes in a system subjected to repeated external mechanical stress. We propose that the progressive shortening of actin filaments under the control of these factors mediates a cellular viscoplastic process that promotes axis elongation. A similar viscoplastic process might operate in vertebrate tissues comprising an epithelial layer surrounded by a contractile layer, such as the internal organs in humans. Notably, high FHOD1 expression correlates with poor prognosis of patients with breast cancer[28]. Such a process might therefore also influence the metastatic properties of tumour cells juxtaposed with contractile cells.

Online content

Any methods, additional references, Nature Research reporting summaries, source data, extended data, supplementary information, acknowledgements, peer review information; details of author contributions and competing interests; and statements of data and code availability are available at https://doi.org/10.1038/s41586-019-1509-4.

Received: 16 May 2018; Accepted: 29 July 2019;
Published online: 28 August 2019

1. Gilmour, D., Rembold, M. & Leptin, M. From morphogen to morphogenesis and back. *Nature* **541**, 311–320 (2017).
2. Martin, A. C., Kaschube, M. & Wieschaus, E. F. Pulsed contractions of an actin–myosin network drive apical constriction. *Nature* **457**, 495–499 (2009).
3. Rauzi, M., Lenne, P. F. & Lecuit, T. Planar polarized actomyosin contractile flows control epithelial junction remodelling. *Nature* **468**, 1110–1114 (2017).
4. Collinet, C., Rauzi, M., Lenne, P. F. & Lecuit, T. Local and tissue-scale forces drive oriented junction growth during tissue extension. *Nat. Cell Biol.* **17**, 1247–1258 (2015).
5. Desprat, N., Supatto, W., Pouille, P. A., Beaurepaire, E. & Farge, E. Tissue deformation modulates twist expression to determine anterior midgut differentiation in *Drosophila* embryos. *Dev. Cell* **15**, 470–477 (2008).
6. Lye, C. M. et al. Mechanical coupling between endoderm invagination and axis extension in *Drosophila*. *PLoS Biol.* **13**, e1002292 (2015).
7. Zhang, H. et al. A tension-induced mechanotransduction pathway promotes epithelial morphogenesis. *Nature* **471**, 99–103 (2011).
8. Behrndt, M. et al. Forces driving epithelial spreading in zebrafish gastrulation. *Science* **338**, 257–260 (2012).
9. Dierkes, K., Sumi, A., Solon, J. & Salbreux, G. Spontaneous oscillations of elastic contractile materials with turnover. *Phys. Rev. Lett.* **113**, 148102 (2014).
10. Vuong-Brender, T. T., Ben Amar, M., Pontabry, J. & Labouesse, M. The interplay of stiffness and force anisotropies drives embryo elongation. *eLife* **6**, e23866 (2017).
11. Munro, E., Nance, J. & Priess, J. R. Cortical flows powered by asymmetrical contraction transport PAR proteins to establish and maintain anterior-posterior polarity in the early *C. elegans* embryo. *Dev. Cell* **7**, 413–424 (2004).
12. Vuong-Brender, T. T., Yang, X. & Labouesse, M. *C. elegans* embryonic morphogenesis. *Curr. Top. Dev. Biol.* **116**, 597–616 (2016).
13. Simões, Sde. M., Mainieri, A. & Zallen, J. A. Rho GTPase and Shroom direct planar polarized actomyosin contractility during convergent extension. *J. Cell Biol.* **204**, 575–589 (2014).
14. Vasquez, C. G., Tworoger, M. & Martin, A. C. Dynamic myosin phosphorylation regulates contractile pulses and tissue integrity during epithelial morphogenesis. *J. Cell Biol.* **206**, 435–450 (2014).
15. Gally, C. et al. Myosin II regulation during *C. elegans* embryonic elongation: LET-502/ROCK, MRCK-1 and PAK-1, three kinases with different roles. *Development* **136**, 3109–3119 (2009).
16. Vuong-Brender, T. T. K., Suman, S. K. & Labouesse, M. The apical ECM preserves embryonic integrity and distributes mechanical stress during morphogenesis. *Development* **144**, 4336–4349 (2017).
17. Rogalski, T. M., Mullen, G. P., Gilbert, M. M., Williams, B. D. & Moerman, D. G. The *UNC-112* gene in *Caenorhabditis elegans* encodes a novel component of cell-matrix adhesion structures required for integrin localization in the muscle cell membrane. *J. Cell Biol.* **150**, 253–264 (2000).
18. Costa, M., Draper, B. W. & Priess, J. R. The role of actin filaments in patterning the *Caenorhabditis elegans* cuticle. *Dev. Biol.* **184**, 373–384 (1997).
19. Priess, J. R. & Hirsh, D. I. *Caenorhabditis elegans* morphogenesis: the role of the cytoskeleton in elongation of the embryo. *Dev. Biol.* **117**, 156–173 (1986).
20. Praitis, V., Ciccone, E. & Austin, J. SMA-1 spectrin has essential roles in epithelial cell sheet morphogenesis in *C. elegans*. *Dev. Biol.* **283**, 157–170 (2005).
21. McCullough, B. R. et al. Cofilin-linked changes in actin filament flexibility promote severing. *Biophys. J.* **101**, 151–159 (2011).
22. Bonakdar, N. et al. Mechanical plasticity of cells. *Nat. Mater.* **15**, 1090–1094 (2016).
23. Doubrovinski, K., Swan, M., Polyakov, O. & Wieschaus, E. F. Measurement of cortical elasticity in *Drosophila melanogaster* embryos using ferrofluids. *Proc. Natl Acad. Sci. USA* **114**, 1051–1056 (2017).
24. Muñoz, J. J. & Albo, S. Physiology-based model of cell viscoelasticity. *Phys. Rev. E* **88**, 012708 (2013).
25. Vanneste, C. A., Pruyne, D. & Mains, P. E. The role of the formin gene *fhod-1* in *C. elegans* embryonic morphogenesis. *Worm* **2**, e25040 (2013).
26. Schönichen, A. et al. FHOD1 is a combined actin filament capping and bundling factor that selectively associates with actin arcs and stress fibers. *J. Cell Sci.* **126**, 1891–1901 (2013).
27. Kühn, S. & Geyer, M. Formins as effector proteins of Rho GTPases. *Small GTPases* **5**, e983876 (2014).
28. Jurmeister, S. et al. MicroRNA-200c represses migration and invasion of breast cancer cells by targeting actin-regulatory proteins FHOD1 and PPM1F. *Mol. Cell. Biol.* **32**, 633–651 (2012).

METHODS

No statistical methods were used to predetermine sample size. The experiments were not randomized. The investigators were not blinded to allocation during experiments and outcome assessment.

Worm strains and conditions of maintenance. The list of strains used is presented in Supplementary Table 5. Worms were propagated on NGM agar plates as previously described[29], maintained at a standard 20 °C. The *gsnl-1(tm2730)* and *viln-1(2413)* worms were outcrossed three times.

Yeast two-hybrid screening. Yeast two-hybrid screening was performed by Hybrygenics Services. The bait component was the N-terminal 294 amino acids of PAK-1 (including the regulatory region of the protein) fused as a C-terminal fusion to LexA. The construct was used as a bait to screen at saturation a highly complex, random-primed *C. elegans* embryo cDNA library[30]. Screening involved a mating approach on a medium lacking Trp, Leu and His, supplemented with 0.5 mM 3-aminotriazole[31]. The strongest hits of the screen can be found in Supplementary Table 2. Reciprocal screens using the spectrin repeat no. 9 or the SH3 domains of SPC-1 as baits identified PAK-1 region 160–206, and no other meaningful prey in the context of the present study.

RNAi screens. A RNAi screen was performed in the *pak-1(tm403)* mutant along with a wild-type control. A collection of 356 essential genes from the Ahringer RNAi library[32]—including adhesion proteins, signalling proteins, phosphatases, kinases, cytoskeleton-associated proteins and proteins important in epithelial morphogenesis—was assembled (Supplementary Table 1), based on a previous screen performed in the *git-1(tm1962)* background (C.G. and M.L., unpublished). The screen was performed in liquid culture on 96-well plates and RNAi knockdown was induced by feeding as previously described[33]. The primary screen was based on enhanced lethality and body morphology defects; the secondary screen focused on very short larvae and elongation defects. We took DIC images for body-length measurements and performed DIC time-lapse imaging for the strongest candidates. We performed two additional RNAi screens. First, we used a *spc-1(ra409) pak-1(tm403)* strain carrying an unstable extrachromosomal rescuing *spc-1::gfp* marker to look for potential suppressors of the retraction phenotype. We selected 13 actin-related proteins from the Ahringer RNAi library[32] that were recently reported to modulate actin remodelling in the early embryo[34] (Supplementary Table 3). RNAi was induced by RNAi feeding on L4 larvae maintained at 20 °C, and the progeny was analysed 20 h to 30 h after feeding; for early-acting essential genes (*cyk-1, pfn-1, unc-60*), worms were maintained at 15 °C, and the progeny was analysed 16 h to 20 h after feeding still inducing more than 14% early embryonic defects. Second, we likewise used a *spc-1(ra409)* mutant carrying an unstable extrachromosomal rescuing *spc-1::gfp* marker to look for potential enhancers of the *spc-1(ra409)* elongation defects. We selected for this enhancer screen genes that had given the strongest defects in the initial screen with 356 genes (Supplementary Table 4). In both cases, young L1 hatchlings were inspected for the presence or absence of a fluoresent *spc-1::GFP* signal and photographed using either a Leica DMI4000 (first screen) or Leica DM6000 (second screen) microscope. Length of the young larvae was measured using ImageJ software.

For specific genes (*spc-1*, *pak-1*, *fhod-1* and *unc-112*), RNAi was induced by injection after preparing the double-stranded RNA (dsRNA) with the Ambion mMessage mMachine kit and purifying the dsRNA with the Qiagen RNeasy MinElute Cleanup kit[35]. The embryos were analysed from 24 h to 48 h after injection. In one case, experiments involving the strain *spc-1(ra409) pak-1(tm403); mcEx1016[spc-1(+)::GFP; Pmyo-2::RFP]* (shown in Extended Data Figs. 3, 4), RNAi against *unc-112* was induced by feeding because the strain barely survived the regular microinjection procedure.

Fluorescent translational reporter constructs. A 12,633-bp genomic sequence including the *spc-1* coding sequence and a 3-kb promoter was inserted in frame with the GFP coding sequence present in the pPD95.75 vector (Addgene). To create the *Ppak-1::pak-1::mKate* reporter construct, first an mKate-containing backbone was created by exchanging the GFP-coding sequence of the pML1572, P*lin-26::vab-10(ABD)::GFP* plasmid[15]. In a following cloning step, a 8,204-bp genomic sequence, including the *pak-1* coding sequence and a 4.5-kb promoter were inserted in frame with the mKate coding sequence present in the vector.

To test whether SPC-1::GFP could rescue the function of SPC-1, we first crossed the different transgenic worms of a wild-type background with *mnDp33; spc-1(ra409)* worms (strain DM3409), and F1 transgenic males again with DM3409 to establish *mnDp33; spc-1(ra409); Ex[spc-1::GFP*. Rescuing transgenes were recognized because all viable progeny was GFP-positive and all (or most) non-viable progeny was GFP-negative, reflecting the loss of the *mnDp33* balancer. To attempt *mnDp33* segregation, we repeatedly transferred single GFP-positive mothers over four generations and examined their progeny, starting from at least two independent extrachromosomal arrays per construct. Thereby, we successfully obtained viable *spc-1(ra409); Ex[Pspc-1::spc-1(+)::gfp* worms, and then viable *spc-1(ra409) pak-1(tm403); Ex[Pspc-1$_1$::spc-1(+)::gfp* worms through crossing and meiotic recombination, which segregated very short retracted GFP-negative embryos. For the FHOD-1 constitutively active construct, a 8,283-bp genomic sequence of *fhod-1* (gift from D. Pruyne[36]) deleted for part of the FH2 domain and the DAD domain was inserted under the control of the epidermis-specific 432-bp *dpy-7* promoter. Deletion of the DAD alone was obtained by inserting back the FH2 domain in the FH2/DAD deleted construct using Hifi DNA assembly cloning kit (New England Biolabs); the FH1/FH2 deleted construct was obtained by deleting the FH1 domain using the Q5 site directed mutagenesis kit protocol (New England Biolabs). All cloning steps relied on the use of the Phusion High-Fidelity DNA Polymerase reaction kit (Fisher Thermo Scientific); the constructs were subsequently verified by sequencing. The constructs were injected at 10 ng μl^{-1} plasmid construct, with 150 ng μl^{-1} pBSK + 5 ng μl^{-1} pCFJ90 (P$_{myo-2}$*::mcherry*) as co-injection markers for the *spc-1::gfp* constructs, or 100 ng μl^{-1} pRF4 (rol) co-injection marker for *pak-1::mKate*.

Fluorescence imaging. DIC images for time-lapse videos were obtained using a Leica DM6000 microscope with Leica LAS-AF software. Observations were done under a 40× oil immersion objective. Mothers were cut up to gain early-staged embryos, which were then transferred onto thin 5% soft agarose pads in a drop of M9. *Z*-stack image series with a 1.5-μm *Z*-step distance were taken in every 5 min during 6 to 10 h. ImageJ software was used to quantify the embryonic length from the end of ventral enclosure/onset of elongation, by taking a segmented line through the midline of the embryos from head to tail. To image the coupling between actin-bundle displacement in the epidermis and muscle contractions, we used a double reporter strain carrying the epidermal *Pdpy-7::LifeAct::GFP* and muscle *Pmyo-3::his-24::mCherry* transgenes (ML2113, Supplementary Table 5), and a spinning-disc DMI6000 Leica microscope equipped with an Andor software (experiments for Fig. 1). Series of five *Z* planes (1 epidermal + 4 muscle) were imaged continuously for 5 min, with 0.5-μm *Z* steps and no averaging. The time interval between two *Z* series was 360 ms. The measurement of actin displacement was done according to the same strategy, and was done using a CSUX1-A1 spinning disc mounted on a Zeiss Axio Observer Z1 inverted microscope with a Roper Evolve camera controlled by the Metamorph software, and a 100× oil immersion objective (experiments for Extended Data Fig. 9). A *Z* stack of 4 focal planes with 0.5-μm step size was acquired using a streaming acquisition mode. The time between two acquisitions was 0.41 s during 300 time frames. To synchronize embryos, mothers were put on an empty NGM agar plate to lay eggs for a short time window, and embryos were left to develop until the stage of interest. For the analysis of the contraction see 'Image analysis and quantification of actin filament contraction, continuity and orientation'. To analyse the in vivo co-localization between PAK-1::mKate, ABD::mcherry and SPC-1::GFP, we used the Zeiss–Roper spinning-disc microscope under a 100× oil immersion objective, keeping the laser intensity at a constant level throughout the experiments. Image processing and computing the co-localization coefficient was done using the Volocity software.

TIRF–SIM. Embryos were mounted between 22-mm square cover glasses (thickness of 0.170 ± 05 μm, Carl Zeiss Microscopy) and 25 × 75-mm teflon-coated glass slides with three depression wells. Embryos were embedded in 2 μl water containing Polybeads acrylate microspheres of 15.4 ± 1.43-μm diameter (Polysciences). Wild-type embryos were at 1.8- to 2-fold stage; *spc-1*(RNAi) *pak-1(tm403)* embryos were aged between twofold and threefold equivalent for a control embryo. TIRF–SIM images[37,38] were acquired on a DeltaVision OMX SR imaging system from GE Healthcare Life Sciences equipped with a 60 × oil immersion objective from Olympus (PlanApo N 60× 1.42 NA). To minimize spherical aberrations, we used Cargille labs immersion oil with a n_D at 25 °C (5893 Å) = 1.5140 ± 0.0002. Imaging was performed using the excitation at 488 nm with laser transmission ranging from 75 to 100% and integration time ranging from 2 to 3 ms. For each embryo, time series of 50 to 100 TIRF–SIM images of 256 × 256 pixels (pixel size of 80 nm) were acquired. Each TIRF–SIM image corresponds to a set of 9 images (3 phases at 3 angles) acquired withing 90.6 to 99.6 ms. Reconstruction of TIRF–SIM images (final pixel size after reconstruction is 40 nm) were performed with the softWoRx software (Applied Precision), which in turn enables a resolution enhancement by a factor of 2 that leads to a final lateral resolution in the order of 100 nm.

Image analysis and quantification of actin-filament contraction, continuity and orientation. The analysis of mechanical displacement in the epidermis was performed on the videos of the dorsoventral actin layer by measuring the distance over time between two landmarks across the region of contraction. The landmarks were set manually on a frame showing relaxed tissue and tracked all over the contraction till the subsequent relaxed state. Landmarks tracking was performed using a statistical template matching approach[39]. The method was implemented as an ImageJ plugin (http://sites.imagej.net/Julienpontabry/), giving as output the landmarks locations, their distance across time and the kymographs. The curves show a pre-contraction state, a minimum (the maximal contraction point) and an ending part where the distance progressively increases again (Fig. 1b, bottom, Extended Data Fig. 9). After a smoothing and interpolation of the curves, the starting, ending and maximal contraction points were extracted by studying the time derivative of the distance and by setting a threshold on the distance itself.

Finally the contraction time was computed as the difference between the ending time and the initial time. The quantification of bending angles was done using a similar strategy; the angles were measured on single bundles at the frame of maximal deformation in a contraction cycle (Extended Data Fig. 5). The analysis of the curves and statistics were done using a MATLAB script. All images were analysed using the ImageJ (FIJI) software (NIH; http://rsb.info.nih.gov/ij/) and MATLAB R2015b (MathWorks). To study the features of actin pattern, we imaged embryos that were put to sleep by oxygen deprivation through a high concentration of bacteria with the Zeiss–Roper spinning-disc using a 100× oil immersion objective. For each experiments, a *Z*-stack of 16 focal planes with 0.2-μm step size was acquired. On the original maximum *Z* projection created by imageJ, a manual ROI was defined on the dorsoventral cells (Fig. 2, Extended Data Fig. 3), from which a high-pass filter in the Fourier space was applied to select only structures smaller than 10 pixels in diameter (Fig. 2, Extended Data Fig. 3).

Continuity. The filtered ROIs were binarized by setting to one all the pixels with a value higher than zero, and setting to zero all the other pixels. The resulting structures were then fitted by ellipses from which the length of the major axis was extracted as a measure of the length of the actin filament. The longer actin filaments are those presenting a more-uniform fluorescence along their length (showing higher continuity). By contrast, short segments result from discontinuity in the fluorescence signal. To avoid noise, only segments longer than four pixels have been considered for the analysis.

Anisotropy of the orientation. The same filtered ROI used for continuity measurements was used to measure the distribution of bundle orientation. Fast Fourier transform (FFT) of these ROIs was computed to work in the frequency domain and more-easily identify repetitive patterns. The resulting power spectrum of the ROIs was represented in polar coordinates to extract the distribution of angles of ROI pattern[40]. The method was implemented in an ImageJ plugin (http://sites.imagej.net/Julienpontabry/), giving as output the angular distribution. To compare the distributions coming from different images the distributions were normalized by their integral (Fig. 2, Extended Data Fig. 3). The more the pattern consists in structures oriented in a preferred direction (the more anisotropic), the highest is the peak of the distribution in that direction. In the case of an isotropic pattern, the angular distribution should show a flat behaviour. As an estimate of the pattern anisotropy, the prominence of the highest peak of the angular distribution was considered (Fig. 2, Extended Data Fig. 4). The analysis of the angular distributions and statistics was performed by a MATLAB script. All images were analysed using the ImageJ (FIJI) software and MATLAB R2015b (MathWorks).

Straightness. For each embryo, we selected an ROI containing the region above the muscles based on a contraction pattern. We selected ROIs containing about ten actin bundles, and we segmented manually seven of them for each ROI (the number of bundles that were on average well-resolved). For each bundle we computed the straightness as the ratio between the length of the segmented bundle and the distance between the initial and final points of the bundle. This quantity has an upper limit equal to one for perfectly straight lines. The manual segmentation and straightness calculation were performed with a custom MATLAB interface.

Bundle organization. For each embryo, we measured the relative contrast in the image between the regions occupied by actin filaments and those in between the filaments as a proxy for bundle composition and organization. The reasoning was that in the extreme case in which bundles separate to generate individual filaments, each filament is likely to have a lower intensity than a bundle made of several filaments, and the contrast between filaments and the intervening space would be less sharp. This should result in a lower variance or standard deviation of the image intensity compared to a wild-type bundle image. To do so we divided the standard deviation by the average intensity.

Statistical analysis. For elongation curves, s.e.m. was measured. For L1 length measurement and rescue experiments we performed paired *t*-test using Prism v.5.00 (GraphPad) and Excel. For contraction time, actin continuity and orientation, we applied for all genotypes a paired *t*-test using MATLAB.

Reporting Summary. Further information on research design is available in the Nature Research Reporting Summary linked to this article.

Data availability

Source Data for Figs. 1d, 2c–f, 3c–e, 4d, e and Extended Data Figs. 1b, d, k, 3b, c, 4c, d, 5d, e, l, 7a, b, 9f, as well as numbers of replicates and *P* values (where applicable) for all figures are provided in the online version of the paper.

Code availability

All MATLAB scripts used for the present analysis are available upon reasonable request.

29. Brenner, S. The genetics of *Caenorhabditis elegans*. *Genetics* **77**, 71–94 (1974).
30. Gomes, J. E. et al. Microtubule severing by the katanin complex is activated by PPFR-1-dependent MEI-1 dephosphorylation. *J. Cell Biol*. **202**, 431–439 (2013).
31. Fromont-Racine, M., Rain, J. C. & Legrain, P. Toward a functional analysis of the yeast genome through exhaustive two-hybrid screens. *Nat. Genet*. **16**, 277–282 (1997).
32. Kamath, R. S. et al. Systematic functional analysis of the *Caenorhabditis elegans* genome using RNAi. *Nature* **421**, 231–237 (2003).
33. Gally, C., Zhang, H. & Labouesse, M. Functional and genetic analysis of VAB-10 spectraplakin in *Caenorhabditis elegans*. *Methods Enzymol*. **569**, 407–430 (2016).
34. Naganathan, S. R. et al. Morphogenetic degeneracies in the actomyosin cortex. *eLife* **7**, e37677 (2018).
35. Bosher, J. M. et al. The *Caenorhabditis elegans vab-10* spectraplakin isoforms protect the epidermis against internal and external forces. *J. Cell Biol*. **161**, 757–768 (2003).
36. Mi-Mi, L., Votra, S., Kemphues, K., Bretscher, A. & Pruyne, D. Z-line formins promote contractile lattice growth and maintenance in striated muscles of *C. elegans*. *J. Cell Biol*. **198**, 87–102 (2012).
37. Gustafsson, M. G. Surpassing the lateral resolution limit by a factor of two using structured illumination microscopy. *J. Microsc*. **198**, 82–87 (2000).
38. Kner, P., Chhun, B. B., Griffis, E. R., Winoto, L. & Gustafsson, M. G. Super-resolution video microscopy of live cells by structured illumination. *Nat. Methods* **6**, 339–342 (2009).
39. Matthews, I., Ishikawa, T. & Baker, S. The template update problem. *IEEE Trans. Pattern Anal. Mach. Intell*. **26**, 810–815 (2004).
40. Gonzalez, R. C. & Woods, R. E. *Digital Image Processing* 3rd edn (Prentice–Hall, 2006).

Acknowledgements The authors thank A. Spang, S. Grill, Y. Bellaïche and R. Voituriez for critical comments on the manuscript and M. Gettings for improving the English. We also thank the *Caenorhabditis* Genetics Center (funded by the NIH Office of Research Infrastructure Programs P40 OD010440) and National BioResource Project at Tokyo Women's Medical University for strains, the IBPS Imaging Facility for advice. This work was supported by the Agence Nationale pour la Recherche, the European Research Council (grant no. 294744), Israel–France Maïmonide exchange program grants, and installation funds from the Centre National de la Recherche Scientifique (CNRS) and University Pierre et Marie Curie (UPMC) to M.L. A.L. was supported by a fellowship from the Fondation pour la Recherche Médicale (FDT201805005501). This work was also made possible by institutional funds from the CNRS, University of Strasbourg and UPMC, the grant ANR-10-LABX-0030-INRT, which is a French State fund managed by the Agence Nationale de la Recherche under the framework programme Investissements d'Avenir labelled ANR-10-IDEX-0002-02 to the IGBMC. The work of P.M. and E.B. was partly supported by the Agence Nationale de la Recherche (contract ANR-11-EQPX-0029 Morphoscope2), the work of S.O. was partly supported by the National Institutes of Health (grant AR048615).

Author contributions M.L. conceived the project. A.L. performed most experiments with initial contributions from G.P. T.F. conceived the modelling, F.L. generated the FHOD-1 variants and the screen reported in Supplementary Table 3, P.M. and E.B. helped with TIRF–SIM imaging, T.F. and J.P. performed image analysis, C.G. shared data from a related screen, S.K. helped with the *spc-1(ra409)* mini-RNAi screen, D.R. provided technical assistance and S.O. provided the outcrossed *gsnl-1* and *viln-1* mutants. M.L. wrote the manuscript, and all authors commented and proofread it (except S.K., who was an intern), A.L. assembled figures, T.F. conceived and wrote the supplementary mathematical modelling material and F.L. prepared the Methods section.

Competing interests The authors declare no competing interests.

Additional information

Supplementary information is available for this paper at https://doi.org/10.1038/s41586-019-1509-4.

Correspondence and requests for materials should be addressed to M.L.

Peer review information *Nature* thanks Edwin Munro, Bruce Vogel and the other, anonymous, reviewer(s) for their contribution to the peer review of this work.

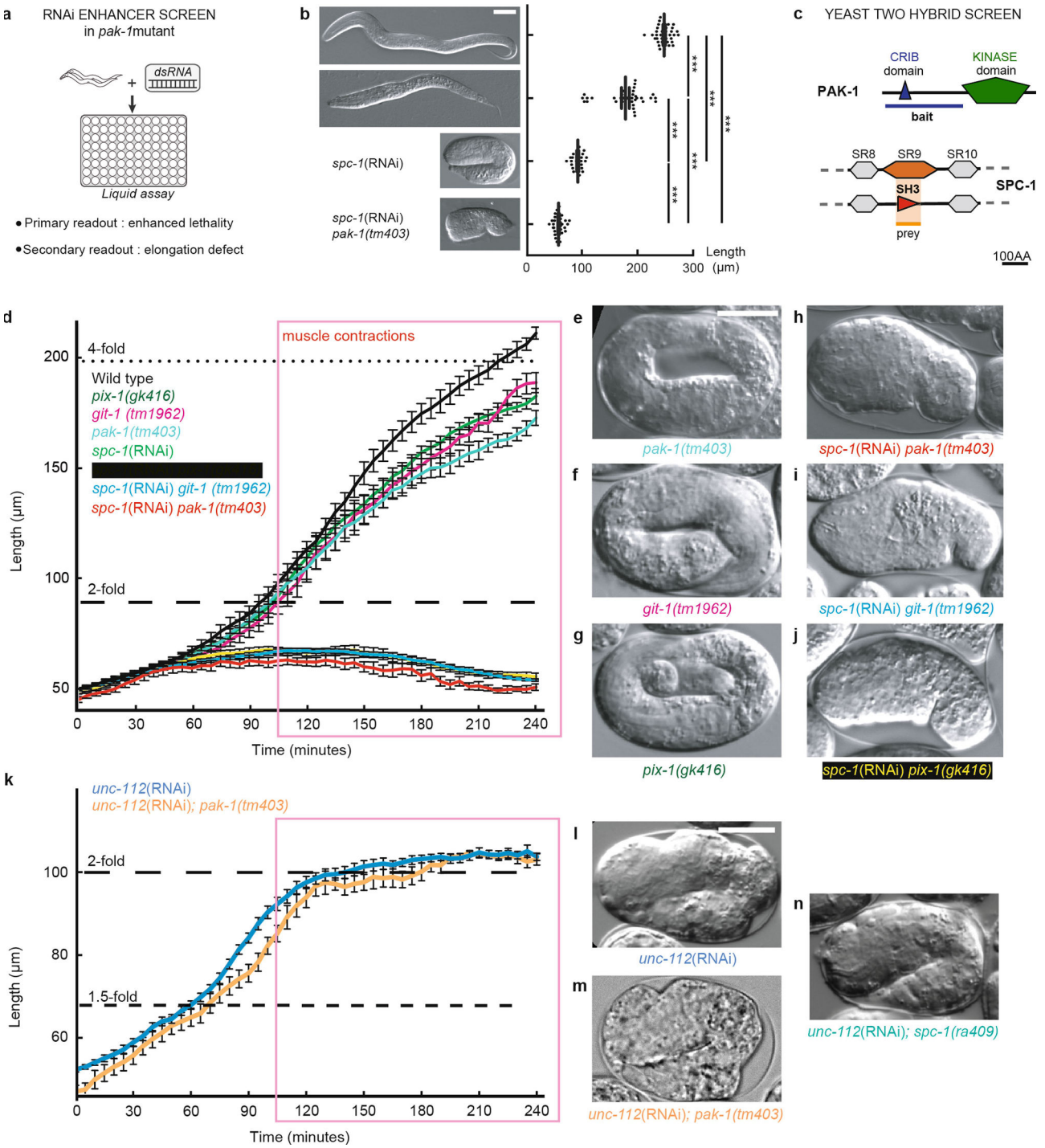

Extended Data Fig. 1 | Genes required to maintain embryonic elongation. a, RNAi screen in a *pak-1* mutant identified *spc-1* as an enhancer (Supplementary Table 1). **b**, DIC images and quantification of newly hatched wild-type body length ($n = 38$ embryos), *pak-1(tm403)* ($n = 32$ embryos), *spc-1*(RNAi) ($n = 26$ embryos) and *spc-1*(RNAi) *pak-1(tm403)* ($n = 36$ embryos). Scale bars, 25 µm (WT and *pak-1*), 10 µm (*spc-1* and *spc-1 pak-1*). Data represent mean values ± s.d. Two-sided paired *t*-test. **c**, A yeast two-hybrid screen using the PAK-1 N-terminal domain as a bait identified the SPC-1 SH3 domain as a prey (orange background) (Supplementary Table 2). **d–j**, Loss of the proteins GIT-1 and PIX-1, acting upstream of PAK-1 in the mechanotransduction pathway promoted by muscle contractions, in the absence of *spc-1* also triggers a retraction phenotype. **d–j**, Elongation curves (**d**) and terminal phenotypes of wild type ($n = 12$ embryos), *pak-1(tm403)* (**e**; $n = 11$ embryos), *git-1(tm1962)* (**f**; $n = 10$ embryos), *pix-1(gk416)* (**g**; $n = 10$ embryos), *spc-1*(RNAi) *pak-1(tm403)* (**h**; $n = 9$ embryos), *spc-1*(RNAi) *git-1(tm1962)* (**i**; $n = 11$ embryos), *spc-1*(RNAi) *pix-1 (tm416)* (**j**; $n = 8$ embryos). Data represent mean ± s.e.m. **k–n**, Elongation curves (**k**) and DIC pictures showing the terminal phenotypes of *unc-112*(RNAi) embryos (**l**; $n = 14$) and *unc-112*(RNAi) *pak-1(tm403)* (**m**; $n = 8$ embryos). **n**, Terminal phenotype of *unc-112*(RNAi) *spc-1(ra409)* obtained by inducing *unc-112*(RNAi) in the strain ML2436 bearing a rescuing extrachromosomal *spc-1::gfp* array and looking for embryos having lost the array; we could only obtain a few embryos of the desired phenotype despite numerous repeats ($n = 4$ embryos), all of which had the phenotype illustrated here, which is similar to that of *spc-1(ra409)* alone. Data represent mean ± s.e.m. Scale bars in **e–j**, **l–n**, 17 µm. $^*P < 0.05$; $^{**}P < 0.001$; $^{***}P < 0.0001$.

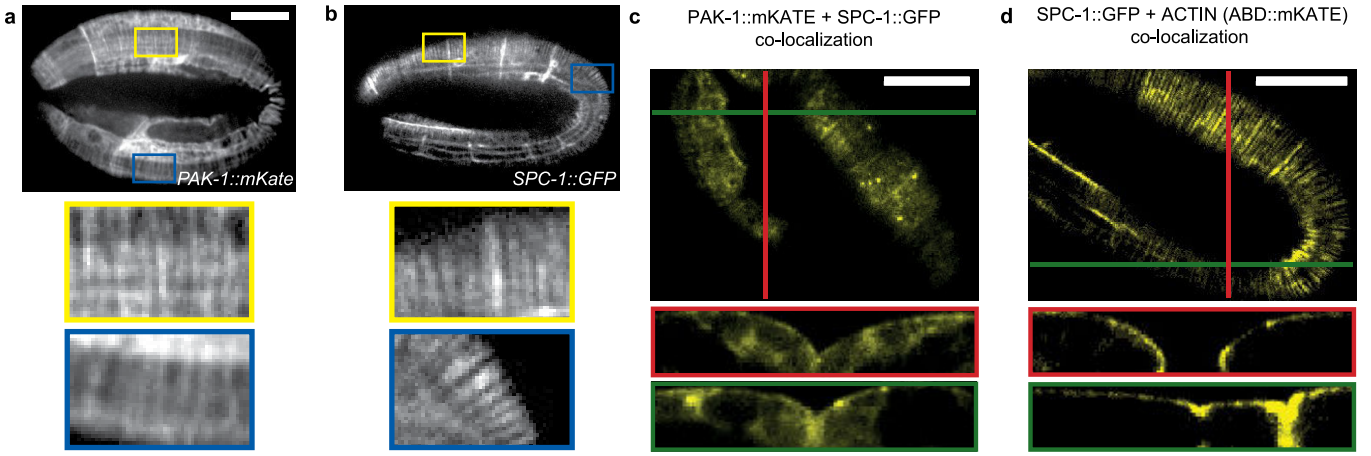

Extended Data Fig. 2 | PAK-1and SPC-1 colocalize with actin filaments. **a**, **b**, Distribution of PAK-1::mKate (**a**; $n = 20$ embryos) and SPC-1::GFP (**b**; $n = 13$ embryos) in a late embryo. Enlarged images of PAK-1 and SPC-1 showing a filamentous distribution in the dorsoventral epidermis similar to actin filaments. **c**, Fluorescence images of PAK-1::mKate (red) and SPC-1::GFP (green) ($n = 20$ embryos). The panel shows the colocalization image for the most-apical focal planes (top image), and full *XZ* (green panel) and *YZ* (red panel) projections. The level of co-localization is high based on Pearson's correlation coefficient (0.7–0.9, $n = 20$ embryos). The highest level of colocalization is detected at the apical cortex. **d**, Fluorescence images of *Plin-26*::VAB-10(ABD)::mKate (red) and SPC-1::GFP (green) ($n = 8$ embryos). The panel shows the colocalization image for the most-apical focal planes (top image), and full *XZ* (green panel) and *YZ* (red panel) projections. The level of colocalization is high based on Pearson's correlation coefficient (0.7–0.9, $n = 8$ embryos). The colocalization is detected almost exclusively at the apical cortex. The gene *lin-26* drives expression in the epidermis; VAB-10(ABD) corresponds to the two actin-binding domains (calponin homology) of the protein VAB-10. Scale bar, 10 μm.

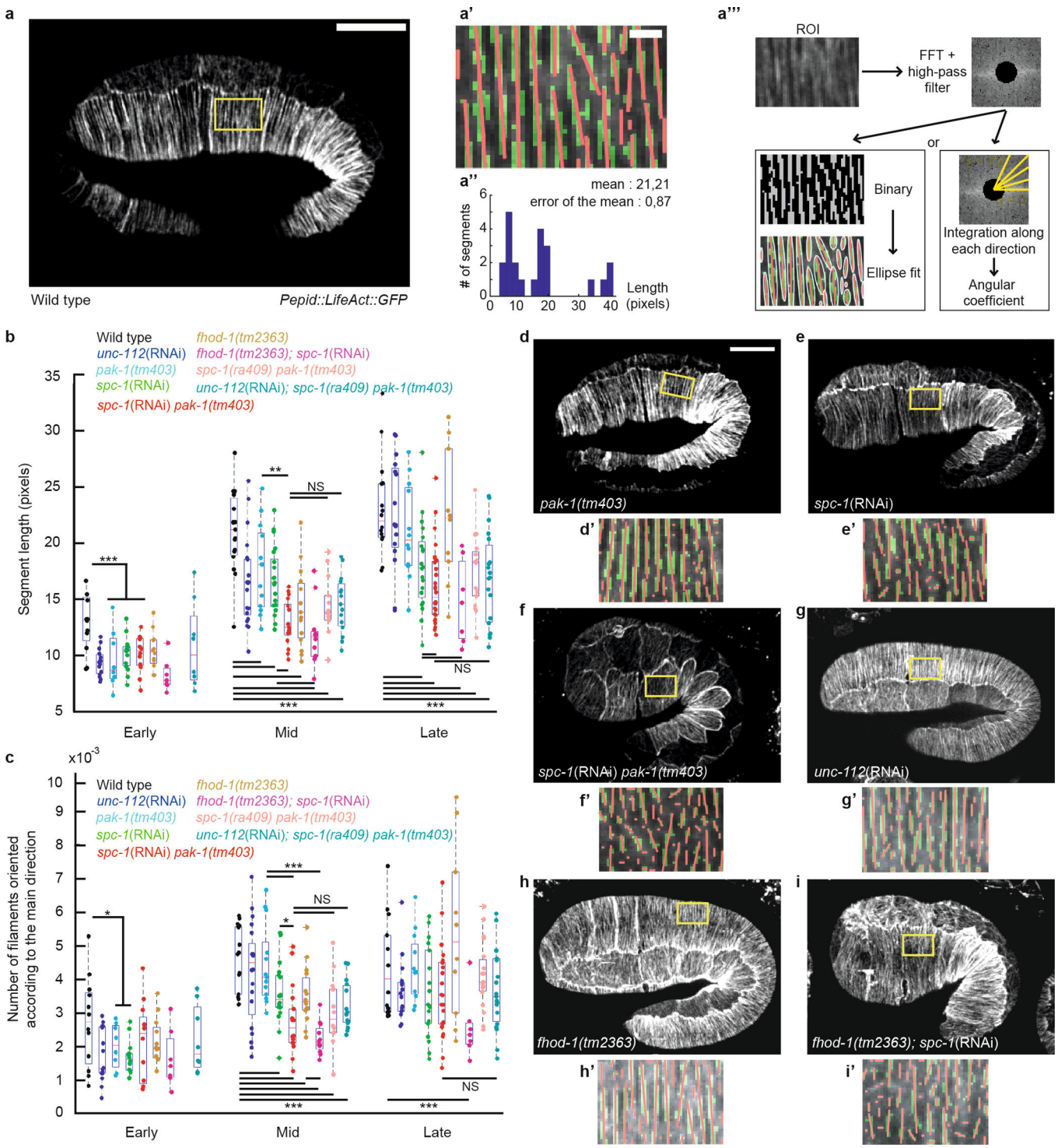

Extended Data Fig. 3 | See next page for caption.

Extended Data Fig. 3 | Actin-filament continuity and orientation at three elongation stages. a, **d–i**, Epidermal actin filaments visualized with the *Pdpy-7::LifeAct::GFP* reporter construct in wild type (**a**), *pak-1(tm403)* (**d**), *spc-1*(RNAi) (**e**), *spc-1*(RNAi) *pak-1(tm403)* (**f**), *unc-112*(RNAi) (**g**), *fhod-1(tm2363)* (**h**) and *fhod-1(tm2363) spc-1*(RNAi) (**i**) at mid-elongation (twofold equivalent) stage. Yellow rectangle, ROI. Scale bar, 10 μm. ROI after binarization (green) and major axis detection (red) (**a**, top middle, **d–i**, bottom), based on three steps of image treatment for continuity and orientation analysis (**a**, right). Actin continuity: distribution of actin segments based on their length (**a**, bottom middle). **b**, Quantification of actin-filament continuity; the graph represents the length (in pixels) along the circumferential axis of actin filaments in early, mid and late (corresponding to 1.7-fold, 2-fold and 3-fold equivalent stages in a wild-type embryo, respectively) embryos of wild-type (early $n = 12$, mid $n = 19$, late $n = 16$), *pak-1(tm403)* (early $n = 16$, mid $n = 21$, late $n = 16$), *spc-1*(RNAi) (early $n = 15$, mid $n = 21$, late $n = 20$), *spc-1*(RNAi) *pak-1(tm403)* (early $n = 12$, mid $n = 17$, late $n = 26$), *unc-112*(RNAi) (early $n = 8$, mid $n = 13$, late $n = 12$), *fhod-1(tm2363)* (early $n = 12$, mid $n = 14$, late $n = 10$), *fhod-1(tm2363); spc-1*(RNAi) (early $n = 7$, mid $n = 11$, late $n = 8$), *spc-1(ra409) pak-1(tm403)* (mid $n = 14$, late $n = 20$) and *unc-112*(RNAi) ; *spc-1(ra409) pak-1(tm403)* (early $n = 8$, mid $n = 15$, late $n = 19$) genotypes. **c**, Actin-filament orientation based on FFT and binarization. Wild-type (early $n = 12$, mid $n = 18$, late $n = 14$), *pak-1(tm403)* (early $n = 16$, mid $n = 20$, late $n = 16$), *spc-1*(RNAi) (early $n = 14$, mid $n = 18$, late $n = 18$), *spc-1*(RNAi) *pak-1(tm403)* (early $n = 12$, mid $n = 18$, late $n = 21$), *unc-112*(RNAi) (early $n = 8$, mid $n = 13$, late $n = 12$), *fhod-1(tm2363)* (early $n = 12$, mid $n = 14$, late $n = 10$), *fhod-1(tm2363); spc-1*(RNAi) (early $n = 7$, mid $n = 11$, late $n = 8$), *spc-1(ra409) pak-1(tm403)* (mid $n = 14$, late $n = 19$) and *unc-112*(RNAi) *spc-1(ra409) pak-1(tm403)* (early $n = 8$, mid $n = 15$, late $n = 19$) genotypes. Note that the characteristics of actin filaments in *spc-1*(RNAi) *pak-1(tm403)* embryos differ mostly at the equivalent of the twofold stage when muscles become active. At earlier and later stages, *spc-1*(RNAi) embryos and *spc-1*(RNAi) *pak-1(tm403)* embryos become similar. Each graph represents median values, 25th and 75th percentiles. The whiskers extend to the most extreme data points not considered outliers. Two-sided paired *t*-test. $*P < 0.05$; $**P < 0.001$; $***P < 0.0001$; n.s, not significant.

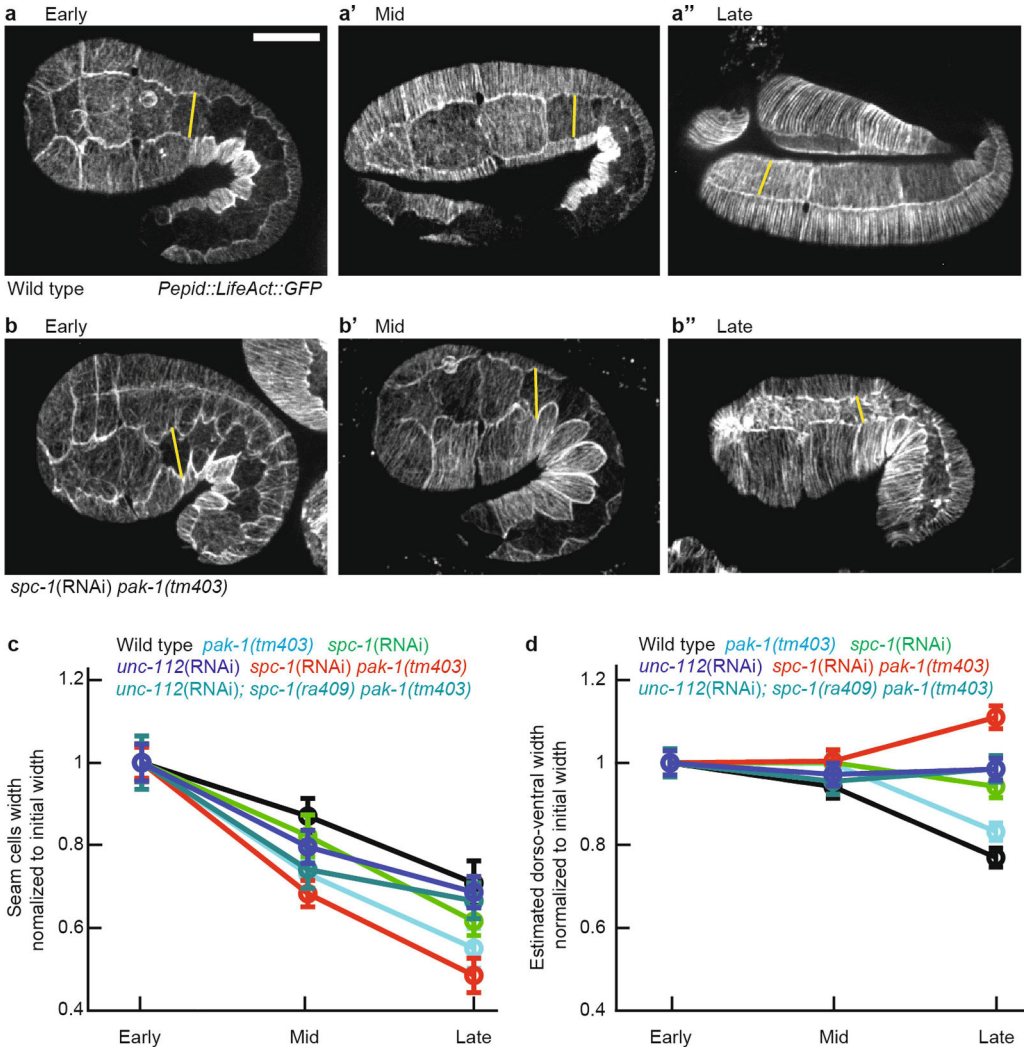

Extended Data Fig. 4 | Changes in embryo diameter during elongation. a, **b**, Fluorescence micrographs of embryos expressing the *Pepid*::*Lifeact*::*GFP* construct in the epidermis at three elongation stages early, middle and late (corresponding to 1.7-fold, 2-fold and 3-fold equivalent stages in a wild-type embryo, respectively) for wild-type (**a**) and *spc-1*(RNAi) *pak-1(tm403)* embryos (**b**). Scale bar, 10 μm. The *Pepid* promoter corresponds to *Pdpy-7*. The yellow lines correspond to the segments used to measure the dorsoventral width of the V1 seam cell. **c**, **d**, Quantification of the average V1 cell circumferential width normalized to the initial width during elongation (**c**), and of the average dorsoventral circumferential width at the level of the V1 seam cell (**d**), which was calculated using the measured embryo length and V1 cell width, taking into consideration the conservation of the total embryo volume, in wild-type (early $n = 38$, mid $n = 10$, late $n = 14$), *pak-1(tm403)* (early $n = 26$, mid $n = 8$, late $n = 20$), *spc-1*(RNAi) (early $n = 24$, mid $n = 26$, late $n = 18$), *spc-1*(RNAi) *pak-1(tm403)* (early $n = 22$, mid $n = 30$, late $n = 38$), *unc-112*(RNAi) (early $n = 8$, mid $n = 9$, late $n = 8$), and *unc-112*(RNAi) *spc-1(ra409) pak-1(tm403)* (early $n = 7$, mid $n = 12$, late $n = 17$) embryos. Error bars, s.e.m. A notable feature of *spc-1*(RNAi) *pak-1(tm403)* embryos is that the circumferential dimension of the seam cells decreased much more than that of their dorsoventral cells, which most probably reflects the actin-filament integrity defects combined with a F_{seam} force largely unchanged.

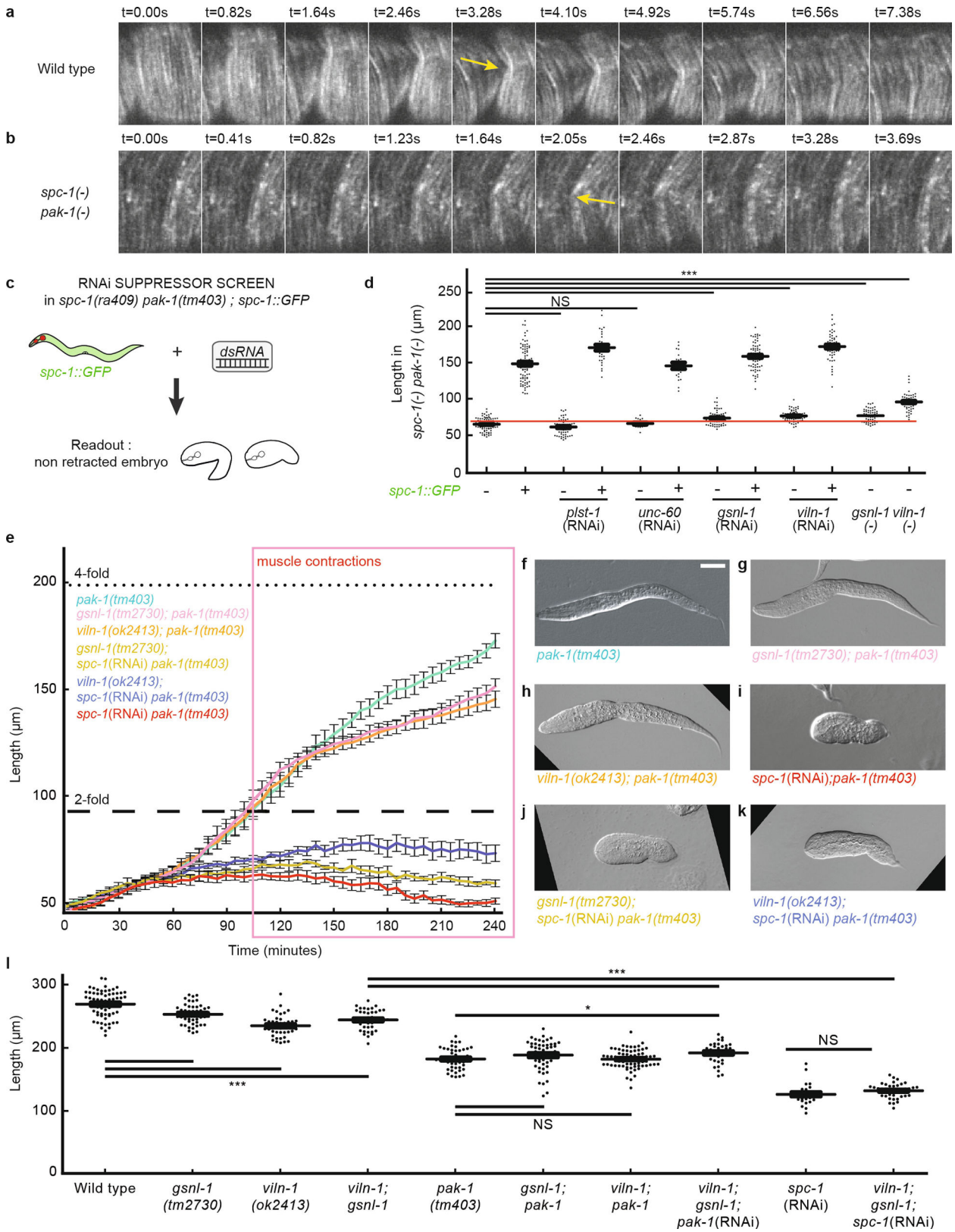

Extended Data Fig. 5 | See next page for caption.

Extended Data Fig. 5 | Bending and severing of actin bundles during muscle contractions. a, **b**, Kymographs of the regions boxed in yellow in Fig. 3a, b after spinning-disc time-lapse imaging of epidermal actin filaments (*Pdpy-7::LifeAct::GFP* reporter) in wild-type (**a**) and *spc-1*(RNAi) *pak-1(tm403)* (**b**) embryos at mid-elongation (twofold equivalent) stage. Scale bar, 5 μm. **c**, Principle of the RNAi screen performed to identify proteins mediating actin remodelling; the recipient strain carried a rescuing, but frequently lost, *spc-1(+)* transgene (green). **d**, Quantification of L1 hatchling length after downregulation or mutation of the indicated genes; the presence of the *spc-1::gfp* transgene is denoted +. Control worms fed on L4440 bacteria. **e**–**k**, Elongation curves (**e**) and DIC images showing the terminal phenotypes of *pak-1(tm403)* (**f**; $n = 11$ embryos), *gsnl-1(tm2730); pak-1(tm403)* (**g**; $n = 9$ embryos), *viln-1(ok2413); pak-1(tm403)* (**h**; $n = 9$ embryos), *gsnl-1(tm2730); spc-1*(RNAi) *pak-1 (tm403)* (**i**; $n = 5$ embryos), *viln-1(ok2413); spc-1*(RNAi) *pak-1(tm403)* (**j**; $n = 11$ embryos) and *spc-1*(RNAi) *pak-1(tm403)* (**k**; $n = 9$ embryos). Pink box in **e**, period of muscle activity. Data represent mean ± s.e.m. Scale bar, 25 μm. **l**, Quantification of the L1 hatchling body length of wild type ($n = 65$ hatchlings), *gsnl-1(tm2730)* ($n = 52$ hatchlings), *viln-1 (ok2413)* ($n = 43$ hatchlings), *viln-1(ok2413); gsnl-1(tm2730)* ($n = 41$ hatchlings), *pak-1(tm403)* ($n = 47$ hatchlings), *gsnl-1(tm2730); pak-1 (tm403)* ($n = 51$ hatchlings), *viln-1(ok2413); pak-1(tm403)* ($n = 70$ hatchlings), *viln-1(ok2413); gsnl-1(tm2730); pak-1*(RNAi) ($n = 35$), *spc-1*(RNAi) ($n = 27$ hatchlings) and *viln-1(ok2413); gsnl-1(tm2730); spc-1*(RNAi) ($n = 41$ hatchlings). Data represent mean ± s.d. Two side paired *t*-test. $^{*}P < 0.05$; $^{**}P < 0.001$; $^{***}P < 0.0001$; n.s, not significant.

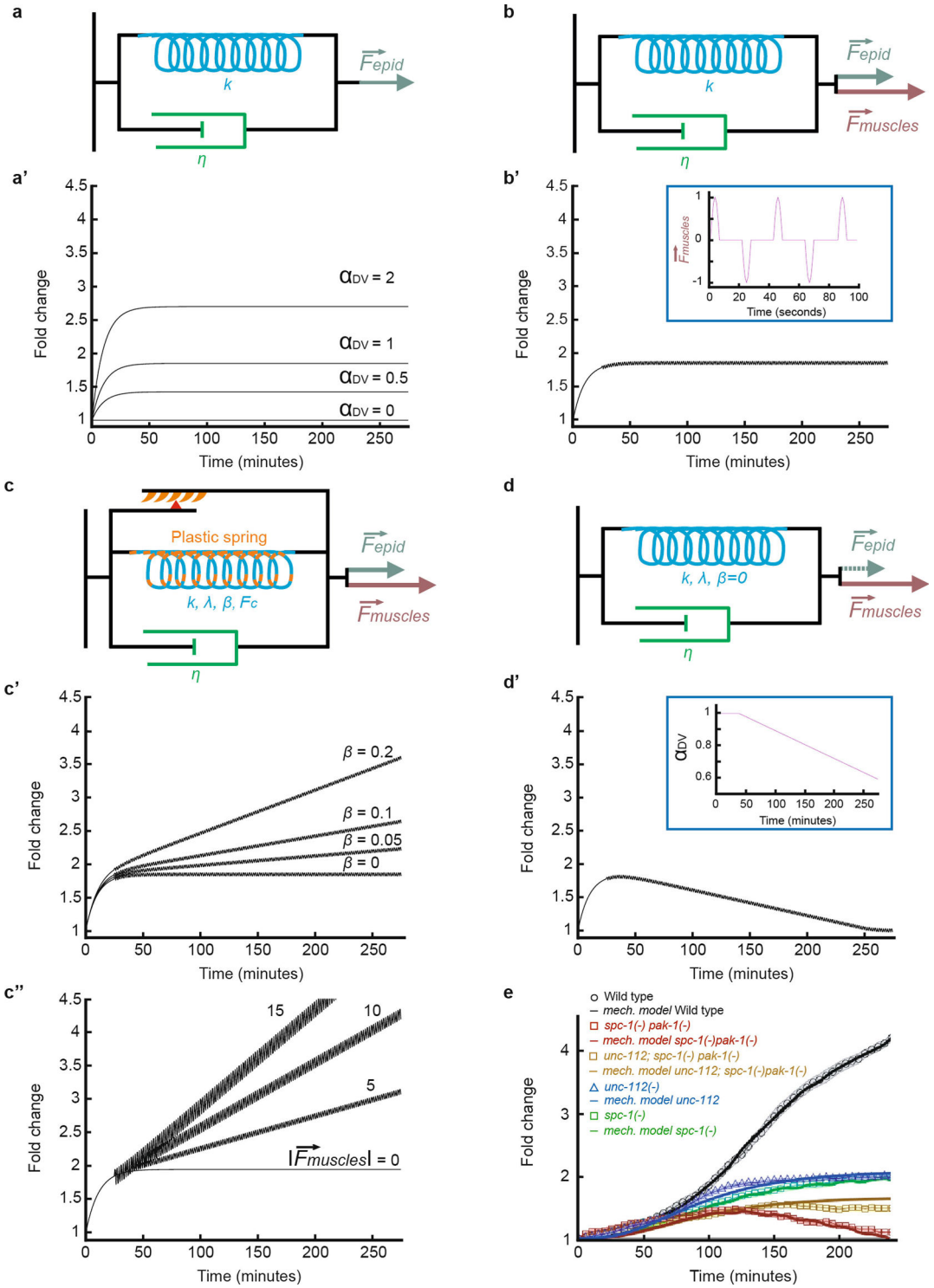

Extended Data Fig. 6 | See next page for caption.

Extended Data Fig. 6 | Time-dependent length of a Kelvin–Voigt model in different conditions. a, A generic Kelvin–Voigt system exposed to a constant force F_{epid}, and its predicted elongation change for $F_{seam} = 0.85$ and four different values of α_{DV} based on the equation $F_{epid} = F_{seam}\,\alpha_{DV}$. **b**, A similar system exposed to two forces, F_{epid} and an oscillating force $\mathbf{F}_{muscles}$, and predicted elongation change using $F_{epid} = 0.85$ and $\mathbf{F}_{muscles}$ with an amplitude equal to 1 and the behaviour depicted in the blue-boxed inset. For simplicity, we will refer to the amplitude of $\mathbf{F}_{muscles}$ as $F_{muscles}$. As the pulsatile force induces both compression and stretching (see Fig. 1c), its net input on elongation is transient and the system oscillates around the maximal value reached without $\mathbf{F}_{muscles}$. In all other panels (except in **a**), $\mathbf{F}_{muscles}$ was set as a periodic function with positive and negative steps of duration 6 s modulated by a cosine function, alternating with periods of null value of duration 15 s (**b**, inset). **c**, A Kelvin–Voigt system with mechanical plasticity introduced according to equations (1), (4), (6) and (7) in the Supplementary Information, and predicted elongation change using $F_{epid} = 0.85$, $F_c = 0$, $F_{muscles} = 3$ and four distinct values of the plasticity factor β, or using $F_{epid} = 0.85$, $F_c = 0$, $\beta = 0.10$ and four distinct values of $F_{muscles}$. **d**, A Kelvin–Voigt system in which the plasticity is defective ($\beta = 0$), and in which there is actin tearing according to equation (7) in the Supplementary Information, inducing a progressive reduction of F_{epid}, and predicted elongation change with an initial value of $F_{epid} = 0.85$, the tearing factor $\gamma = 0.15$ and $F_{muscles} = 3$; the inset outlined in blue shows the behaviour of $\alpha_{DV}(t)$ over time. In **a**–**d**, the elastic constant of the spring is $k = 1$, the initial resting length has the value $\lambda(t = 0) = 1$, and the viscosity is $\eta = 10$. **e**, Result of the fit for the following genotypes: WT, *unc-112(−)* alone *spc-1(−)* alone, *spc-1(−) pak-1(−)* double, *unc-112(−); spc-1(−) pak(−)* according to equations (1), (4), (9) to (11) in the Supplementary Information. The values of the parameters are specified in paragraphs 1.5 and 1.6 in the Supplementary Information. The shallow decrease in length for the curve of *unc-112(−); spc-1(−) pak-1(−)* after 150 min is due to a deformation of the embryos under the effect of *unc-112* knockdown but not to retraction, which is why the fit has been evaluated on the first 150 min of the curve.

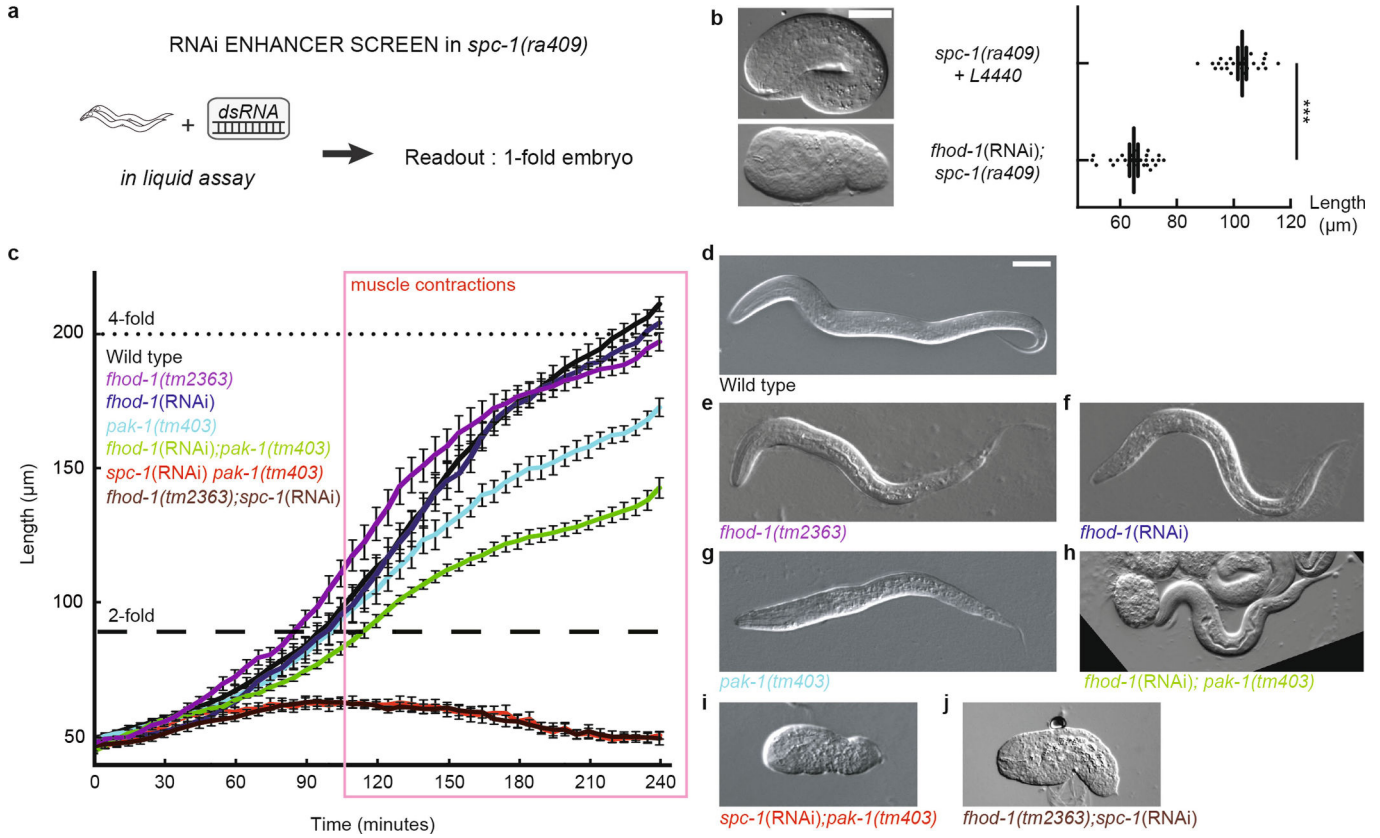

Extended Data Fig. 7 | Comparable retraction phenotypes after the combined loss of SPC-1 and PAK-1 or SPC-1 and FHOD-1. a, Principle of the retraction screen in a *spc-1* mutant that identified *fhod-1*. **b**, DIC image of *spc-1* deficient embryos after feeding on L4440 control ($n = 21$ hatchlings) or *fhod-1*(RNAi) ($n = 25$ hatchlings) bacteria, and quantification of *spc-1(ra409)* L1 hatchling body length after feeding. Data represent mean ± s.d. Two-sided paired *t*-test. **c**–**j**, Elongation curves and (**d**) corresponding DIC images showing the terminal phenotypes at hatching of wild type (**d**; $n = 12$ embryos), *fhod-1(tm2363)* (**e**; $n = 10$ embryos), *fhod-1*(RNAi) (**f**; $n = 10$ embryos), *pak-1(tm403)* (**g**; $n = 11$ embryos), *fhod-1*(RNAi) *pak1(tm403)* (**h**; $n = 10$ embryos), *spc-1*(RNAi) *pak-1(tm403)* (**i**; $n = 8$ embryos) and *fhod-1(tm2363); spc-1*(RNAi) (**j**; $n = 9$ embryos). Data in **c** represent mean ± s.e.m. Scale bar, 25 µm.

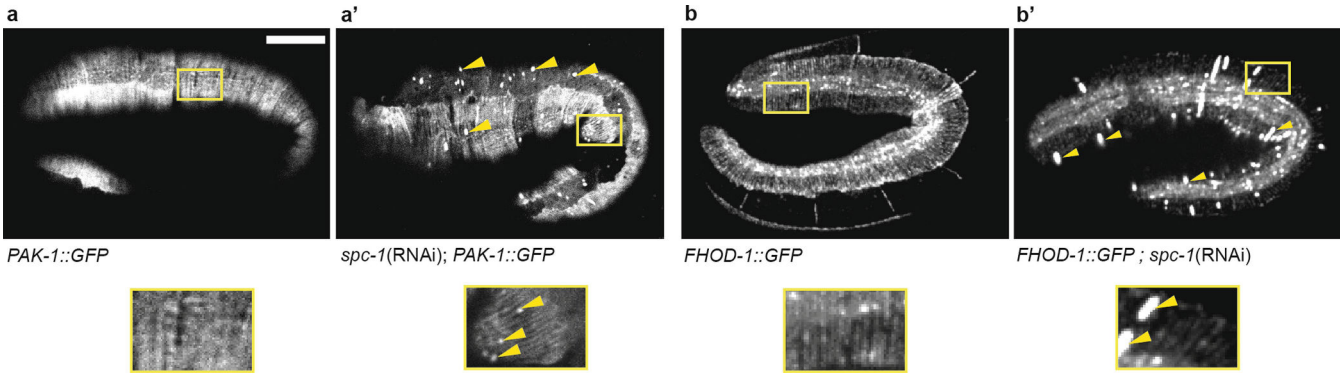

Extended Data Fig. 8 | PAK-1 and FHOD-1 form aggregates in *spc-1*(RNAi) loss of function. a, PAK-1::GFP localization in wild-type and *spc-1*(RNAi) embryos. Yellow box, area enlarged below the panel. Note the punctae in SPC-1 deficient embryos. **b**, FHOD-1 localization in wild-type and *spc-1*(RNAi) embryos. Note the aggregates (arrowheads). Note also that FHOD-1::GFP displayed a filamentous organization reminiscent of actin filaments. Scale bar, 10 μm.

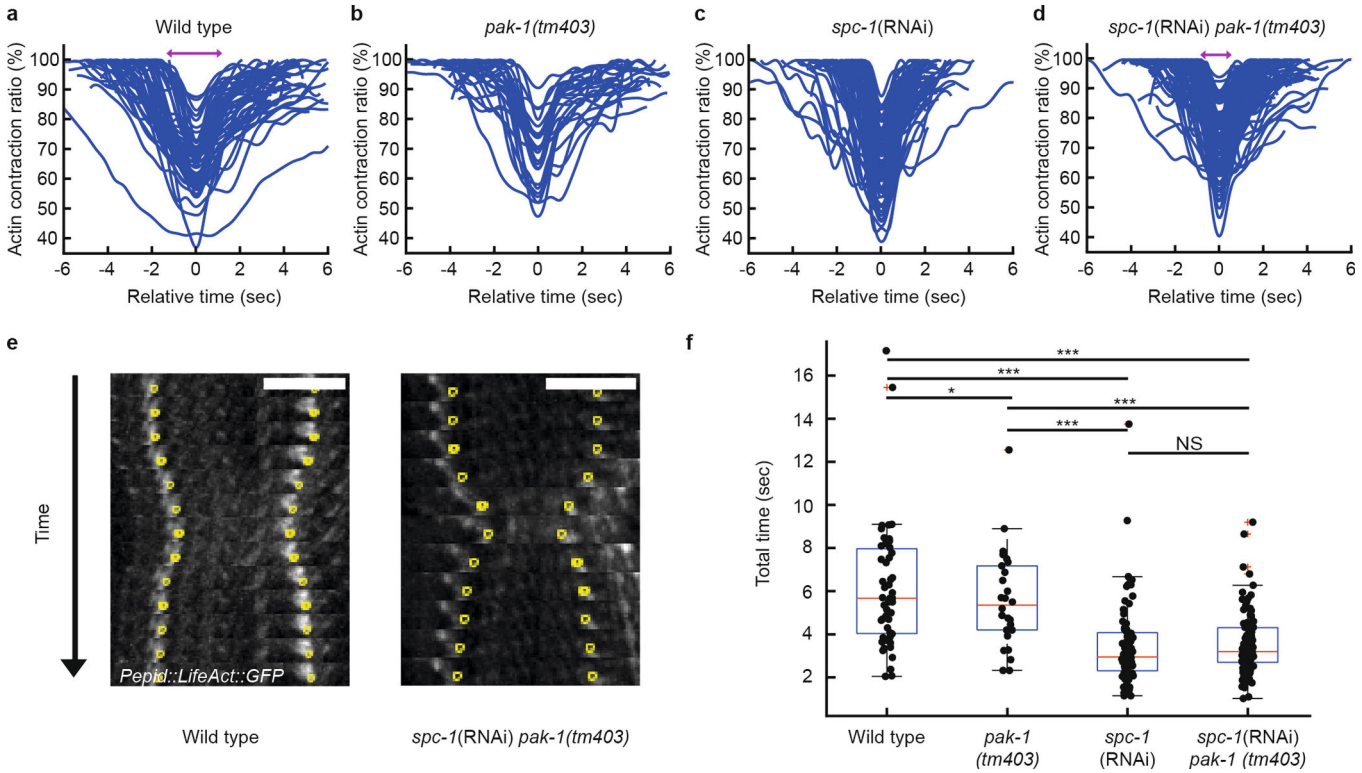

Extended Data Fig. 9 | Actin displacement ratio. a–**d**, Spinning-disc microscopy tracking of actin filaments visualized with a *Pdpy-7::Lifeact::GFP* marker specifically expressed in the epidermis. Individual displacement tracks of wild-type (**a**), *pak-1(tm403)* (**b**), *spc-1*(RNAi) (**c**) and *spc-1*(RNAi) *pak-1(tm403)* (**d**) embryos at a stage equivalent to twofold in a wild-type embryo. Scale bar, 10 μm. **e**, Typical kymographs of the Lifeact::GFP–labelled actin filaments in wild-type and *spc-1*(RNAi) *pak-1(tm403)* embryos from which the tracks in **a**–**d** were derived. Time interval between two images is 0.41 s. Yellow dots correspond to landmarks for quantitative analysis. **f**, Quantification of the displacement duration in (N = number of embryos, n = number of contractions): wild type, $N = 11$, $n = 51$; *pak-1(tm403)*, $N = 11$, $n = 26$; *spc-1*(RNAi), $N = 11$, $n = 73$; *spc-1*(RNAi) *pak-1(tm403)*, $N = 11$, $n = 89$. Data represent median values, 25th and 75th percentiles. The whiskers extend to the most extreme data points not considered outliers. Two-sided paired t-test. $^*P < 0.05$; $^{**}P < 0.001$; $^{***}P < 0.0001$; n.s., not significant.

nature research

Corresponding author(s): Michel Labouesse

Reporting Summary

Nature Research wishes to improve the reproducibility of the work that we publish. This form provides structure for consistency and transparency in reporting. For further information on Nature Research policies, see Authors & Referees and the Editorial Policy Checklist.

Statistical parameters

When statistical analyses are reported, confirm that the following items are present in the relevant location (e.g. figure legend, table legend, main text, or Methods section).

n/a	Confirmed	
☐	☒	The exact sample size (*n*) for each experimental group/condition, given as a discrete number and unit of measurement
☐	☒	An indication of whether measurements were taken from distinct samples or whether the same sample was measured repeatedly
☐	☒	The statistical test(s) used AND whether they are one- or two-sided *Only common tests should be described solely by name; describe more complex techniques in the Methods section.*
☒	☐	A description of all covariates tested
☒	☐	A description of any assumptions or corrections, such as tests of normality and adjustment for multiple comparisons
☐	☒	A full description of the statistics including central tendency (e.g. means) or other basic estimates (e.g. regression coefficient) AND variation (e.g. standard deviation) or associated estimates of uncertainty (e.g. confidence intervals)
☐	☒	For null hypothesis testing, the test statistic (e.g. *F*, *t*, *r*) with confidence intervals, effect sizes, degrees of freedom and *P* value noted *Give P values as exact values whenever suitable.*
☒	☐	For Bayesian analysis, information on the choice of priors and Markov chain Monte Carlo settings
☒	☐	For hierarchical and complex designs, identification of the appropriate level for tests and full reporting of outcomes
☒	☐	Estimates of effect sizes (e.g. Cohen's *d*, Pearson's *r*), indicating how they were calculated
☐	☒	Clearly defined error bars *State explicitly what error bars represent (e.g. SD, SE, CI)*

Our web collection on statistics for biologists may be useful.

Software and code

Policy information about availability of computer code

Data collection	DIC images for time-lapse videos were obtained using a Leica DM6000 microscope 360 with a Leica LAS-AF software and with an inverted DMI 4000 microscope (Leica) equipped with a Coolsnap fx (Photometrix) digital camera controlled by micromanager software. Fluorescent images were acquired with a spinning-disk DM 6000 Leica microscope equipped 371 with an Andor software, a CSUX1-A1 spinning-disk controlled by the Metamorph software and a DeltaVision OMX SR imaging system from GE Healthcare Life Sciences. Reconstruction of TIRF-SIM images were performed with the softWoRx software (Applied Precision, Inc).
Data analysis	All images were analysed using the 405 ImageJ (FiJi) software (NIH, Bethesda, Maryland, USA; http://rsb.info.nih.gov/ij/) and 406 MATLAB R2015b (The MathWorks Inc., Natick, MA).

For manuscripts utilizing custom algorithms or software that are central to the research but not yet described in published literature, software must be made available to editors/reviewers upon request. We strongly encourage code deposition in a community repository (e.g. GitHub). See the Nature Research guidelines for submitting code & software for further information.

Data

Policy information about availability of data

All manuscripts must include a data availability statement. This statement should provide the following information, where applicable:

- Accession codes, unique identifiers, or web links for publicly available datasets
- A list of figures that have associated raw data
- A description of any restrictions on data availability

Supplementary Tables 1-4

Field-specific reporting

Please select the best fit for your research. If you are not sure, read the appropriate sections before making your selection.

☒ Life sciences ☐ Behavioural & social sciences ☐ Ecological, evolutionary & environmental sciences

For a reference copy of the document with all sections, see nature.com/authors/policies/ReportingSummary-flat.pdf

Life sciences study design

All studies must disclose on these points even when the disclosure is negative.

Sample size	Sample size was determined by checking the stability of the standard deviation.
Data exclusions	For Figure 1, we excluded all embryos for which the simultaneous tracking of actin and muscles nuclei was not possible. For Figure 2, we excluded out of focus embryos or blurred embryos due to their fast movements. For Extended data 3, 4, 5, 8 and 9, we excluded all the out of focus embryos. For Extended data 9, we excluded embryos for which we could not track a full cycle of contractions. For others figures, nothing was excluded.
Replication	Data were replicated at least 3 independant times.
Randomization	We did not use randomization.
Blinding	For Supplementary 3 and Supplementary 9, experiments were done in Strasbourg and Paris by two different persons signing the manuscript, reaching the same conclusions.

Reporting for specific materials, systems and methods

Materials & experimental systems

n/a	Involved in the study
☒	☐ Unique biological materials
☒	☐ Antibodies
☒	☐ Eukaryotic cell lines
☒	☐ Palaeontology
☐	☒ Animals and other organisms
☒	☐ Human research participants

Methods

n/a	Involved in the study
☒	☐ ChIP-seq
☒	☐ Flow cytometry
☒	☐ MRI-based neuroimaging

Animals and other organisms

Policy information about studies involving animals; ARRIVE guidelines recommended for reporting animal research

Laboratory animals	C. elegans
Wild animals	None
Field-collected samples	None

nature

SUPPLEMENTARY INFORMATION

https://doi.org/10.1038/s41586-019-1509-4

In the format provided by the authors and unedited.

An actin–based viscoplastic lock ensures progressive body–axis elongation

Alicia Lardennois[1,6], Gabriella Pásti[2,6], Teresa Ferraro[1], Flora Llense[1], Pierre Mahou[3], Julien Pontabry[2,4], David Rodriguez[2], Samantha Kim[2], Shoichiro Ono[5], Emmanuel Beaurepaire[3], Christelle Gally[2] & Michel Labouesse[1,2]*

[1]CNRS UMR7622, Institut de Biologie Paris–Seine (IBPS), Sorbonne Université, Paris, France. [2]IGBMC –CNRS UMR 7104, INSERM U964, Development and Stem Cells Department, Université de Strasbourg, Illkirch, France. [3]INSERM U1182 – CNRS/ UMR7645, Laboratoire d'Optique et Biosciences, Ecole Polytechnique, Paris, France. [4]RS2D, Mundolsheim, France. [5]Departments of Pathology and Cell Biology, Winship Cancer Institute, Emory University School of Medicine, Atlanta, GA, USA. [6]These authors contributed equally: Alicia Lardennois, Gabriella Pásti. *e-mail: michel.labouesse@sorbonne-universite.fr

SUPPLEMENTARY MATERIAL

An actin-based viscoplastic lock ensures progressive body axis elongation

Alicia Lardennois[1]*, Gabriella Pásti[2]*, Teresa Ferraro[1], Flora Llense[1], Pierre Mahou[3], Julien Pontabry[2,4], David Rodriguez[2], Samantha Kim[2], Shoichiro Ono[5], Emmanuel Beaurepaire[3], Christelle Gally[2], Michel Labouesse[1,2] #

CONTENT

1-Supplementary Mechanical Modeling

1.1 Background information. During its morphogenesis, the *C. elegans* embryo undergoes a process of elongation whereby it becomes four times as long as the eggshell long axis (50 µm). Cell proliferation and cell intercalation are absent, therefore the process of axis elongation relies only on the ability of the embryo to extend in the anterior-posterior direction. The outer epithelium (epidermis) plays an essential role in this process.

Changing the status of any physical entity requires the involvement of a force (mechanical or chemical), and the *C. elegans* embryo is no exception to this rule of physics. During the first phase of elongation and until muscles become active, the machinery driving elongation involves an active force in the lateral epidermis (also called seam cells), and a passive force exerted by the dorsal and ventral epidermal cells (called DV cells) adjacent to the seam cells (Fig. 1a). Seam cells have a high concentration of non-muscle myosin II, which has a non-polarized distribution and does not display pulsatile flows[41,42], as observed for instance during *Drosophila* germband elongation[43]. Nevertheless, the stress generated by the seam cells is anisotropic and globally oriented along the DV axis (see cyan box in Fig. 1a)[42]. The stress anisotropy results mainly from the presence of circumferential F-actin filament bundles in DV epidermal cells, which create a global stiffness anisotropy (see yellow box in Fig. 1a). Electron microscopy suggests that these bundles are made of three to five actin filaments[44,45].

The DV epidermal cells do not contribute to generate active stress (Fig. 1a), as their myosin II is kept mostly silent through the activity of the RhoGAP RGA-2[41,42,46]. The interplay between stress anisotropy in seam cells, stiffness anisotropy from the DV epidermis, and hydrostatic pressure resulting from the reduction of embryo diameter, induces a force oriented along the AP direction that is sufficient to extend the embryo until it reaches the 2-fold stage[42]. Note that here as well as in the main text we refer to each elongation phase based on the ratio between the actual embryo length and that of the eggshell long axis (50 µm), i.e. 1.7-fold or 2-fold means that the embryo has reached roughly 85 µm or 100 µm, respectively. Importantly, in mutant embryos which extend slower, we refer to

embryo stages based on the length that a wild-type embryo would reach after the same time duration, with t_0 corresponding to the beginning of elongation (see extension curves in Fig. 2d).

During embryogenesis, muscles organize and assemble in four rows located under the epidermis (Fig. 1a). Muscles are attached to the extracellular matrix that separates them from the epidermis, and that in turn serves to anchor the epidermis through hemidesmosome-like junctions[41]. Muscle organization and maturation is a progressive process, such that muscle activity starts with small contractions at the 1.7-fold, which progressively become more robust. The mechanical activity of muscles can be summarized as an alternation of contractions followed by relaxation. Since muscles are tightly connected to the epidermis, their contractions locally and repeatedly induce an anterior-posterior compression and extension of the epidermis, which can be visualized through the displacement of the actin cables (Fig. 1b-c, Extended Data Fig. 7). The stress exerted by muscle contractions on the epidermis induces a mechanotransduction pathway (2nd yellow box in Fig. 1a), which is essential to promote hemidesmosome maturation and embryo elongation[47]. Of note, when embryos reach the 3.5-fold stage, they start secreting a collagenous cuticle acting as a rigid exoskeleton that limits further muscle-driven elongation.

1.2 Viscoplastic model. For simplicity, let us call the net force in the AP direction produced by the epidermis the epidermal cell force (F_{epid}). This force is not enough to explain the elongation up to the 4-fold stage, since genetic analysis has established that embryos with non-functional muscles do not elongate beyond the 2-fold stage (Fig. 2b)[48]. Therefore, muscles provide a second active force driving elongation beyond the 2-fold stage, which we will call $F_{muscles}$.

The *C. elegans* epidermis can be modelled as a visco-elastic body, more specifically as a Kelvin-Voigt system with a spring and dashpot in parallel, subject to two main active forces: the epidermal force F_{epid}, which is a continous positive force, and the muscle force $F_{muscles}$, which is a pulsatile force since muscles alternatively contract and relax. The first force is present since the beginning of elongation, whereas the second force starts only after the 1.7-fold stage. The elastic reaction of the epidermis to active forces can be captured by Hooke's law; the damped nature of the reaction can be expressed by a viscous term. Overall the length of the embryo over time $l(t)$ can be captured by the equation:

$$\eta \frac{dl}{dt} = -k\,(l-\lambda) + F_{epid} + F_{muscles} \qquad (1)$$

where k is the body stiffness, λ is the worm resting length and η is the coefficient of viscosity. Inertia has been neglected given the low Reynolds number of the system. Eq. (1) corresponds to the so-called Kelvin-Voigt viscoelastic model[49,50] that captures the behavior of viscoelastic solids under stress or deformation. For constant forces, the solution of Eq. (1) is given by:

$$l(t) = \frac{F_{epid} + F_{muscles}}{k}\,(1 - e^{-t/\tau}) + \lambda \qquad (2)$$

meaning that the length of the system relaxes to the plateau value $\frac{F_{epid} + F_{muscles}}{k} + \lambda$ in a relaxation time of $\tau = \eta/k$.

F_{epid} can promote elongation until the 2-fold stage (Extended Data Fig. 6a'). Beyond, the pulsatile force originating from muscles, $F_{muscles}$, alternates periods of positive, negative or null contribution, so that its temporal average $< F_{muscles} >_\theta$ is null:

$$< F_{muscles} >_\theta = \frac{1}{\theta}\int_0^\theta F_{muscles}(t)\ dt = 0, \text{for } \theta = nT \qquad (3)$$

where θ is the integration period, T is the period and n is a positive integer. As a consequence, on average, $F_{muscles}$ will not contribute to the steady state length (l_{ss}) of the embryo (see Extended Data Fig. 6a-a') that is set by $l_{ss} = \frac{F_{epid}}{k} + \lambda$.

A way to introduce a positive contribution to embryo lengthening is to allow some plasticity, in the physical sense, or ability of the system to get reorganized. For example, let consider a stretching pulse due to muscle activity during which the embryo increases its length *l(t)* with an increment *dl*, such that the embryo will be temporarily *l(t)+dl* long at the end of the pulse. During the subsequent relaxation phase, due to elasticity in the system, the embryo should return to the initial length *l(t)* it had before muscles had locally extended it. However, if it undergoes a permanent plastic deformation, then the body will permanently keep a portion of the stretched length. This situation corresponds to a permanent rearrangement, and it has been observed and modeled in biological systems undergoing stresses[51,52]. In biological terms we imagine the rearrangement process as follows: during the compression phases, muscle contractions locally squeeze the embryo along the AP axis, which generates an increased circumferential stress due to volume conservation. In particular, circumferential actin cables become bent, which certainly introduces a state of increased stress along their length. As argued in the main text, our new results (Figs 2 and 3), together with published results on the effect of actin filament bending[53], suggest that the compression phases will induce actin filament severing. Thus, muscle contractions create the conditions for actin filament remodeling in the subsequent relaxation and stretching phases toward filament shortening, hence they create the conditions for plasticity.

Similarly to[52], a simple mathematical solution to introduce plasticity consists in having an adjustable resting length λ. We impose that $\lambda(t)$ evolves with the same law as the length *l(t)* according to:

$$\frac{d\lambda}{dt} = \beta\ \frac{dl}{dt}\mathrm{H}(\alpha_{DV}) \quad \text{if } \frac{dl}{dt} > 0 \text{ and } l - \lambda > F_c/k \qquad (4)$$

where $0 \leq \beta < 1$ is a proportionality factor called 'plasticity factor'; the case of $\beta = 0$ corresponds to an absence of plasticity. The condition $\frac{dl}{dt} > 0$ ensures that there is rearrangement only during the extension phases; the condition $l - \lambda > F_c/k$ means that the rearrangement takes place only if the applied force exceeds a critical force F_c. The term $\mathrm{H}(\alpha_{DV})$ is the Haeviside step function, which expresses that dorso-ventral

rearrangement is possible only in presence of resistance. For the description of the α_{DV} term, see next paragraph. Given the form of Eq. 4, the resting length will not increase indefinitely for an applied constant positive force since it is proportional to the derivative of l, which evolves as a spring. This equation also implies that the ability to remodel to an applied force is finite, which is the case for natural systems. Indeed Eq. (4) is equivalent to $\lambda = \lambda(0)\,(1-\beta) + \beta\, l$ assuming that $\lambda(0)$ is the length and the resting length at time 0 , $F_c = 0$ and $\alpha_{DV} > 0$. With these choices and with a constant positive force *F*, Eq. (1) has the following solution:

$$l(t) = \frac{1}{(1-\beta)}\frac{F}{k}\left(1 - e^{-t(1-\beta)/\tau}\right) + \lambda(0) \qquad (5)$$

Hence, the plasticity condition effectively reduces the body stiffness k to $k(1-\beta)$ enabling the system to reach a longer final size compared to the one allowed by the Kelvin-Voigt system alone, and increasing the relaxation time. By introducing a plasticity factor like in Eq. (4), the body progressively gains length at each stretching phase (Fig S5d-d'). Indeed, the length $l(t)$ is an increasing function of the plasticity factor β (Extended Data Fig. 6c').

We are aware that the general form of Eq. 4 is one of some other possibilities to capture the phenomenology of the process. It potentially implies an important plasticity response for very fast-applied deformations and an almost elastic behavior for very slowly applied deformation. We did not explore a large range of deformation speeds in our system since it was in the ~1 μm/s range for all of the mutants we examined (Extended Figure 9). Thus deformation speed does not discriminate any mutant.

There are other options to express the equation giving the deformation of a Kelvin-Voigt material under stress than our choice for Eq. 4. Indeed, according to the classical formulation of plasticity reported in our ref. 24 (Munoz and Albo, PRE 88, 012708)}, the resting length could evolve proportionally to the deformation according to:

$$\frac{d\lambda}{dt} = \beta\,(l-\lambda)\mathrm{H}(\alpha_{DV}) \quad \text{if } \frac{dl}{dt} > 0 \text{ and } l - \lambda > {F_c}/{k} \qquad (4\text{ bis})$$

For F_c bigger than a limit value and for large values of $F_{muscles}$, this equation accounts for elongation and positive dependency on $F_{muscles}$; for example by posing $F_c \geq 1$ $F_{muscles} > 10$ with all parameters set to $\eta = 10$, $k = 1$, $Fepid = 0.85$, and $l(0) = \lambda(0) = 1$. On the other hand, for smaller values of F_c and β, elongation takes place also in absence of $F_{muscles}$. which is contradictory with the experimental data. Therefore, we decided to privilege the Eq. 4 for plasticity (see above), since its qualitative behavior recapitulates the experimental phenomenology in a parameter independent manner. We discuss the linear version of Eq. 4bis in section 1.8.

1.3 The consequences of actin stability defects. As reminded above, the intensity of F_{epid} relies on two components: the constant contractility of the seam cell actomyosin network, and the stiffness of the actin cables in DV cells. We can then represent it like:

$$F_{epid} = F_{seam}\ \alpha_{DV} \quad (6)$$

where the force F_{seam} represents the active force generated by myosin II in the lateral cells and α_{DV} is the passive component given by the presence of actin filament bundles in the DV cells. The biomechanical significance of equation (6) is that both F_{seam} and α_{DV} positively contribute to F_{epid}, and that if one is absent $F_{epid}=0$. This captures the fact that in the absence of myosin II there will be no pulling force because the active component is absent, and that if actin cables are lost myosin II is missing the resistance structure onto which it can pull, resulting in a null epidermis AP force. From Eq. 2 the size of $\frac{F_{seam}\ \alpha_{DV}}{k}$ sets the maximal elongation that the embryo can achieve in the absence of muscle activity (Extended Data Fig. 6a-a').

As shown in the main text (Fig. 3), the absence of SPC-1 and PAK-1, combined with the mechanical input from muscles, induces actin integrity defects in DV cells. To translate this situation in mathematical terms, we chose to write the passive component α_{DV} as follows:

$$\frac{d\alpha_{DV}}{dt} = \gamma\ \frac{dl}{dt} \quad if\ \ \frac{dl}{dt} < 0\ and\ \alpha_{DV} \geq 0 \quad (7)$$

where $\gamma \geq 0$ is a proportionality factor defined as a 'tearing factor'. The condition $\frac{dl(t)}{dt} < 0$ implies that α_{DV} decreases at each cycle of muscle activity (a cycle is a sequence of positive and negative net force). In addition, we are imposing that $\gamma=0$ corresponds to an absence of tearing, as in wild-type embryos. The biological significance of this choice is the following (see section 1.2 for further details). When muscles contract and locally squeeze the embryo along the A/P axis (Extended Data Fig. 4, Video 1), they bend actin filaments (Fig. 3) and produce an increased circumferential stress. As a consequence, their integrity in response to the stress originating from muscle activity is not maintained in *spc-1 pak-1* double mutants (see Fig. 3). For this reason, α_{DV} should progressively decrease at each cycle. The condition $\alpha_{DV} \geq 0$ prevents α_{DV} from assuming negative values. Thus with α_{DV} decreasing, F_{epid} will progressively decrease, and as consequence the system length will shorten (see Extended Data Fig. 5e and Fig. 4e).

1.4 Equations summary. In summary, we describe the embryo body as a plastic Kelvin-Voigt solid according to the following system of equations:

- <u>Kelvin-Voigt with adjusting resting length subject to $F_{epid}+F_{muscles}$</u>

$$\eta\ \frac{dl}{dt} = -k\ (l-\lambda) + F_{epid} + F_{muscles} \quad (1)$$

- <u>Plasticity condition</u>

$$\frac{d\lambda}{dt} = \beta\ \frac{dl}{dt}\ \mathrm{H}(\alpha_{DV}) \quad \text{if } \frac{dl}{dt} > 0\ ,\ 0 \leq \beta < 1 \text{ and } l-\lambda > {}^{F_c}/_{k} \quad (4)$$

- <u>Tearing condition</u>

$$\frac{d\alpha_{DV}}{dt} = \gamma\ \frac{dl}{dt} \quad if\ \ \frac{dl}{dt} < 0\ and\ \alpha_{DV} \geq 0 \quad (7)$$

- <u>Equation of epidermal force</u>

$F_{epid} = F_{seam}\ \alpha_{DV}$ as described in Eq. (6).

We assume that γ=*0* for wild-type, meaning that the resistance of dorso-ventral actin filament bundles remains unaffected by the body length changes caused by muscle activity, and that γ=*0* for *unc-112* defective embryos, which are muscle-defective.

The equations (1), (4), (5), (6) and (7) have seven parameters: η, *k*, F_{seam}, $\alpha_{DV}(0)$, $F_{muscles}$, β and γ. In order to reduce the parameter space we fixed some of them:

- for simplicity we set **k=1**;
- from the laser ablation experiments performed in reference[42], the relaxation time of epidermal actin filaments following the laser cut is in the order of a few seconds. Being the relaxation time in a Kelvin-Voigt system given by $\tau = \eta/k$, we set $\boldsymbol{\eta}$**=3** so that the relaxation time is 3 seconds.
- F_{epid} is the multiplication of two parameters, and thus from the parameter point of view can be considered as a single parameter that we formally set to $\boldsymbol{F_{seam}}$**=1** letting $\alpha_{DV}(0)$ as a free parameter.
- The size of the critical force F_c has been chosen to be half F_{seam} ($\boldsymbol{F_c = 0.5}$). Thereby, we consider that low intensity forces cannot trigger a plastic response.
- Regarding $F_{muscles}$, we specified its details on the basis of the measured contraction durations for embryos between 1.7 and 2-fold stages (Extended Data Fig. 7). For wild-type embryos, the duration of positive and negative periods has been set to 6 seconds and the period of null contribution has been set to 15 seconds, whereas for *spc-1* mutants and *spc-1 pak-1* double mutants the duration of non-null activity has been set to 3 seconds and the duration of null contribution is set to 15 seconds. In wild-type embryos, the intensity of $F_{muscles}$ has been left as a fit parameter together with α_{DV}, β and γ in order to be determined by comparing with the data. The muscle force amplitude for *spc-1* and *spc-1 pak-1* mutants has been set to **50% of the *wt* intensity** according to our experimental observations. In our model, the length of the embryo is an increasing function of the intensity of the muscle force $F_{muscles}$, (Extended Data Fig. 6c'').

To better adapt to the experimental observations, both F_{seam} and $F_{muscles}$ have been modified by introducing an initial transient that sets their behavior from zero to the regime of maximal intensity; the detailed form of these transients are reported in the paragraph 'Refining model details'.

1.5 Fitting procedure. In order to determine the remaining four free parameters: intensity of $F_{muscles}$, $\alpha_{DV}(0)$ (the initial value of actin strength), β (the plasticity factor) and γ (the tearing factor) we fitted different genotypes. We started with muscle-defective *unc-112* and wild-type embryos. As shown in Figs. 2 and S3, their elongation rate is quite similar until the 2-fold stage, at which point *unc-112* embryos have no muscle force ($F_{muscles}$=0), and they both have an identical actin pattern (γ=*0*). Therefore, we fitted together the two elongation curves to find the values of the three parameters $\alpha_{DV}(0)$, β and $F_{muscles}$ that capture the main features of the two genotypes; we then refined the minor differences by allowing a 20% tolerance with respect to the parameters values determined through the common fit. To estimate the value of $F_{muscles}$ intensity in *spc-1* and *spc-1 pak-1*

embryos, we considered that it was half the wild-type value, based on the observation that the muscle contraction/relaxation cycles were roughly twice shorter in these embryos (Extended Data Fig. 7). The notion that $F_{muscles}$ is lower in *spc-1* mutant embryos is consistent with the observation that muscles make an angle of 20° with the anterior-posterior axis, instead of 6° in wild-type embryos, predicting that their input should be reduced[54]. The wild-type value of the plasticity factor was used as the upper limit for the variability range of β for *spc-1* and *spc-1 pak-1* embryos. We then proceeded by fitting the *spc-1* and *spc-1 pak-1* elongation curves to determine the values of $\alpha_{DV}(0), \beta$ and the tearing factor γ (see below for the method).

The best fit parameters were determined by minimalizing the following cost function:

$$\xi = \sum_g \sum_i [(curve_{data}(i) - curve_{model}(i))^2]_g \qquad (8)$$

where $curve_{data}(i)$ is the value of the data elongation curve at the time point i and $curve_{model}(i)$ is the solution of the model interpolated at the time point *i*; *g* refers to the genotypes considered for a fit. To minimize the cost function, a Covariance Matrix Adaptation Evolution Strategy (CMA-ES) algorithm was used[55]. The algorithm has an available MATLAB code at http://www.lri.fr/~hansen/cmaes_inMATLAB.html.

In the Supplementary Table 7, we report the values of the fitted parameters for the different genotypes presented in the Fig. 1d and Extended Data Fig. 6e. Errors have been obtained by fitting the mean curves plus and minus their standard errors respectively and by taking the maximal deviation from the parameters obtained from the mean.

1.6 Refining model details. Ablation experiments in seam cells[42] have shown that the circumferential stress is not constant during development but increases from the 1.3-fold to 1.7-fold stages. To better adapt our model to this observation, we introduced a time dependent function for F_{epid} that saturates to a plateau value within a time τ_s :

$$F_{epid}(t) = F_{seam}\ \alpha_{DV}\ (1 - \exp\left(-\frac{t}{\tau_s}\right))^{h_s} \qquad (9)$$

where h_s is an exponent that sets the steepness of the function in reaching the plateau and $F_{seam}\ \alpha_{DV}$ is the plateau value. We set τ_s=*50* min and h_s=*4*, since this choice produces slow elongation for the first 50 minutes, as was observed for all the genotypes (see Fig. 2). Much like the epidermis force, the muscle force $F_{muscles}$ also starts at a small amplitude, then progressively evolves with a behavior similar to equation (8):

$$F_{muscles}(t) = \begin{cases} A \quad \Theta(t)\left(1 - \exp\left(-\frac{(t-t_{init})}{\tau_m}\right)\right)^{h_m} & for\ t > t_0 \\ 0 \qquad otherwise \end{cases} \qquad (10)$$

where A is the maximum amplitude, *Θ(t)* is the periodic function made of a composition of cosines described in Extended Data Fig. 5c; h_m sets the steepness of the function to reach the plateau; t_0 is the time at which muscles get active and τ_m is the time necessary for the function to reach its plateau.

We started to measure the elongation curves immediately before the comma stage, which represents our initial time. We set t_{init}=*90 min*, since around this point of elongation wild type embryos are 1.7-fold long and they start to contract muscles; we also assume that after the 2-fold stage the muscle force has reached its maximum amplitude, which is why we fixed τ_m=*15 min* (the time necessary for a wild type embryo to go from 1.7 to 2 fold; h_m has been arbitrarely set to 1).

The model summarized in Eqs. (5) and (9) has no plateau; however *C. elegans* embryos extend up to 4-fold whithin ≤150 minutes, then stay at this length for ~100 additional minutes before hatching. We do not know why the body length stops at 4-fold and this issue is not the focus of this work. We can speculate that the ability of the body to remodel is not illimited and may also be restricted by cuticle secretion. In this framework, we can modify Eq.(5) by introducing a multiplicative term under the form of a Hill function to account for the saturation of the elongation:

$$\frac{d\lambda}{dt} = \beta \frac{dl}{dt} \mathrm{H}(\alpha_{DV}) Hill(\lambda) \quad \text{if } \frac{dl}{dt} > 0\,,\ 0 \le \beta < 1 \text{ and } l - \lambda > {}^{F_c}/_{k} \qquad (11)$$

where $Hill(\lambda) = \frac{L^d}{L^d + \lambda^d}$, with *L* upper threshold for the resting length and *d* an exponent[56]**.** We set **L=3.2** and **d=15** to account for a rapid saturation of elongation after the 3.2-fold stage, since the wild type embryos show, after this length, a rapid reduction of the elongation rate. By introducing these aditional functions, we can improve the agrement between the data and the model results (Fig. 4j). The Equations presented above have been solved numerically by the Euler method implemented in a MATLAB script, with the choice of intitial length $l(0) = \lambda(0) = 1$.

The Supplementary Table 8 is a summary of the parameter values that we fixed on the basis of experimental observations and therefore were not used as free parameters.

1.7 Predictive value of the model. The aim of the model is to give a mesoscopic physical description and interpretation of embryo elongation, rather than a detailed mechanistic formulation. Nevertheless its predictions are strongly connected with some experimental findings.

Fitting the parameters as described in section 1.5 predicts a value close to zero for the plasticity factor of *spc-1 pak-1* mutants associated with a tearing factor different from zero (see Table 1). It means that *spc-1 pak-1* mutants are unable to remodel their cytoskeleton to reduce the circumferential size of the actin filaments in the dorso-ventral epidermal cells. Consistent with this view, Extended Data Fig. 4 shows that the circumferential size of *spc-1 pak-1* defective embryos actually increases once muscles become active, showing that the actin filaments did not shorten. The model also predicts a very small plasticity factor but with a low tearing factor for single *spc-1* mutants. These mutants can slightly decrease their circumference (Extended Data Fig. 4), meaning that their actin filaments have a small ability to remodel. Finally, we note that equations (1) and (7) predict that there should be no retraction if $F_{muscles}$ equals zero, which is what we observed for *spc-1 pak-1* embryos in which muscle activity is compromised by knocking-

down *unc-112* (Fig. 1). In those embryos, fitting the *unc-112*; *spc-1 pak-1* elongation curve gives a value of $\alpha_{DV} = 0.66 \pm 0.01$, which is very similar to that predicted for *spc-1 pak-1* double mutants.

1.8 Kelvin-Voigt-type model versus other models. In the present work we decided to model the *C. elegans* embryo as a viscoelastic solid with the ability to rearrange its resting length during elongation, and using this model we show that changing the behavior of the epidermal force can account both for elongation and retraction. The Maxwell model[50], as a dashpot and a spring in series, would also account for elongation when the system is under a positive force. The solution for the length $l(t)$ would be of the form[52]: $l(t) = l_0(1 + \frac{F}{k}\left(1 + \frac{tk}{\eta}\right))$, with l_0 initial length, F a constant force, k the elastic constant of the spring and η the viscosity of the dashpot. A Maxwell-type material would keep extending over time as soon as a positive force acts on it; such a behavior would not account for the elongation arrest of muscle-defective embryos. We have also considered an alternative model suggested in refs [51,52], in which the rate of change of resting length is proportional to the difference between the length and the resting length. The dynamic system would obey the following equations:

$$\eta \frac{dl}{dt} = -k\,(l - \lambda) + F \qquad (12)\text{ (same type as our Eq. 1)}$$

$$\frac{d\lambda}{dt} = \beta\,(l - \lambda) \qquad (13)\text{ (instead of our Eq. 4)}$$

where F is a positive constant and $l(0) = \lambda(0) = l_0$. The solution of this system has the following form:

$$l(t) = l_0 + \frac{F((\,k\,(1-\exp[-\left(\beta+\frac{k}{\eta}\right)t])+t(\beta^2\eta+\beta k))}{(\beta\eta+k)^2} \qquad (14)$$

$$\lambda(t) = l_0 + \frac{F(\beta\eta(\,\exp\left[-\left(\beta-\frac{k}{\eta}\right)t\right]-1)+t(\beta^2\eta+\beta k))}{(\beta\eta+k)^2} \qquad (15)$$

When time t tends to ∞, the forms of equations (14) and (15) imply a linear increase for both $l(t)$and $\lambda(t)$. Again, this behavior cannot account for the muscle-defective arrest of elongation, unless $\beta = 0$.

2-Supplementary references

41 Vuong-Brender, T. T., Yang, X. & Labouesse, M. C. elegans Embryonic Morphogenesis. *Curr Top Dev Biol* **116**, 597-616, doi:10.1016/bs.ctdb.2015.11.012 (2016).

42 Vuong-Brender, T. T., Ben Amar, M., Pontabry, J. & Labouesse, M. The interplay of stiffness and force anisotropies drive embryo elongation. *Elife* **6**, doi:10.7554/eLife.23866 (2017).

43 Rauzi, M., Lenne, P. F. & Lecuit, T. Planar polarized actomyosin contractile flows control epithelial junction remodelling. *Nature* **468**, 1110-1114, doi:nature09566 [pii] 10.1038/nature09566 (2010).
44 Costa, M., Draper, B. W. & Priess, J. R. The role of actin filaments in patterning the Caenorhabditis elegans cuticle. *Dev Biol* **184**, 373-384, doi:10.1006/dbio.1997.8530 (1997).
45 Priess, J. R. & Hirsh, D. I. *Caenorhabditis elegans* morphogenesis: the role of the cytoskeleton in elongation of the embryo. *Dev Biol* **117**, 156-173 (1986).
46 Diogon, M. *et al.* The RhoGAP RGA-2 and LET-502/ROCK achieve a balance of actomyosin-dependent forces in C. elegans epidermis to control morphogenesis. *Development* **134**, 2469-2479, doi:dev.005074 [pii] 10.1242/dev.005074 (2007).
47 Zhang, H. *et al.* A tension-induced mechanotransduction pathway promotes epithelial morphogenesis. *Nature* **471**, 99–103, doi:10.1038/nature09765 (2011).
48 Williams, B. D. & Waterston, R. H. Genes critical for muscle development and function in *Caenorhabditis elegans* identified through lethal mutations. *J Cell Biol* **124**, 475-490. (1994).
49 Vincent, J. in *Structural Biomaterials: Third Edition* 1-28 (Princeton University Press, 2012).
50 Meyers, M. A. & Chawla, K. K. *Mechanical Behavior of Materials*. (Cambridge University Press, 2008).
51 Doubrovinski, K., Swan, M., Polyakov, O. & Wieschaus, E. F. Measurement of cortical elasticity in Drosophila melanogaster embryos using ferrofluids. *Proc Natl Acad Sci U S A* **114**, 1051-1056, doi:10.1073/pnas.1616659114 (2017).
52 Munoz, J. J. & Albo, S. Physiology-based model of cell viscoelasticity. *Phys Rev E Stat Nonlin Soft Matter Phys* **88**, 012708, doi:10.1103/PhysRevE.88.012708 (2013).
53 McCullough, B. R. *et al.* Cofilin-linked changes in actin filament flexibility promote severing. *Biophys J* **101**, 151-159, doi:10.1016/j.bpj.2011.05.049 (2011).
54 Norman, K. R. & Moerman, D. G. Alpha spectrin is essential for morphogenesis and body wall muscle formation in Caenorhabditis elegans. *The Journal of cell biology* **157**, 665-677, doi:10.1083/jcb.200111051 (2002).
55 Hansen, N. & Ostermeier, A. Completely derandomized self-adaptation in evolution strategies. *Evol Comput* **9**, 159-195, doi:10.1162/106365601750190398 (2001).
56 Alon, U. (Chapman & Hall/CRC, Boca Raton, 2007).

Supplementary Table 1 | Enhancer RNAi screen in a *pak-1(-)* mutant RNAi screen was performed in the pak-1(tm403) mutant along with a wild type control, testing a collection of 356 essential genes from the Ahringer RNAi library. The table recapitulates all the genes tested and the score of their interactions for the strongest.

A	Reproducible 50-100% enhanced defect* compared to wild-type
B	Reproducible 20-50% enhanced defect* compared to wild-type
C	Reproducible 5-20% enhanced defect* compared to wild-type

* Defect refers to lethality and body morphology defects

Targeted gene	Function	Strength of interaction
(III) ani-1	Anilin	A
(IV) cap-1	F-actin capping protein α subunit	A
(II) cap-2	β subunit of actin capping protein	A
(V) cdc-25.2	Putative homolog of Cdc25 phosphatase	A
(II) cdc-42	RHO GTPase	A
(III) dlc-1	Dynein light chain	A
(IV) epi-1	Laminin α chain	A
(I) hmp-2	β-catenin	A
(IV) lam-1	Laminin β	A
(I) let-502	Rho-binding Ser/Thr kinase	A
(III) mlc-5	Myosin II essential light chain ortholog	A
(I) pfn-1	Profilin	A
(V) sma-1	βH-spectrin	A
(X) spc-1	α-spectrin	A
(I) sur-6	Regulatory subunit of serine/threonine protein phosphatase 2A	A
(X) tni-1	Troponin	A
(II) dsh-2	Dishevelled (Dsh) homolog	B
(I) goa-1	Ortholog of the heterotrimeric G protein α subunit Go	B
(I) hmr-1	Cadherin	B
(I) kin-10	Putative regulatory (β) subunit of casein kinase II	B
(V) mom-2	Member of the Wnt family	B
(II) mpk-2	Mitogen activated protein (MAP) kinase	B
(I) pfd-3	Putative prefoldin, orthologous to human VBP1	B
(II) aakg-5	AMP kinase	C
(V) arx-2	Subunit of the actin related protein of the conserved Arp2/3 complex	C
(III) arx-3	Subunit of the actin related protein of the conserved Arp2/3 complex	C
(I) bub-1	Serine/threonine kinase	C
(V) chk-1	CHK1-like serine threonin protein kinase	C
(I) chp-1	Protein containing two CHORD domains	C
(I) csnk-1	Ortholog of human CSNK1G3, CSNK1G1 and CSNK1G2	C
(II) ect-2	Putative RHO guanine nucleotide exchange factor (RhoGEF)	C
(I) ekl-1	Ortholog of members of the human TDRD	C
(IV) fln-1	Filamin	C
(X) ifa-3	Intermediate filament protein	C
(III) klp-19	Plus-end-directed microtubule motor protein	C
(III) lit-1	Serine threonine protein kinase	C
(I) mei-2	Novel protein containing a region similar to the p80-targeting subunit of katanin	C
(V) mrck-1	Serine/threonine-protein kinase	C
(III) par-2	Protein containing a C3HC4-type RING-finger	C
(III) pfd-5	Putative prefoldin 5 subunit	C
(I) sys-1	Novel protein that contains three divergent armadillo repeats	C
(II) spv-1	Ortholog of human GMIP	C
(I) tbcd-1	Puatative β-tubulin folding cofactor D	C
(I) usp-5	Ortholog of human USP5 and USP13	C
(II) Y19D2B.1	Structural constituent of cytoskeleton	C

Supplementary Table 1 | Enhancer RNAi screen in a *pak-1(-)* mutant

No enhanced defect* compared to wild-type

* Defect refers to lethality and body morphology defects

(I) afd-1	*(II) aak-1*	*(III) abce-1*	*(IV) arp-11*	*(V) air-1*	*(X) aakb-1*
arx-7	*arp-1*	*abi-1*	*ced-5*	*cct-7*	*aakg-2*
aspm-1	*C27H5.4*	*arf-1.2*	*dli-1*	*F14H3.12*	*abl-1*
chs-1	*cacn-1*	*cct-5*	*dnc-1*	*gck-2*	*dyn-1*
col-53	*cal-2*	*cct-6*	*dyci-1*	*knl-3*	*efn-3*
cpn-1	*ccm-3*	*cls-1*	*eps-8*	*mig-6*	*F20B6.1*
cutl-13	*cct-1*	*cls-2*	*frk-1*	*noca-1*	*frm-9*
dhc-1	*cct-2*	*col-94*	*gex-2*	*pak-2*	*hpk-1*
dlc-6	*cct-4*	*col-97*	*gex-3*	*par-1*	*ifa-2*
eak-6	*cdc-25.4*	*cra-1*	*klp-10*	*rbx-1*	*kin-29*
egg-5	*cpn-2*	*cyk-4*	*klp-11*	*spas-1*	*lam-2*
egg-6	*dep-1*	*daf-4*	*klp-5*	*sun-1*	*lin-18*
ekl-4	*ebp-2*	*fem-2*	*let-60*	*syx-5*	*lpr-3*
erm-1	*eff-1*	*frm-2*	*let-92*	*unc-112*	*nck-1*
fhod-1	*egg-3*	*gei-4*	*M116.5*	*unc-70*	*pak-1*
gei-17	*evl-20*	*gop-3*	*nsp-1*		*pfn-2*
gfi-2	*F59A6.5*	*ina-1*	*par-5*		*pfn-3*
gsa-1	*frm-5.2*	*inft-1*	*pfd-1*		*pqn-34*
gsk-3	*glb-12*	*kin-18*	*pld-1*		*unc-97*
gsp-3	*gpb-1*	*klp-6*	*pmk-2*		
gsp-4	*klp-1 / unc-104*	*klp-7*	*pmk-3*		
kca-1	*klp-17*	*let-805*	*ptp-4*		
lim-9	*let-268*	*mpk-1*	*rac-1 / ced-10*		
mel-26	*lrr-1*	*mtm-3*	*rack-1*		
mfap-1	*max-2*	*nfm-1*	*unc-33*		
mom-5	*mel-11*	*pef-1*	*wsp-1*		
nab-1	*mig-5*	*plk-1*	*zen-4*		
ned-8	*mlt-8*	*pph-6*			
nkb-1	*nsy-1*	*ptp-1*			
nmy-2	*pfd-2*	*pxl-1*			
npp-4	*pink-1*	*rfl-1*			
ocrl-1	*pir-1*	*tbb-2*			
pes-7	*ptc-3*	*ten-1*			
pfd-6	*ptp-2*	*tlk-1*			
ppk-1	*ptp-3*	*trd-1*			
rga-2	*saps-1*	*unc-116*			
rsa-1	*scpl-2*	*wrm-1*			
smgl-1	*sds-22*				
spd-1	*spdl-1*				
tba-2	*tac-1*				
ttx-7	*tba-4*				
unc-35	*unc-52*				
unc-59	*vab-19*				
unc-73	*vab-9*				
unc-94	*vhp-1*				
vab-10	*vps-11*				
viln-1	*vps-32*				
vps-20	*W0761.1*				
wve-1	*zyg-9*				

Supplementary Table 2 | Primary and secondary Y2H screens Yeast two-hybrid screening performed by Hybrygenics Services (Paris, France) using the N-terminus of PAK-1 up to the kinase domain as a bait (Primary Screen), or two different regions of the SPC-1 protein spanning the SH3 domain (Secondary Screens). The table recapitulates the strongest interactions.

Global Predicted Biological Score (*categories computed and established by Hybrigenics, to assess the interaction reliability)*

A Very high confidence in the interaction

B High confidence in the interaction

C Good confidence in the interaction

D Moderate confidence in the interaction
(either due to false-positive interactions or due to interactions that are hardly detectable by the Y2H technique)

Strongest candidates
(Prey library: C. elegans embryo)

Primary Yeast Two Hybrid Screen
(Bait: CePAK-1 N-terminal amino acids: 1-294)

* Positive controls (PAK-1 itself + its known interactors)

Secondary Yeast Two Hybrid Screen
† *Bait I: CeSPC-1 SR8-10(aa:796-1243)*
‡ *Bait II: CeSPC-1 SH3 (aa:986-1041)*
§ *Common hits using Bait I and Bait II*

Interactor candidate	Protein Function	Global PBS
SPC-1	α-spectrin	A
F47B10.1	β-chain succinyl-co-A ligase	A
CHW-1	RhoU homolog	A
GCK-1	STE20-family kinase	A
NCK-1	NCK adaptor	A
PIX-1 *	ARHGEF7 homolog β-Pix	A
CDC-42 *	Small GTPase	A
PAK-1 *	P21-activated Ser/Tre kinase (multiple hits through kinase domain)	A
CED-10 *	Rac-1 / Small GTPase	B
POD-2	Predicted acetyl-coA carboxylase	B
Y39E4A.3	Transketolase	B
EEL-1	HECT-ubiquitin ligase	C
NPP-21	Nuclear pore protein	C
TAG-143	Transcription factor	C
UNC-44	Ankyrin	D
HIPR-1	SLA2 and Hip related	D
T05C1.4	Conserved calmodulin-binding TFs	D
Y53F4B.13	RNA methyltransferase	D
PTP-3	LAR-like receptor tyr-protein phosphatase	D
COGC-6	Conserved Oligomeric Golgi (COG) Component	D
DAF-21	Hsp90 molecular chaperone family member	D
GCK-1 variant	STE20-family kinase	D

Interactor candidate	Protein Function	Global PBS
PAK-1 §	p21-activated kinase	A
LIM-8 §	LIM domain muscle component	A
F44.E2.3 ‡	ARGLU1 ortholog	A
CSN-5 ‡	COP9-subunit ortholog E3 ubiquitin ligase interactor	A
DEB-1 ‡	Vinculin	A
DnaJ ‡	DNAJ/ZRF1/MPP11 ortholog ribosome-associated chaperone	B
CYLD-1 ‡	Human CYLD1 ortholog NF-κβ signalling interactor	B
VAB-3 / VAR-1 †	Homeodomain protein PAX6 ortholog	B
GRL-4 ‡	Hedgehog-like protein	C
UNC-34 ‡	Enabled/VASP homolog	C
T04F8.6 †	Human ninein and ninein-like (GSK3B interactor) ortholog	D
ALR-1 †	Human ARX (aristaless) ortholog homeodomain transcription factor	D
ATN-1 †	α-actinin homolog	D
MMCM-1 †	Methylmalonyl-CoA mutase	D
UNC-70 †	β_G-spectrin	D
VAB-10 †	Spectraplakin	D
F26A10.2 ‡	Zinc-finger containing protein	D
F43C1.1 ‡	Human PHLPP1&PHLPP2 ortholog	D
ALP-1 ‡	Enigma family member ALP (α-actinin associated LIM Protein) ortholog	D
CIT-1.2 ‡	Cyclin T ortholog	D
FLH-1 ‡	FLYWCH zinc finger transcription factor homolog	D
SHW-1 ‡	Human KCNC3 voltage-gated SHaW family potassium channel ortholog	D

Supplementary Table 3 | Secondary RNAi screen in *spc-1(ra409) pak-1(tm403)* background Additional RNAi screen in a spc-1(ra409) pak-1(tm403) mutant maintained by an exctrachromosomal spc-1(+)::GFP transgene of 13 actin related proteins from the Ahringer RNAi library that were recently reported to modulate actin remodeling in the early embryo (see text).

A Longer compared to *spc-1(-) pak-1(-)* (no retraction phenotype)

B Not longer compared to *spc-1(-) pak-1(-)* (retraction phenotype)

Targeted gene	Function	Strength of interaction
(I) viln-1	Ortholog of human SVIL (supervillin)	A
(V) gsnl-1	Gelsolin-related proteins	A
(X) tth-1	Thymosin beta ortholog	A
(I) pfn-1	Profilin	B
(II) cap-2	Beta subunit of actin capping protein	B
(III) ani-1	Anillin	B
(III) cyk-1	Formin homologous to Drosophila diaphanous and human DIAPH1	B
(III) fli-1	Orthologous to Drosophila and human Flightless I	B
(IV) cap-1	F-actin capping protein alpha subunit	B
(IV) fln-1	Ortholog of human filamin A	B
(IV) plst-1	Ortholog of human PLS1, PLS3 and LCP1	B
(V) arx-2	Subunit of the actin related protein of the conserved Arp2/3 complex	B
(V) unc-60	Actin depolymerizing factor(ADF)/cofilin	B

Supplementary Table 4 | Secondary RNAi screen in *spc-1(ra409)* background Additional RNAi screen in a spc-1(ra409) mutant maintained by an exctrachromosomal spc-1(+)::GFP transgene. Genes that gave the strongest defects in the initial RNAi screen (Supplementary Table 1) were tested again.

A Shorter compared to *spc-1(-)*

B Not shorter compared to *spc-1(-)*

Targeted gene	Function	Strength of interaction
(I) fhod-1	Formin	A
(I) hmr-1	Cadherin	A
(I) hmp-2	β-catenin	A
(II) cdc-42	RHO GTPase	A
(II) spdl-1	Coiled-coil protein	A
(II) vps-11	Ortholog of human VPS11	A
(III) mtm-3	Myotubularin lipid phosphatase	A
(III) mlc-5	Myosin II essential light chain ortholog	A
(IV) dnc-1	Ortholog of the dynactin complex subunit p150/GLUED/DCTN1	A
(IV) epi-1	Laminin α chain	A
(I) goa-1	Ortholog of the heterotrimeric G protein α subunit Go	B
(I) kin-10	Putative regulatory (β) subunit of casein kinase II	B
(I) mec-8	mRNA processing factor	B
(I) nmy-2	Non-muscle myosin II	B
(I) unc-94	Tropomodulin	B
(II) cap-2	β subunit of actin capping protein	B
(II) evl-20	Ortholog of human ADP-ribosylation factor-like protein 2	B
(II) spv-1	Ortholog of human GMIP	B
(II) unc-52	Perlecan	B
(III) klp-7	Ortholog of human KIF2A, 2B and 2C	B
(III) mup-4	Transmembrane protein	B
(IV) cap-1	F-actin capping protein α subunit	B
(IV) eps-8	Cell signaling adaptor protein	B
(IV) frk-1	Non-receptor tyrosine kinase	B
(IV) unc-33	Conserved member of the CRMP/TOAD/Ulip/DRP family	B

Supplementary Table 5 | List of strains used in this study

Name	Genotype
DM3409	*mnDp33 (X;IV)/+ IV.; spc-1(ra409) X.*
DWP10	*fhod-1(tm2363) I.; qaIs8001 [unc-119(+) fhod-1::gfp]*
ML1694	*pix-1(gk416)X.*
ML1725	*mcEX567 [spc-1::GFP, myo-2p::mcherry]*
ML1943	*mcIs55[pak-1::GFP;pRF4]*
ML1911	*git-1(tm1962)X.*
ML2113	*mcIs67 [dpy7p::LifeAct::GFP; unc-119(+)] V.; stIs10088[hlh-1::his-24::mCherry, unc-119(+)]*
ML2129	*pak-1(tm403) X.*
ML2200	*pak-1(tm403) X.; mcIs67 [dpy7p::LifeAct::GFP; unc-119(+)] V; stIs10088[hlh-1::his-24::mCherry, unc-119(+)]*
ML2419	*mcEx915[ppak-1::pak-1::mkate;pR4(rol);pBSK]*
ML2436	*spc-1(ra409) X.; mcEx636 [spc-1p::spc-1::GFP]*
ML2446	*pak-1(tm403) X.; spc-1(ra409) X.; mcEx636 [spc-1p::spc-1::GFP]*
ML2465	*mcIs91[linc26p::ABD::mkate; myo-2p::mcherry]*
ML2684	*mcEx1008 [fhod-1ΔFH2/DAD]*
ML2688	*pak-1(tm403) X.; mcEx1009 [fhod-1ΔFH2/DAD]*
ML2853	*pak-1(tm403) X.; mcEx1002 [fhod-1ΔFH1/FH2/DAD]*
ML2854	*pak-1(tm403) X.; mcEx1003 [fhod-1ΔDAD]*
ML2855	*pak-1(tm403) X.; mcEx1004 [fhod-1 full length]*
ML2856	*mcEx1005 [fhod-1ΔFH1/FH2/DAD]*
ML2857	*mcEx1006 [fhod-1ΔDAD]*
ML2858	*mcEx1007 [fhod-1 full length]*
ML2898	*fhod-1(tm2363) I.; mcIs67 [dpy7p::LifeAct::GFP; unc-119(+)] V.*
ML2903	*spc-1(ra409) X.; pak-1(tm403) X.; mcEx1016 [spc-1p::spc-1::GFP] line 1*
ML2904	*spc-1(ra409) X.; pak-1(tm403) X.; mcEx1016 [spc-1p::spc-1::GFP] line 3*
ML2906	*spc-1(ra409) X.; pak-1(tm403) X.; mcEx1016 [spc-1p::spc-1::GFP] line 4*
ML2929	*mcIs67 [dpy7p::LifeAct::GFP; unc-119(+)] V.; spc-1(ra409) X.; pak-1(tm403) X.; mcEx1016 [spc-1p::spc-1::GFP]*
ML2931	*viln-1(ok2413) I.; pak-1(tm403) X.*
ML2932	*gsnl-1(tm2730) V.; pak-1(tm403) X.*
ON204	*gsnl-1(tm2730) V.* (3x outcrossed)
ON206	*viln-1(ok2413) I.* (3x outcrossed)
ON218	*viln-1(ok2413) I.; gsnl-1(tm2730) V.*
N2	*Bristol*
XA8001	*fhod-1(tm2363) I.*

Supplementary Table 6 | List of Ex and Is used in this study

Name	Genotype
mcEx567	*[spc-1::GFP, myo-2p::mcherry]*
mcEx636	*[spc-1p::spc-1::GFP]*
mcEx915	*[ppak-1::pak-1::mkate;pR4(rol);pBSK]*
mcEx1002	*[fhod-1ΔFH1/FH2/DAD]*
mcEx1003	*[fhod-1ΔDAD]*
mcEx1004	*[fhod-1 full length]*
mcEx1005	*[fhod-1ΔFH1/FH2/DAD]*
mcEx1006	*[fhod-1ΔDAD]*
mcEx1007	*[fhod-1 full length]*
mcEx1008	*[fhod-1ΔFH2/DAD]*
mcEx1009	*[fhod-1ΔFH2/DAD]*
mcEx1016	*[spc-1p::spc-1::GFP]*
mcIs55	*[pak-1::GFP;pRF4]*
mcIs67	*[dpy7p::LifeAct::GFP; unc-119(+)] V.*
mcIs91	*[lin26p::ABD::mkate; myo-2p::mcherry]*

Supplementary Table 7 | Results of model fit Values of the fitted parameters for the different genotypes

	wild-type (n=12 embryos)	*unc-112* (n=14 embryos)	*spc-1* (n=8 embryos)	*spc-1 pak-1* (n=7 embryos)	*unc-112; spc-1 pak-1* (n=7 embryos)
Initial actin stiffness $\alpha_{DV}(0)$	1.4 ± 0.2	1.04 ± 0.02	0.93 ± 0.04	0.68 ± 0.02	0.66 ± 0.02
Plasticity factor β	0.11 ± 0.01	0.10 ± 0.03	0.040 ± 0.015	0.03 ± 0.03	0.02 ± 0.01
Intensity $F_{muscles}$	3.9 ± 0.1	Ø	1.95	1.95	Ø
Tearing factor γ	Ø	Ø	0.02 ± 0.01	0.15 ± 0.01	Ø

Supplementary Table 8 | Model parameters Summary of the parameter values

Spring	$k = 1$
Dashpot	$\eta = 3$
F_{epid}	$F_{seam} = 1,\ \tau_s = 50,\ \ h_s = 4$
$F_{muscles}$	$\tau_m = 15,\ h_m = 1,\ \ t_{init} = 90$
Saturation function	$L = 3.2,\ d = 15$
Critical force *Fc*	0.5

REFERENCES

REFERENCES

Adams, D.S. et al. The mechanics of notochord elongation, straightening and stiffening in the embryo of *Xenopus laevis*. Development. 110:115-130. (1990).

Adhikari, S. et al. Unraveling the mechanism of the cadherin-catenin-actin catch bond. PLoS Comput Biol. 14(8):e1006399. (2018).

Affolter, M. et al. Tube or not tube: remodeling epithelial tissues by branching morphogenesis. Dev Cell. 4(1):11-8. (2003).

Alberts, B. et al. Molecular Biology of the Cell (5th ed.). Garland Science. p. 1321. (2007).

Altmann, S.M. et al. Pathways and intermediates in forced unfolding of spectrin repeats. Structure. 10(8):1085-96. (2002).

Ambros, V. Control of developmental timing in *Caenorhabditis elegans*. Curr Opin Genet Dev. 10: 428-433. (2000).

Amin, N.M. et al. A Zn-finger/FH2-domain containing protein, FOZI-1, acts redundantly with CeMyoD to specify striated body wall muscle fates in the *Caenorhabditis elegans* postembryonic mesoderm. Development. 134:19-29. (2007).

An, Y. et al. Apical constriction is driven by a pulsatile apical myosin network in delaminating *Drosophila* neuroblasts. Development. 144(12):2153-2164. (2017).

Anthis, N.J. et al. The structure of an integrin/talin complex reveals the basis of inside-out signal transduction. EMBO J. (22): 3623-3632. (2009).

Antoshechkin, I. and Han, M. The *C. elegans evl-20* gene is a homolog of the small GTPase ARL2 and regulates cytoskeleton dynamics during cytokinesis and morphogenesis. Dev Cell 2, 579-591. (2002).

Aratyn-Schaus, Y. et al. Dynamic and structural signatures of lamellar actomyosin force generation. Mol Biol Cell. 22(8):1330-9. (2011).

Ardiel, E.L. et al. Visualizing Calcium Flux in Freely Moving Nematode Embryos. Biophys J. 112(9):1975-1983. (2017).

Armenti, S.T. and Nance J. Adherens junctions in *C. elegans* embryonic morphogenesis. Subcell Biochem. 60:279-99. (2012).

Backholm, M. and Bäumchen, O. Micropipette force sensors for in vivo force measurements on single cells and multicellular microorganisms. Nat Protoc. 14(2):594-615. (2019).

Baines, A.J. Evolution of spectrin function in cytoskeletal and membrane networks. Biochem Soc Trans. 37 (Pt 4):796-803. (2009).

Ballestrem, C. et al. Marching at the front and dragging behind: differential alphaVbeta3-integrin turnover regulates focal adhesion behavior. J Cell Biol. 155(7):1319-32. (2001).

Barstead, R.J. et al. Cloning, sequencing, and mapping of an alpha-actinin gene from the nematode *Caenorhabditis elegans.* Cytoskeleton. 20(1):69-78. (1991).

Batchelder, E.L. et al. Cytokinesis is not controlled by calmodulin or myosin light chain kinase in the *Caenorhabditis elegans* early embryo. FEBS Lett. 581:4337-41. (2007).

Bechtold, M. et al. FHOD proteins in actin dynamics-a formin class of its own. Small GTPases 5:e973765. (2014).

Becker, P.M. et al. Pulmonary vascular permeability and ischemic injury in gelsolin-deficient mice. Am J Respir Cell Mol Biol. 28(4):478-84. (2003).

Begg, D.A. et al. The visualization of actin filament polarity in thin sections. Evidence for the uniform polarity of membrane-associated filaments. J Cell Biol. 79(3):846-52. (1978).

Bennett, V. The spectrin-actin junction of erythrocyte membrane skeletons. Biochim Biophys Acta. 988(1):107-21. (1989).

Bennett, V. and Baines, A.J. Spectrin and ankyrin-based pathways: metazoan inventions for integrating cells into tissues. Physiol Rev. 81(3):1353-1392. (2001).

Bercher, M. et al. *mua-3*, a gene required for mechanical tissue integrity in *Caenorhabditis elegans*, encodes a novel transmembrane protein of epithelial attachment complexes. J Cell Biol. 154(2):415-26. (2001).

Berg, J.M. et al. Biochemistry. 5th edition. New York: W H Freeman. Section 34.3. Kinesin and Dynein Move Along Microtubules. (2002).

Bergs, A. et al. Rhodopsin optogenetic toolbox v2.0 for light-sensitive excitation and inhibition in *Caenorhabditis elegans*. PLoS One. 13(2):e0191802. (2018).

Bertet, C. et al. Myosin-dependent junction remodelling controls planar cell intercalation and axis elongation. Nature. 429(6992):667-71. (2004).

Bialkowska, K. et al. SH3 domain of spectrin participates in the activation of Rac in specialized calpain-induced integrin signaling complexes. J Cell Sci. 118(Pt 2):381-95. (2005).

Bianco, A. et al. Expanding the genetic code of *Drosophila melanogaster*. Nat Chem Biol. 8(9):748-50. (2012).

Bird, A.F. and Bird, J. The structure of nematodes. Academic Press, San Diego, CA. (1991).

Biro, M. et al. Cell cortex composition and homeostasis resolved by integrating proteomics and quantitative imaging. Cytoskeleton (Hoboken). 70(11):741-54. (2013).

Blanchard, G.B. et al. Cytoskeletal dynamics and supracellular organisation of cell shape fluctuations during dorsal closure. Development. 137(16):2743-52. (2010).

Blanchoin, L. et al. Actin dynamics, architecture, and mechanics in cell motility. Physiol Rev. 94(1):235-63. (2014).

Blankenship, J.T. et al. Multicellular rosette formation links planar cell polarity to tissue morphogenesis. Dev Cell. 11(4):459-70. (2006).

Blaser, H. et al. Migration of zebrafish primordial germ cells: a role for myosin contraction and cytoplasmic flow. Dev Cell. 11(5):613-27. (2006).

Bodine, D.M. et al. Spectrin deficient inherited hemolytic anemias in the mouse: characterization by spectrin synthesis and mRNA activity in reticulocytes. Cell. 37(3):721-9. (1984).

Bornslaeger, E.A. et al. Breaking the connection: displacement of the desmosomal plaque protein desmoplakin from cell-cell interfaces disrupts anchorage of intermediate filament bundles and alters intercellular junction assembly. J Cell Biol. 134(4):985-1001. (1996).

Bosher, J.M. et al. The *Caenorhabditis elegans* vab-10 spectraplakin isoforms protect the epidermis against internal and external forces. J Cell Biol. 161(4):757-68. (2003).

Bossinger, O. et al. Zonula adherens formation in *Caenorhabditis elegans* requires *dlg-1*, the homologue of the *Drosophila* gene discs large. Dev Biol. 230,29-42. (2001).

Bosveld, F. et al. Mechanical control of morphogenesis by Fat/Dachsous/Four-jointed planar cell polarity pathway. Science. 336(6082):724-727. (2012).

Bournier, O. et al. Spectrin interacts with EVL (Enabled/vasodilator-stimulated phosphoprotein-like protein), a protein involved in actin polymerization. Biol Cell. 98(5):279-93. (2006).

Breitsprecher, D. et al. Rocket launcher mechanism of collaborative actin assembly defined by single-molecule imaging. Science. 336,1164-1168. (2012).

Breitsprecher, D. and Goode, B.L. Formins at a glance. J Cell Sci. 126:1-7. (2013).

Brenner, S. The genetics of *Caenorhabditis elegans*. Genetics. 77,71-94. (1974).

Broadie, K.S. et al. Extracellular matrix and its receptors in *Drosophila* neural development. Dev Neurobiol. 71(11):1102-1130. (2011).

Broderick, M.J. and Winder, S.J. Spectrin, alpha-actinin, and dystrophin. Adv Protein Chem. 70:203-46. (2005).

Brown, J.W. et al. The Physiological Molecular Shape of Spectrin: A Compact Supercoil Resembling a Chinese Finger Trap. PLoS Comput Biol. 11(6):e1004302. (2015).

Brown, N.H. et al. Integrins as mediators of morphogenesis in *Drosophila*. Dev Biol. 223(1):1-16. (2000).

Bryant, D.M. and Mostov, K.E. From cells to organs: building polarized tissue. Nat Rev Mol Cell Biol. 9(11):887-901. (2008).

Buechner, M. et al. Cystic canal mutants in *Caenorhabditis elegans* are defective in the apical membrane domain of the renal (excretory) cell. Dev Biol. 214(1):227-41. (1999).

Burlacu, S. et al. Distribution of actin filament lengths measured by fluorescence microscopy. Am J Physiol. 262(3 Pt 1):C569-77. (1992).

Burnette, D.T. et al. A role for actin arcs in the leading-edge advance of migrating cells. Nat Cell Biol. 13(4):371-81. (2011).

Campbell, H.K. et al. PAK2 links cell survival to mechanotransduction and metabolism. J Cell Biol. 218(6):1958-1971. (2019).

Carmon, A. et al. Dumpy interacts with a large number of genes in the developing wing of *Drosophila melanogaster.* Fly. 4(2):117-27. (2010).

Cassada, R.C. and Russell, R.L. The dauer larva, a postembryonic developmental variant of the nematode *Caenorhabditis elegans.* Dev Biol. 46:326-342. (1975).

Cearns, M.D. et al. Microtubules, polarity and vertebrate neural tube morphogenesis. J Anat. 229(1):63-74. (2016).

Chanet, S. and Martin, A.C. Mechanical force sensing in tissues. Prog. Mol. Biol. Transl. Sci. 126,317-352 (2014).

Chauhan, B. et al. Epithelial morphogenesis: the mouse eye as a model system. Curr Top Dev Biol. 111:375-99. (2015).

Chen, C.S. et al. Cell shape provides global control of focal adhesion assembly. Biochem Biophys Res Commun. 307(2):355-61. (2003).

Chen, C.S. Mechanotransduction - a field pulling together? J Cell Sci. 121(Pt 20):3285-92. (2008).

Chen, T.W. et al. Membrane domain modulation by Spectrins in *Drosophila* photoreceptor morphogenesis. Genesis. 47(11):744-50. (2009).

Chesarone, M.A. et al. Unleashing formins to remodel the actin and microtubule cytoskeletons. Nat Rev Mol Cell Biol. 11:62-74. (2010).

Chisholm, A.D. and Hardin, J. Epidermal morphogenesis. WormBook. 1:1-22. ed. The *C. elegans* Research Community. WormBook. (2005).

Choe, C.P. and Crump, J.G. Dynamic epithelia of the developing vertebrate face. Curr Opin Genet Dev. 32:6672. (2015).

Choe, H. et al. The calcium activation of gelsolin: Insights from the 3A structure of the G4-G6/actin complex. J Mol Biol. 324,691-702. (2002).

Chugh, P. et al. Actin cortex architecture regulates cell surface tension. Nat. Cell Biol. 19,689-697. (2017).

Ciarletta, P. et al. Continuum model of epithelial morphogenesis during *Caenorhabditis elegans* embryonic elongation. Phil. Trans. R. Soc. A. 367(1902):3379-3400. (2009).

Clark, A.G. et al. Stresses at the cell surface during animal cell morphogenesis. Curr Biol. 24,R484-R494. (2014).

Claudiu, A. et al. Cell Identification and Cell Lineage Analysis. Methods Cell Biol. 106: 325-341. (2011).

Colas, J.F. Schoenwolf, G.C. Towards a cellular and molecular understanding of neurulation. Dev Dyn. 221(2):117-45. (2001).

Collinet, C. et al. Local and tissue-scale forces drive oriented junction growth during tissue extension. Nat Cell Biol. 17(10):1247-58. (2015).

Conti, M.A. and Adelstein, R.S. Nonmuscle myosin II moves in new directions. J Cell Sci. 121(Pt 1):11-8. (2008).

Cook, S.J. et al. Whole-animal connectomes of both *Caenorhabditis elegans* sexes. Nature. 571(7763):63-71. (2019).

Cooper, G.M. The Cell: A Molecular Approach. 2nd edition. Sunderland (MA): Sinauer Associates. (2000).

Corsi, A.K. et al. A Transparent window into biology: A primer on *Caenorhabditis elegans*. WormBook:1-31. ed. The *C. elegans* Research Community. WormBook. (2015).

Corsi, A.K. et al. A Transparent Window into Biology: A Primer on *Caenorhabditis elegans*. Genetics. 200(2):387-407. (2015).

Costa, M. et al. The role of actin filaments in patterning the *Caenorhabditis elegans* cuticle. Dev Biol. 184, 373-384. (1997).

Costa, M. et al. A putative catenin-cadherin system mediates morphogenesis of the *Caenorhabditis elegans* embryo. J Cell Biol. 141(1):297-308. (1998).

Cox, E.A. and Hardin, J. Sticky worms: adhesion complexes in *C. elegans*. J Cell Sci. 117(Pt 10):1885-97. (2004).

Cox-Paulson, E.A. et al. Tropomodulin protects α-catenin-dependent junctional-actin networks under stress during epithelial morphogenesis. Curr Biol. 22(16):1500-5. (2012).

da Silva, S.M. and Vincent, J.P. Oriented cell divisions in the extending germband of *Drosophila*. Development. 134(17):3049-54. (2007).

Dai, J. et al. Myosin I contributes to the generation of resting cortical tension. Biophys J. 77(2):1168-76. (1999).

David, D.J. et al. The PAR complex regulates pulsed actomyosin contractions during amnioserosa apical constriction in *Drosophila*. Development. 137(10):1645-55. (2010).

David, D.J. et al. Bazooka inhibits aPKC to limit antagonism of actomyosin networks during amnioserosa apical constriction. Development. 140(23):4719-29. (2013).

Davidson, L.A. No strings attached: new insights into epithelial morphogenesis. BMC Biol. 20;10:105. (2012).

Davidson, L. and Keller, R. Measuring mechanical properties of embryos and embryonic tissues. Methods Cell Biol. 83:425-439. (2007).

Davies, A.G. e.t al. Functional overlap between the *mec-8* gene and five *sym* genes in *Caenorhabditis elegans*. Genetics. 153(1):117-34. (1999).

Davis, L. and Greiss, S. Genetic Encoding of Unnatural Amino Acids in *C. elegans*. Methods Mol Biol. 1728:389-408. (2018).

De Matteis, M.A. and Morrow, J.S. Spectrin tethers and mesh in the biosynthetic pathway. J Cell Sci. 113 (Pt 13):2331-2343. (2000).

del Rio, A. et al. Stretching single talin rod molecules activates vinculin binding. Science. 323:638-641. (2009).

Delon, I. and Brown, N.H. Integrins and the actin cytoskeleton. Curr Opin Cell Biol. 19(1):43-50. (2006).

Delva, E. The desmosome. Cold Spring Harbor Perspectives in Biology. 1 (2): a002543. (2009).

Deng, H. et al. The Flightless I homolog, *fli-1*, regulates anterior/posterior polarity, asymmetric cell division and ovulation during *Caenorhabditis elegans* development. Genetics. 177,847-860. (2007).

DePianto, D. and Coulombe, P.A. Intermediate filaments and tissue repair. Exp Cell Res. 301(1):68-76. (2004).

Desai, A. and Mitchison, T.J. Microtubule polymerization dynamics. Annu Rev Cell Dev Biol. 13:83-117. (1997).

Desrochers, G. et al. Molecular basis of interactions between SH3 domain-containing proteins and the proline-rich region of the ubiquitin ligase Itch. J Biol Chem. 292(15):6325-6338. (2017).

Dickinson, D.J. et al. Engineering the *Caenorhabditis elegans* genome using cas9-triggered homologous recombination. Nat Methods. 10(10):1028-1034. (2013).

Dickinson, D.J et al. Streamlined Genome Engineering with a Self-Excising Drug Selection Cassette. Genetics. 200(4):1035-49. (2015).

Ding, M. et al. The cytoskeleton and epidermal morphogenesis in *C. elegans*. Exp Cell Res. 301(1):84-90. (2004).

Diogon, M. et al. The RhoGAP RGA-2 and LET-502/ROCK achieve a balance of actomyosin-dependent forces in *C. elegans* epidermis to control morphogenesis. Development. 134, 2469-2479. (2007).

Discher, D.E. and Carl, P. New insights into red cell network structure, elasticity, and spectrin unfolding--a current review. Cell Mol Biol Lett. 6(3):593-606. (2001).

Dixon, S.J. and Roy, P.J. Muscle arm development in *Caenorhabditis elegans.* Development. 132(13):3079-92. (2005).

Diz-Muñoz, A. et al. Use the force: membrane tension as an organizer of cell shape and motility. Trends Cell Biol. 23,47-53. (2013).

Diz-Muñoz, A. et al. In pursuit of the mechanics that shape cell surfaces. Nat. Phys. 14,648-652. (2018).

Doherty, G.J. and McMahon, H.T. Mediation, modulation, and consequences of membrane-cytoskeleton interactions. Annu Rev Biophys. 37:65-95. (2008).

dos Remedios, C.G. et al. Actin binding proteins: regulation of cytoskeletal microfilaments. Physiol Rev. 83(2):433-73. (2003).

Doubrovinski, K. et al. Measurement of cortical elasticity in *Drosophila melanogaster* embryos using ferrofluids. Proc Natl Acad Sci USA. 114,1051-1056. (2017).

du Roure, O. et al. Force mapping in epithelial cell migration. Proc Natl Acad Sci USA. 102:2390-2395. (2005).

Dubreuil, R.R. et al. A beta-spectrin isoform from *Drosophila* (beta H) is similar in size to vertebrate dystrophin. J Cell Biol. 111(5 Pt 1):1849-58. (1990).

Dubreuil, R.R. et al. *Drosophila* beta spectrin functions independently of alpha spectrin to polarize the Na,K ATPase in epithelial cells. J Cell Biol. 149(3):647-656. (2000).

Dupont, S. et al. Role of YAP/TAZ in mechanotransduction. Nature. 474,179-183. (2011).

Edelstein-Keshet, L. and Ermentrout, G.B. Bull. Math. Biol. 60: 449. (1998).

Edwards, D.N. et al. An activity-dependent network of interactions links the Rel protein Dorsal with its cytoplasmic regulators. Development. 124(19):3855-64. (1997).

El Mouridi, S. et al. Reliable CRISPR/Cas9 Genome Engineering in *Caenorhabditis elegans* Using a Single Efficient sgRNA and an Easily Recognizable Phenotype. G3. 5 1429-1437. (2017).

Ellertsdóttir, E. et al. Vascular morphogenesis in the zebrafish embryo. Dev Biol. 341(1):56-65. (2010).

Elliott, P.R. et al. The Structure of the talin head reveals a novel extended conformation of the FERM domain. Structure. 18(10):1289-99. (2010).

Elliott, T.S. Et al. Proteome labeling and protein identification in specific tissues and at specific developmental stages in an animal. Nat Biotechnol. 32(5):465-72. (2013).

Elzinga, M. et al. Complete amino-acid sequence of actin of rabbit skeletal muscle. Proc Natl Acad Sci USA. 70(9):2687-91. (1973).

Engler, A.J. et al. Matrix elasticity directs stem cell lineage specification. Cell. 126(4):677-689. (2006).

Ewald, A.J. et al. Collective epithelial migration and cell rearrangements drive mammary branching morphogenesis. Dev Cell. 14(4):570-581. (2008).

Fang-Yen, C. et al. Illuminating neural circuits and behaviour in *Caenorhabditis elegans* with optogenetics. Philos Trans R Soc Lond B Biol Sci. 370(1677):20140212. (2015).

Fehon, R.G. et al. Organizing the cell cortex: the role of ERM proteins. Nat Rev Mol Cell Biol. 11(4):276-287. (2010).

Feldman, J. L. and Priess, J. R. A role for the centrosome and PAR-3 in the hand-off of MTOC function during epithelial polarization. Curr Biol. 22,575-582. (2012).

Feldt, J. et al. Structure, regulation and related diseases of the actin-binding protein gelsolin. Expert Rev Mol Med. 20:e7. (2019).

Feng, L. et al. Full-contact domain labeling: Identification of a novel phosphoinositide binding site on gelsolin that requires the complete protein. Biochemistry. 40, 904-913. (2001).

Fernandez-Gonzalez, R. et al. Myosin II dynamics are regulated by tension in intercalating cells. Dev Cell. 17(5):736-43. (2009).

Fernandez-Gonzalez, R. and Zallen, J.A. Oscillatory behaviors and hierarchical assembly of contractile structures in intercalating cells. Phys Biol. 8(4):045005. (2011).

Firestein, B.L. and Rongo, C. DLG-1 is a MAGUK similar to SAP97 and is required for adherens junction formation. Mol. Biol. Cell. 12,3465-3475. (2001).

Fischer, R.S. and Fowler, V.M. Thematic minireview series: The state of the cytoskeleton in 2015. J Biol Chem. 290(28):17133-6. (2015).

Flanagan, L.A. et al. Neurite branching on deformable substrates. Neuroreport. 13(18):2411-2415. (2002).

Fletcher, G.C. et al. The Spectrin cytoskeleton regulates the Hippo signalling pathway. EMBO J. 34(7):940-954. (2015).

Forest, E. et al. The apical scaffold big bang binds to spectrins and regulates the growth of *Drosophila melanogaster* wing discs. J Cell Biol. 217(3):1047-1062. (2018).

Francis, G.R. and Waterston, R.H. Muscle organization in *Caenorhabditis elegans*: localization of proteins implicated in thin filament attachment and band organization. J. Cell Biol. 101(4):1532-1549. (1985).

Francis, G.R. and Waterston, R.H. Muscle cell attachment in *Caenorhabditis elegans*. J Cell Biol. 114(3):465-479. (1991).

Franke, J.D. et al. Nonmuscle myosin II generates forces that transmit tension and drive contraction in multiple tissues during dorsal closure. Curr Biol. 15(24):2208-21. (2005).

Frantz, C. et al. The extracellular matrix at a glance. J Cell Sci. 123(24): 4195-4200. (2010).

Fritzsche, M. et al. Self-organizing actin patterns shape membrane architecture but not cell mechanics. Nat. Commun. 8,14347. (2017).

Frøkjær-Jensen, C. et al. Random and targeted transgene insertion in *C. elegans* using a modified Mosl transposon. Nat Methods. 11(5):529-534. (2014).

Frøkjær-Jensen, C. et al. Single copy insertion of transgenes in *C. elegans*. Nat Genet. 40(11):1375-1383. (2008).

Fromont-Racine, M. et al. Toward a functional analysis of the yeast genome through exhaustive two-hybrid screens. Nat Genet. 16, 277-282. (1997).

Fu, R. et al. The spectraplakins of *Caenorhabditis elegans:* Cytoskeletal crosslinkers and beyond. Semin Cell Dev Biol. 69:58-68. (2017).

Fyrberg, C. et al. Genes encoding actin-related proteins of *Drosophila melanogaster*. J Mol Biol. 241(3):498-503. (1994).

Fyrberg, C. et al. The actin protein superfamily. Soc Gen Physiol Ser. 49:173-178. (1994).

Galkin, V.E. Et al. Actin filaments as tension sensors. Curr Biol. 22(3):R96-101. (2012).

Gally, C. et al. Myosin II regulation during *C. elegans* embryonic elongation: LET-502/ROCK, MRCK-1 and PAK-1, three kinases with different roles. Development. 136, 3109-3119. (2009).

Gally, C. et al. Functional and Genetic Analysis of VAB-10 Spectraplakin in *Caenorhabditis elegans*. Methods Enzymol. 569:407-30 (2016).

Garcia, A.J. and Reyes, C.D. Bio-adhesive surfaces to promote osteoblast differentiation and bone formation. J Dent Res. 84(5):407-413. (2005).

Gardel, M.L. et al. Mechanical integration of actin and adhesion dynamics in cell migration. Annu Rev Cell Dev Biol. 26:315-33. (2010).

Gasteier, J.E. et al. Activation of the Rac-binding partner FHOD1 induces actin stress fibers via a ROCK-dependent mechanism. J Biol Chem. 278:38902-12. (2003).

Gatewood, B.K. and Bucher, E.A. The *mup-4* locus in *Caenorhabditis elegans* is essential for hypodermal integrity, organismal morphogenesis and embryonic body wall muscle position. Genetics. 146(1):165-83. (1997).

Gauthier, N.C. et al. Temporary increase in plasma membrane tension coordinates the activation of exocytosis and contraction during cell spreading. Proc Natl Acad Sci USA. 108,14 467-14 472. (2011).

Gauthier, N.C. et al. Mechanical feedback between membrane tension and dynamics. Trends Cell Biol. 22(10):527-35. (2012).

Gendreau, S.B. et al. The potential to differentiate epidermis is unequally distributed in the AB lineage during early embryonic development in *C. elegans*. Dev Biol. 166(2):770-81. (1994).

Gettner, S.N. et al. Characterization of beta pat-3 heterodimers, a family of essential integrin receptors in *C. elegans*. J Cell Biol. 129(4):1127-41. (1995).

Ghoshdastider, U. et al. The expanding superfamily of gelsolin homology domain proteins. Cytoskeleton (Hoboken). 70(11):775-95. (2013).

Giannone, G. et al. Periodic lamellipodial contractions correlate with rearward actin waves. Cell. 116(3):431-43. (2004).

Giannone, G. et al. Lamellipodial actin mechanically links myosin activity with adhesion-site formation. Cell. 128(3):561-75. (2007).

Gibson, D.G. et al. Enzymatic assembly of DNA molecules up to several hundred kilobases. Nature Methods. 6 (5): 343-345. (2009).

Gibson, D.G. Enzymatic assembly of overlapping DNA fragments. Methods Enzymol. 498:349-61 (2011).

Gieseler, K. Development, structure, and maintenance of *C. elegans* body wall muscle. WormBook, ed. The *C. elegans* Research Community, WormBook, (2017).

Gilmour, D. et al. From morphogen to morphogenesis and back. Nature. 541,311-320. (2017).

Gingras, A.R. et al. Mapping and consensus sequence identification for multiple vinculin binding sites within the talin rod. J Biol Chem. 280,37217-37224. (2005).

Gingras, A.R. et al. Structural determinants of integrin binding to the talin rod. J Biol Chem. 284,8866-8876. (2009).

Gomes, J.E. et al. Microtubule severing by the katanin complex is activated by PPFR-1-dependent MEI-1 dephosphorylation. J Cell Biol. 202, 431-439. (2013).

Gonzalez, R.C. and Woods, R.E. Digital Image Processing (3rd Edition). Prentice-Hall, Inc. (2006).

Goode, B.L. and Eck, M.J. Mechanism and function of formins in the control of actin assembly. Annu Rev Biochem. 76:593-627. (2007).

Goshima, M. et al. Characterization of a novel Ras-binding protein Ce-FLI-1 comprising leucine-rich repeats and gelsolin-like domains. Biochem Biophys Res Commun. 257,111-116. (1999).

Graceffa, P. and Dominguez R. Crystal structure of monomeric actin in the ATP state. Structural basis of nucleotide-dependent actin dynamics. J Biol Chem. 278 (36): 34172-80. (2003).

Greenquist, A.C. et al. The spectrin phosphorylation reaction in human erythrocytes. Prog Clin Biol Res. 20:1-24. (1978).

Greiss, S. and Chin, J.W. Expanding the genetic code of an animal. J Am Chem Soc. 133(36):14196-9. (2011).

Grum, V.L. Et al. Structures of two repeats of spectrin suggest models of flexibility. Cell. 98(4):523-35. (1999).

Guillot, C. and Lecuit, T. Mechanics of epithelial tissue homeostasis and morphogenesis. Science. 340(6137):1185-9. (2013).

Gunning, P.W. et al. The evolution of compositionally and functionally distinct actin filaments. J Cell Sci. 128(11):2009-19. (2015).

Gupton, S.L. and Waterman-Storer, C.M. Spatiotemporal feedback between actomyosin and focal-adhesion systems optimizes rapid cell migration. Cell. 125(7):1361-74. (2006).

Gushchina, L.V. et al. High-resolution crystal structure of spectrin SH3 domain fused with a proline-rich peptide. J Biomol Struct Dyn. 29(3):485-95. (2011).

Gustafsson, M.G. Surpassing the lateral resolution limit by a factor of two using structured illumination microscopy. J Microsc. 198,82-87 (2000).

Hahn, B.S. and Labouesse, M. Tissue integrity: Hemidesmosomes and resistance to stress. Curr Biol. 11(21):R858-861. (2001).

Haimo, L.T. and Rosenbaum, J.L. Cilia, flagella, and microtubules. J Cell Biol. 91(3 Pt 2):125s-130s. (1981).

Haining, A.W.M. et al. All subdomains of the talin rod are mechanically vulnerable and may contribute to cellular mechanosensing. ACS Nano. 10,6648-6658. (2016).

Hajne, J. et al. Determination of the persistence length of actin filaments on microcontact printed myosin patterns. Proc. SPIE 9337. (2015).

Halder, G. et al. Transduction of mechanical and cytoskeletal cues by YAP and TAZ. Nat. Rev. Mol. Cell Biol. 13,591-600. (2012).

Hall, S. and Ward, R.E. Septate Junction Proteins Play Essential Roles in Morphogenesis Throughout Embryonic Development in *Drosophila.* G3 (Bethesda). 6(8): 2375-2384. (2006).

Ham, H. et al. Dedicator of cytokinesis 8 interacts with talin and Wiskott-Aldrich syndrome protein to regulate NK cell cytotoxicity. J Immunol. 190:3661-3669. (2013).

Hamada, T. et al. Lateral phase separation in tense membranes. Soft Matter. 7,9061. (2011).

Hammarlund, M. et al. Mutations in beta-spectrin disrupt axon outgrowth and sarcomere structure. J Cell Biol. 149(4):931-42. (2000).

Hammarlund, M. et al. Axons break in animals lacking beta-spectrin. J Cell Biol. 176(3):269-75. (2007).

Han, S. et al. Expanding the genetic code of *Mus musculus*. Nat Commun. 8:14568. (2017).

Hannemann, S. et al. The Diaphanous-related Formin FHOD1 associates with ROCK1 and promotes Src-dependent plasma membrane blebbing. J Biol Chem. 283:27891-903. (2008).

Hardin, J. The role of secondary mesenchyme cells during sea urchin gastrulation studied by laser ablation. Development. 103:317-324. (1988).

Hardin, J. and Lockwood, C. Skin tight: cell adhesion in the epidermis of *Caenorhabditis elegans*. Curr Opin Cell Biol. 16(5):486-92. (2004).

Harris, A.R. et al. Mechanotransduction by the actin cytoskeleton: Converting mechanical stimuli into biochemicals signals. Annu Rev Biophys. 47,617-631. (2018).

Hartsock, A. and Nelson, W.J. Adherens and tight junctions: structure, function and connections to the actin cytoskeleton. Biochim Biophys Acta. 1778(3):660-9. (2008).

Hartwig, J.H. Actin-binding proteins. 1: Spectrin super family. Protein Profile. 2(7):703-800. (1995).

Hayakawa, K. et al. Actin filaments function as a tension sensor by tension-dependent binding of cofilin to the filament. J Cell Biol. 195,21-727. (2011).

Hayakawa, K. et al. Single-molecule imaging and kinetic analysis of cooperative cofilin-actin filament interactions. Proc Natl Acad Sci USA. 111,9810-9815. (2014).

Hayes, P. and Solon, J. *Drosophila* dorsal closure: An orchestra of forces to zip shut the embryo. Mech Dev. 144(Pt A):2-10. (2017).

He, L. et al. Tissue elongation requires oscillating contractions of a basal actomyosin network. Nat Cell Biol. 12(12):1133-42 (2010).

Heasman, J. et al. Fates and states of determination of single vegetal pole blastomeres of *X. laevis*. Cell. 37(1):185-94. (1984).

Hegsted, A. et al. INF2- and FHOD related formins promote ovulation in the somatic gonad of *C. elegans.* Cytoskeleton (Hoboken). 73: 712-728. (2016).

Heisenberg, C. P. and Bellaiche, Y. Forces in tissue morphogenesis and patterning. Cell. 153(5): 948-962. (2013).

Herrmann, H. and Wiche, G. Plectin and IFAP-300K are homologous proteins binding to microtubule-associated proteins 1 and 2 and to the 240-kilodaltonsubunit of spectrin. J Biol Chem. 262(3)1320-1325. (1987).

Hesse, M. et al. Targeted deletion of keratins 18 and 19 leads to trophoblast fragility and early embryonic lethality. EMBO J. 19(19):5060-5070. (2000).

Hetherington, S. et al. PAT-12, a potential anti-nematode target, is a new spectraplakin partner essential for *Caenorhabditis elegans* hemidesmosome integrity and embryonic morphogenesis. Dev Biol. 350(2):267-78. (2011).

Hetmanski, J.H.R. et al. Membrane tension orchestrates rear retraction in matrix directed cell migration. Sneak Peak. (2018).

Hirata, H. et al. Force-dependent vinculin binding to talin in live cells: a crucial step in anchoring the actin cytoskeleton to focal adhesions. AJP Cell Physiol. 306,C607-C620. (2014).

Hiscock, T.W. and Megason, S.G. Orientation of Turing-like Patterns by Morphogen Gradients and Tissue Anisotropies. Cell Systems. 1(6):408-416. (2015).

Hodgkin, J. et al. Nondisjunction Mutants of the Nematode *Caenorhabditis elegans*. Genetics.91(1):67-94. (1979).

Hollenbeck, P.J. et al. Intermediate filament collapse is an ATP-dependent and actin-dependent process. J Cell Sci. 92(Pt 4):621-31. (1989).

Holt, M.R. et al. Quantifying cell-matrix adhesion dynamics in living cells using interference reflection microscopy. J Microsc. 232(1):73-81. (2008).

Hong, L. et al. MUP-4 is a novel transmembrane protein with functions in epithelial cell adhesion in *Caenorhabditis elegans*. J Cell Biol. 154(2):403- 414. (2001).

Houk, A.R. et al. Membrane tension maintains cell polarity by confining signals to the leading edge during neutrophil migration. Cell. 148,175-188. (2012).

Howard, J. Molecular motors: structural adaptations to cellular functions. Nature. 389(6651):561-567. (1997).

Hresko, M.C. et al. Assembly of body wall muscle and muscle cell attachment structures in *Caenorhabditis elegans*. J Cell Biol. 124(4):491-506. (1994).

Hresko, M.C. et al. Myotactin, a novel hypodermal protein involved in muscle-cell adhesion in *Caenorhabditis elegans*. J Cell Biol. 146(3):659-72. (1999).

Hu, R.J. et al. Characterization of human brain cDNA encoding the general isoform of beta-spectrin. J Biol Chem. 267(26):18715-18722. (1992).

Hu, X. et al. Molecular stretching modulates mechanosensing pathways. Protein Sci. 26(7):1337-1351. (2017).

Huber, F. et al. Emergent complexity of the cytoskeleton: from single filaments to tissue. Adv Phys. 62(1):1-112. (2013).

Humphries, J.D. et al. Vinculin controls focal adhesion formation by direct interactions with talin and actin. J Cell Biol. 179,1043-1057. (2007).

Hunt-Newbury, R. et al. High-throughput *in vivo* analysis of gene expression in *Caenorhabditis elegans*. PLoS Biol. 5(9):e237. (2007).

Husson, S.J. et al.Optogenetic manipulation of neural activity in *C. elegans*: from synapse to circuits and behaviour. Biol Cell. 105(6):235-50. (2013).

Hutson, M.S. et al. Forces for morphogenesis investigated with laser microsurgery and quantitative modeling. Science. 300(5616):145-9.. (2003).

Ingber, D.E. Mechanical control of tissue growth: function follows form. Proc Natl Acad Sci USA. 102(33):11571-2. (2005).

Ingber, D.E. Cellular mechanotransduction: putting all the pieces together again. FASEB J. 20(7):811-27. (2006).

Ipsaro, J.J. et al. Crystal structure and functional interpretation of the erythrocyte spectrin tetramerization domain complex. Blood. 115(23):4843-52. (2010).

Irvine, K.D. and Wieschaus, E. Cell intercalation during *Drosophila* germband extension and its regulation by pair-rule segmentation genes. Development. 120(4):827-41. (1994).

Iskratsch, T. et al. Formin follows function: a muscle-specific isoform of FHOD3 is regulated by CK2 phosphorylation and promotes myofibril maintenance. J Cell Biol. 191,1159-1172. (2010).

Iskratsch, T. et al. Two distinct phosphorylation events govern the function of muscle FHOD3. Cell Mol Life Sci. 70:893-908. (2013).

Italia, J.S. et al. Expanding the genetic code of mammalian cells. Biochem Soc Trans. 45(2):555-562. (2017).

Jaalouk, D.E. and Lammerding, J. Mechanotransduction gone awry. Nat. Rev. Mol. Cell Biol. 10,63-73 (2009).

Jagannathan, B. et al. Direct observation of a force-induced switch in the anisotropic mechanical unfolding pathway of a protein. Proc Natl Acad Sci USA. 109(44):17820-5. (2012).

Jahraus, A. et al. ATP-dependent Membrane Assembly of F-Actin Facilitates Membrane Fusion. Mol Biol Cell. 12(1): 155-170. (2011).

Janmey, P.A. et al. Phosphoinositide-binding peptides derived from the sequences of gelsolin and villin. J Biol Chem. 267, 11818-11823. (1992).

Jansen, K.A. et al. A guide to mechanobiology: Where biology and physics meet. Biochim Biophys Acta. 1853(11 Pt B):3043-52. (2015).

Jiang, B. et al. Sodium sulfite is a potential hypoxia inducer that mimics hypoxic stress in *Caenorhabditis elegans*. J Biol Inorg Chem. 16(2):267-74. (2011).

Johansson, M. et al. Activation of endosomal dynein motors by stepwise assembly of Rab7-RILP-p150Glued, ORP1L, and the receptor betalll spectrin. J Cell Biol. 176(4):459-471. (2007).

Johnson, C.P. et al. Pathogenic proline mutation in the linker between spectrin repeats: disease caused by spectrin unfolding. Blood. 109, 3538. (2007).

Johnson, C.P. et al. Forced unfolding of proteins within cells. Science. 317(5838):663-6. (2007).

Johnston, D. and Ahringer J. Cell polarity in eggs and epithelia: parallels and diversity. Cell. 141(5):757-74. (2010).

Johnston, R.J. et al. An unusual Zn-finger/FH2 domain protein controls a left/right asymmetric neuronal fate decision in *C. elegans*. Development. 133:3317-3328. (2006).

Jun, Y. et al. Calibration of optical tweezers for *in vivo* force measurements: how do different approaches compare? Biophys J. 107(6):1474-84. (2014).

Kalwat, M.A. and Thurmond, D.C. Signaling mechanisms of glucose-induced F-actin remodeling in pancreatic islet β cells. Exp Mol Med. 45:e37. (2013).

Kamath, R.S. et al. Systematic functional analysis of the *Caenorhabditis elegans* genome using RNAi. Nature. 421, 231-237 (2003).

Kan-O, M. et al. Mammalian formin Fhod3 plays an essential role in cardiogenesis by organizing myofibrillogenesis. Biol. Open. 1:889-896. (2012).

Katic, I. et al. CRISPR/Cas9 Genome Editing in *Caenorhabditis elegans*: Evaluation of Templates for Homology-Mediated Repair and Knock-Ins by Homology-Independent DNA Repair. G3. 3;5(8):1649-56. (2015).

Kazlauskas, A. et al. Large-Scale Screening of Preferred Interactions of Human Src Homology-3 (SH3) Domains Using Native Target Proteins as Affinity Ligands. Mol Cell Proteomics. 15(10):3270-3281. (2016).

Keller, R. and Danilchik, M. Regional expression, pattern and timing of convergence and extension during gastrulation of *Xenopus laevis*. Development. 103:193-209. (1988).

Keller, R. and Jansa, S. *Xenopus* Gastrulation without a blastocoel roof. Dev Dyn. 195:162-176. (1992).

Keller, R. et al. The forces that shape embryos: physical aspects of convergent extension by cell intercalation. Phys. Biol. 5(1):1-22. (2008).

Keller, R.E. et al. The function and mechanism of convergent extension during gastrulation of *Xenopus laevis*. J Embryol Exp Morphol. 89:185-209. (1985).

Kelley, M. et al. FBN-1, a fibrillin-related protein, is required for resistance of the epidermis to mechanical deformation during *C. elegans* embryogenesis. Elife. 4: e06565. (2015).

Kelsell, D.P. et al. Human diseases: clues to cracking the connexin code? Trends Cell Biol. 11(1):2-6. (2001).

Keren, K. Cell motility: the integrating role of the plasma membrane. Eur. Biophys J. 40,1013-1027. (2011).

Keys, D.N. et al. Control of intercalation is cell-autonomous in the notochord of Ciona intestinalis. Dev Biol. 246:329-340. (2002).

Khaitlina, S.Y. Functional specificity of actin isoforms. Int Rev Cytol. 202:35-98. (2001).

Kiehart, D.P. et al. Multiple forces contribute to cell sheet morphogenesis for dorsal closure in *Drosophila*. J Cell Biol. 149(2):471-90. (2000).

Kim, H.S. et al. VAB-10 spectraplakin acts in cell and nuclear migration in *Caenorhabditis elegans*. Development. 138 (18) 4013-4023. (2011).

Kim, H.Y. and Davidson, L.A. Punctuated actin contractions during convergent extension and their permissive regulation by the non-canonical Wnt-signaling pathway. J Cell Sci. 124(Pt 4):635-46. (2011).

Kimble, J. and Hirsh, D. The postembryonic cell lineages of the hermaphrodite and male gonads in *Caenorhabditis elegans*. Dev Biol. 70(2):396-417. (1979).

Kirschner, M. and Mitchison, T. Beyond self-assembly: from microtubules to morphogenesis. Cell. 45(3):329-42. (1986).

Kizhatil, K. et al. Ankyrin-G and beta2-spectrin collaborate in biogenesis of lateral membrane of human bronchial epithelial cells. J Biol Chem. 282(3):2029-2037. (2007).

Klaavuniemi, T. et al. *Caenorhabditis elegans* gelsolin-like protein 1 is a novel actin filament-severing protein with four gelsolin-like repeats. J Biol Chem. 283(38):26071-80. (2008).

Klein, J.S. et al. Design and characterization of structured protein linkers with differing flexibilities. Protein Eng Des Sel. 27(10):325-330. (2014).

Kloda, A. and Martinac, B. Mechanosensitive channels in archaea. Cell Biochem Biophys. 34:349-381. (2001).

Kner, P. et al. Super-resolution video microscopy of live cells by structured illumination. Nat Methods. 6(5):339-42. (2009).

Knust, E. and Müller, H.J. *Drosophila* morphogenesis: orchestrating cell rearrangements. Curr Biol. 8(23):R853-5. (1998).

Koestler, S.A. et al. Differentially oriented populations of actin filaments generated in lamellipodia collaborate in pushing and pausing at the cell front. Nat Cell Biol. 10(3):306-13. (2008).

Kolega, J. Effects of mechanical tension on protrusive activity and microfilament and intermediate filament organization in an epidermal epithelium moving in culture. J Cell Biol. 102(4):1400-11. (1986).

Komada, M. and Soriano, P. [Beta]IV-spectrin regulates sodium channel clustering through ankyrin-G at axon initial segments and nodes of Ranvier. J Cell Biol. 156(2):337-348. (2002).

Kong, D. et al. Forces directing germ-band extension in *Drosophila* embryos. Mech Dev. 144(Pt A):11-22. (2017).

Koppen, M. et al. Cooperative regulation of AJM-1 controls junctional integrity in *Caenorhabditis elegans* epithelia. Nat. Cell Biol. 3, 983-991. (2001).

Korsgren, C. and Lux, S.E. The carboxyterminal EF domain of erythroid alpha-spectrin is necessary for optimal spectrin-actin binding. Blood. 116(14):2600-2607. (2010).

Korsgren, C. et al. Protein 4.2 binds to the carboxyl-terminal EF-hands of erythroid alpha-spectrin in a calcium- and calmodulin-dependent manner. J Biol Chem. 285(7):4757-4770. (2010).

Kovar, D.R. et al. Control of the assembly of ATP- and ADP-actin by formins and profilin. Cell. 124(2):423-35. (2006).

Krendel, M. and Mooseker, M.S. Myosins: tails (and heads) of functional diversity. Physiology (Bethesda). 20:239-51. (2005).

Kreplak, L. and Fudge, D. Biomechanical properties of intermediate filaments: from tissues to single filaments and back. Bioessays. 29(1):26-35. (2007).

Krieg, M. et al. Mechanical control of the sense of touch by β-spectrin. Nat Cell Biol. 16(3):224-33. (2014).

Kuhn, J.R. and Pollard, T.D. Real-time measurements of actin filament polymerization by total internal reflection fluorescence microscopy. Biophys J. 88(2):1387-402. (2005).

Kumar, A. et al. Talin tension sensor reveals novel features of focal adhesion force transmission and mechanosensitivity. J Cell Biol. 213(3): 371-383. (2016).

Kurochkina, N. and Guha, U. SH3 domains: modules of protein-protein interactions. Biophys Rev. 5(1): 29-39. (2013).

Kusunoki, H. et al. Structural insights into the stability and flexibility of unusual erythroid spectrin repeats. Structure. 12(4):645-56. (2004).

Kutscheidt, S. et al. FHOD1 interaction with nesprin-2G mediates TAN line formation and nuclear movement. Nat Cell Biol. 16(7):708-15. (2014).

Kwiatkowski, D. J. et al. Identification of critical functional and regulatory domains in gelsolin. J Cell Biol. 108, 1717-1726. (1989).

Labouesse, M. Rac GTPase signaling in mechanotransduction during embryonic morphogenesis. Small GTPases. 2(6):305-309 (2011).

Labouesse, M. Role of the extracellular matrix in epithelial morphogenesis: a view from *C. elegans*. Organogenesis. 8(2):65-70. (2012).

Labouesse, M. Epithelial junctions and attachments. WormBook. ed. The *C. elegans* Research Community. WormBook. (2006).

Lappalainen, P. Actin-binding proteins: the long road to understanding the dynamic landscape of cellular actin networks. Mol Biol Cell. 27(16):2519-22. (2016).

Lautscham, LA. et al. Biomembrane-mimicking lipid bilayer system as a mechanically tunable cell substrate. Biomaterials. 35(10):3198-207. (2014).

Law, R. et al. Cooperativity in forced unfolding of tandem spectrin repeats. Biophys J. 84, 533. (2003).

Le Roux, A.L. et al. The plasma membrane as a mechanochemical transducer. Phil. Trans. R. Soc. B. 374.(2019).

Lecuit, T. and Lenne, P.F. Cell surface mechanics and the control of cell shape, tissue patterns and morphogenesis. Nat Rev Mol Cell Biol. 8(8):633-44 (2007).

Lecuit, T. and Yap, A.S. E-cadherin junctions as active mechanical integrators in tissue dynamics. Nat Cell Biol. 17(5):533-9. (2015).

Lee, H.G. et al. The cell adhesion molecule Roughest depends on beta(Heavy)-spectrin during eye morphogenesis in *Drosophila*. J Cell Sci. 123(Pt 2):277-285. (2010).

Legouis, R. et al. LET-413 is a basolateral protein required for the assembly of adherens junctions in *Caenorhabditis elegans*. Nat Cell Biol. 2(7):415-22. (2000).

Levayer, R. and Lecuit, T. Biomechanical regulation of contractility: spatial control and dynamics. Trends Cell Biol. 22(2):61-81. (2012).

Lieber, A.D. et al. Membrane tension in rapidly moving cells is determined by cytoskeletal forces. Curr Biol. 23,1409-1417. (2013).

Lieber, A.D. et al. Front-to-rear membrane tension gradient in rapidly moving cells. Biophys J. 108,1599-1603. (2015).

Lin, X. et al. *C. elegans* PAT-6/actopaxin plays a critical role in the assembly of integrin adhesion complexes *in vivo*. Curr Biol 13(11): 922-932. (2003).

Litjens, S.H. et al. Current insights into the formation and breakdown of hemidesmosomes. Trends Cell Biol. 16(7):376-83. (2006).

Liu, Z. et al. Distinct roles of four gelsolin-like domains of *Caenorhabditis elegans* gelsolin-like protein-1 in actin filament severing, barbed end capping, and phosphoinositide binding. Biochemistry. 49(20):4349-60. (2010).

Lodish, H. et al. Molecular Cell Biology. (4th edition). New York: W. H. Freeman. Section 19.4, Cilia and Flagella: Structure and Movement. (2000).

Lodish, H. et al. Molecular Cell Biology. (7th edition). pp. 775-815. (2013).

Long, F. et al. A 3D digital atlas of *C. elegans* and its application to single-cell analyses. Nat. Meth. 6:667-672. (2009).

Loranger, A. et al. Simple epithelium keratins are required for maintenance of hepatocyte integrity. Am J Pathol. 151(6):1673-1683. (1997).

Lorenzo, D.N. et al. Spectrin mutations that cause spinocerebellar ataxia type 5 impair axonal transport and induce neurodegeneration in *Drosophila*. J Cell Biol. 189(1):143-158. (2010).

Lux, S.E. Anatomy of the red cell membrane skeleton: unanswered questions. Blood. 127(2):187-99. (2016).
Machnicka, B. et al. Spectrin-based skeleton as an actor in cell signaling. Cell Mol Life Sci. 69(2):191-201. (2012).

Machnicka, B. et al. Spectrins: a structural platform for stabilization and activation of membrane channels, receptors and transporters. Biochim Biophys Acta. 1838(2):620-34. (2014).

Mackinnon, A.C. et al. *C. elegans* PAT-4/ILK functions as an adaptor protein within integrin adhesion complexes. Curr Biol. 12(10):787-97. (2002).

Maki, K. et al. Nano-mechanical characterization of tension-sensitive helix bundles in talin rod. Biochem Biophys Res Commun. 484,372-377. (2017).

Mancuso, V.P. et al. Extracellular leucine-rich repeat proteins are required to organize the apical extracellular matrix and maintain epithelial junction integrity in *C. elegans*. Development. 139(5):979-90. (2012).

Mango, S.E. The *C. elegans* pharynx: a model for organogenesis. WormBook. 22:1-26. (2007).

Marchesi, V.T. and Steers, E. Selective solubilization of a protein component of the red cell membrane. Science. 159(3811):203-4. (1968).

Marciano, D.K. A Holey Pursuit: Lumen formation in the Developing Kidney. Pediatr Nephrol. 32(1): 7-20. (2017).

Marieb, E.M. Human Anatomy and Physiology (3rd ed.). Benjamin/Cummings. pp. 103-104. (1995).

Marshall, W.F. and Rosenbaum, J.L. Cell division: The renaissance of the centriole. Curr Biol. 9(6):R218-20. (1999).

Marston, D.J. and Goldstein, B. Actin-based forces driving embryonic morphogenesis in *Caenorhabditis elegans*. Curr Opin Genet Dev. 16(4):392-8. (2006).

Martin, A.C. and Goldstein B. Apical constriction: themes and variations on a cellular mechanism driving morphogenesis. Development. 141(10):1987-98. (2014).

Martin, A.C. et al. Pulsed contractions of an actin-myosin network drive apical constriction. Nature. 457(7228):495-9. (2009).

Martin, A.C., et al. Integration of contractile forces during tissue invagination. J Cell Biol. 188(5):735-749. (2010).

Martinac, B. et al. Ion channels in microbes. Physiol Rev. 88:1449-1490. (2008).

Martinez, J.C. and Serrano, L. The folding transition state between SH3 domains is conformationally restricted and evolutionarily conserved. Nat Struct Biol. 6(11):1010-6. (1999).

Martino, F. et al. Cellular Mechanotransduction: From Tension to Function. Front Physiol. 9:824. (2018).

Mason, F.M. and Martin, A.C. Tuning cell shape change with contractile ratchets. Curr Opin Genet Dev. 21(5):671-9. (2011).

Mathur, J. and Hülskamp, M. Microtubules and microfilaments in cell morphogenesis in higher plants. Curr Biol. 12(19):R669-76. (2002).

Matthews, I. et al. The template update problem. IEEE Trans Pattern Anal Mach Intell. 26(6):810-5. (2004).

McCullough, B.R. et al. Cofilin-linked changes in actin filament flexibility promote severing. Biophys J 101, 151-159. (2011).

McGough, A. et al. Cofilin changes the twist of F-actin: implications for actin filament dynamics and cellular function. J Cell Biol. 138,771-781. (1997).

McGough, A.M. and Josephs, R. On the structure of erythrocyte spectrin in partially expanded membrane skeletons. Proc Natl Acad Sci USA. 87(13):5208-12. (1990).

McKay, S.J. et al. Gene expression profiling of cells, tissues, and developmental stages of the nematode *C. elegans*. Cold Spring Harb Symp Quant Biol. 68:159-69. (2003).

McKeown, C. et al. *sma-1* encodes a betaH-spectrin homolog required for *Caenorhabditis elegans* morphogenesis. Development. 125(11):2087-98. (1998).

McMahon, L. et al. Assembly of *C. elegans* apical junctions involves positioning and compaction by LET-413 and protein aggregation by the MAGUK protein DLG-1. J Cell Sci. *114*, 2265-2277. (2001).

Mehboob, S. et al. Crystal structure of the nonerythroid alpha-spectrin tetramerization site reveals differences between erythroid and nonerythroid spectrin tetramer formation. J Biol Chem. 285(19):14572-84. (2010).

Meier, S. Development of the chick embryo mesoblast: morphogenesis of the prechordal plate and cranial segments. Dev Biol. 83(1):49-61. (1981).

Meili, R. et al. Myosin II is essential for the spatiotemporal organization of traction forces during cell motility. Mol Biol Cell. 21(3):405-17. (2010).

Meng, W. and Takeichi, M. Adherens Junction: Molecular Architecture and Regulation. Cold Spring Harb Perspect Biol. 1(6): a002899. (2009).

Mi-Mi, L. et al. Z-line formins promote contractile lattice growth and maintenance in striated muscles of *C. elegans*. J Cell Biol. 198, 87-102. (2012).

Mi-Mi, L. and Pruyne, D. Loss of Sarcomere-associated Formins Disrupts Z-line Organization, but does not Prevent Thin Filament Assembly in *Caenorhabditis elegans* Muscle. J Cytol Histol. 6:318. (2015).

Miura, T. Models of lung branching morphogenesis. J Biochem. 157(3):121-7. (2015).

Miyazaki, K. and Takenouchi. M. Creating random mutagenesis libraries using megaprimer pcr of whole plasmid. Biotechniques. 33(5):1033-4. (2002).

Moerman, D.G., and Fire, A. Muscle: Structure, function and development. In *C. elegans* II, D.L. Riddle, T. Blumenthal, B.J. Meyer, and J.R. Priess, eds. (Cold Spring Harbor: Cold Spring Harbor Press), pp. 417-470. (1997).

Moerman, D.G. and Williams, B.D. Sarcomere assembly in *C. elegans* muscle. WormBook. 16:1-16. ed. The *C. elegans* Research Community. WormBook. (2006).

Mohler, W.A. et al. Dynamics and ultrastructure of developmental cell fusions in the *Caenorhabditis elegans* hypodermis. Curr Biol. 8(19):1087-90. (1998).

Montell, D.J. Morphogenetic Cell Movements: Diversity from Modular Mechanical Properties. Science. 322(5907):1502-1505. (2008).

Moore, S.W. et al. The dorsal involuting marginal zone stiffens anisotropically during its convergent extension in the gastrula of *Xenopus laevis*. Development. 121:3131-3140. (1995).

Moorthy, S. et al. *Caenorhabditis elegans* beta-G spectrin is dispensable for establishment of epithelial polarity, but essential for muscular and neuronal function. J Cell Biol. 149(4):915-30. (2000).

Munjal, A. et al. A self-organized biomechanical network drives shape changes during tissue morphogenesis. Nature. 524(7565):351-5. (2015).

Munoz, J. J. and Albo, S. Physiology-based model of cell viscoelasticity. Phys Rev E Stat Nonlin Soft Matter Phys. 88, 012708. (2013).

Munro, E. et al. Cortical flows powered by asymmetrical contraction transport PAR proteins to establish and maintain anterior-posterior polarity in the early *C. elegans* embryo. Dev Cell. 7(3):413-24. (2004).

Munro, E.M. and Odell, G.M. Polarized basolateral cell motility underlies invagination and convergent extension of the ascidian notochord. Development. 129:13-24. (2002).

Munro, M.J. et al. Hypotensive extremely low birth weight infants have reduced cerebral blood flow. Pediatrics. 114(6):1591-6 (2004).

Murrell, M. et al. Forcing cells into shape: the mechanics of actomyosin contractility. Nat Rev Mol Cell Biol. 16(8):486-98. (2015).

Naganathan, S.R. et al. Morphogenetic degeneracies in the actomyosin cortex. Elife. 7. (2018).

Neuhuber, B. et al. Reevaluation of *in vitro* differentiation protocols for bone marrow stromal cells: disruption of actin cytoskeleton induces rapid morphological changes and mimics neuronal phenotype. J Neurosci Res. 77(2):192-204. (2004).

Nicholson-Dykstra, S. et al. Actin dynamics: growth from dendritic branches. Curr Biol. 15(9):R346-57. (2005).

Nievers, N.G. et al. Biology and function of hemidesmosomes. Matrix Biol. 18(1):5-17. (1999).

Nishikawa, M. et al. Controlling contractile instabilities in the actomyosin cortex. Elife. 6. pii:e19595. (2017).

Nishimura, T. et al. Planar cell polarity links axes of spatial dynamics in neural-tube closure. Cell. 149:1084-1097. (2012).

Nolz, J.C. et al. WAVE2 regulates high-affinity integrin binding by recruiting vinculin and talin to the immunological synapse. Mol Cell Biol. 27:5986-6000. (2007).

Nomura, K. and Ono, S. ATP-dependent regulation of actin monomer-filament equilibrium by cyclase-associated protein and ADF/cofilin. Biochem J. 453 (2) 249-259. (2013).

Norman, K.R., and Moerman, D.G. Alpha spectrin is essential for morphogenesis and body wall muscle formation in *Caenorhabditis elegans*. J Cell Biol. May 13;157(4):665-77. (2002).

Ohashi, K. et al. Roles of the cytoskeleton, cell adhesion and rho signaling in mechanosensing and mechanotransduction. J Biochem. 161,245-254. (2017).

Ortega, E. et al. The structure of the plakin domain of plectin reveals a non-canonical SH3 domain interacting with its fourth spectrin repeat. J Biol Chem. 286 (14) 12429-12438. (2011).

Page, A.P. and Johnstone, I.L. The cuticle. WormBook. 19:1-15. ed. The *C. elegans* Research Community. WormBook. (2007).

Page, B.D. et al. ELT-1, a GATA-like transcription factor, is required for epidermal cell fates *in Caenorhabditis elegans* embryos. Genes Dev. 11(13),1651-1661. (1997).

Paluch, E.K. and Heisenberg, C.P. Biology and physics of cell shape changes in development. Curr Biol. 19(17): R790-799. (2009).

Paluch, E.K. et al. Mechanotransduction: use the force(s). BMC Biol. 13: 47. (2015).

Pan, L. et al. Super-Resolution Microscopy Reveals the Native Ultrastructure of the Erythrocyte Cytoskeleton. Cell Rep. 22(5):1151-1158. (2018).

Paramore, S. and Voth, G.A. Examining the influence of linkers and tertiary structure in the forced unfolding of multiple-repeat spectrin molecules. Biophys J. 91, 3436. (2006).

Pardee, J.D. and Spudich, J.A. Purification of muscle actin. Methods Enzymol. 85, 164-181. (1982).

Parkinson, N.J. et al. Mutant beta-spectrin 4 causes auditory and motor neuropathies in quivering mice. Nat Genet. 29(1):61-65. (2001).

Parton, R.G. and Simons, K. The multiple faces of caveolae. Nat. Rev. Mol. Cell Biol. 8,185-194. (2007).

Partridge, M.A. and Marcantonio, E.E. Initiation of attachment and generation of mature focal adhesions by integrin-containing filopodia in cell spreading. Mol. Biol. Cell. 17(10):4237-48. (2006).

Pascual, J. et al. Solution structure of the spectrin repeat: a left-handed antiparallel triple-helical coiled-coil. J Mol Biol. 273(3):740-51. (1977).

Pasternak, C. et al. Capping of surface receptors and concomitant cortical tension are generated by conventional myosin. Nature. 341:549-551. (1989).

Pásti, G. and Labouesse, M. Epithelial junctions, cytoskeleton, and polarity. WormBook. ed. The *C. elegans* Research Community. WormBook. (2014).

Patel, A.A. et al. *Drosophila* and human FHOD family formin proteins nucleate actin filaments. J Biol Chem. 293(2):532-540. (2018).

Pelham, R.J. and Wang, Y.I. Cell locomotion and focal adhesions are regulated by substrate flexibility. Proc Natl Acad Sci USA. 94(25):13661-5. (1997).

Peralta, X.G. et al. Upregulation of forces and morphogenic asymmetries in dorsal closure during *Drosophila* development. Biophys J. 92:2583-2596. (2007).

Pestonjamasp, K.N. et al. Supervillin (p205): A novel membrane-associated, F-actin-binding protein in the villin/gelsolin superfamily. J Cell Biol. 139 (5): 1255-69. (1997).

Phillips, M.D. and Thomas, G.H. (2006). Brush border spectrin is required for early endosome recycling in *Drosophila*. J Cell Sci. 119(7):1361-1370. (2006).

Piekny, A.J. et al. Embryonic morphogenesis in *Caenorhabditis elegans* integrates the activity of LET-502 Rho-binding kinase, MEL-11 myosin phosphatase, DAF-2 insulin receptor and FEM-2 PP2c phosphatase. Genetics. 156:1671-89. (2000).

Piekny, A.J. et al. The *Caenorhabditis elegans* non-muscle myosin genes nmy-1 and nmy-2 function as redundant components of the let-502/Rho-binding kinase and mel-11/myosin phosphatase pathway during embryonic morphogenesis. Development. 130(23):5695-5704. (2003).

Piekny, A.J. et al. Squeezing an egg into a worm: *C. elegans* embryonic morphogenesis. ScientificWorldJournal. 3:1370-81. (2003).

Pilhofer, M. et al. Microtubules in bacteria: ancient tubulins build a five-protofilament homolog of the eukaryotic cytoskeleton. PLoS Biol. 9(12):e1001213. (2011).

Pilot, F. and Lecuit T. Compartmentalized morphogenesis in epithelia: from cell to tissue shape. Dev Dyn. 232(3):685-94. (2005).

Plastino, J. and Blanchoin, L. Dynamic stability of the actin ecosystem. J Cell Sci. 132(4). (2018).

Podbilewicz, B. Cell fusion. WormBook. ed. The *C. elegans* Research Community. WormBook. (2000).

Podbilewicz, B. and White, J.G. Cell fusions in the developing epithelial of *C. elegans*. Dev Biol. 161(2):408-24. (1994).

Pollard, T.D. and Borisy, G.G. Cellular motility driven by assembly and disassembly of actin filaments. Cell. 112(4):453-65. (2003).

Pollard, T.D. and Cooper, J.A. Actin, a central player in cell shape and movement. Science. 326(5957):1208-12. (2009).

Polte, T.R. et al. Extracellular matrix controls myosin light chain phosphorylation and cell contractility through modulation of cell shape and cytoskeletal prestress. Am J Physiol., Cell Physiol. 286(3):C518-28. (2004).

Pontes, B. et al. Membrane tension controls adhesion positioning at the leading edge of cells. J Cell Biol. 216,2959. (2017).

Pontes, B. et al. Membrane tension: a challenging but universal physical parameter in cell biology. Semin Cell Dev Biol. 71,30-41. (2017).

Ponti, A. et al. Two distinct actin networks drive the protrusion of migrating cells. Science. 305(5691):1782-6. (2004).

Pope, B. et al. Localization of the calcium-sensitive actin monomer binding site in gelsolin to segment 4 and identification of calcium binding sites. Biochemistry. 34,1583-1588. (1995).

Pope, R.K. et al. Cloning, characterization, and chromosomal localization of human superillin (SVIL). Genomics. 52(3):342-51. (1998).

Praitis, V., et al. SMA-1 spectrin has essential roles in epithelial cell sheet morphogenesis in *C. elegans*. Dev Biol. 283,157-170 (2005).

Priess, J.R. and Hirsh, D.I. *Caenorhabditis elegans* morphogenesis: the role of the cytoskeleton in elongation of the embryo. Dev Biol. 117, 156-173 (1986).

Prout, M. et al. Autosomal mutations affecting adhesion between wing surfaces in *Drosophila melanogaster*. Genetics. 146:275-85. (1997).

Pruyne, D. Revisiting the Phylogeny of the Animal Formins: Two New Subtypes, Relationships with Multiple Wing Hairs Proteins, and a Lost Human Formin. PLoS One. 11: e0164067. (2016).

Quintin, S. et al. Non-centrosomal epidermal microtubules act in parallel to let-502/rock to promote *C. elegans* elongation. Development. 143(1):160-173. (2016).

Raharjo, W.H. et al. Cell architecture: surrounding muscle cells shape gland cell morphology in the *Caenorhabditis elegans* pharynx. Genetics. 189(3):885-97. (2011).

Rahikainen, R. et al. Mechanical stability of talin rod controls cell migration and substrate sensing. Sci. Rep. 7:3571. (2017).

Randles, L.G. et al. Spectrin domains lose cooperativity in forced unfolding. Biophys J. 92(2):571-7. (2007).

Rauzi, M. et al. Nature and anisotropy of cortical forces orienting *Drosophila* tissue morphogenesis. Nat Cell Biol. 10(12):1401-10. (2008).

Rauzi, M. et al. Planar polarized actomyosin contractile flows control epithelial junction remodelling. Nature. 468(7327):1110-4. (2010).

Rauzi, M. et al. Embryo-scale tissue mechanics during *Drosophila* gastrulation movements. Nat Commun. 6:8677. (2015).

Reed, R.A. et al. Morphogenesis of the primitive gut tube is generated by Rho/ROCK/myosin II-mediated endoderm rearrangements. Dev Dyn. 238(12):3111-3125. (2009).

Refai, O. et al. Tissue-Specific Functions of fem-2/PP2c Phosphatase and fhod-1/formin During *Caenorhabditis elegans* Embryonic Morphogenesis. G3 (Bethesda). 8(7): 2277-2290. (2018).

Reisler, E. Actin molecular structure and function. Curr Opin Cell Biol. 5 (1): 41-7. (1993).

Rid, R. et al. The last but not the least: the origin and significance of trailing adhesions in fibroblastic cells. Cell Motil. Cytoskeleton. 61(3):161-71. (2005).

Rief, M. et al. The mechanical stability of immunoglobulin and fibronectin III domains in the muscle protein titin measured by atomic force microscopy. Biophys J. 75(6):3008-14. (1998).

Rief, M. et al. Single molecule force spectroscopy of spectrin repeats: low unfolding forces in helix bundles. J Mol Biol. 286(2):553-61. (1999).

Risca, V.I. et al. 2012. Actin filament curvature biases branching direction. Proc Natl Acad Sci USA. 109,2913-2918.

Rivera-Pérez, J.A. and Hadjantonakis, A.K. The Dynamics of Morphogenesis in the Early Mouse Embryo. Cold Spring Harb Perspect Biol. 7(11). pii: a015867. (2014).

Rodriguez-Boulan, E. and Macara, I.G. Organization and execution of the epithelial polarity programme. Nat Rev Mol Cell Biol. 15(4):225-242. (2014).

Rogalski, T.M. et al. Mutations in the unc-52 gene responsible for body wall muscle defects in adult *Caenorhabditis elegans* are located in alternatively spliced exons. Genetics. 139(1):159-69. (1995).

Rogalski, T. M., et al. The UNC-112 gene in *Caenorhabditis elegans* encodes a novel component of cell-matrix adhesion structures required for integrin localization in the muscle cell membrane. J Cell Biol. 10:150(1):253-264 (2000).

Rogers, K.K. et al. The Rho family of small GTPases is involved in epithelial cystogenesis and tubulogenesis. Kidney Int. 63(5):1632-1644. (2003).

Roh-Johnson, M. et al. Triggering a cell shape change by exploiting preexisting actomyosin contractions. Science. 335(6073):1232-5 (2012).

Rohs, R. et al. Unraveling proteins: a molecular mechanics study. Biophys J. 76(5):2760-8. (1999).

Roper, K. et al. The 'spectraplakins': cytoskeletal giants with characteristics of both spectrin and plakin families. J Cell Sci. 115(Pt 22):4215-25. (2002).

Rottner, K. and Stradal, T.E. Actin dynamics and turnover in cell motility. Curr Opin Cell Biol. 23(5):569-78. (2011).

Ruff, C. et al. Single-molecule tracking of myosins with genetically engineered amplifier domains. Nat Struct Biol. 8(3):226-9. (2001).

Sackmann, E. How actin/myosin crosstalks guide the adhesion, locomotion and polarization of cells. Biochim Biophys Acta. 1853(11 Pt B):3132-42. (2015).

Saha, S. et al. Joining forces: crosstalk between biochemical signalling and physical forces orchestrates cellular polarity and dynamics. Phil. Trans. R. Soc. B. 373,20170145. (2018).

Saifee, O. et al. The *Caenorhabditis elegans* unc-64 locus encodes a syntaxin that interacts genetically with synaptobrevin. Mol Biol Cell. 9(6):1235-52. (1998).

Sakakibara, A. et al. Microtubule dynamics in neuronal morphogenesis. Open Biol. 3(7):130061. (2013).

Salbreux, G. et al. Actin cortex mechanics and cellular morphogenesis. Trends Cell Biol. 22(10):536-45. (2012).

Sawada, Y. et al. Force sensing by mechanical extension of the Src family kinase substrate p130Cas. Cell. 127:1015-1026. (2006).

Sawyer, J.K. et al. A contractile actomyosin network linked to adherens junctions by canoe/afadin helps drive convergent extension. Mol Biol Cell. 22(14):2491-508. (2011).

Sawyer, J.M. et al. Apical constriction: a cell shape change that can drive morphogenesis. Dev Biol. 341(1):5-19. (2009).

Schierenberg, E. et al. Cell lineages and developmental defects of temperature-sensitive embryonic arrest mutants in *Caenorhabditis elegans*. Dev Biol. 76(1):141-59. (1980).

Schmitz, C. et al. Axon guidance genes identified in a large-scale RNAi screen using the RNAi-hypersensitive *Caenorhabditis elegans* strain *nre-1(hd20) lin-15b(hd126*). Proc Natl Acad Sci USA. 104(3): 834-839. (2007).

Schonichen, A. et al. FHOD1 is a combined actin filament capping and bundling factor that selectively associates with actin arcs and stress fibers. J Cell Sci. 126, 1891-1901. (2013).

Schulte, A. et al. The human formin FHOD1 contains a bipartite structure of FH3 and GTPase binding domains required for activation. Structure. 16:1313-23. (2008).

Segbert, C. et al. Molecular and functional analysis of apical junction formation in the gut epithelium of *Caenorhabditis elegans*. Dev Biol. 266, 17-26. (2004).

Sens, P. and Plastino, J. Membrane tension and cytoskeleton organization in cell motility. J Phys Condens Matter. 27,273103. (2015).

Severson, A.F. et al. A Formin Homology Protein and a Profilin Are Required for Cytokinesis and Arp2/3-Independent Assembly of Cortical Microfilaments in *C. elegans*. Curr Biol. 12:2066-2075. (2002).

Shaye, D.D. and Greenwald, I. The Disease-Associated Formin INF2/EXC-6 Organizes Lumen and Cell Outgrowth during Tubulogenesis by Regulating F-Actin and Microtubule Cytoskeletons. Dev Cell. 32:743-755. (2015).

Shaye, D.D. and Greenwald, I. A network of conserved formins, regulated by the guanine exchange factor EXC-5 and the GTPase CDC-42, modulates tubulogenesis *in vivo*. Development. 143:4173-4181. (2016).

Shelton, C.A. et al. The nonmuscle myosin regulatory light chain gene mlc-4 is required for cytokinesis, anterior-posterior polarity, and body morphology during *Caenorhabditis elegans* embryogenesis. J Cell Biol. 146(2):439-51. (1999).

Shih, J. and Keller R. Patterns of cell motility in the organizer and dorsal mesoderm of *Xenopus laevis*. Development. 116:915-930. (1992).

Shimozawa, T. and Ishiwata, S. Mechanical distortion of single actin filaments induced by external force: detection by fluorescence imaging. Biophys J. 96,1036-1044. (2009).

Shindo, A. Models of convergent extension during morphogenesis. Wiley Interdiscip Rev Dev Biol. 7(1). (2018).

Siang, L.C. et al. Modeling cell intercalation during *Drosophila* germband extension. Phys Biol. 15(6):066008. (2018).

Simoes, S.M. et al. Rho GTPase and Shroom direct planar polarized actomyosin contractility during convergent extension. J Cell Biol. 204(4):575-89. (2014).

Simon, C. et al. Interplay between membrane tension and the actin cytoskeleton determines shape changes. Phys. Biol. 15,65004. (2018).

Simsek, AN. et al. Substrate-rigidity dependent migration of an idealized twitching bacterium. Soft Matter. 23. (2019).

Singh, A. et al. Polarized microtubule dynamics directs cell mechanics and coordinates forces during epithelial morphogenesis. Nat Cell Biol. 20(10):1126-1133. (2018).

Sit, S.T. and Manser, E. Rho GTPases and their role in organizing the actin cytoskeleton. J Cell Sci. (2011).

Slack, F. and Ruvkun, G. Temporal pattern formation by heterochronic genes. Annu. Rev. Gen. 31: 611-634. (1997).

Smith, S.A. et al. Dysfunction in the βII spectrin-dependent cytoskeleton underlies human arrhythmia. Circulation. 131(8):695-708. (2015).

Sokolow, A. et al. Cell ingression and apical shape oscillations during dorsal closure in *Drosophila*. Biophys J. 102(5):969-79. (2012).

Solon, J. et al., Pulsed forces timed by a ratchet-like mechanism drive directed tissue movement during dorsal closure. Cell. 137(7):1331-42 (2009).

Somlyo, A.P. and Somlyo, A.V. Signal transduction by G-proteins, rho-kinase and protein phosphatase to smooth muscle and non-muscle myosin II. J Physiol. 522:177-85. (2000).

Sonnenberg, A. and Liem, R.K.H. Plakins in development and disease. Exp Cell Res. 313(10):2189-203. (2007).

Sonnenberg, A. et al. The structure of a tandem pair of spectrin repeats of plectin reveals a modular organization of the plakin domain. J Mol Biol. 368(5)1379-1391. (2007).

Sönnichsen, B. et al. Full-genome RNAi profiling of early embryogenesis in *Caenorhabditis elegans*. Nature. 434(7032):462-9. (2005).

Sotomayor, M. and Schulten, K. Single-molecule experiments *in vitro* and in silico. Science. 316(5828):1144-8. (2007).

Stankewich, M.C. et al. Targeted deletion of betaIII spectrin impairs synaptogenesis and generates ataxic and seizure phenotypes. Proc Natl Acad Sci USA. 107(13):6022-6027. (2010).

Stokke, B.T. et al. Spectrin, human erythrocyte shapes, and mechanochemical properties. Biophys J. 49(1): 319-327. (1986).

Stossel, T.P. et al. Cell surface actin remodeling. J Cell Sci. 119(Pt 16):3261-4. (2006).

Stricker, J. et al. Mechanics of the F-actin cytoskeleton. J Biomech. 43(1):9-14. (2010).

Sullivan-Brown, J. and Goldstein, B. Neural tube closure: the curious case of shrinking junctions. Curr Biol. 22(14):R574-6. (2012).

Sulston, J.E. and Horvitz, H.R. Post-embryonic cell lineages of the nematode, *Caenorhabditis elegans*. Dev Biol. 56(1):110-56. (1977).

Sulston, J.E. et al. The embryonic cell lineage of the nematode *Caenorhabditis elegans*. Dev Biol. 100(1):64-119. (1983).

Suman, S.K. et al. The *C. elegans* plectin homologue VAB-10 acts as a hemidesmosome mechanosensor. BioRxiv. (2019).

Summerbell, D. and Wolpert L. Cell density and cell division in the early morphogenesis of the chick wing. Nat New Biol. 239(88):24-6. (1972).

Summerbell, D. and Wolpert L. Precision of development in chick limb morphogenesis. Nature. 244(5413):228-30. (1973).

Sun, H.Q. et al. The actin side-binding domain of gelsolin also caps actin filaments. Implications for actin filament severing. J Biol Chem. 269, 9473-9479. (1994).

Sun, H.Q. et al. Gelsolin, a multifunctional actin regulatory protein. J Biol Chem. 274(47):33179-82. (1999).

Suozzi, K.C. et al. Spectraplakins: master orchestrators of cytoskeletal dynamics. J Cell Biol. 197 (4) 465-475. (2012).

Supatto, W. et al. *In vivo* modulation of morphogenetic movements in *Drosophila* embryos with femtosecond laser pulses. Proc Natl Acad Sci USA. 102:1047-1052. (2005).

Suraneni, P. A mechanism of leading-edge protrusion in the absence of Arp2/3 complex. Mol Biol Cell. 26(5): 901-912. (2015).

Svitkina, T.M. and Borisy, G.G. Arp2/3 complex and actin depolymerizing factor/cofilin in dendritic organization and treadmilling of actin filament array in lamellipodia. J Cell Biol. 145(5):1009-26. (1999).

Svitkina, T.M. et al. Analysis of the actin-myosin II system in fish epidermal keratocytes: mechanism of cell body translocation. J Cell Biol. 139(2):397-415. (1997).

Takeichi, M. Dynamic contacts: rearranging adherens junctions to drive epithelial remodelling. Nat Rev Mol Cell Biol. 15(6):397-410. (2014).

Takeya, R. et al. The mammalian formin FHOD1 is activated through phosphorylation by ROCK and mediates thrombin-induced stress fibre formation in endothelial cells. EMBO J. 27:618-28. (2008).

Tang, N. and Marshall, W.F. Centrosome positioning in vertebrate development. Cell Sci. 125(Pt 21):4951-61. (2012).

Taniguchi, K. et al. Mammalian formin fhod3 regulates actin assembly and sarcomere organization in striated muscles. J Biol Chem. 284, 29873-29881. (2009).

Theocharis, A.D. et al. Extracellular matrix structure. Adv Drug Deliv Rev. 97:4-27. (2016).

Thomas, G.H. and Kiehart, D.P. βHeavy-spectrin has a restricted tissue and subcellular distribution during *Drosophila* embryogenesis. Development. 120, 2039-2050. (1994).

Thompson, A.W. On Growth and Form. Cambridge University Press. (1917).

Topczewski, J. et al. The zebrafish glypican knypek controls cell polarity during gastrulation movements of convergent extension. Dev Cell. 1:251-264. (2001).

Townes, P.L. and Holtfreter, J. Directed movements and selective adhesion of embryonic amphibian cells. Exp Zool A Comp Exp Biol. 301(9):701-6. (1955).

Trelstad, R.L. Cell contact during early morphogenesis in the chick embryo. Dev Biol. 16(1):78-106. (1967).

Tsopoulidis, N. et al. T cell receptor-triggered nuclear actin network formation drives CD4+ T cell effector functions. Sci Immunol. 4(31). pii: eaav1987. (2019).

Tsujita, K. et al. Feedback regulation between plasma membrane tension and membrane-bending proteins organizes cell polarity during leading edge formation. Nat. Cell Biol. 17,749-758. (2015).

Turing, A.M. The Chemical Basis of Morphogenesis. Bull Math Biol. 52(1-2):153-97; discussion 119-52. (1952).

Urwyler, O. et al. *Drosophila* sosie functions with β(H)-Spectrin and actin organizers in cell migration, epithelial morphogenesis and cortical stability. Biol Open. 1(10):994-1005. (2012).

Uyeda, T.Q. et al. Stretching actin filaments within cells enhances their affinity for the myosin II motor domain. PLoS One. 6,e26200. (2011).

Vale, R.D. et al. Identification of a novel force-generating protein, kinesin, involved in microtubule-based motility. Cell. 42(1):39-50. (1985).

Valencia, R.G. et al. Intermediate filament-associated cytolinker plectin 1c destabilizes microtubules in keratinocytes. Mol. Biol. Cell. 24(6)768-784. (2013).

Vanneste, C.A., et al. The role of the formin gene *fhod-1* in *C. elegans* embryonic morphogenesis. Worm. 2(3):e25040. (2013).

Vasquez, C.G. et al. Dynamic myosin phosphorylation regulates contractile pulses and tissue integrity during epithelial morphogenesis. J Cell Biol. 206(3):435-50. (2014).

Verkhovsky, A.B. et al. Myosin II filament assemblies in the active lamella of fibroblasts: their morphogenesis and role in the formation of actin filament bundles. J Cell Biol. 131(4):989-1002. (1995).

Verstraeten, B. et al. Zebrafish teeth as a model for repetitive epithelial morphogenesis: dynamics of E-cadherin expression. BMC Dev Biol. 10:58. (2010).

Vicente-Manzanares, M. et al. Regulation of protrusion, adhesion dynamics, and polarity by myosins IIa and IIb in migrating cells. J Cell Biol. 176(5):573-80. (2007).

Vicente-Manzanares, M. et al. Non-muscle myosin II takes centre stage in cell adhesion and migration. Nat Rev Mol Cell Biol. 10(11):778-90. (2009).

Vinson, V. Expanding the genetic code in vertebrates. Science. 355(6320):36. (2017).

Vogel, V. and Sheetz, M.P. Cell fate regulation by coupling mechanical cycles to biochemical signaling pathways. Curr Opin Cell Biol. 21:38-46. (2009).

Von Ehrenstein, G. and Schierenberg, E. Cell lineages and development of *Caenorhabditis elegans* and other nematodes. In Nematodes as biological models Vol. I, Behavioral and developmental models (ed. Zuckerman, B.M.). Chapter 1. pp 2-68. Academic Press, New York. (1980).

Von Stetina, S.E. and Mango, S.E. PAR-6, but not E-cadherin and β-integrin, is necessary for epithelial polarization in *C. elegans.* Dev Biol. 403(1):5-14. (2015).

Vuong-Brender, T.T. et al. The interplay of stiffness and force anisotropies drives embryo elongation. Elife. 6. (2017).

Vuong-Brender, T.T. et al. The apical ECM preserves embryonic integrity and distributes mechanical stress during morphogenesis. Development. 144, 4336-4349. (2017).

Vuong-Brender, T.T. et al. *C. elegans* Embryonic Morphogenesis. Curr Top Dev Biol. 116, 597-616. (2016).

Walko, G. et al. Molecular architecture and function of the hemidesmosome. Cell Tissue Res. 360(2):363-78. (2015).

Wallingford, J.B. and Harland, R.M. Neural tube closure requires dishevelled-dependent convergent extension of the midline. Development. 129:5815-5825. (2002).

Wallingford, J.B. et al. Convergent extension: the molecular control of polarized cell movement during embryonic development. Dev Cell. 2(6):695-706. (2002).

Walsh, E.P. and Brown, N.H. A screen to identify *Drosophila* genes required for integrin-mediated adhesion. Genetics. 150:791-805. (1198).

Wang N, and Suo Z. Long-distance propagation of forces in a cell. Biochem Biophys Res Commun. 328(4):1133-8. (2005).

Wang, N. Review of cellular mechanotransduction. J Phys D Appl Phys. 50(23). pii: 233002. (2017).

Wang, S. et al. Characterization and development of photoactivatable fluorescent proteins for single molecule-based super resolution imaging. Proc Natl Acad Sci USA. 111(23):8452-8457. (2014).

Wang, Y. and Kanchanawong, P. Three-dimensional super resolution microscopy of F-actin filaments by interferometric photoactivated localization microscopy (iPALM). JoVE. 118,e54774. (2016).

Waterston, R.H. Muscle. In The nematode *C. elegans*. (W. B. Wood ed.) pp281-335. Cold Spring Harbor Laboratory Press, New York. (1988).

Waterston, R.H. The minor myosin heavy chain, mhcA, of *Caenorhabditis elegans* is necessary for the initiation of thick filament assembly. EMBO J. 8(11):3429-36 (1989).

Way, M. et al. Identification of a region in segment 1 of gelsolin critical for actin binding. EMBO J. 9,4103-4109. (1990).

Weaver, V.M. et al. Reversion of the malignant phenotype of human breast cells in three-dimensional culture and *in vivo* by integrin blocking antibodies. J Cell Biol. 137:231-245. (1997).

Weber, A. et al. Role of the N- and C-terminal actin-binding domains of gelsolin in barbed filament end capping. Biochemistry. 30,9327-9334. (1991).

Weisenberg. R.C. Microtubule formation *in vitro* in solutions containing low calcium concentrations. Science. 177(4054):1104-5. (1972).

Weisenberg, R.C. et al. Tubulin-nucleotide interactions during the polymerization and depolymerization of microtubules. Biochemistry. 15(19):4248-4254. (1976).

Weliky, M. et al. Notochord morphogenesis in *Xenopus laevis*: simulation of cell behavior underlying tissue convergence and extension. Development. 113(4):1231-44. (1991).

White, J.G. et al. The structure of the nervous system of the nematode *Caenorhabditis elegans*. Phil. Trans. R. Soc. Lond. B. (1165):1-340. (1986).

White, J.G. et al. Getting into the mind of a worm - a personal view. ed. The *C. elegans* Research Community. WormBook. k. 1-10. (2013).

Wieschaus, E. et al. Convergence and Extension during Germband Elongation in *Drosophila* Embryos. In: Keller R., Clark W.H., Griffin F. (eds) Gastrulation. Bodega Marine Laboratory Marine Science Series. Springer, Boston, MA. (1991).

Willecke, K. et al. Structural and functional diversity of connexin genes in the mouse and human genome. Biol Chem. 383(5):725-737. (2002).

Williams, B.D. and Waterston, R.H. Genes critical for muscle development and function in *Caenorhabditis elegans* identified through lethal mutations. J Cell Biol. 124(4):475-90 (1994).

Williams, M. et al. Distinct apical and basolateral mechanisms drive planar cell polarity-dependent convergent extension of the mouse neural plate. Dev Cell. 29:34-46. (2014).

Williams-Masson, E.M. et al. An actin-mediated two-step mechanism is required for ventral enclosure of the *C. elegans* hypodermis. Development. 124:2889-2901. (1997).

Williams-Masson, E.M. et al. The cellular mechanism of epithelial rearrangement during morphogenesis of the *Caenorhabditis elegans* dorsal hypodermis. Dev Biol. 204,263-276. (1998).

Winder, S.J. and Ayscough, K.R. Actin-binding proteins. J Cell Sci. 118(Pt 4):651-4. (2005).

Wirshing, A.C.E. and Cram, E.J. Spectrin regulates cell contractility through production and maintenance of actin bundles in the *Caenorhabditis elegans* spermatheca. Mol Biol Cell. 29(20):2433-2449. (2018).

Wissmann, A. et al. The *Caenorhabditis elegans mel-11* myosin phosphatase regulatory subunit affects tissue contraction in the somatic gonad and the embryonic epidermis and genetically interacts with the Rac signaling pathway. Dev Biol. 209(1):111-27. (1999).

Wissmann, A. et al. *Caenorhabditis elegans* LET-502 is related to Rho-binding kinases and human myotonic dystrophy kinase and interacts genetically with a homolog of the regulatory subunit of smooth muscle myosin phosphatase to affect cell shape. Genes Dev. 11(4):409-22. (1997).

Wolpert, L. et al. Principles of Development. 1st edition, Oxford University Press. (1998).

Wu, M. and Herman, M.A. A novel noncanonical Wnt pathway is involved in the regulation of the asymmetric B cell division in *C. elegans*. Dev Biol. 293:316-329. (2006).

Xu, K. et al. Actin, spectrin and associated proteins form a periodic cytoskeletal structure in axons. Science. 339(6118): 10.1126. (2013).

Yamashita, R.A. et al. Identification and analysis of the myosin superfamily in *Drosophila*: a database approach. J Muscle Res Cell Motil. 21(6):491-505. (2000).

Yan, Y. et al. Crystal structure of the repetitive segments of spectrin. Science. 262(5142):2027-30. (1993).

Yogesha, S.D. et al. Crystal structure of vinculin in complex with vinculin binding site 50 (VBS50), the integrin binding site 2 (IBS2) of talin. Protein Sci. 21(4):583-8. (2012).

Young, P.E. et al. Dynamic changes in the distribution of cytoplasmic myosin during *Drosophila* embryogenesis. Development. 111,1-14. (1991).

Yu, F.X. et al. Identification of a polyphosphoinositide-binding sequence in an actin monomer binding domain of gelsolin. J Biol Chem. 267(21):14616-21. (1992).

Yu, Y. and Elble, R.C. Homeostatic signaling by cell-cell junctions and its dysregulation during cancer progression. J Clin Med. 5(2):427-430. (2016).

Zahreddine, H. et al. CRT-1/calreticulin and the E3 ligase EEL-1/HUWE1 control hemidesmosome maturation in *C. elegans* development. Curr Biol. 20(4):322-7. (2010).

Zamir, E. et al. Dynamics and segregation of cell-matrix adhesions in cultured fibroblasts. Nat. Cell Biol. 2(4):191-6. (2000).

Zelenka, P.S. Regulation of cell adhesion and migration in lens development. Int J Dev Biol. 48(8-9):857-65. (2004).

Zhang, H. et al. A tension-induced mechanotransduction pathway promotes epithelial morphogenesis. Nature. 471(7336):99-103. (2011).

Zhang, J. et al. Design and optimization of a linker for fusion protein construction. Prog Nat Sci. 19(10):1197-1200. (2009).

Zhang, R. et al. Spectrin: structure, function and disease. Sci China Life Sci.56(12):1076-85. (2013).